Technical University of Denmark

DTU

Chemically Structured Products: Simultaneous model-based design of process and assisting structured materials

Soni, Vipasha; Jonsson, Gunnar Eigil; Gani, Rafiqul; Abildskov, Jens

[Link back to DTU Orbit](#)

DTU Library
Technical Information Center of Denmark

Simultaneous model-based design of process and assisting structured materials

Vipasha Soni

January 13, 2008

Computer Aided Process Engineering Center
Department of Chemical Engineering
Technical University of Denmark

Preface

This thesis is submitted as partial fulfillment of the requirements for the Ph.D.-degree at Danmarks Tekniske Universitet (Technical University of Denmark). The work has been carried out at Institut for Kemiteknik (Department of Chemical Engineering) from Nov 2004 to December 2007 under the supervision of Professor Rafiqul Gani, Professor Gunnar Jonsson and Associate Professor Jens Abildskov. Financial support from Danisco is highly appreciated.

My sincerest thanks to my supervisors Professor Rafiqul Gani, Professor Gunnar Jonsson and Associate Professor Jens Abildskov who have provided all possible help and guidance when and where required. A very special thanks to my main supervisor Professor Rafiqul Gani for patient hearings and long hours of discussions which were a great help to me for completing this Ph.D. project. Being in a very international and dynamic group such as Computer Aided Process/Property Engineering Center (CAPEC) at the Department of Chemical Engineering at Technical University of Denmark and numerous travels have given me an insight to international research.

I am obliged to Professor Vlasis Mavrantzas and his group at ICE-FORTH, Patras, Greece for giving me an opportunity to visit the institute and do research with them. My heartiest thanks to Nikos Karayiannis and Rico Bagger Jorgensen for valuable data for the project.

I would like to thank all the coworkers at CAPEC for their support, technical and non-technical discussions and encouragement in all those years of research. My special thanks to Piotr Mitkowski, for countless hours of professional and personal discussions, endless dinners in late working hours and for calling me to wake me up every morning for years for me to be on time for work. My heartiest thanks to Ana, Jakob, Oscar and Florin for being around, for travels, coffee and cake breaks and helping me out whenever I needed.

Last but not the least, heartfelt thanks are due to my family and friends, who have morally supported me throughout the time. I would be failing in my duty if I do not thank Archana for being my moral and emotional support during the longest three months of thesis writing. My very special thanks to my parents, Vinod and Viney Soni and brother Vikrant, who have not left any stone unturned in every aspect to support and encourage me in my pursuit of academic excellence.

Lyngby, November 2007

Vipasha Soni

Abstract

This thesis describes the development and application of a general model-based design framework for the simultaneous design of processes and products. Products in this case are referred to structured materials that assist the process by enhancing their performance. Conventionally, most process-product design problems employ an iterative, trial and error experiment-based procedure. Since experiments are usually expensive and time consuming, the search space for optimal design is limited. Applying computer-aided model-based framework has the potential to save time and expenses, and, widen the search domain for the design alternatives for the process and the products.

The key factors for the simultaneous design of the processes and the assisting structured materials are the dependence of the process performance on the properties of the assisting structured material and the dependence of the assisting structured material properties on their microscopic structures. Thus, properties play a central role in the simultaneous process-product design. It is observed that, separating the constitutive equations representing the properties of the assisting structured material from the process model, can reduce the computational complexity of the design problem by not having to solve multilevel models (macro-level equations representing the process and micro-level equations representing the structured material) together. This is achieved by employing the reverse algorithm that first defines the design targets in terms of properties of the assisting structured material corresponding to a desired process performance (stage 1), and then determine structured materials that match the property targets (stage 2). In this way, the process model does not need a property model for the structured material, since the properties are the unknown variables in stage 1. Once the values for the property targets are obtained from the first stage, structured materials corresponding to these properties can be found using property models that relate the properties to the microscopic structure of the structured materials.

The application of molecular modeling in generating property data for the assisting structured materials as a function of the microscopic structure of the structured materials has been investigated and found to add a new dimension to the simultaneous process-product design problem. It has been possible to generate very useful property data through this option.

The application for the model-based design framework have been illustrated through case studies involving membrane-based separation processes. In particular, membrane-based gas separation and membrane-based liquid separation with a phase change have been investigated. The design framework is however general enough to be applicable to other chemical process and product design problems.

Resumé på Dansk

Denne afhandling beskriver udviklingen og anvendelsen af en general modelbaseret designrammestruktur for simultan design af processer og produkter. Produkterne i dette tilfælde er strukturerede materialer, som assisterer og forbedrer processerne. Normalt inkluderer de fleste proces-produktdesignproblemstillinger eksperimentelle iterative "trial and error" procedurer, men da eksperimenter normalt er forbundet med store omkostninger og stort tidsforbrug, er søgemulighederne for optimalt design dermed begrænsede. Potentielt kan der opnås både økonomiske og tidsmæssige besparelser ved anvendelse af computer-aided model-based framework (computerassisteret modelbaseret rammestruktur), hvilket også kan udvide spektret af søgemuligheder for alternative design af processer og produkter.

Hovedfaktorerne bag simultan design af processer og de dertilhørende assisterende strukturerede materialer er procesydeevnens afhængighed af de assisterende strukturerede materialers egenskaber og de assisterende strukturerede materialers egenskabers afhængighed af deres mikroskopiske struktur. Dermed spiller egenskaberne en central rolle i simultan proces-produktdesign. Det er observeret, at ved at adskille de grundlæggende ligninger, som repræsenterer de assisterende strukturerede materialers egenskaber, fra procesmodellen kan designproblemstillingens udregningsmæssige kompleksitet reduceres ved ikke at skulle løse multiniveaumodeller sammen (makroniveauligninger som repræsenterer processen og mikroniveauligninger som repræsenterer de strukturerede materialer). Dette opnås ved anvendelse af en omvendt algoritme, som først definerer designmålet med hensyn til de assisterende strukturerede materialers egenskaber, som svarer til en ønsket procesydeevne (fase 1), og derefter bestemmer strukturerede materialer, som matcher egenskabsmålene (fase 2). På den måde behøver procesmodellen ikke en egenskabsmodel for det strukturerede materiale, idet egenskaberne er de ukendte variable in fase 1. Når egenskabsmålenes værdier er opnået fra fase 1, kan strukturerede materialer, som svarer til disse egenskaber, findes ved brug af egenskabsmodeller, som relaterer egenskaberne til de strukturerede materialers mikroskopiske struktur.

Anvendelsen af molekylærmodellering til generering af egenskabsdata for de assisterende strukturerede materialer som funktion af deres mikroskopiske struktur er blevet undersøgt og synes at tilføje simultan proces-produktproblemstillingen en ny dimension. Gennem denne mulighed har det vret muligt at genererer meget brugbare egenskabsdata.

Den modelbaserede designrammestrukturs anvendelse er blevet illustreret ved case studies, som involverer membranbaserede separationsprocesser. Særligt er membranbaseret gasseparation og membranbaseret vskeseparation med faseomdannelse blevet undersøgt. Imidlertid er designrammestrukturen general nok til at blive anvendt i forbindelse med andre kemiske proces- og produktdesignproblemstillinger.

Contents

List of Tables

List of Figures

4

1

Introduction

1.1 Background and motivation

A *chemical process* is a means by which raw materials are changed or separated into useful *end-use products* [86]. Each process can be broken down into a series of steps called, *unit operations*. These unit operations are the building blocks of different processes and have common techniques that are based on same scientific principals. In a process, each of the unit operations commonly occur in individual vessels or sections of the process called *process units*.

The chemical process could either be a single unit operation or a combination of several operations involving, for example, reactions and separations. Often, one or more chemical reactions are involved, but other ways of changing chemical (or material) composition may be used, such as mixing or separation processes. In this work, separation processes are studied in particular. A *separation process* may be used to transform a mixture of substances into two or more compositionally-distinct products. The classification of separation processes can be based on the means of separation: mechanical or chemical. Depending on the raw material, various processes can be employed to separate the materials.

In order to obtain desired physical and/or chemical transformation of materials, the process must be designed accordingly. The *process design* essentially amounts to deciding which unit operations to perform on the given raw material or feed streams to achieve optimal end-use product streams at minimal costs (Nishida et al., 1981). Process design involves the design of a new process and/or the modification or expansion of an existing process. Model-based process design is a quantitative problem solving approach, including the use of heuristics, simulation, and optimization. An important first step should include developing or obtaining a detailed mathematical model for the process and identifying the most important design variables to which the process is sensitive to.

In many cases, the chemical processes are assisted by special chemicals like catalysts, solvents etc.. These special chemicals assisting the processes are termed in this thesis as the *formulated/structured chemical materials*. Some common examples are catalysts for reaction systems, solvents for solvent based separations/reactions, polymers for membrane-based separation processes, polymeric micro-capsules for controlled-delivery systems and many more. Any process that requires these assisting structured materials depends very much on their properties, which in turn, depend on their structure. So, in order to design a process which is assisted by

structured materials, it is important to design these materials as well, together with the process. The simultaneous design of the process and the assisting structured material is the main topic of research in this work. The design of processes that is considered in this work are membrane-based liquid and gas separation processes using polymeric membranes and the assisting structured material in this case is the polymer that is used as the membrane.

A *membrane-based separation process* separates an influent stream into two effluent streams known as the permeate and the retentate with the help of a membrane. The *membrane* can be defined essentially as a barrier, which separates two phases and restricts transport of various chemicals in a selective manner. The stream that permeates through the membrane is the permeate stream and the one retained by the membrane is the retentate. Either of the two streams could be the end-use products in a membrane-based separation process. If the aim is concentration, the retentate will usually be the end-use product stream. However, in the case of purification, both the retentate or the permeate can yield the desired end-use product depending on the impurities that have to be removed [89]. In this work, membrane-based gas separation and liquid separation with phase change that employ polymeric membranes for the separation are investigated.

Polymeric membranes can be classified as: porous membranes and non-porous membranes [89]. A *porous membrane* is very similar in structure and function to a conventional filter [6]. It has rigid, highly voided structure with randomly distributed, interconnected pores. These pores are normally in the order of 0.01-10μm in diameter. All particles larger than these pores are completely rejected by the membrane. Particles smaller than the largest pores, but larger than the smallest pores are partially rejected, according to the pore size distribution of the membrane. Separation in these kind of membranes is dependent on both the molecular size and pore size distribution [6].

Non-porous membranes (also referred as dense membranes), consist of a dense film through which permeants are transported by diffusion under the driving force of a pressure, concentration, or electrical potential gradient. The separation is mainly determined by the diffusivity and solubility of the permeants in the membrane material. Thus, non-porous membranes can separate permeants of similar sizes, given their solubility is significantly different [6].

Membrane-based gas separation is an important separation process that has been extensively used for many gas separations, for example, separation of hydrogen from gaseous mixtures of nitrogen and/or methane, recovery of hydrogen from product streams in ammonia production process, separation of methane from biogas produced by oxidation of biomass, enrichment of oxygen from an air stream for medical or combustion purposes, removal of water vapor and/or carbon dioxide and/or hydrogen sulphide from natural gas and removal of volatile organic chemicals (VOC) from air or exhaust streams.

Usually non-porous polymeric membranes are utilized for membrane-based gas sepa-

ration. As mentioned earlier, selectivity to the permeants is imparted by membrane based on the solubility and diffusivity of the permeants in the polymer material. Polymers in glassy state are generally more effective for separation. Glassy polymers predominantly differentiate in terms of diffusivity. Due to the thermal motion of the polymer segments, local gaps are formed along the polymer chains and small molecules of penetrants move among polymer chains according to the formation of these gaps. The factors that affect the diffusivity are free volume of the polymer, its distribution and local changes of distribution [48].

Porous membranes can also be utilized for membrane-based gas separation. The pore diameter must be smaller than the mean free path of gas molecules. Under normal condition (100 kPa, 300 K) it is about 50 nm. Then the gas flux through the pore is proportional to molecules velocity, i.e., inversely proportional to square root of the molecule mass. This transport phenomena is known as Knudsen diffusion. Gas flux through a porous membrane is higher than through non-porous membranes, by about 3 to 5 orders of magnitude, while the separation efficiency is moderate.

Membrane-based separation processes are also used for liquid separations. Typical examples are concentration and purification in various types of industry (especially in the food industry) as well as in water and wastewater treatment are typical applications in liquid separations using membranes. They have a wide application range in chemical industry, dairy industry, food and beverage industry, fermentation and biotechnology and waste water treatment [6].

Liquid separation using membranes can mainly be divided in two groups: one where there is a phase change and one where there is not. Pervaporation and membrane distillation are examples of liquid separation using membranes with phase change, while nano- and microfiltration are examples of liquid separation using membranes without phase change. In this work, however, we are only focusing on liquid separation using membranes with phase change. The membranes used in these processes are classified according to the nature of the separation being performed. *Hydrophilic membranes* are used to remove water from organic solutions. These types of membranes are typically made of polymers with glass transition temperatures above room temperatures. Polyvinyl alcohol is an example of a hydrophilic membrane (i.e. as assisting structured material). *Organophilic membranes* are used to recover organic chemicals from solutions. These membranes are typically made up of elastomer materials (polymers with glass transition temperatures below room temperature). The flexible nature of these polymers make them ideal for allowing organic compounds to pass through. Examples include nitrile, butadiene rubber and styrene butadiene rubber [89].

So, in order to design membrane-based separation processes (both for gas and liquid separations with phase change) and the assisting structured materials (in this case polymers) using a model-based process design, it is required to develop/obtain mathematical models for both the processes and the property models for the polymers (note: unless otherwise stated, the term "structured materials" will be used in the rest of the thesis for "assisting structured materials"). Mathematical modeling

and model-based design of these processes is not only interesting but also a very important research area. It is anticipated that the simultaneous design of the process and the structured material will lead to a better design for both. Therefore, this project is devoted to investigate different scenarios where the simultaneous process-product design can be applied and to improve the already existing design procedures.

Section 1.2 covers the current state of the art in the relevant research areas. Based on the state of the art, the objectives of this work is presented in Section 1.3. In order to achieve the objectives, the main tasks needed are then enumerated (Section 1.4). In the end, the organization of the whole thesis is given.

1.2 Current state of the art

Based on a literature survey, the current state-of-the-art with respect to mathematical modeling of membrane-based separation processes for gas and liquid separations, property modeling for the properties of polymers that affect separation, property modeling for pure component properties of the chemical compounds present in the process streams and procedures for simultaneous process-product design are reviewed in this section. This helps in getting an idea of the groundwork that has already been done and to identify the missing connections and research work needed for the simultaneous design of the processes and the assisting structured materials.

1.2.1 Membrane based separation processes

Membrane processes have wide industrial applications, that includes many existing and emerging uses in chemical, petrochemical, petroleum, environmental, water treatment, pharmaceutical, medical, food, dairy, beverage, paper, textile, and electronic industry. Processes using membranes are generally separation processes, i.e., membranes are primarily used for separation [48]. Membrane based separation processes are replacing conventional separation processes at a large scale owing to the advantages of these processes over conventional processes, which are listed below [89, 48]:

- Membrane-based separation processes are often more capital efficient compared to conventional separation processes with appreciable energy savings.

- Membrane technology is environmentally benign and in general a clean technology with operational ease.

- Membrane units and devices are usually compact and modular with less demanding mechanical properties.

- Membrane processes usually require less vapor spaces and operate on low pressures.

Due to numerous advantages and falling cost of membrane-based separation technologies in past few years, there has been a huge acceptance of these technologies [37]. Continued focus on research and development has led to innovations, growth

and improved membrane performances .

A general membrane based separation process can be represented by the schematic diagram shown in Fig. 1.1.
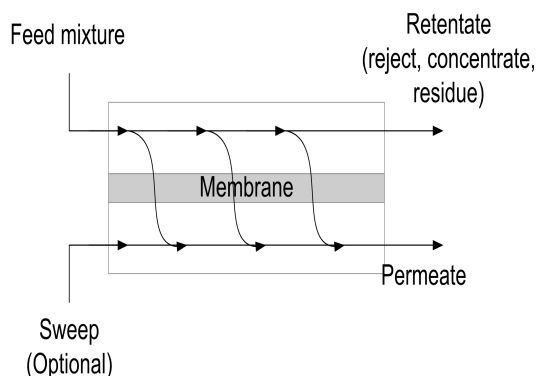
Figure 1.1: General membrane process

As shown in Fig. 1.1, the feed stream enters the membrane-based separation unit and is separated into a *retentate* (that part of the feed that does not pass through the membrane, i.e., is retained) and a *permeate* (that part of the feed that does pass through the membrane). The membrane is selective to one of the chemicals. One bulk phase is enriched in one of the chemicals while the other is depleted of it. A membrane-based separation process then allows a selective and controlled transfer of one species from one bulk phase to another bulk phase separated by the membrane. The selectivity of the membrane is based on difference of chemical or physical properties of the chemicals to be separated such as size (filtration, microfiltration, dialysis etc.), vapor pressure (membrane distillation), affinity (reverse osmosis, nanofiltration, gas separation, pervaporation etc.), charge (ion exchange, electrodialysis) etc. [89]. The movement of any chemical across the membrane is caused by one or more driving forces. These driving forces arise from a gradient of chemical potential or electrical potential. A gradient in chemical potential may be due to concentration gradient or pressure gradient or both [48].

The membrane based separation processes can be divided into mainly three classes: membrane based gas separation, liquid separation with phase change using membranes and liquid separation without phase change. Some examples of each kind of separation are shown in Fig. 1.2

In this work, we are dealing with membrane-based liquid separations with phase change and gas separations. Liquid separation processes considered are: Pervaporation (PV) and various kinds of membrane distillation (MD) processes including Vacuum membrane distillation (VMD), Sweep gas membrane distillation (SGMD), Direct contact membrane distillation (DCMD) and Osmotic membrane distillation (OMD). A general model for these membrane based separation processes is proposed.
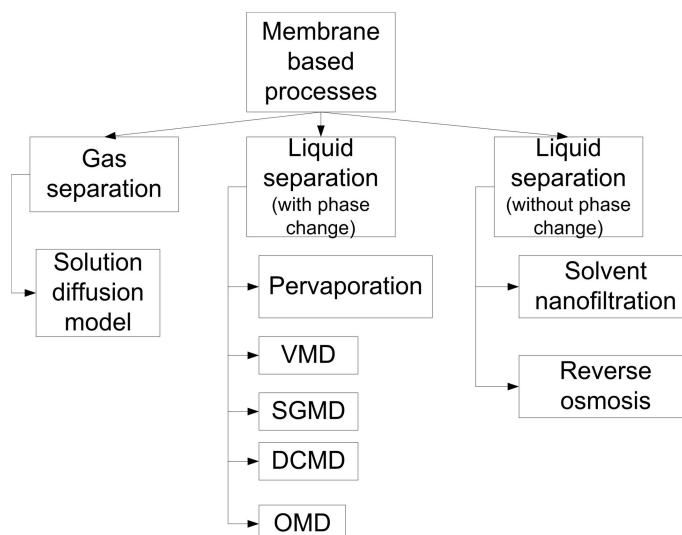
Figure 1.2: General membrane process

Similar work has been published by Marriot et.al [81, 80].

1.2.1.1 Membrane distillation

In the "Workshop on Membrane Distillation" in Rome on May 5, 1986 a committee was formed with the task of preparing a terminology for membrane distillation. Smolders et.al.(1989) have listed terms, definitions and symbols including different embodiments of membrane distillation, which are generally used in the field of membrane distillation, that were agreed upon in this workshop [106]. They have also discussed in brief, a qualitative analysis of various membrane parameters on the process performance. The term "membrane distillation" should be applied for membrane-based operations having the following characteristics [106]:

- The membrane should be porous.

- The membrane should not be wetted by the process liquids.

- No capillary condensation should take place inside the pores of the membrane.

- Only vapor should be transported through the pores of the porous membrane.

- The membrane must not alter the vapor-liquid equilibrium of the different components in the process liquids.

- At least one side of the membrane should be in direct contact with the process liquid.

- For each component the driving force of this membrane operation is a partial pressure gradient in the vapor phase.

Membrane distillation (MD) is a relatively new process, which is attracting increasing research interest because it is a low cost, energy saving alternative to conventional separation processes such as distillation, absorption etc. [48]. Lower

operating temperature is making MD an attractive option for applications such as fruit juice concentration [19, 55] In an MD process, a heated feed solution is brought into contact on the feed side of a hydrophobic, microporous membrane. Due to the repellent effect of the membrane on liquid water, water will only enter the membrane pores if the pressure exceeds the so called "liquid entry pressure of water", which is determined by the membrane material, the pore size and the surface tension of water. The hydrophobic nature of the membrane prevents penetration of the aqueous solution in the pores, resulting in a vapor-liquid interface at each pore entrance (see Fig. 1.3) [73].
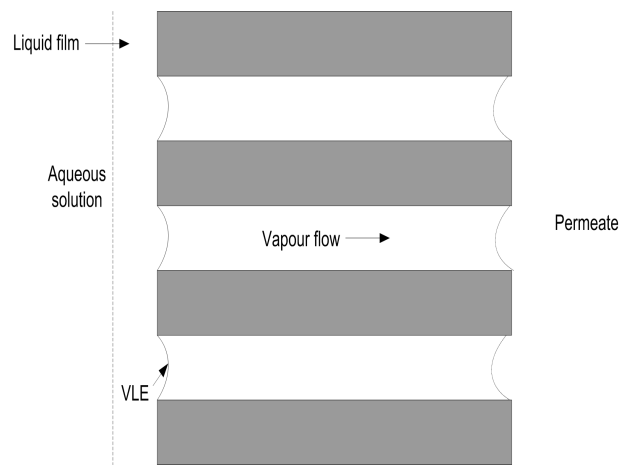
Figure 1.3: Vapor liquid interface in Membrane distillation [73]

In an MD process, the differences in temperature at the membrane interfaces causes the difference in vapor pressures of the species being separated, which is the driving force of the process [29]. To obtain equilibrium, the liquid on the hot side (the feed side) will vaporize at the feed side membrane surface, and then travel through the membrane pores to the membrane surface at the cold side (the permeate side), where the vapor will condense again. The microporous membrane acts only as a support for a vapor-liquid interface. Depending on the membrane pore size and system operating conditions, the membrane may impart some selectivity based on individual Knudsen diffusivities of diffusing species, but the largest degree of separation is realized as a result of the vapor-liquid equilibrium conditions at the membrane-solution interface.

As highlighted by Smolders et.al.(1989), there are different types of MD, depending on how the driving force is imposed [106]. Fig. 1.4 illustrates several common configurations of the MD process that may be utilized to establish the required driving force.

For the different embodiments of membrane distillation the following terms are defined by Smolders et.al.(1989):

13
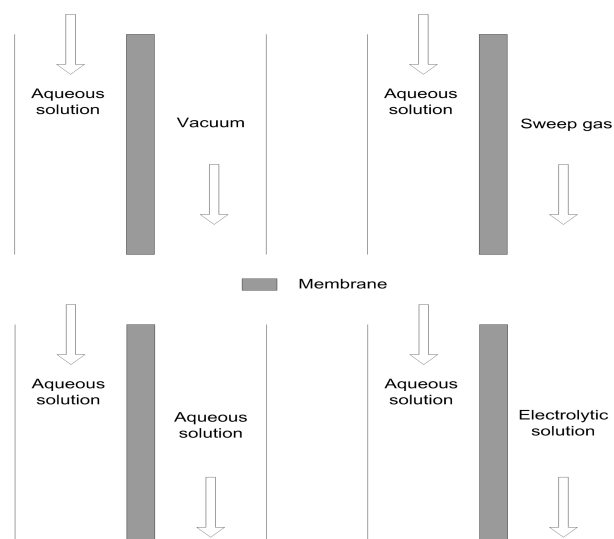
Figure 1.4: Different configuration of membrane distillation

- *Direct contact membrane distillation (DCMD)* for a system in which the liquid on both sides of the membrane is in direct contact with the membrane and in which the liquid on the downstream side is used as the condensing medium.

- *Vacuum membrane distillation (VMD)* In this system a low pressure is applied downstream and the condensation of the permeate takes place outside the module.

- *Sweeping gas membrane distillation (SGMD)* In this system a sweeping gas (e.g., nitrogen) is passed through the downstream side of the membrane and the condensation of the permeate takes place outside the module.

  In addition to the above proposed by by Smolders et.al., another method with the use of a salt solution on the permeate side, called osmotic membrane distillation has also been proposed [5].

- *Osmotic membrane distillation (OMD)* An electrolyte solution is passed on the downstream side which acts as the condensing medium.

Lawson et.al(1997) gave several advantages of membrane distillation over other conventional membrane based separation processes [73]:

- MD is a thermally driven process, so the process is operated at low pressures as compared to pressure driven processes like reverse osmosis (RO).

- MD process is governed by vapor liquid equilibrium at the interface, so a 100% (theoretical) rejection of ions, macromolecules, colloids, cells, and other non-volatile constituents can be achieved.

- Operating at low pressures greatly reduces the mechanical demands on the microporous membranes.

- Membrane fouling is less of a problem in MD as compared to RO or ultrafiltration (UF) because of relatively large pores, which are not easily clogged.

A phenomena in membrane distillation that has a large negative effect on the driving force is *polarization*. It has two aspects: *Temperature Polarization (TP)* and *Concentration Polarization (CP)*. Formation of temperature and concentration polarization layers on either side of a microporous hydrophobic membrane results in a reduced vapor pressure difference. Such polarization layers lead to decreased permeate flux due to reduced vapor pressure difference [48]. TP appears because of evaporation of one side and condensation on the other side. Thus, the temperature difference will be lower resulting in a smaller driving force. CP arises when the one of the component moves faster through the membrane than the other. Due to convective forces the slower component moves from the bulk to the interface but does not pass through the membrane that fast so it inevitably accumulates at the membrane interface until a steady state is attained. An increase in concentration of this component lowers the vapor pressure of the other component and hence the driving force. Sakai et.al (1988) explained the concentration and temperature polarization with experiments done on pure water, aqueous solution, bovine plasma and bovine blood using a temperature controlled stirred cell of original design to see water vapor permeability in membrane distillation [101].

Vacuum membrane distillation VMD: It is a pressure driven process, and the partial pressure difference across the membrane is maintained by creating vacuum pressures on the permeate side of the membrane. The mean free path of gases, is inversely proportional to the pressure. Due to low pressures on the permeate side of the membrane in the case of VMD, leads to high values of the mean free path of the gas molecules. Besides, in most VMD systems the membrane pores are extremely small compared to the mean free path of the diffusing molecules. Therefore the number of molecule-molecule collision is negligible compared to the number of molecule - pore wall collisions, and the molecular diffusion resistance can be omitted [71]. Additionally, molecular diffusion resistance is proportional to the partial pressure of the air in the membrane pores. Since, VMD normally operates at total pressures of 10-50 kPa, which is much below the vapor pressures of most diffusing species, only trace amounts of air can reside in the membrane pores. So, the transmembrane flux through the membrane is according to Knudsen mechanism. But in a case of comparable size of the membrane pores to the mean free path, Knudsen-Viscous diffusion mechanism should be used [7] to calculate the fluxes. Many authors have postulated transmembrane flux for Vacuum membrane distillation. A detailed model for transmembrane flux based on Knudsen and viscous diffusion is presented by Lawson et.al.(1996) [71] and Banat et.al.(1996) [7]. Lawson et.al.(1996) have validated the model with pure water fluxes and also with ethanol-water separation system. Various factors affecting flux in VMD have been discussed. While, Bandini et.al.(1999,2002) have modeled VMD processes with Knudsen-diffusion mechanism [11, 10]. They have shown the role of transport resistances within the liquid phase, due to both the heat and mass transport qualitatively.

Normally, resistances to mass and heat transfer in any kind of membrane distil-

lation module are modeled analogously to resistances in series model [73]. Main resistances are the boundary layer on each side of the membrane and the membrane itself. The boundary layer resistance is modeled by temperature polarization (TP) and concentration polarization (CP). The vacuum on the permeate side of the membrane prevents the formation of a boundary layer, so the corresponding boundary layer resistance may be omitted. This is due to the fact that there is only convective transfer, so the concentration does not change on the permeate side of the membrane [73]. A polarization model could be used to model the resistances in the boundary layer. Izquierdo et.al. (2003) presented an experimental and theoretical investigation of the influence of concentration polarization and temperature polarization on the flux and selectivity of binary aqueous mixtures of ethanol for vacuum membrane distillation (VMD) processes [51]. These effects are normally be modeled by film theory which requires the evaluations of heat and mass transfer resistance coefficients. Mengual et.al.(2004) have shown models for heat and mass transfer in vacuum membrane distillation with special focus on estimation of heat and mass transfer coefficients in the membrane module [87]. Similar models have been proposed by many authors previously [8, 11, 43]. All these models have very similar forms but the equation parameters are different. Most of the times bulk temperature is used to evaluate the heat and the mass transfer coefficients. However, if there is a great temperature difference between the bulk and the membrane wall, most authors employ a viscosity correction factor.

Sweeping gas membrane distillation (SGMD): SGMD involves: (a) the evaporation of water at the hot feed side; (b) transport of water vapor through dry pores of hydrophobic membranes due to transmembrane vapor pressure, which is the driving force; (c) collection of the permeating water vapor by an inert cold sweeping gas; and (d) condensation out of the membrane module [62]. The membrane acts only as a support for a vapor-liquid interface and does not contribute to the separation mechanism. Khayet et.al.(2000) presented a theoretical model that describes sweeping gas membrane distillation (SGMD) processes through porous hydrophobic membranes [63]. Same authors then presented an improved model for SGMD, by adding temperature polarization effects and the heat and mass transfer mechanisms that permits to obtain the temperature profiles in the system, both for the liquid phase and for the gas phase [64]. The effects of the process parameters, liquid feed flow rate, feed temperature, air flow rate and salt concentration on the distillate flux have been investigated by Khayet et.al (2003). A theoretical model that considers the heat and mass transfer through microporous and hydrophobic membranes as well as the temperature and concentration polarization effects is developed and validated with the experimental data of distilled water and saturated aqueous feed solutions [62]. This is a very detailed and well explained model.

Direct contact membrane distillation (DCMD): DCMD is a thermally driven process, where both liquid feed and liquid permeate are kept in contact with the membrane. The temperature difference between two solutions gives rise to transmembrane flux. Lower temperature is maintained on the permeate side by an aqueous permeate stream. The flux obtained by this kind of membrane process is typically very high and is comparable to that of reverse osmosis. For majority of DCMD

processes, such as desalination or concentration of fruit juices, the general model based on dusty gas model can be reduces to account for only two components, water and air. The transmembrane flux in the membranes usually used for DCMD are due to molecular and/or Knudsen diffusion. The influence of the membrane properties and of the operating conditions on mass transfer rate and energy efficiency is also discussed [8]. Lawson et.al.(1996) gave the equation for transmembrane flux by Knudsen-molecular diffusion mechanism and an experimental validation is given [72]. It has been shown [103] that in DCMD applications the net flux of air across the membrane is extremely small as compared to the flux of water. Also, viscous flux can be neglected in case where process solutions have not been degassed. With these assumptions, the model reduces to the Knudsen-molecular diffusion transition mechanism.

Schofield et.al.(1987) [103] described the heat and mass transfer in DCMD and gave the corresponding equations with an emphasis on effect of temperature polarization on the overall process performance. Bandini et.al.(1991) presented a simple criterion for direct contact membrane distillation (DCMD) to predict whether the overall permeation rate is mass or heat transfer controlled, simply based on the knowledge of the physical properties and of the transport coefficients of each intervening phase. Temperature and concentration polarization effects are dominant in DCMD. A detailed analysis of temperature polarization effect in DCMD was done by Gryta et.al.(1998) [45]. Martinez et.al.(2000) proposed a method that permits to evaluate the membrane mass transfer coefficient, the membrane heat transfer coefficient and the boundary layer heat transfer coefficient in a membrane distillation system [83]. Martinez et.al.(2007) have recently analyzed different experimental membrane/module configurations to show the dependence of the resistances introduced on membrane and module characteristics, and on operating conditions (temperatures, type of feed and feed concentration) [82].

Osmotic membrane distillation (OMD): In OMD a macroscopic hydrophobic separates two aqueous solutions having different osmotic pressures. Water evaporates in the solution of higher chemical potential and the vapor crosses the membrane before being condensed in the solution of lower water potential [68]. The polarization effects can also be seen in this kind of membrane distillation. Kunz et.al.(1996) have given model equations for transmembrane flux and boundary layer effects. Temperature effects and heat transfer mechanism in OMD is explained by Gostoli (1999) [43]. They have modeled transmembrane flux with molecular diffusion as the controlling mechanism. In general OMD is very similar to DCMD and a very similar model can be used to model OMD systems. However, there are some differences, that results from the fact that the driving force in DCMD process is formed by the temperature gradient, whereas, in OMD by the concentration gradient [44]. Temperature polarization effect is prevalent in the case of OMD as well, however, the temperature profiles formed in the DCMD and OMD are different. In DCMD, $T_1 > T_2$, whereas in OMD is inversely, $T_1 < T_2$. The temperature gradient is obtained due to the evaporation at the feed side and the condensation at the distillate side, even if the bulk temperatures of two liquids are equal, like in OMD. Conduction of heat from the brine to feed induces a decrease of the polarization

effect in OMD. In the case of DCMD, the situation is reversed, heat associated with the mass transfer as well as conducted through the membrane flows in the same direction, i.e. from the feed to distillate side, therefore the temperature polarization effect increases [44]. Nagaraj et.al.(2006) have shown model equations for Knudsen and molecular diffusion through membranes [92].

In general, mathematical models for all MD modules are available in literature that explains important underlying physical phenomena for these processes. A lot of experimental data has also been reported. However, not a lot of literature was found that have addressed systematic model-based design of the MD processes. Property prediction of the pure component properties of the compounds present in the process streams that would be required for the model solution are not discussed explicitly.

Application of MD

Applications such as desalination, concentration of aqueous solutions (fruit juices), blood, treating waste/process water is best suited for DCMD, where water is main permeate component. The process has been successfully applied to textile waste water contaminated with dyes, pharmaceutical waster water containing taurine, waste water contaminated with heavy metals, sulfuric acid solutions rich in lanthane compounds [73].

To avoid low efficiency of heat utilization using DCMD, air gap membrane distillation (AGMD) can be used. There is a trade-off though, that the mass transfer increases, reducing AGMD fluxes. AGMD can be used for all DCMD applications but also to remove trace volatile components from aqueous solution. It has been successfully been applied to pure water production and concentration of various non-volatile solutes. An application in the area of water and hydrochloric acid or propionic acid azeotropes can be either broken or shifted to higher acid concentration has been done.

In case of removal of volatile organic or a dissolved gas from an aqueous solution either SGMD or VMD can be used. Conductive heat losses through the membrane are negligible in case of VMD.

OMD can be used for removal of water from dilute aqueous solutions, such as liquid foods or natural colors, concentrating them, while retaining the organoleptic and nutritional properties [5]. It is regarded with great interest in the processing of liquid foodstuffs or aqueous solutions of thermally labile pharmaceutical products and biologicals, since a concentration level as high as that currently obtained by evaporation can be reached but avoiding any thermal damage or loss of the solutes [20].

1.2.1.2   Pervaporation

Pervaporation (PV) is a membrane separation process that has elements in common with reverse osmosis and membrane-based gas separation. Permeation through the

membrane during liquid permeation followed by evaporation was termed as perva-
poration by Kober (1917) [67]. In pervaporation, the liquid mixture to be separated
(feed) is placed in contact with one side of a membrane and the permeated product
(permeate) is removed as a low pressure vapor from the other side. The permeate
vapor can be condensed and collected or released as desired. The chemical poten-
tial gradient across the membrane is the driving force for the mass transport. The
driving force can be created by applying either a vacuum pump or an inert purge
(normally air or steam) on the permeate side to maintain the permeate vapor pres-
sure lower than the partial pressure of the feed liquid [32].

Pervaporation separation is governed by the chemical nature of the macromolecules
that comprise the membrane, the physical structure of the membrane, the physio-
chemical properties of the mixtures to be separated, and the permeant-permeant
and permeant-membrane interactions. Pervaporation transport is usually described
to be a three-step process [34]:

- Selective absorption into the membrane at the feed side of the membrane.

- Selective diffusion through the membrane.

- Desorption into vapor phase at the permeate side of the membrane.

The separation is based on the fact that the membrane imparts selectivity to the
components based on their solubility and diffusivity, i.e., the physical-chemical in-
teractions between the membrane material and the permeating molecules, and not
the relative volatility as in distillation (see Fig. 1.5). Therefore, pervaporation is
commonly considered to be a profitable substitute to distillation for the separation
of azeotropic and close-boiling mixtures, which requires at present the use of energy-
intensive processes. Binning et.al.(1961) proposed a solution-diffusion mechanism
for the transport of liquids through homogeneous membranes [13]. The original
solution-diffusion mechanism was proposed by Lonsdale et.al(1965), that described
the flux of a component through a homogeneous membrane [75].
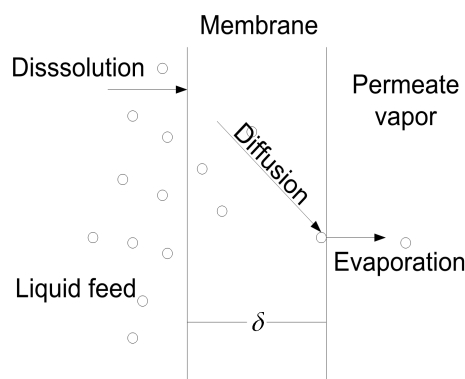
Figure 1.5: Solution-diffusion mechanism in pervaporation

Pervaporation can be operated at low feed pressures and at ambient temperature
or even below this, and no additional chemicals are needed for separation. There-

fore, pervaporation can be applied in biotechnology for the concentration of heat-, stress-, and/or chemical sensitive biochemicals.

Compared with other membrane processes such as reverse osmosis or ultrafiltration, the permeation fluxes in pervaporation are generally low since pervaporation membranes are dense and nonporous. Thus, the concentration polarization in pervaporation is often assumed to be insignificant. However, it has been shown experimentally that for some cases the concentration polarization can be of significance on the overall pervaporation performance, in particular for the removal of trace organic compounds from aqueous solutions. Currently, the resistance-in-series model is mainly used to study the effect of concentration polarization in pervaporation [120]. According to this model, the overall mass transfer resistance is the sum of the membrane resistance and the boundary layer resistance. Starting from the basic equations for mass transport, Feng et.al.(1994), pursued a theoretical approach to describe the concentration polarization in pervaporation processes [32]. A detailed discussion on the mechanisms involved in the pervaporation process and the factors affecting the performance is reviewed in a review paper by Feng et.al.(1997) [34]. An excellent review on solution-diffusion model is given by Wijmans et.al.(1995), where the equation have been derived from basics [120]. The model was extended by Wijmans (2004) to include the role of permeant molar volume in the solution-diffusion model transport equations [119]. Later Feng et.al.(1996) have shown a method to estimate the activity energy for permeation in pervaporation process [33].

Concluding, transmembrane flux in pervaporation is mostly modeled by solution-diffusion mechanism. A lot of literature is available for the polarization effects and solution-diffusion model. The estimation of permeabilities of vapor through membranes have not been reported in many publications. However, use of polymer properties to design the pervaporation process have not been addressed.

Applications of pervaporation

The applications of pervaporation can be classified into three categories: (i) dehydration of organic solvents, (ii) removal of organic compounds from aqueous solutions, (iii) separation of azeotropic mixtures, and (iv) separation of anhydrous organic mixtures. Currently, pervaporation has been commercialized for two applications: one is the dehydration of alcohols and other solvents, and the other is the removal of small amounts of organic compounds from contaminated waters [34]. In the latter application, pollution control and solvent recovery are effected simultaneously. There are also some other promising applications such as aroma recovery and beer dealcoholization in the food industry [74].

1.2.1.3 Membrane based gas separation

Membrane gas separators split a gas stream into two product streams, a high pressure retentate one and a low pressure permeate one, by providing a selective mass transfer layer. Chemical potential differences make the species permeate through the membrane material at different rates. Membrane-based separation processes

compete with technology alternatives such as adsorption, cryogenic distillation etc. in niche application areas [89]. This process is very similar to PV.

Gas separation mechanisms Similar to the liquid separation with phase change using membranes, gas separation mechanism also depend on the structure of the membrane. Fig. 1.6 schematically shows different membrane structures and the corresponding mechanism. The permeation of gas through membranes with larger pores can have either a convective flow (very large pores, no separation), Knudsen diffusion, Poiseuille flow or molecular sieving [61, 48]. The proportions of Knudsen to Poiseuille flow depend on the ratio of pore radius (r) to the mean free path (λ). For $r/\lambda < 1$, Knudsen flow dominates and for $r/\lambda > 5$, Poiseuille flow predominates ($> 90\%$). There can be an enhancement of the transport rates through Knudsen diffusion membranes by other mechanisms like surface diffusion, in which molecules absorb to the surface of the pores and then diffuse along the surface. If the pores are small enough, large molecules are unable to pass through them and are excluded by the membrane. This molecular sieving is useful in separating molecules of different sizes. Detailed discussion about these kind of mechanisms can be found in literature [61]. In this work, we are focusing on membrane based gas separation through dense or non-porous membranes.
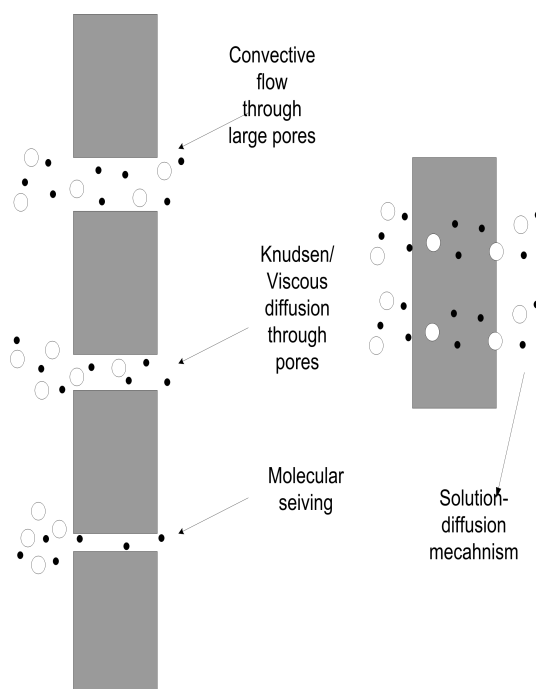
Figure 1.6: Mechanism for gas separation using membranes

In non-porous membranes, the gas molecules gets absorbed and then diffuse through the membrane matrix. The separation mechanism thus takes place in three steps, (i) absorption or adsorption of the gas molecules on the upstream side of the membrane, (ii) diffusion through the membrane, and (iii) dissolution or evaporation from the downstream side of the membrane. Membrane based gas separation also follows

solution-diffusion mechanism just like pervaporation process [97]. It is driven by difference in thermodynamic activity on both sides of the membrane. Thus, permeation is a thermodynamically and kinetically driven process. For small gases permeating through polymers, permeability is a product of solubility (thermodynamic aspect) and diffusivity (kinetic aspect) of the small gas molecule through the polymeric matrix [84]. One of the earlier works in membrane based gas separation include analysis of design parameters, operating variables, physical properties, flow patterns etc. in hollow-fiber membranes for design purposes by Antonson et.al.(1977) [4]. They also gave the differential pressure drop equation to account for the pressure drop in the fiber bore.

The performance of polymeric dense membranes for gas separations, working in solution-diffusion regime, is influenced by the following different structural levels [48]:

- First level: Chain conformation, branch frequency and/or orientation and polymer architecture.

- Second level: The monomer repeat unit of the polymer that forms the selective membrane layer.

- Third level: Morphology of membrane separating layer.

- Fourth level: The overall membrane structure, including structural relationships between the separating layer and the rest of the membrane.

The first two levels are microscopic and involve polymer chemistry and influence on the rate at which the gas diffuses through the membrane. At the third level, membranes can be classified as being symmetric or asymmetric. Commercial membranes for solution-diffusion transport mechanism are asymmetric in nature. The fourth level involves the active layer and the support layer in the overall membrane structure.

Continuous membrane column (CMC) concept was introduced by Hwang et.al.(1980) which is not only interesting from theoretical point of view but has also found extensive industrial applications [49]. The CMC is very similar to a distillation column without reboiler. It consists of two counter-current membrane modules with feed gas introduced between both modules. The top product, which is enriched in fast permeating components, is partially recompressed and recycled to the high pressure side top of the column.

Chern et.al.(1985) have presented an interesting model for the separation of binary gas mixtures by hollow-fiber module [22]. Instead of using the solution-diffusion model they have used dual-mode model which introduces a component dependency of the permeabilities. This model, however, is applicable only to binary mixtures. A more simplified model for a hollow-fiber module for the separation of binary mixtures has been presented by Rautenbach et.al.(1986) [97]. An initial differential model including pressure drop equations for both permeate and feed side and an axial backmixing term is reduced to a model consisting only if differential material

balance equations. The model is further simplified to obtain an analytical solution of the differential equations.

Kao et.al.(1987) have shown the effect of axial diffusion term on the model describing the separation of binary mixture using hollow-fiber permeator [56]. Axial diffusion becomes important when the convective flow in the capillaries is small. Axial backmixing tends to level out composition gradients in the axial direction and therefore reduced the driving force resulting in a poor separation. Fattah et.al.(1992) have taken into account the non-ideal behavior of gas phases by equation of states [31]. They have reported large differences between ideal and non-ideal models for the investigated cases.

Coker et.al.(1998) have given models for multicomponent mixtures separated by hollow-fiber co-current and counter-current flow patters [23]. Gorissen et.al.(1987) have considered temperature effects in connection with gas permeation due to Joule-Thomsen effect [42]. The integral energy balance for permeator is based on the assumption of isenthalpic operation of the module. Furthermore, the module is assumed to behave like an ideal heat exchanger.

Ruthven et.al.(1995) have presented design model for membrane separation for binary mixtures to design cascades of membrane units which were economically compared to a competitive pressure swing adsorption [100]. Their model is formulated in terms of the differential material balances for the binary mixture. In a work by Lababidi et.al.(1996), a design model which is used for economic optimization calculations of different permeator configurations have been presented. The three systems considered are the single stage, the two stage, and the continuous membrane column (CMC). The design model consists of integral material balances around each module together with flux relations for the mass transfer through the membrane [69].

Concluding, mathematical models have been developed by various researchers, for membrane-based gas separation following solution-diffusion mechanism and dual-mode mechanism. In some cases, approximate models have been derived in order to simplify the differential models. Very few papers have addressed temperature effects involved in membrane-based gas separation processes. Non-ideal behavior of gases is not taken into account in many papers. There is a scope of improving the existing design procedures by incorporating the model-based design approach and simultaneous design of polymers. Experimental permeability data is available in many articles but not as much is presented for the prediction of the permeability of gases in polymers.

Applications of membrane based gas separations

The membrane gas separation has been used for hydrogen separation and recovery, ammonia purge gas, refinery hydrogen recovery, 'syngas' separation in petrochemicals industry, carbon dioxide enhanced oil recovery, natural gas processing, landfill gas upgrading, air separation, nitrogen production, air dehydration, helium recovery etc. [111].

1.2.2 Property modeling

This section is divided into two subsections: One dealing with membrane (polymer) properties and other with pure component property prediction of chemical compounds present in the process streams.

1.2.2.1 Membrane properties

Polymeric membrane-based separation processes depend very much on the properties of the polymers used as membranes. The separation factors, flux, selectivity, etc., all depend on various polymer properties which in turn depend on the polymer structure. The kinds of processes that are considered in this work use non-porous (dense) polymeric membranes and porous polymeric membranes. The mechanisms for different processes are different and thus depend on different properties of the polymer. Table 1.1 lists different processes and the kind of polymer that is used for the separation in that process. Different separation mechanism and the corresponding key property of membrane that enhances and retards the separation are also shown. The transport of material through porous membranes depends on Knudsen, viscous and/or molecular diffusivities of the components through the polymer matrix. These diffusivities depend on the membrane parameters like K_0, K_1 and B_0, which in turn depend on the porosity (ϵ), pore size (r) and tortousity (τ) of the membrane.

Process	Mechanism	Polymer	Property
Membrane distillation	Knudsen/ Viscous / Molecular diffusion	Porous	Porosity, toutousity, pore size
Pervaporation	Solution diffusion mechanism	Dense	Solubility, diffusivity of vapor in the membrane
Gas separation	Solution diffusion mechanism	Dense	Solubility, diffusivity of gas in the membrane

Table 1.1: Mechanism of different kinds of membrane processes and corresponding polymer properties

Permeability

In the case of non-porous membranes, the governing mechanism is solution-diffusion mechanism. According to solution-diffusion mechanism, gas permeation is a complex process controlled by the diffusion of the penetrant gas molecules in the membrane matrix. Solution equilibrium is assumed to be established between the gas in contact with the membrane interfaces and the gas dissolved in the membrane at these interfaces [107]. In the case where, the solubility of a penetrant gas in a polymer is sufficiently low to be within the Henrys law limit, it is a constant at a given temperature. The diffusion coefficient is then often also a constant, this is the case for supercritical gases in "rubbery" polymers over wide ranges of pressure. In such

a case the permeability is simply a product of the diffusivity and the solubility of
that gas in the polymer [61]. So, the polymer property that enhances or retards
the separation process and determines the product purity is the permeability of the
gas molecules being transported through the polymer. Permeation is a thermody-
namically and kinetically driven process, and it very much depends on structural
parameters related to the monomer structure of the polymer and also on the mi-
croscopic architecture of the polymer like chain length, branch length, branching
frequency or orientation etc.. Developing such models requires information on how
properties (density, diffusivity, solubility, etc.) vary as a function of polymer struc-
ture and architecture (length, branching etc.).

The process of gas diffusion in polymers can often be described satisfactorily on
a macroscopic (continuum) level by suitable solutions of Ficks laws [26, 110]. On a
microscopic level, models provide expressions for gas diffusion coefficients or perme-
ability coefficients, or both, derived from free-volume, statistical-mechanical, energy,
structural, or other considerations [107]. However, phenomenological models are
not predictive because the model parameters are not directly related to the polymer
structure. To have a connection between the permeability properties and the struc-
ture of the polymer, group contribution models and computer simulations employing
atomistic simulations can be used.

Van Krevelan (1990) [114] have given models for properties of polymers and corre-
lations that gives property values as a function of the chemical structure, numerical
estimations of the properties and prediction from additive group contribution based
models. For both diffusivity and solubility of small gases, reasonable estimates are
possible if some basic data of the permeating molecules (e.g. critical temperature
and collision diameter) and of the polymer (structure, glass transition temperature,
crystallinity) are known. Krevelan has given simple equations and equation parame-
ters for both diffusivity and solubility of small gases through various polymer repeat
units.

Park et.al.([95]) have attempted to develop a group contribution method for predict-
ing permeabilities of small gases in polymers based on free volume of the polymer.
The method used involves an empirical modification of a free volume scheme that
has been used in the past with some success. The diffusion coefficient of a gas in a
polymer depends more profoundly on the nature of the polymer, than the solubility
coefficient. One of the most important factors influencing gas sorption and diffusion
is the free volume of the polymer [115]. This suggests a strong correlation between
the permeability coefficient of the solved gas and fractional free volume. They have
given correlations for predicting permeability of six gases through structurally dif-
ferent polymers. Extensive work has been presented by Zielinski et.al.(1992) on the
free-volume theory as well as attempts to obtain a purely predictive model for sol-
vents in polymers [122]. An extension of the free-volume theory for large molecules
was presented by Vrentas et.al.(1996) [116].

Solubilities and diffusivities are governed by the penetrant size and interactions
with the polymer as well as by the shape, size, connectivity, and time scales of

thermal rearrangement of unoccupied space within the polymer [60]. A lot of work has been done in molecular modeling to formulate more detailed descriptions of the mechanisms of gas transport in polymers. These molecular models attempt to analyze specific motions of penetrant molecules and surrounding polymer chains relative to each other and take into consideration the pertinent intermolecular forces [107]. Takeuchi et.al.(1990) have calculated diffusion of simple gas molecules in polymers using molecular dynamics (MD) computer simulations [109]. The self diffusion coefficients of the small gas molecules were obtained from mean squared displacement of the gas molecules.

Diffusivity

At high temperatures (higher than glass transition temperatures), the picture of penetrant diffusion as a sequence of infrequent jumps breaks down; diffusion is limited mainly by the mobility of the polymer chains. Diffusion of small molecules in polymer melts can be safely calculated by employing MD and invoking the Einstein relation, in the long-time, hydrodynamic or Fickian limit [112]. Pant et.al.(1995) carried out molecular dynamics simulations of diffusion of a small-molecule penetrant in an amorphous polymer matrix for methane in polyethylene (PE) and methane in polyisobutylene (PIB) over a very wide range of temperatures [94]. They calibrated the non-bonded potentials (Lennard-Jones potential) representing the polymer-polymer bead interactions in the matrix.

At low temperatures, however, penetrant motion is characterized by periods of localization interspersed with large diffusive jumps. Diffusion at the lower temperatures therefore seems to be limited by the number of sites available to the penetrant in the polymer matrix and the distribution of intersite energy barriers [108]. In a glassy polymer, diffusion is too slow (by about 2-3 orders of magnitude) that it takes a long time to predict the diffusion coefficient by brute-force MD [112]. In this case, the distribution of rate constants characterizing the elementary diffusive jumps of a low molar mass substance through the polymer matrix can be calculated by applying transition-state theory (TST) [46]. Nikos et.al.(2004) have shown the use of transition-state theory to calculate the rate constants of diffusive jumps between sorption sites, and hence the low concentration self-diffusivity of gas molecules [60].

Solubility

Many predictive models for solubility of small gases in polymers are available in literature. In this work, however, the main focus is on molecular modeling because it correlates the solubilities with microscopic structure of the polymer. With the advance of computer technologies, molecular simulation methods based on force field technologies are regarded as promising alternatives for predicting solubilities values. If the external pressures of interest are sufficiently low, a good estimate of the solubilities of small gases in polymers can be obtained from the Henry's law constant [36]. Murad et.al.(2000) have given a simple algorithm to predict Henry's law constants using Monte Carlo techniques [90]. The algorithm is based on a molecular dynamics system of representing a gaseous compartment separating a gas from the solvent

using a semi-permeable membrane, permeable only to the gas molecules. The system is then allowed to come to equilibrium at the desired density and temperature. They have shown the determination of Henry's law constants at equilibrium using simple thermodynamics. Under equilibrium conditions, the number of absorbed molecules per unit volume is proportional to the Henry's law constant and external pressure [36]. Murad et.al.(2001) have then applied this algorithm to the case of oxygen dissolved in liquid benzene and have achieved very accurate predictions [91].

For polymeric systems, Widom insertion method [118] coupled with canonical ensemble (NVT) molecular simulations can be used to calculate Henrys law constants (HLCs) of common gas molecules [121]. From the Henry's law constants, the solubilities of the gas molecules can be calculated. The idea of the Widom insertion method is to uniformly insert the test particles in the configuration space. The insertion can be randomly placed, which requires a good random number generator. After each insertion the energy of the system is calculated. The calculated energy that includes intermolecular energy between sorbate molecules, interaction energy between sorbate molecules and the polymer matrix and the total intramolecular energy of the sorbate molecules. Based on this energy compared to the energy before insertion, the insertion is accepted or rejected. Henry's constant is then calculated at equilibrium. Economou (2001) has given semi-empirical two-body potential models that allows accurate representation of the pure water vapor-liquid equilibria, including the critical region. These models are also used for the calculation of water-hydrocarbon low and high pressure phase equilibria [30]. Theodorou et.al.(2001) have shown the use of Monte-Carlo simulation for solubility prediction of non-polar solute molecules in water. Results are analyzed with respect to the free energy of cavity formation for hosting the solute molecule in the solvent and the free energy of interactions between the solute molecule and the solvent [15].

Molecular modeling is a well established modeling approach to predict structural, static and thermodynamic properties of a wide variety of materials including polymers. Methods for predicting barrier properties of polymers using molecular modeling have been reported by several researchers. However, most of the papers employ the "united atom" approach to perform the simulations. United atom is an approximation of a real system, as instead of taking all the atoms explicitly, united atoms represent a group of atoms. For example, instead of treating all four atoms of a CH3 methyl group explicitly (or all three atoms of CH2 methylene group), one represents the whole group with a single pseudo-atom. This considerably reduces CPU time but for barrier property estimation the predictions would be precise of all the atoms are considered explicitly. Not much data has been found that predicts barrier properties with all atoms approach.

1.2.2.2 Pure Component properties

Component properties play a very crucial role in the separation process and hence their precise prediction is very important for the process model to be accurate within a reasonable error. There are a number of pure component properties that are required in order to solve the process model. These include pure component liquid

density (ρ_i), liquid viscosity (μ_i), specific heat (Cp_i), thermal conductivity (k_i), infinite dilution diffusion coefficients (D_i), gas viscosity (μ_{gi}), heat of vaporization (δH_i), vapor pressure (P^{sat}), Critical temperature (T_C), etc. and mixture properties like activity coefficients (γ_i). In case of osmotic membrane distillation component activity coefficients are also required in salt solution. Experimental values should always be a first choice wherever possible. But since these properties depend on process parameters like temperature, there is a need to have a correlation that gives the temperature dependency where temperature changes with time and/or length and to evaluate the properties at each discrete time or length point such a correlation is required. For some common compounds experimental values of these properties at various temperatures are usually available, which then needs to be regressed in order to obtain closed form of end use property models. In other cases where experimental data is not available, it is then required to predict these properties at different temperatures using predictive models.

Considerable work has been done in the field of property prediction of chemicals, giving methods for the estimation of a wide range of properties. Jaksland et.al.(1996) subdivided properties and their prediction into two classes: primary properties (predicted on the basis of molecular structure) and secondary properties (predicted using primary properties and/or temperature or pressure) [52]. Franklin in 1949 described a group contribution approach, where the properties of a compound are expressed in terms of functions of the number of occurrences of predefined fragments (groups) in the molecule [35]. Group contribution methods such as by Joback et.al.(1983) [53], Constantinou and Gani (2004) [24], van Krevelan [114], etc., have been applied regularly for pure component property prediction.

1.2.3 Product and process design

Gani and Constantinou (1996) have identified relationships between molecular structures, properties and design and highlighted how they can be exploited in process-product simultaneous design [38]. The objective was to evaluate and analyze molecular structure based methods for estimation of properties with respect to their use in process-product design. The idea is to get target properties from the process design part of the design problem and then find the molecular structures of the products that has those property values. Harper et.al.(1999) have developed a Computer-aided molecular design (CAMD) technique that provides a means for determining molecules or mixtures of molecules (CAMMD) having a desirable set of physico-chemical properties [47]. While Harper et.al. used group contribution methods for molecular design, Meniai et.al.(1992) used a molecular graphics system coupled with mainframe Monte Carlo simulations to predict liquid phase solute-solvent interaction energies for design of solvent for liquid liquid extraction [88]. Macchietto et.al.(1990) have also shown the use of group contribution for solvent design where a mathematical optimization problem is formulated and the optimal solvent or solvent mixture is found by selecting the number and type of structural groups in the solvent molecule, subject to chemical feasibility and engineering constraints [76]. Derringer et.al.(1985) have tackled a common problem in polymer science of finding a polymer which can meet a number of property constraints. A methodology

is presented in which a computer generates polymer structures and estimates their properties using empirical relationships. An optimization method is then employed to select the candidate polymers which best comply with a set of property specifications [28]. Gani et.al.(2002) shows the role of properties in three ways: service role, advice role and solve role [41]. In this work, product design is considered as the design problem that determines the specification of a product together with the design of the process. Thus, a simultaneous product-process design problem starts with the definition of the product specification and ends with the optimal process that produces the specified product.

1.3 Objectives of the PhD-thesis

Section 1.2 reviewed the current state-of-the-art in the area of membrane based separation processes and simultaneous process and product design. There are some interesting issues in connection with simultaneous design of membrane based separation processes and product (in this case polymers) design that have not yet been addressed in the open literature. This PhD-thesis intends to fill in some of these gaps in the area of process-product modeling, analysis and design of membrane-based separation processes simultaneously with the design of the assisting structured materials.

The main objective of this PhD project is to simultaneously design process and the assisting structured material for better performance of both the process and the structured material. For this there is a need for a systematic design framework for the design, analysis and validation of both the process and the product. The key factor in the simultaneous design of the processes and the assisting structured materials is the dependence of the process performance on the properties of the structured materials and the dependence of their properties on their structure (See Fig. 1.7). This also forms the basis for the need for multilevel modeling. This simultaneous design of the process and the structured material will tackle the design problem in two ways: (i) designing the process in terms of process/operating conditions (macrolevel process design) and (ii) by designing of the assisting structured material (microlevel product design).
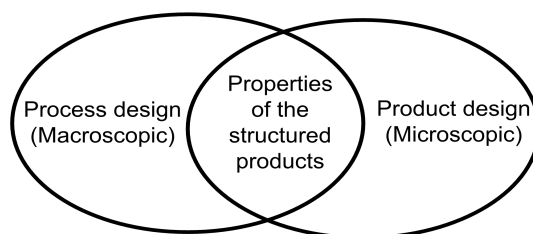
Figure 1.7: Process - product - property relationship

For the development of a model-based design framework, there is a need for mathematical model libraries. Models representing the processes that correlates the physical behavior of the system with design variables that affects the process are im-

portant in design. The model libraries should also include various property models for the computation of the needed pure component and mixture properties of the streams in the process. And also the property models that relates the properties of the structured products to their microscopic structure should be incorporated. Apart from models, it is also required to have robust solution algorithms that are computationally inexpensive and can be applied to a wide variety of process-product design problems.

The main tasks needed in order to achieve the objectives of this PhD project are listed in the next section.

1.4   Main tasks needed

A systematic computer-aided multilevel model-based design framework should be developed for the design of the process simultaneously with the design of the assisting structured materials. This design framework should comprise of model libraries for different membrane-based separation processes and properties of chemicals and structured materials (polymers). The models should be implemented in such a way that the model equations can be re-arranged in different ways to solve them in the forward way or the reverse way. The architecture of the design framework should be general so that can be applied to a variety of processes and structured materials.

There is a vital connection from process demands to the properties of the assisting structured materials, which is in turn depend on their microscopic structure. This connection of the process performance, properties of the structured materials and their microscopic structure should be highlighted conceptually and demonstrated with case studies. This should include the development of process models, identifying the key properties of the structured materials and then obtaining the property data through appropriate property models that relates the properties to the structure of the materials.

Since the design problem at hand is multilevel due to the presence of macroscopic process models and microscopic property models for the structured materials, a robust design approach should be developed that is able to handle the different levels and dimensions of the simultaneous process-product design problem. The design approach should be versatile in nature, that is, it should be able to handle wide variety of design problems.

It is in general a good idea to have the process and product models as rigorous as possible. If needed, assumptions can be applied to simplify the models for the required process. These kind of models make it convenient for a computer-based system to generate individual process models by application of assumptions corresponding to them. A general model for membrane-based separation processes including liquid separation with phase change and membrane-based gas separation should be developed.

Molecular modeling could be used to predict barrier properties of the polymers for various penetrant molecules and not much literature data have been found so far to connect this modeling approach to membrane-based separation processes to design the process and the polymers simultaneously. Molecular modeling should be used to establish the connection between structured material properties and their microscopic structure. A lot of theory is available in literature for this kind of calculations but there is a need for step-by-step hierarchal procedure to predict barrier properties of gases through the polymers.

Group contribution methods for property predictions could be used for both pure component physical properties of the compounds in the process streams and also for predicting properties of the polymers and relating them to their repeat unit structure. This will help in handling the process-product design problem at a repeat unit level.

The methodologies and the developed design algorithms should be validated by applying to various case studies from the field of membrane-based separation process.

1.5 Organization of the thesis

The PhD-thesis consists of six chapters and two appendices. The computer-aided model-based design framework for simultaneous process and product design is presented and explained in Chapter 2. This chapter describes all the components of the developed design framework in terms of various process and property models and different solution algorithms. A conceptual study highlighting the application and salient features of the design algorithms is presented. Various computational tools and software that are employed in this work for the solution of model equations for both process and property models, simultaneous design of membrane-based separation process and the polymers used as membranes, prediction of pure component properties etc. have been listed and described.

Chapter 3 presents the theoretical background of molecular modeling. Both techniques of molecular modeling: molecular dynamics and Monte-Carlo simulations are described with the relevant equations. A general idea about various ensembles in molecular modeling, potentials and force fields is given. At the end of the chapter, prediction methods for diffusivity and solubility of penetrants in the polymer matrix employing molecular modeling techniques, is presented.

Chapter 4 gives the general model structure for various process models developed/used in this work for the membrane-based separation processes. Development of detailed models for liquid separation with phase change and for membrane-based gas separation have been described in detail. Various pure component property models needed by the process models and the design framework are presented. Property models for predicting barrier properties of the polymers used as membranes is also presented. A hierarchal approach for predicting permeability of small gases through polymers of different structures and at different conditions is presented in this chap-

ter.

Chapter 5 illustrates various steps in the design framework and reverse design approach with case studies from membrane-based separation processes. This chapter is mainly divided into two sections. In the first section demonstrates the application/development of property models to predict pure component and polymer properties. In the second section, motivating examples illustrating the employment of the design framework developed in Chapter 2 for simultaneous process-product design are presented. Section 5.1 dealing with property prediction, describes in a step by step procedure to predict solubility and diffusivity of oxygen and nitrogen in polyisobutylene at various temperatures. This section also presents pure component property prediction of aroma compounds found in black currant juice, using group contribution models. Section 5.2 demonstrates the process-product design for the case of enrichment of oxygen from air and of carbon dioxide from natural gas. A process-product design of recovery of aroma compounds from black currant juice is also presented in this section. A comparative study of process performance in terms of flux and product concentration factor for various membrane distillation processes is presented.

Chapter 6 presents the main conclusions, discussion of major achievements of this PhD thesis and some recommendations for future work.

In the end, there are two appendices. Appendix A gives modeling details for pervaporation and various types of membrane distillation processes considered in this work.

Appendix B gives the full forms of some polymers whose abbreviations are used in the case study given is section 5.2.1 and 5.2.2.

2

Design framework for process-product design

2.1   Introduction

In a chemical process, raw materials are changed or separated into useful end-use products. These processes could either be single unit operations or a combination of several operations or hybrid processes involving reaction - separation or separation - separation schemes. Sometimes these processes are also assisted by other formulated/structured chemical products. Fig. 2.1 illustrates the relation between process and its performance in terms of end-use products and the properties of assisting structured materials.
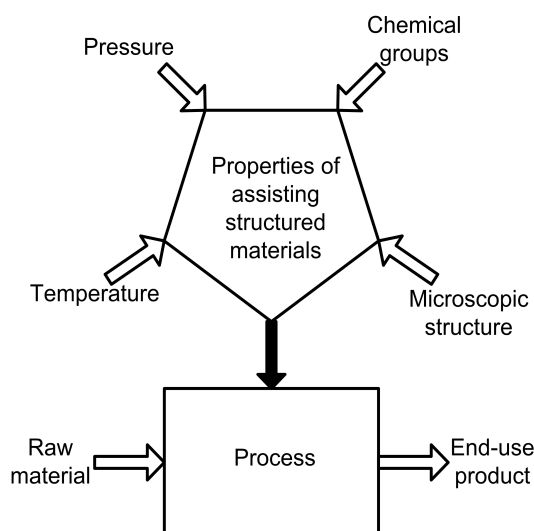
Figure 2.1: Relation between process and and the properties of assisting structured materials.

The properties of these assisting structured materials significantly affect the performance of the processes where they are used. These properties depend on temperature, pressure etc., and are also assumed to be intimately related to the chemical groups representing the structured materials and their microscopic structure [38], [114]. So, the process performance not only depends on the process variables and parameters like temperature, flow rate etc., but also on the microscopic structure of the structured materials. This dependence of process (macro-scale) and the structured material parameters (micro-scale) on the performance of the process, in terms of end-use product specifications, makes the whole design procedure multi-scaled.

Model-based designing, optimizing and conceptualizing such a process would require development of process models, property models for pure component physical properties of all chemical species present in the system and property models for the structured materials (models that relate the macroscopic properties to the microscopic structure of the structured material). In order to simultaneously design the process and the structured materials, it is advantageous and convenient to solve different scales of models together, systematically integrated in a single design framework.

The central point in the development of a design framework for the simultaneous process-product design are the properties which play an important role in any process-product design procedure. The properties of the chemical species and structured material both affect the process output and both are affected by the process conditions and structure of the structured materials. So, in general the composition, purity, recovery of the end-use product of the process directly depends on the operating condition and the properties of the chemical species and structured materials, and thus depend on the structure of the chemical species and structured materials. For example, for a membrane based separation process where a polymer membrane is used, the process performance could be measured by the concentration factor of the desired compound in the outlet. In such a case, the polymer used as the membrane is the structured material that assists the membrane-based separation process. This very much depends on the driving force applied to the system and the permeability properties of the polymer used as a membrane. The driving force may depend on the operating conditions like T, P and/or composition, and, the permeation properties may depend on operating conditions and structure of the polymer (both at the repeat unit level and the microscopic structure like average chain length, branch length, etc.). So, the design procedure depends on the relationship of properties of the structured material (polymer permeability) and hence its structure, to the process performance. A higher permeability of the desired component will result in a higher separation, while a higher permeability ratio of different compounds in the mixture will result in higher recovery. This relation of the structured material properties and process performance makes the basis for the simultaneous product-process design.

The next section, (Section 2.2) gives the general definition of the design problem along with the definition of important variables that either represent the process or affect the process performance. Section 2.3 describes the need for a systematic design framework for the simultaneous design of process and product followed by the description of the design framework and its main elements. That is followed by different design algorithms to solve the simultaneous design problem and their comparison is presented. Later, in Section 2.4, a conceptual study with a motivational example is presented that explains different steps of the design algorithms. Section 2.5 presents the discussions and conclusions of this chapter.

2.2 Definition of the Design problem

The design problem considered in this PhD thesis involves simultaneous process and product (in this case, assisting structured materials needed to obtain the end-use products from the process) design. Schematic diagram of a process with an structured materials is shown in Fig. 2.2.
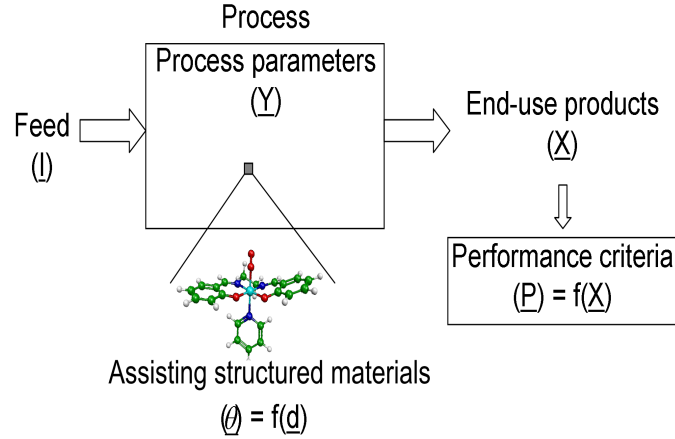
Figure 2.2: Schematic diagram of the process

The different variables shown in the figure are explained below:

- I = *Inlet variables:* Vector $\underline{I}$ defines feed inlet variables like the feed flow rate, temperature, pressure, composition etc..

- $\underline{X}$ = *Outlet variables:* End-use product parameters are given by vector $\underline{X}$, e.g. product composition, purity etc..

- $\underline{Y}$ = *State variables:* Vector $\underline{Y}$ represents the state variables like temperature, pressure etc. (process parameters).

- $\underline{P}$ = *Performance criteria:* Vector $\underline{P}$ defines the performance criteria of the process like product recovery, concentration factor as compared to the feed etc., which is normally a function of the outlet variables $\underline{X}$.

- $\underline{\theta}$ = *Properties of the assisting structured materials:* The properties of the assisting structured materials that effect the process are defined by vector $\underline{\theta}$. These properties depend on variables defined by vector $\underline{d}$, which could either be state variables $\underline{Y}$ or microscopic structural parameters of the materials denoted by $\underline{S}$ like chemical structure, branch length/frequency (if material is made of polymer) etc..

- $\underline{M}$ = *Geometry of the process unit:* The performance of the process also depends on the geometry of the process module (defined by vector $\underline{M}$), for example, reactor geometry, membrane separator structure, like length or height of the module, thickness of the membrane or membrane area, co-current or counter-current flow etc. [14, 104].

Based on the above definition of the variables, the design problem is defined as follows.

For given feed conditions ($\underline{\text{I}}$), the objective is to design the process to match the desired performance criteria ($\underline{\text{P}}$) set by market or individual demands for the end-use products.

So, for a known $\underline{\text{I}}$ and $\underline{\text{P}}$, the design variables could be related to, the process conditions ($\underline{\text{Y}}$), the structural parameters of the assisting structured materials ($\underline{\text{S}}$) and/or the unit geometry ($\underline{\text{M}}$). For an already existing plant, due to economic reasons, it is sometimes not possible to alter the unit geometry or the structured materials. In such a case, the design variables would only be related to the process conditions, which will also have an impact on the properties of the structured materials in most cases.

In a case of a new process design, there is more freedom to choose the design variables. The design variables could be a combination of process and structured material parameters for simultaneous product-process design. In case of the design of the structured material only (where design variables are only the parameters related to the structured material), the procedure requires to relate the end-use product targets to the properties of the structured material and then use the relation between the properties and the microscopic structural parameters to design the structured material.

2.3   Design framework

The architecture of a general design framework for simultaneous process-product design is highlighted in Fig. 2.3. The salient features of the design framework includes model generation, model validation and model application. Model generation involves development of all multilevel process and structured material property models. Once the models are developed, it is important to validate the models with experiments. The validated models can be employed for process and product design. In this work, this is done by using a reverse design algorithm. All these features are explained in the subsequent sections.

2.3.1   Need for a systematic model-based design framework

Most process-product design problems are solved on an experimental-based trial and error procedure. While they provide validation of the process-product, they are time consuming, expensive and do not guarantee an optimal product or use of a wide search space. Validated models coupled to easy generation of models and flexible use of models for purposes of design, can eliminate some of the time and expenses in process-product development. As highlighted in Fig. 2.3 of the model-based design framework, a systematic procedure for the simultaneous process-product design is shown. The process models and the product models could be of different scales, that need to be solved simultaneously. It is thus important to have a framework that

gives a step wise procedure to solve different levels of interdependent models with relevant design algorithms together in a way that leads to a simultaneous process and product design with computational ease.

A design framework, including macro-scale process models and meso-/micro-scale models for properties of structured materials, has been developed and shown in Fig. 2.3. The model-based design framework divides the design procedure in subsets representing model generation, model validation and model application step in a systematic way. Various components of this design framework are explained in the subsections below.
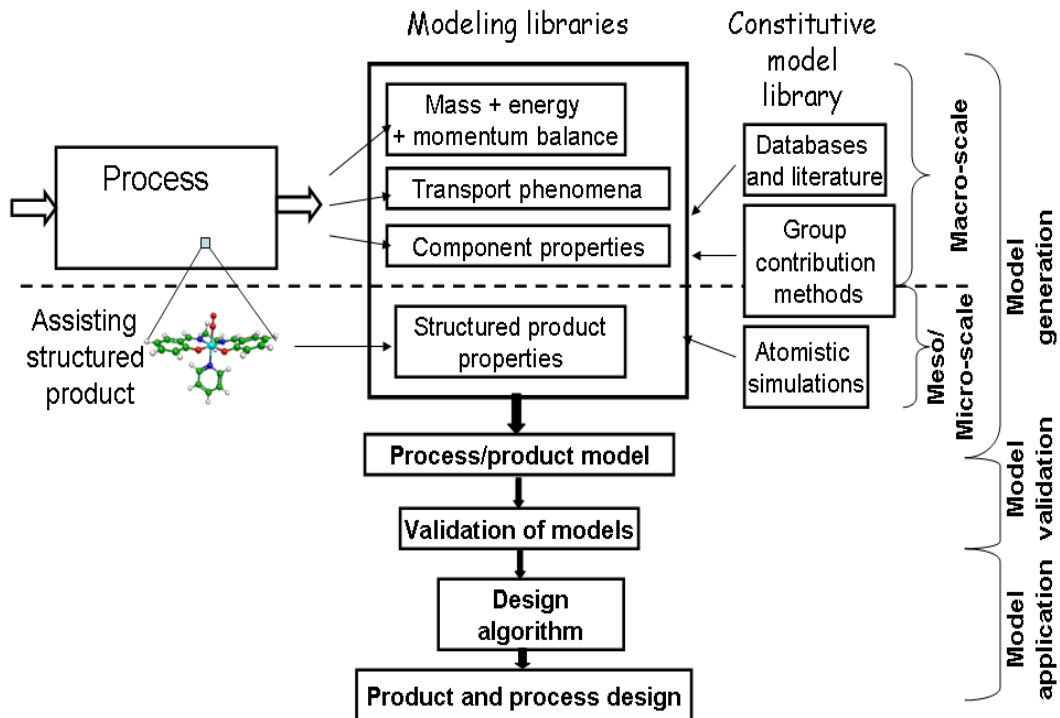
Figure 2.3: Architecture of a model-based design framework

2.3.2 Multilevel modeling

For a model-based product-process design procedure, it is required to develop or obtain a rigorous process model, that relates the raw material conditions, process conditions, component properties, flow behavior, transport phenomena, structured material properties, equipment geometry etc.. Process models may be considered to be composed of balance equations (mass, energy, momentum), constitutive equa-

tions and conditional equations (equilibrium, controller, defined relations) [99]. The constitutive models may include physical and chemical properties of the chemical species present in the system or phenomena models and their dependence on the process conditions. Another kind of constitutive models could be the property models for the structured materials giving the properties as a function of their structure. As mentioned in the section above, there is a need to integrate different levels of process and product models in one framework in order to perform simultaneous process-product design. For a process shown in Fig. 2.2, various equations, variables, constitutive models etc. are enumerated below:

- *Balance equations:* For a given boundary for a process, balance equations can be derived based on mass, energy and momentum conservation principals. For any given process (see Fig. 2.2), if state variables like temperature, pressure, composition etc. are defined by vector $\underline{Y}$, then the balance equations can in general be written as:

$$\frac{d\underline{Y}}{dz} = f\left(\underline{Y}, \underline{X}, \underline{\theta}, \underline{I}, \underline{M}, \underline{\xi}\right) \tag{2.1}$$

  s.t.

$$I.C. : \underline{Y}(z = 0) = \underline{Y}_0 \tag{2.2}$$

$$B.C. : \underline{Y}(z = z_{end}) = \underline{Y}_z \tag{2.3}$$

  Where, z is the independent variable, that could be time or space, vector $\underline{X}$ is the outlet variables, vector $\underline{\theta}$ is structured materials properties, vector $\underline{I}$ is inlet variables, vector $\underline{M}$ is variables related to geometry of the process unit and vector $\underline{\xi}$ is the chemical and physical properties of the various chemical species in the system. For the evaluation of the balance equations there is a need of evaluating different variables and integration of different scales of constitutive models. The balance equations give profiles of composition, temperature, pressure etc. with respect to time and/or space.

- *Control/definition equations:* These are normally conditional equations, for example, equilibrium, control or defined relations [99]. Another example of *control/definition* equations are the equations defining the performance criteria of the process like product recovery or concentration factor as compared to the feed, given in terms of the outlet variables. Since these conditions must be satisfied in order to obtain a "feasible" design.

$$\underline{P} = f\left(\underline{X}\right) \tag{2.4}$$

  The performance criteria $\underline{P}$, is usually a function of the outlet variables $\underline{X}$.

- *Constitutive equations 1: Component properties* From Eq. 2.1 it can be noted that the process model needs the evaluation of some chemical and physical properties of the chemical species (defined by $\underline{\xi}$) present in the system. These properties could be the density, viscosity, activity coefficients, specific heat,

38

molecular weight, vapor pressure etc.. $\underline{\xi}$ are generally a function of state variables $\underline{Y}$ and chemical formula $(\underline{c_f})$ [52]. And since these states change over time and/or space (see Eqn. 2.1), the property models should also be a function of state variables to see the change over the independent variable.

$$\underline{\xi} = f(\underline{Y}, \underline{c_f}) = f(T, P, \underline{x}, \underline{c_f}) \tag{2.5}$$

In this work, the pure component properties have been estimated using property models based on group contribution methods. In these models, the property of a compound is estimated as a summation of the contributions of the functional groups like $CH_3, CH_2, OH...$ etc., which can occur in the molecular structure [53, 98]. The general form of this kind of models is:

$$f\left(\underline{\xi}\right) = \sum_i N_i C_i \tag{2.6}$$

where, $f\left(\underline{\xi}\right)$ is a property function for the property $\underline{\xi}$ to be estimated, N_i is number of times the group G_i appears in the molecule, and C_i is the contribution of the group G_i to the property function $f\left(\underline{\xi}\right)$. In order to regress the contributions C_i to reliably predict the properties, it is required to have ample amount of experimental property data.

There are some newer group contribution techniques based on higher level of functional groups [25, 78]. Estimation is performed at three levels. The primary level uses contributions from simple first-order groups that allow describing a wide variety of organic compounds, while the higher levels involve poly-functional and structural groups that provide more information about molecular fragments whose description through first-order groups is not possible. The general form of these kind of models is [78]:

$$f\left(\underline{\xi}\right) = \sum_i N_i C_i + \omega \sum_j M_j D_j + z \sum_k O_k E_k \tag{2.7}$$

where, D_j the contribution of the second-order group of type-j that occurs M_j times and E_k the contribution of the third-order group of type-k that has O_k occurrences in a compound. A computational program called Pro-Pred [78] has been used in this work, that uses the contributions for these different levels of functional groups and predicts the properties of various chemical species.

Another property prediction method that can be used, is based on the valance connectivity indices $(^\nu\chi)$ described by [65]. This leads to a group contribution$^+$ (GC$^+$) method of wider application range than before because of the new groups that can be created through the regressed contributions of a set of zero-order and first-order connectivity indices [39].

Once the properties of different compounds are obtained at a particular set of process conditions, similar data can be obtained at various temperatures and pressures. These properties can then be regressed to have close form relation

like in Eqn. 2.5 to be easily used in process models. More details about these methods is presented in Chapter 4 under the section of property prediction.

- *Constitutive equations 2: Structured material property models* The process performance depends on some key properties of the structured materials defined by vector $\underline{\theta}$. These properties could be reaction rate constant or dissociation constant for reactive systems, driving force for distillation or liquid-liquid extraction etc., thermodynamic or kinetic properties for solution diffusion kind of separation, selectivity of solvents for solvent based separation, polymer structure like porosity, tortuosity for membrane based separation etc. The property parameters $\underline{\theta}$ in turn depend on variables $\underline{d}$, which could either be a function of the process variables $\underline{Y}$ or the function of microscopic structural parameters of the structured materials $\underline{S}$. This dependence of properties on structure or process variables is usually given by different *property models* of the general form:

$$\underline{\theta} = f\left(\underline{d}\right) \tag{2.8}$$

Three different calculation approaches have been used in this work to obtain properties $\underline{\theta}$ as a function of process variables or variables related to the structured materials (Eq. 2.8) are given below:

1. Extensive literature survey where property values are readily available for specific structured materials that could either be experimentally measured or predicted from empirical models. These kinds of models can only be used for materials listed in the databases.

2. Group contribution models, where variables $\underline{d}$ are the values of the weights of the groups that form the chemical formula of the structured material. This approach provides more freedom to choose the product composition and the ability to design the structured material with more versatility compared to a simple database search.

3. The properties, as mentioned earlier are intimately related to not only its chemical composition but also molecular conformation. For most structured materials, "true" and strategic experiments to predict the properties do not exist or could be very expensive and time- consuming. Theoretical and simulation advances along with the revolution in computational technology are now making it possible to address such design challenges of novel materials through advanced atomistic simulations.

   Once property data has been obtained using atomistic simulations for different structures and process conditions, closed-form models relating the properties with structures and architectures of the materials could be obtained by regression.

2.3.3 Solution approaches

For the simultaneous process product design, the widely used conventional used design algorithm is designated in this PhD-thesis as the forward solution approach.

Due to obvious limitations in the use of this solution approach such as being computationally expensive and iterative in nature, a new reverse design approach is proposed. The reverse solution approach (reverse algorithm) that splits the design procedure into two stages hence solving different scales of models separately, and thereby making the design procedure computationally simple and efficient. The two algorithms are compared with each other below.

The model has N equations where $N = N_N + N_P + N_{SM}$; (N_N process equations plus N_P performance equations and N_{SM} structural material property equations), with M variables (out of which, M_X are number of output variables, M_Y are number of process variables, M_I are number of input variables, M_θ are number of structural material property variables, M_M are number of process geometry variables and M_ξ are number of chemical species property variables). The degrees of freedom is $D_F = M - (N_N + N_{SM})$ which means that D_F variables out of M_X, M_Y, M_I, M_θ, M_M and M_ξ must be specified to solve the $N_N + N_{SM}$ model equations.

In the forward approach, M_X, M_Y, M_θ and M_ξ are calculated for given values of M_I and M_M. Using the calculated values of $\underline{X}$, the specified values of $\underline{P}$ are checked (through N_P equations). If they do not match, new sets of M_I and/or M_M are specified and the procedure is repeated.

In the reverse approach, from the specified values of $\underline{P}$, using N_P performance equations N_P number of outlet variables, say $\underline{X_{NP}}$ out of total $\underline{X}$ outlet variables, are calculated. This means that $M_{X_{NP}}$ variables (calculated from N_P equations) are no longer unknown variables in the original $N_N + N_{SM}$ equation set. So, for the original model, number of equations and variables have not changed but now $M_{X_{NP}}$ variables that were originally unknown have become known variables in the model. This means that since the number of unknown variables in the original model is the same, $M_{X_{NP}}$ number of variables from the set of structural property variables M_{SM} can now be the unknown variables in the new formulation of the same model. So, the same model can be solved to calculate the structured material property variables (giving values of the target property variables $\underline{\theta}$).

The common requirements for both the algorithms are the availability of process models, identification of the design variables, setting the performance criteria for the end-use products, identification of the key properties of the structured material and availability of the property models for the key properties. Once all of these have been obtained the design algorithms can be used.

2.3.3.1 Forward design algorithm

Forward design algorithm is diagrammatically shown in Fig. 2.4. Various steps of the algorithm are explained below.

Step I: For a given feed $\underline{I}$ and performance criteria $\underline{P}$, obtain the process model and identify the process design variables ($\underline{d_1}$), and the structured material design variable ($\underline{d_2}$).

Step II: Choose the process conditions ($\underline{d_1}$) and the structured material ($\underline{d_2}$) that could be used for this process. This fixes the design variables ($\underline{d_2}$) as the the structure of the structured material $\underline{S}$ is fixed through the selection of the material.

Step III: Calculate the properties of structured material ($\underline{\theta}$) using the property models embedded in the process model, where properties are a function of $\underline{S}$ and/or process conditions.

Step IV: Solve the process model to determine the values of the outlet variables $\underline{X}$.

Step V: Compare the calculated ($\underline{X}$) against the performance criterion ($\underline{P}$). If the criteria are satisfied, stop. Otherwise, repeat from **Step II**.

The new set could have different process conditions, different structure of the structured material or a completely different structured material. This procedure should be repeated until the desired performance criteria $\underline{P}$ is achieved.
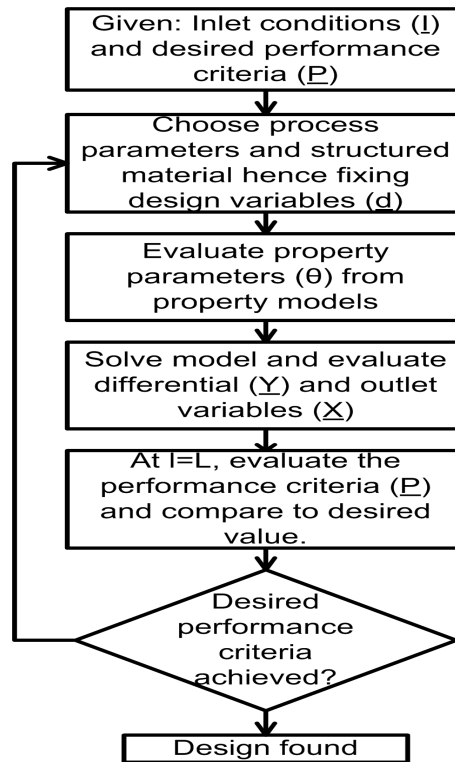
Figure 2.4: Forward design algorithm

2.3.3.2 Reverse design algorithm

In contrast to the forward approach, this work employs a (two design and one validation stage) reverse solution approach. In the first stage only the process model is solved while in the second stage the property models for the structured material are solved independently of the process models. Reverse design algorithm is diagram-

matically shown in Fig. 2.5. Various steps of the algorithm are explained below.

Stage A: Setting the targets

Step A-I: Similar to forward design algorithm, for a given feed $\underline{I}$ and performance criteria $\underline{P}$, the first step is to obtain the rigorous process model and identify the design variables.

Step A-II: Calculate the outlet variables ($\underline{X}$) using the values of the performance criteria ($\underline{P}$).

Step A-III: Calculate the target property values, defined by $\underline{\theta}_{target}$, with specified inlet and outlet variables.

Stage B: Obtaining the targets

Step B-IV: Use different property models to identify the structured materials matching the targets ($\underline{\theta}_{target}$) for the properties. In this stage, an extensive database search could also be made to identify the structured material with ($\underline{\theta}_{target}$) property values.

This procedure gives a set of options for the structured material and the best choice is made based on if the material is readily available or is a new material. At this point, it is also important to investigate if it is feasible to manufacture the structured material economically.

Stage C: Validating the design

Step C-V: Validate the different selection from **Step B-IV**, through rigorous simulations.

2.3.3.3 Comparison of algorithms

Forward design algorithm is essentially a trial and error procedure. For each proposed design in terms of process variables (process design) or variables related to the structured material (product design) the process model has to be solved iteratively. All the steps of the algorithm have to be repeated until one of the proposed designs matches the performance criteria. This could be quite cumbersome. While in the case of reverse design algorithm, the structured material property variables are unknown variables in the model. For a given feed and performance criteria, these variables are calculated from the model. So, there is no trial and error or iterations required saving the computational time and power.

With forward design approach, since the properties of the structured material chosen need to be evaluated during the solution of the process model, the constitutive model for these properties is embedded in the process-product model. It should be noted is that the constitutive model must be specified before the solution can be
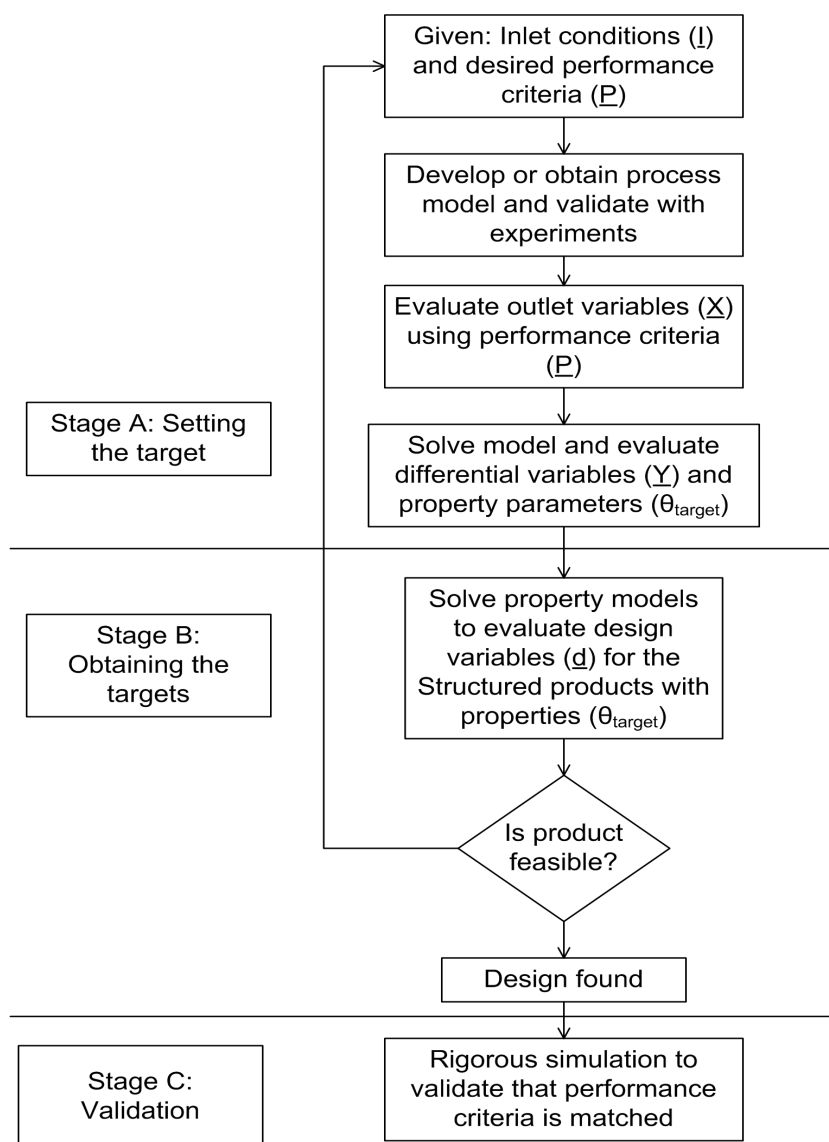
Figure 2.5: Reverse design algorithm

attempted. Therefore the design depends on the choice of this model. In contrast, reverse design algorithm is independent of the choice of the constitutive model. In the second stage of the algorithm, as many constitutive models as available can be used to predict the structure of the material having the target properties ($\underline{\theta}_{target}$), calculated in stage I.

Another disadvantage of having the property models embedded in the process model is that it may become computationally demanding to solve both models together. For instance, for pervaporation process the key property that affects the solution-diffusion mechanism is permeability. Its calculation generally needs diffusivity and solubility data, which for a given component/polymer system can be predicted by using a group contribution method. The above-mentioned calculations depend on the composition, temperature and pressure at each spatially discrete point of the membrane module. Consequently, incorporating them in the membrane model while possible, is not simple. On the other hand in the reverse design algorithm, many polymers may be designed (identified) without having to repeatedly solve the membrane process model coupled with the corresponding polymer property model .

2.3.4 Computational tools

Since the model-based design framework is also a computer based approach, a number of different computer aided tools are necessary. Note that the choice of the computational tools is specific to the design problem. For the simultaneous design of membrane based separation processes and polymers that can be used as membranes the computational tools used are given below.

ICAS-MoT: It is an equation-based modeling tool capable of handling steady-state simulations (models based on algebraic equations), lumped and/or dynamic system simulations (models based on differential algebraic equations), distributed systems simulation (models based on partial differential equations), steady-state optimization and dynamic parameter optimization [102]. It is a modeling test-bed for model translation, solution, analysis and validation of mathematical models. Most of the process models in this work were solved using ICAS-MoT.

Pro-Pred: It is a pure component property estimation tool [78] with an interface for drawing molecular structures and prediction of functional properties of pure components for a wide range of temperatures. This tool uses first or higher order group contribution methods for the property predictions [66], [25]. For the estimation of pure component properties for various components involved in the case studies, Pro-Pred was used.

TML: This tool is a Thermodynamic Model Library (TML) for predicting thermodynamic properties of mixtures. This tool is a part of a process simulator called ICAS [40]. For prediction of activity coefficients of compounds in liquid solution, TML was used.

LAMMPS: LAMMPS, which stands for Large-scale Atomic/Molecular Massively

Parallel Simulator is a molecular dynamics program [70]. LAMMPS has potentials for soft materials (biomolecules, polymers) and solid-state materials (metals, semiconductors) and coarse-grained systems. It can be used to model atoms or, more generically, as a parallel particle simulator at the meso-scale or continuum levels. LAMMPS runs on single-processor machines or in parallel using message-passing techniques and a spatial-decomposition of the simulation domain. The code is designed to be easy to modify or extend with new functionality. LAMMPS is distributed by Sandia National Laboratories, a US Department of Energy (DOE) laboratory. Extensive equilibration of trajectories for molecular modeling to predict permeability of different structures of polymers, was done with LAMMPS.

Materials Studio 4.0: Material Studio by Accelrys is a comprehensive suite for modeling and simulation solutions for studying chemicals and materials, including crystal structure and crystallization processes, polymer properties, catalysis, and structure-activity relationships. In this work it was used to predict the solubility and diffusivity of small gas molecules through polymers at different temperatures.

2.3.5 Validation of the process-product design and analysis

The process design and the design of the structured material obtained through the reverse design algorithm needs to be validated as a final check (even though matching of the target guarantees that the model equations are satisfied). This can be done through rigorous model (if available) or through experiment. This means that the investment on experiments is reserved for a small set of design alternatives within which the optimal can be found.

2.4 A Conceptual study

A conceptual study to demonstrate the use of the design algorithms is presented in this section. In this study, the model equations are solved using two different design algorithms and the differences in the solution steps are pointed out. The first step is to have the mathematical equations that constitute the process model. It is therefore important to define different kind of equations (eg. balance equations, constitutive equations, constraint equations etc.) and to define different kind of variables (eg. differential variables, design variables, known and unknown variables etc.). The model and variable analysis is very important in order to know the degrees of freedom and which equations needs to be manipulated, and how to do so in order to solve the models using either of the algorithms.

2.4.1 Design problem definition

For a given process, assisted by structured materials, the modeling goal is to find out the values of the design variables in the model that will satisfy certain performance criteria. The design variables can be related to either the process (process design) or the structured material (product design).

2.4.2 Model equations and characterizing variables

If $\underline{Y}$ represents the state variables that vary as a function of the dependent variable (time or space) within the process boundaries, then the balance equations can be derived from the laws of conservation of mass, momentum and energy. For the conceptual study, the balance equations are given in the form:

$$0 = C_1 \left(Y_1 \cdot A_1 + \theta_1 / X_2 \right) \tag{2.9}$$

$$0 = C_2 \left(Y_2 \cdot A_2 - \theta_2 \cdot X_1 \right) \tag{2.10}$$

$$0 = C_1 \cdot X_2 + \theta_1 \cdot Y_3 - A_1 \tag{2.11}$$

Assuming steady state left hand side (LHS) of Eq. 2.9 to 2.11 is set to zero. $\underline{X}$ and $\underline{A}$ are vectors of constitutive variables that needs to be evaluated for every evaluation of the RHS of Eqn. 2.9- 2.11 and $\underline{C}$ is a vector of known parameters.

The constitutive equations for variables $\underline{X}$ and $\underline{A}$ for this conceptual study are given as:

$$A_1 = \theta_1 \cdot X_1 + Y_1 \cdot X_2^2 \tag{2.12}$$

$$A_2 = \theta_2 / X_2 + Y_2 X_1^2 \tag{2.13}$$

$$X_1 = \frac{A_1 \cdot Y_1 \cdot t}{A_1 + A_2} \tag{2.14}$$

$$X_2 = (A_2 + Y_2)/t \tag{2.15}$$

where, $\underline{\theta}$ is the vector of properties of the assisting structured material ans t is the residence time. A set of constitutive equations to evaluate the properties ($\underline{\theta}$) is required. θ_1 and θ_2 are functions of the design variables Z_1 and Z_2 and the state variables. Therefore, the properties θ_1 and θ_2 can be calculated using the constitutive equations given below:

$$\theta_1 = \frac{Z_1 Z_2 Y_1}{Z_1 + Z_2} \tag{2.16}$$

$$\theta_2 = \frac{Z_1^2 + Z_2^2}{Y_2} \tag{2.17}$$

If θ_1 and θ_2 are the property values then the design variables Z_1 and Z_2 affecting the property values could be macroscopic (eg. state variables like temperature or pressure), mesoscopic (eg. chemical composition of the species) or microscopic (eg. microscopic structural parameters like orientation or alignment of certain functional groups etc.) in nature.

In the model shown above, X_1 and X_2 are the desired output (unknown) variables. The constraint equations would give the optimal/desired values of X_1 and X_2 that need to be satisfied. These values could come from market demands for the end use products and/or if these are intermediate products with certain properties or values.

$$P - P_1(\underline{X}, \underline{P}) = 0 \tag{2.18}$$

$$P - P_2(\underline{X}, \underline{P}) = 0 \tag{2.19}$$

Eq. 2.9 to 2.19 represents the model. The variables in this model are defined in Table 2.1.

Variable	Type
Y_1 and Y_2	Dependent (differential or state) variables
Z_1 and Z_2	Design Variables
θ_1 and θ_2	Property parameters
X_1 and X_2	Desired output variables (unknown)
P_1 and P_2	Performance criteria
C_1 and C_2	Known parameters

Table 2.1: Variables definition

Here, X_1 and X_2 are indirectly dependent on the design variables Z_1 and Z_2. So, the idea is to find out the values of the design variables Z_1 and Z_2 that will give the "target" or "desired" values of X_1 and X_2 that will satisfy the constraints (Eq. 2.18 and 2.19).

2.4.3   Solution approaches

2.4.3.1   Forward design algorithm

Step 1: Assume values of design variables Z_1 and Z_2.

Step 2: Evaluate property parameters θ_1 and θ_2 using Eq. 2.16 and 2.17 respectively.

Step3: Solve model equations 2.9 to 2.17 for Y_1, Y_2, Y_3, A_1, A_2, θ_1, θ_2, X_1 and X_2 with Z_1 and Z_2 as known variables (guessed).

Step4: Check if Eq. 2.18 and 2.19 are satisfied. If yes, stop. Otherwise assume different values of Z_1 and Z_2 and repeat from Step 2. This stepwise procedure is shown in Fig. 2.6.

2.4.3.2   Reverse design algorithm

Step 1: Use known values of P_1 and P_2 and Eq. 2.18 and 2.19 to calculate X_1 and X_2.
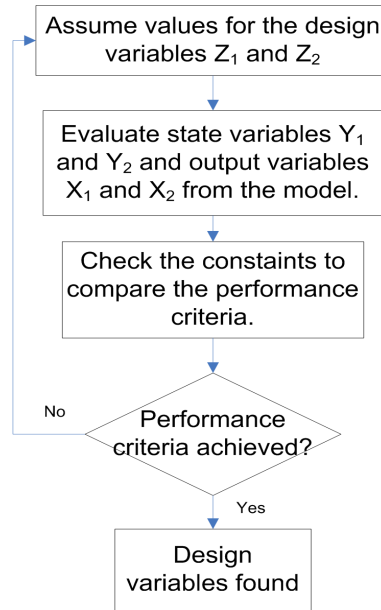
Figure 2.6: Forward design approach - conceptual study

Step 2: Divide the model in two subsets, Eq. 2.9 to 2.15 in one subset and Eq. 2.16 to 2.17 in another subset.

Step 3: Solve equations Eq. 2.9 to 2.15 for Y_1, Y_2, Y_3, A_1, A_2, θ_1 and θ_2 for known X_1 and X_2.

Step 4: Use calculated θ_1 and θ_2 to find out Z_1 and Z_2 from Eq. 2.16 and 2.17.

Note that there is no need to iterate if a consistent set of $\underline{P}$ was specified. This stepwise procedure is shown in Fig. 2.7.
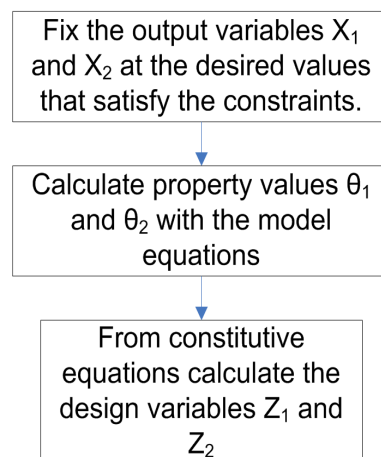
Figure 2.7: Reverse design approach - conceptual study

With this conceptual case-study, it can be highlighted that disintegrating the model equations to solve the property models not only does avoid the iterative

trial and error approach but also makes the solution of equations computationally easier.

2.5 Discussion/Conclusion

In this chapter, a general design framework for simultaneous design of process and product has been presented. Components of this framework include multilevel models for process and structured materials, design algorithms, computational tools, databases etc.. It has been conceptually shown that the reverse design algorithm is superior to the forward design algorithm when it comes to the simultaneous product and process design. For the success of both the design framework and design algorithms, it is however important to have very good process models and product models. For membrane based separation processes all relevant models required for the design framework are presented in the next chapter.

3

Molecular modeling - theoretical background

3.1   Molecular modeling

Computer based experiments play a very important role in science today. The advent of high speed computers, which started to be used in the 1950s, have brought a new element in between experiment and theory: the computer based experiment. In a computer based experiment, a model is provided by theory (or an approximation of it) and the calculations are carried out by the computer by following an algorithm, implemented in a suitable programming language. In this way, varying degrees of complexity can be introduced and many more systems can be investigated, leading to a better understanding of the reality.

Molecular modeling is a collective term that refers to theoretical methods and computational techniques to model or mimic the behavior of molecules. The techniques are used in the fields of computational chemistry, computational biology and materials science for studying molecular systems ranging from small chemical systems to large biological molecules and material assemblies. The simplest calculations can be performed by hand, but inevitably computers are required to perform molecular modeling of any reasonably sized system. The common feature of molecular modeling techniques is the atomistic level description of the molecular systems; the lowest level of information is individual atoms (or a small group of atoms). This is in contrast to quantum chemistry (also known as electronic structure calculations) where electrons are considered explicitly. The benefit of molecular modeling is that it reduces the complexity of the system, allowing many more particles (atoms) to be considered during simulations.

The two main families of molecular modeling are molecular dynamics (MD) and Monte Carlo (MC) simulations. There is also a whole range of hybrid techniques which combine features from both. In this work, however, MD has been used for extensive equilibration of the polymeric systems. The obvious advantage of MD over MC is that it gives a route to dynamical properties of the system, such as, transport coefficients, time-dependent responses to perturbations, rheological properties and spectra.

Molecular models have been employed to formulate detailed descriptions of the mechanisms of gas transport in polymers [90, 46, 108]. These models attempt to analyze specific motions of penetrant molecules and surrounding polymer chains relative to

each other and take into consideration the pertinent intermolecular forces. Recent advances in the computer simulation of polymer microstructures and the greatly increased capability of computers should make possible the formulation of much more realistic molecular models of gas transport through polymers.

Part of this work involves predicting barrier properties of polymers employing molecular modeling. The steps that are employed to predict these properties include extensive equilibration of the polymer matrix using an MD simulation, followed by diffusivity of small gases by brute-force MD simulations and predicting solubility of small gas molecules in polymers by MC simulations. So, in this chapter an introduction to both MD and MC method and to important aspects of these two methods is presented.

3.2 Molecular Dynamics simulations

Molecular dynamics (MD) is a computer simulation technique where the time evolution of a set of interacting atoms is followed by integrating their equations of motion. Molecular dynamics simulations generate information at the microscopic level, including atomic positions and velocities [36]. The mechanical or microscopic state of a system is defined by the atomic positions, q, and momenta, p; these can also be considered as coordinates in a multidimensional space called phase space [96]. For a system of N particles, this space has $6N$ dimensions. A single point in phase space, describes the state of the system. An ensemble is a collection of such points in phase space satisfying the conditions of a particular thermodynamic state. A molecular dynamics simulations generates a sequence of points in phase space as a function of time. These points belong to the same ensemble, and they correspond to the different conformations of the system and their respective momenta. This microscopic information is converted to macroscopic observables such as pressure, energy, heat capacities, etc., usually by statistical mechanics. Statistical mechanics is fundamental to the study of polymeric systems by molecular dynamics simulation. The connection between microscopic simulations and macroscopic properties is made via statistical mechanics which provides the rigorous mathematical expressions that relate macroscopic properties to the distribution and motion of the atoms and molecules of the N-body system; molecular dynamics simulations provide the means to solve the equation of motion of the particles and evaluate these mathematical formulas. With molecular dynamics simulations, one can study both thermodynamic properties and/or time dependent (kinetic) phenomenon [3].

3.2.1 Calculating Averages from a Molecular Dynamics Simulation

An experiment is usually made on a macroscopic sample that contains an extremely large number of atoms or molecules sampling an enormous number of conformations. In statistical mechanics, averages corresponding to experimental observables

are defined in terms of ensemble averages [36]. One justification for this is that there has been good agreement with experiment. An ensemble average is average taken over a large number of replicas of the system considered simultaneously. In statistical mechanics, average values are defined as ensemble averages.

If $A(p^N, r^N)$ is any observable quantity of interest and it is expressed as a function of the momenta, p, and the positions, r, of the system. The integration is over all possible values of r and p. The ensemble average is then given by [36]:

$$\langle A \rangle_{ensemble} = \int \int dp^N dr^N A(p^N, r^N) \rho(p^N, r^N) \tag{3.1}$$

The probability density function of the ensemble is given by:

$$\rho(p^N, r^N) = \frac{1}{Q} exp \left[-H(p^N, r^N)/k_B T \right] \tag{3.2}$$

where H is the Hamiltonian, T is the temperature, k_B is Boltzmanns constant and Q is the partition function, given as [36]:

$$Q = \int \int dp^N dr^N exp \left[-H(p^N, r^N)/k_B T \right] \tag{3.3}$$

This integral is generally extremely difficult to calculate because one must calculate all possible states of the system. In a molecular dynamics simulation, the points in the ensemble are calculated sequentially in time, so to calculate an ensemble average, the molecular dynamics simulations must pass through all possible states corresponding to the particular thermodynamic constraints.

Another way, as done in an MD simulation, is to determine a time average of A, which is expressed as [96, 36]:

$$\langle A \rangle_{time} = \lim_{t \to \infty} \frac{1}{\tau} \int_{t=0}^{\tau} A(p^N(t), r^N(t)) dt \approx \frac{1}{M} \sum_{t=1}^{M} A(p^N, r^N) \tag{3.4}$$

where t is the simulation time, M is the number of time steps in the simulation and $A(p^N, r^N)$ is the instantaneous value of A.

The dilemma appears to be that one can calculate time averages by molecular dynamics simulation, but the experimental observables are assumed to be ensemble averages. Resolving this leads us to one of the most fundamental axioms of statistical mechanics, the ergodic hypothesis, which states that the time average equals the ensemble average. The Ergodic hypothesis states [96, 36, 3]:

$$\langle A \rangle_{ensemble} = \langle A \rangle_{time} \tag{3.5}$$

The basic idea is that if one allows the system to evolve in time indefinitely, that system will eventually pass through all possible states. One goal, therefore, of a molecular dynamics simulation is to generate enough representative conformations such that this equality is satisfied. If this is the case, experimentally relevant information concerning structural, dynamic and thermodynamic properties may then be calculated using a feasible amount of computer resources. Because the simulations are of fixed duration, one must be certain to sample a sufficient amount of phase space.

3.2.2 Ensembles

An ensemble is a collection of all possible systems which have different microscopic states but have an identical macroscopic or thermodynamic state. There exist different ensembles with different characteristics. Most commonly used ensembles are [112]:

- Microcanonical ensemble (NVE) : In the microcanonical, or NVE ensemble, the system is isolated from changes in moles (N), volume (V) and energy (E). It corresponds to an adiabatic process with no heat exchange. A microcanonical molecular dynamics trajectory may be seen as an exchange of potential and kinetic energy, with total energy being conserved.

- Canonical Ensemble (NVT): In the canonical ensemble, moles (N), volume (V) and temperature (T) are conserved. It is also sometimes called constant temperature molecular dynamics (CTMD). In NVT, the energy of endothermic and exothermic processes is exchanged with a thermostat.

  A variety of thermostat methods are available to add and remove energy from the boundaries of an MD system in a realistic way, approximating the canonical ensemble. Popular techniques to control temperature include the Nose-Hoover thermostat and Langevin dynamics.

- Isobaric-Isothermal Ensemble (NPT): In the isothermal-isobaric ensemble, moles (N), pressure (P) and temperature (T) are conserved. In addition to a thermostat, a barostat is needed. It corresponds most closely to laboratory conditions with a flask open to ambient temperature and pressure.

- Grand canonical Ensemble (μVT): The thermodynamic state for this ensemble is characterized by a fixed chemical potential, μ, a fixed volume, V, and a fixed temperature, T.

3.2.3 Classical mechanics formulation

There exists three different formulations of the classical equations of motion. They all lead to exactly the same motions of the particles in the system but one form may be more convenient to use than another, dependent on both the system and properties studied. The different formulations are Vectorial, Lagrangian and Hamiltonian formulations [36]. Here only the well known vectorial formulation is described.

Molecular dynamics simulation consists of the numerical time evolution of a set of interacting atoms followed by solution of the classical equations of motion, which for a simple atomic system may be written as [96]

$$F_i = m_i a_i \tag{3.6}$$

for each atom i in a system constituted by N atoms. Here, m_i is the atom mass, $a_i = d^2 r_i / dt^2$ its acceleration, and F_i the force acting upon it, due to the interactions with other atoms. Therefore, in contrast with the Monte Carlo method, molecular dynamics is a deterministic technique: given an initial set of positions and velocities, the subsequent time evolution is in principle completely determined.

3.2.4 Molecular dynamics algorithms

The potential energy is a function of the atomic positions (3N) of all the atoms in the system. Due to the complicated nature of this function, there is no analytical solution to the equations of motion; they must be solved numerically. Numerous numerical algorithms have been developed for integrating the equations of motion. In this work, Velocity Verlet algorithm is used. This algorithm can also be implemented directly for the NVE and NVT ensembles without an iterative procedure. For the other ensembles, an iterative procedure is required.

Assuming that the set of initial conditions, that is coordinates and velocities at time t, $x_i(t)$ and $\dot{x}_i(t)$ are known. Then these initial values can be used to calculate the accelerations at the same time $\ddot{x}_i(x_i(t), \dot{x}_i(t))$. The velocity Verlet integration scheme, is then given by [96, 3]:

$$x_i(t + \delta t) = x_i(t) + \dot{x}_i(t)\delta t + \frac{1}{2}\ddot{x}_i(t)\delta t^2 + O(\delta t^3) \qquad (3.7)$$

$$\dot{x}_i(t + \delta t) = \dot{x}_i(t) + \frac{1}{2}\left[\ddot{x}_i(t)(t + \delta t) + \ddot{x}_i(t)\right] + O(\delta t^3) \qquad (3.8)$$

The coordinates are advanced using the first relation (Eq. 3.7). The problem then is, that the accelerations at t + δt depend on the velocities at the same time, such that the second relation (Eq. 3.8) can not be used directly to advance the velocities. One needs to predict these velocities with an extra expression [96, 3].

$$\dot{x}_i^P(t + \delta t) = \dot{x}_i(t + \delta t) + 2\ddot{x}_i(t)\delta t + O(\delta t^3) \qquad (3.9)$$

to predict the velocity at t + δt. This expression predicts the velocity to the same order as the velocity in the second relation (Eq. 3.8). The predicted velocities $\dot{x}^P(t + \delta t)$ are used to determine the acceleration at t + δt [96, 3]:

$$\ddot{x}_i(t + \delta t) = \ddot{x}_i\left(x_i(t + \delta t), \dot{x}_i^P(t + \delta t)\right) \qquad (3.10)$$

and the advanced velocities are calculated from the second relation (Eq. 3.8). If different from the predicted velocities, the new velocities may be used in a new determination of $\ddot{x}_i(t + \delta t)$ and a subsequent new determination of the advanced velocities until convergence. It should be fast, since the predicted velocities are determined to the same order in δt as the final velocities.

3.2.5 Potentials and forces

To integrate the equation of motion Eq. 3.6, it is required to calculate the forces F_i acting on the atoms, and these are usually derived from a potential energy $U(r^N)$, where $r^N = (r1; r2; ...r^N)$ represents the complete set of $3N$ atomic coordinates. The computer calculates a trajectory in a $6N$-dimensional phase space ($3N$ positions and $3N$ momenta). The main ingredient of a simulation is a model for the physical system. For a molecular dynamics simulation this amounts to choosing the potential which is essentially a function $V(r_1, r_2..., r_N)$ of the positions of the

nuclei, representing the potential energy of the system when the atoms are arranged in that specific configuration [36]. This function is translationally and rotationally invariant, and is usually constructed from the relative positions of the atoms with respect to each other, rather than from the absolute positions.

Forces are then derived as the gradients of the potential with respect to atomic displacements:

$$F_i = -\nabla_{r_i} V\left(r_1, r_2 ..., r_N\right) \tag{3.11}$$

This form implies the presence of a conservation law of the total energy $E = K + V$, where K is the instantaneous kinetic energy.

The simplest choice for V is to write it as a sum of pairwise interactions [36]:

$$V\left(r_1, r_2 ..., r_N\right) = \sum_i \sum_{j>i} \phi\left(|r_i - r_j|\right) \tag{3.12}$$

The clause $j > i$ in the second summation has the purpose of considering each atom pair only once.

Non-bonded interactions

The part of the potential energy $U_{non-bonded}$ representing non-bonded interactions between atoms is traditionally split into 1-body, 2-body, 3-body . . . terms [2]:

$$U_{non-bonded}\left(r^N\right) = \sum_i u\left(r_i\right) + \sum_i \sum_{j>i} v\left(r_i, r_j\right) \tag{3.13}$$

The $u(r)$ term represents an externally applied potential field or the effects of the container walls (it is usually dropped for fully periodic simulations of bulk systems). Also, it is usual to concentrate on the pair potential $v(r_i; r_j) = v(r_{ij})$ and neglect three-body (and higher order) interactions. There is an extensive literature on the way these potentials are determined experimentally, or modeled theoretically [2].

The Lennard-Jones potential is the most commonly used form:

$$v^{LJ}(r) = 4\epsilon\left[\left(\frac{\sigma}{r}\right)^{12} - \left(\frac{\sigma}{r}\right)^6\right] \tag{3.14}$$

with two parameters, σ the diameter, and ϵ the well depth. For applications in which attractive interactions are of less concern than the excluded volume effects which dictate molecular packing, the potential may be truncated at the position of its minimum, and shifted upwards to give what is usually termed the WCA model [117]. If electrostatic charges are present, appropriate Coulomb potentials are added:

$$v^{Coulomb}(r) = \frac{Q_1 Q_2}{4\pi\epsilon_0 r} \tag{3.15}$$

where Q_1, Q_2 are the charges and ϵ_0 is the permittivity of free space. The correct handling of long-range forces in a simulation is an essential aspect of polyelectrolyte simulations.

Intramolecular bonded interactions

For molecules the intramolecular bonding interactions must also be considered. The simplest molecular model will include terms with 2-body, 3-body and 4-body interactions. 2-body interaction are also called *bond stretching potential*. The simplest of all is called Harmonic bond stretching portential given as [2]:

$$U_r = \frac{1}{2} \sum_{bonds} k_{ij}^r \left(r_{ij} - r_{eq} \right)^2 \tag{3.16}$$

Fig. 3.1 illustrates the geometry of a simple chain molecule. The bonds will typically involve the separation $r_{ij} = |r_i - r_j|$ between adjacent pairs of atoms in a molecular framework.
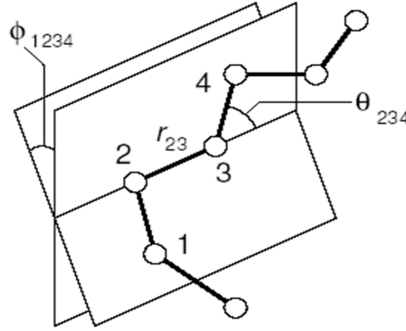
Figure 3.1: Geometry of a simple chain molecule, illustrating the definition of interatomic distance r_{23}, bend angle θ_{234}, and torsion angle ϕ_{1234}.

The bend angles θ_{ijk} are between successive bond vectors such as $r_i - r_j$ and $r_j - r_k$ and therefore involve three atom coordinates [2]:

$$cos\theta_{ijk} = \hat{r}_{ij} \cdot \hat{r}_{jk} = \left(r_{ij} \cdot r_{ij} \right)^{-1/2} \left(r_{jk} \cdot r_{jk} \right)^{-1/2} \left(r_{ij} \cdot r_{jk} \right) \tag{3.17}$$

Usually this bending term is taken to be quadratic in the angular displacement from the equilibrium value. As shown in the harmonic bend angle potential is given as [2]:

$$U_\theta = \frac{1}{2} \sum_{bend\ angles} k_{ijk}^\theta \left(\theta_{ijk} - \theta_{eq} \right)^2 \tag{3.18}$$

The torsion angles ϕ_{ijkl} are defined in terms of three connected bonds, hence four atomic coordinates:

$$cos\phi_{ijkl} = -\hat{n}_{i}jk \cdot \hat{n}_{j}kl, \ where \ n_{ijk} = r_{ij} \times r_{jk}, \ n_{jkl} = r_{jk} \times r_{kl} \tag{3.19}$$

where, $\hat{n}$ is the unit normal to the plane defined by each pair of bonds. Usually the torsional potential involves an expansion in periodic functions of order m = 1,2,... as seen in the potential function for torsional potential given below [2]:

$$U_\phi = \frac{1}{2} \sum_{torsion\ angles} \sum_m k_{ijkl}^{\phi,m} \left(1 + cos(m\phi_{ijkl} - \gamma_m)\right) \qquad (3.20)$$

It is important at this point to define the so called "united-atom" and "all-atom" description of the force field model. A united-atom is a particle that incorporates a group of atoms but can approximately represent the molecular mechanical properties of the group on a scale of size that is larger than atomic scale. It is also called pseudo-atom.

The united-atom model is a good approximation to simulate molecular systems in which the intermolecular motion is much more important than the intramolecular motion, or the intramolecular motion is much less significant than the intermolecular motion [16, 93]. For example, in many materials that are composed of stable chemical compounds (i.e. they do not react with each other to form new compounds or break into smaller units), the way how these molecules interact as whole groups with each other often determines the physical and chemical properties of the bulk materials. These potentials are typically less accurate and less transferable than the all-atom potentials, but significantly less expensive. While an all-atom force field is usually very accurate in predictions but is computationally extremely expensive. In this work, both the approaches have been used. United-atom approach is used for the initial extensive equilibration of the system and all-atom approach is used to predict diffusion coefficients and solubility of small gases in the polymer matrix.

3.3   Monte Carlo simulations

Monte Carlo methods are a widely used class of computational algorithms for simulating the behavior of various physical and mathematical systems, and for other computations. They are distinguished from other simulation methods (such as molecular dynamics) by being stochastic, that is nondeterministic in some manner (usually by using random numbers) as opposed to deterministic algorithms.

Monte Carlo molecular modeling is the application of Monte Carlo methods to molecular problems. These problems can also be modeled by the molecular dynamics method. The difference is that this approach relies on statistical mechanics rather than molecular dynamics. Instead of trying to reproduce the dynamics of a system, it generates states according to appropriate Boltzmann probabilities [36]. In mathematics, a Markov chain, named after Andrey Markov, is a discrete-time stochastic process with the Markov property. Having the Markov property means the next state solely depends on the present state and does not directly depend on the previous states. So, MC modeling employs a Markov chain procedure in order to determine a new state for a system from a previous one [3]. According to its stochastic nature, this new state is accepted at random. Each trial usually

counts as a move. The avoidance of dynamics restricts the method to studies of static quantities only, but the freedom to choose moves makes the method very flexible.

There are biased and unbiased Monte Carlo algorithms, in this work however, Metropolis Monte Carlo method is used. This method is simple and mostly applicable. To describe a Metrolopis Monte Carlo method, it is first necessary to describe some notation. The system is initially in a configuration r^N, which is denoted by o (old), which has a non-vanishing Boltzmann factor $exp[-\beta U(o)]$, where β is the Boltzmann factor and U is the energy of the system. A new trial configuration can generated r'^N, denoted by n (new), by adding a small random displacement Δ to o. The Boltzmann factor of this trial configuration is $exp[-\beta U(n)]$.

The algorithm should now decide whether the trial configuration be accepted or rejected. On an average the probability of finding the system in a configuration n is proportional to the probability density $N(n)$. The probably density may be defined as [36]:

$$N(n) = \frac{exp[-\beta U(n)]}{\int dr^N exp[-\beta U(n)]} \tag{3.21}$$

If the probability of accepting a trial move from o to n is $acc(o \rightarrow n)$, then [36]:

$$N(o) \times acc(o \rightarrow n) = N(n) \tag{3.22}$$

From the above two equations, it follows:

$$\frac{\times acc(o \rightarrow n)}{\times acc(n \rightarrow o)} = \frac{N(n)}{N(o)} = exp[-\beta U(n) - U(o)] \tag{3.23}$$

Suppose that a trial move from state o to state n have been generated, with $U(n) \, U(o)$. According to Eq. 3.23 this trial move should be accepted with a probability

$$acc(o \rightarrow n) = exp-\beta[U(n) - U(o)] < 1 \tag{3.24}$$

In order to decide whether to accept or reject the trial move, a random number is generated, denoted by R, from a uniform distribution in the interval $[0, 1]$. The probability that R is less than $acc(o \rightarrow n)$ is equal to $acc(o \rightarrow n)$. The trial move is accepted if $R < acc(o \rightarrow n)$ and reject it otherwise. This rule guarantees that the probability to accept a trial move from o to n is indeed equal to $acc(o \rightarrow n)$ [36]. Obviously, it is very important that the random-number generator does indeed generate numbers uniformly in the interval $[0, 1]$.

So, here Metropolis method is introduces as a Markov process in which random walk is constructed in such a way that the probability of visiting a particular point r^N is proportional to the Boltzmann factor $exp[-\beta U(r^N)]$. There are many ways to construct such a random walk. In the approach introduced by Metropolis et al. (1953) and quoted by Frenkel and Smit (2002) [36], the following scheme is proposed:

1. Select a particle at random, and calculate its energy $U(r^N)$.

2. Give the particle a random displacement, $r' = r + \Delta$, and calculate its new energy $U(r'^N)$.

3. Accept the move from r^N to r'^N with probability

$$acc(o \rightarrow n) = min\left(1, exp-\beta[U(r'^N) - U(r^N)]\right) \qquad (3.25)$$

Monte Carlo algorithm is mainly used for the solubility calculations of small gas molecules in polymer matrix. This is explained in the next section.

3.4 Barrier properties

This section presents the prediction of permeability of small gases in polymers. Mathematically, defining the permeability of a polymer to a small molecule gas amounts to calculating the product of diffusivity and solubility of the gas in the polymer. While for diffusivity calculation, MD simulations are used, for solubility calculation MC simulation is employed.

3.4.1 Diffusivity of small gases in polymer matrix

Solubilities and diffusivities are governed by the penetrant properties such as size, interactions with the polymer and by the shape, size, connectivity, and time scales of thermal rearrangement of unoccupied space (free volume) within the polymer. The mechanism of a gas diffusing in a polymer matrix is explained as a "hopping mechanism". At temperatures well above the glass transition temperature of the polymer Tg, polymer matrix undergoes fast thermal motions. The small gas molecules (penetrants) reside in the accessible cavities and due to fast thermal motions of the polymer matrix, a micro-channel appears, joining another cavity and hence permitting the gas molecule to hop from one cavity to another resulting in an effective motion. Hence, the penetrant diffuses through large succession of small local moves. Diffusion of small molecules in polymer melts using MD simulation is most frequently calculated by means of the Einstein relationship given as [60, 96]:

$$D_\alpha = \frac{1}{6N_\alpha} \lim_{t \to \infty} \frac{d}{dt} \sum_{i=1}^{N_\alpha} \left\langle [r_i(t) - r_i(0)]^2 \right\rangle \qquad (3.26)$$

where, r_i denotes the position vector of center of mass of species α, and angular brackets denote averaging over all choices of time origin within a dynamic trajectory. From an MD run, long enough to ensure that the system has reached the normal diffusive regime (when slope of the log of mean square displacement (MSD) as a function of log(t) is close to unity), a few well equilibrated and uncorrelated trajectories are extracted. The mean-square displacement (MSD) averaged over number of atoms ($N\alpha$) is plotted against time. A plot of the mean square displacement as a function of time should give a straight line, if the molecular motion is described by the diffusion equations, and the diffusion coefficient may be determined from the

slope of the line [57]. This expression is usually easier to use in practice than the velocity time correlation function expression.

Charati et.al.(1998) [21] have found that a penetrant molecule must travel a distance of at least one unit cell (20 Å) in a microstructure in order to pass from "anomalous" to "normal" (Einstein) diffusion. The time required by a penetrant molecule to travel such a distance increases with an increase in the rigidity of the polymer, i.e., with a decrease in its intra-segmental mobility, as reflected by a rise in the glass transition temperature, Tg, of the polymer. Hence, the time necessary for the simulation of normal diffusive motion of a given penetrant molecule in a polymer also increases with an increase in the Tg of the polymer.

3.4.2 Solubility of small gases in polymer matrix

A series of fixed pressure simulations are used to plot the pressure vs. average loading curve to predict the solubility of small gases in a polymer matrix. In a fixed pressure simulation, the configurations are sampled from a grand canonical ensemble. In the grand canonical ensemble, the fugacities of all components, as well as the temperature, are fixed as if the framework was in open contact with an infinite sorbate reservoir with a fixed temperature.

The probability of a configuration, n, in the grand canonical ensemble is given by [121]

$$\rho_n = CF(N_n)exp[-\beta U(n)] \tag{3.27}$$

where, where C is an arbitrary normalization constant, $\beta = 1/k_B T$ is the reciprocal temperature, and $U(n)$ is the total energy of configuration n. The set of sorbate loadings of all components in configuration m is denoted by N_n. For a single component, the function F(N) is given by [121]:

$$F(N) = \left(\frac{(\beta\phi V)^N}{N!}\right) exp\left[-\beta N\mu_{intra}\right] \tag{3.28}$$

where ϕ is the fugacity, μ_{intra} is the intramolecular chemical potential, and N is the loading of the component. For a mixture of components, $F(N_n)$ factorizes to a product of functions (Eq. 3.27) for each component.

The total energy of a configuration, $U(n)$, is given by [1]:

$$U_n = U_{n,SS} + U_{n,SF} + U_{n,S} \tag{3.29}$$

where, $U_{n,SS}$ is the intermolecular energy between the sorbates molecules, $U_{n,SF}$ is the interaction energy between the sorbates molecules and the framework, and $U_{n,S}$ is the total intramolecular energy of the sorbates molecules.

Metropolis method described before is employed here to generate a chain of configurations with the ensemble density. Different step types provided by Metropolis Monte Carlo method are [1]:

- *Conformer:* The conformation of the selected sorbate is replaced with a randomly chosen conformation from the trajectory for that species. The new conformer is given the position and orientation of the old conformer. If a trajectory of conformations has not been supplied for the selected sorbate component (or the trajectory document contains only one frame) a conformer swap will not be attempted.

- *Rotation:* The selected sorbate is rotated about its center of geometry by an angle of $\delta\theta$ about an axis, A. The rotation $\delta\theta$ is drawn from a uniform distribution between $-\Delta r$ and Δr, where r is the maximum rotation amplitude as specified at the start of the Sorption run. The axis A is the vector from a random point on a sphere to its origin.

- *Translation:* The selected sorbate is translated by a distance of δr along an axis, A. The translation r is drawn from a uniform distribution between $\Delta_{t'}$ and Δt, where t is the maximum translation amplitude as specified at the start of the Sorption run. The axis A is the vector from a random point on a sphere to its origin.

- *Creation:* The center of geometry of a sorbate of a randomly selected component is inserted at a random position within the framework. The sorbate is rotated about the center of geometry by an angle of $\delta\theta$ along an axis, A. The rotation $\delta\theta$ is drawn from a uniform distribution between -180 and $+180^o$. The axis is the vector from a random point on a sphere to its origin.

- *Deletion:* A sorbate of a randomly selected component is deleted from the framework.

Each step of the Sorption run starts with the selection of a step type using the weights set at the start of the Sorption run. This could be a sorbate exchange with the reservoir or a translation, rotation, or torsion change of an existing sorbate etc.. After a step type is selected, a random component is chosen and the step type is applied to a random sorbate of that component. The Monte Carlo method is then used to decide whether to accept or reject the change. After a large number of steps, the average loading, N, is evaluated in the grand canonical ensemble, for that pressure [1]. Similar runs are made at different pressures, and then the average loading is plotted against pressure. The slope of this plot then gives the Henry's constant, inverse of which gives the solubility of the sorbate in the polymer matrix.

3.5 Discussion/Conclusion

This chapter briefly introduces the molecular modeling methods and concepts. Both Molecular dynamics and Monte Carlo methods are explained and how they can be used to predict the barrier properties of the small gases through polymers. A hierarchal procedure that could be followed to make the calculations for the barrier properties using molecular modeling is presented in the next chapter. Calculations for polyisobutylene (PIB) are then presented in Chapter 5 to exemplify the hierarchal procedure. These methods are very good to relate the microscopic structure of the

polymer to the properties. The only disadvantage is that they are very expensive as far as time and computational power is concerned.

4

Multilevel modeling of membrane-based separation processes

As already established in Chapter 2 that, in order to design the process and the assisting structured material simultaneously, it is required to solve the process and the property models for the structured material together in one design framework (as illustrated in the Fig. 2.3 in Section 2.3 from Chapter 2). Usually the process models are macro-scale models and the property models that relate the properties of the structured materials to their microscopic structure are micro-scale models. Developing and solving mathematical models of different scales is usually the case when solving process-product design problem and are referred in this work as *multilevel models*.

In this work, for the simultaneous design of membrane-based separation processes and the polymer used as a membrane (assisting structured material), it is required to have multilevel mathematical models representing:

- Detailed process models representing underlying physical phenomena (macro-level models).

- Property models for the properties of pure components and mixtures present in the process. These models relate the chemical structure of the components to their physical and chemical properties, for example, predictive models with parameters depending on chemical structure of the component or group contribution models (meso-level models).

- Property models for polymers (assisting structured materials) that assist in the separation process at a repeat unit level, e.g. group contribution models (meso-level models).

- Property models for polymers, where properties are a function of the microscopic structure of the polymer like chain length and branch length. This kind of relations can be obtained through models like molecular dynamics or Monte-Carlo simulations (micro-scale models).

In this chapter, multilevel models required for membrane based separation processes are presented. Section 3.1 gives the overall picture of the model structure and how various process and product models are related to each other. Section 3.2 lists all the process scenarios, assumptions and modeling objectives. This will be followed by

model derivation for the membrane-based separation processes and the structured products in Section 3.3. Section 3.4 lists various process-product modeling scenarios followed by conclusions and discussion in Section 3.5.

4.1 Theoretical background

Membranes for membrane-based separation processes are available in mainly two configurations: *flat* and *tubular* configurations (see Fig. 4.1). Flat membranes are used in plate and frame and spiral wound systems whereas tubular membranes are used in hollow-fiber (diameter < 0.5 mm), capillary (diameter < 0.5-5 mm) and tubular systems (diameter > 5 mm) [89].

(a) Hollow-fiber membrane   (b) Flat membrane
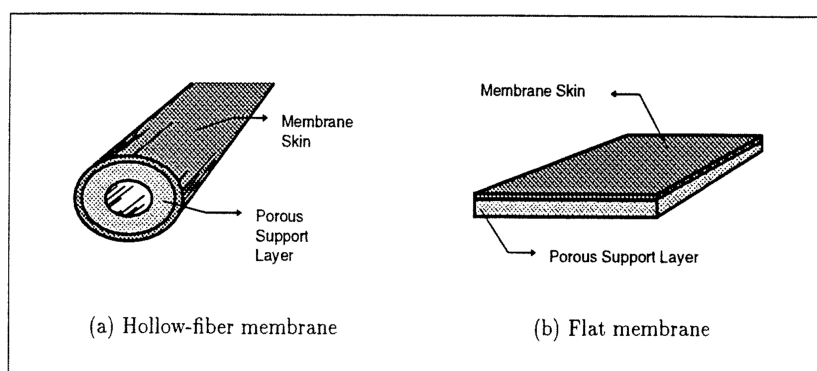
Figure 4.1: Geometries of commercial membranes for membrane-based separation processes

Depending on the manufacturer, the commercially available configurations are either hollow-fiber or spiral-wound modules. The membrane assembly for both designs is schematically illustrated in Fig. 4.2 [48]. The schematic diagram of hollow-fiber modules is shown in Fig. 4.1(a). The fibers usually between 100-500 μm in diameter, are arranged in bundles parallel to each other and are pass through tube-sheets at either one or both ends of the device (Fig. 4.2(a)). The membrane is then inserted into a pressure vessel, usually a standard metal tube (shell). Size of pressure housings range approximately 1 to 6 m in length and 10 to 30 cm in diameter. The feed is normally fed to the shell side (but not always necessary) and the components permeate at different rates to the fiber bore. Due to better separation characteristics the commercial hollow-fiber modules are normally operated in counter-current flow patterns.

For spiral-wound membrane modules, the membrane is manufactured in flat sheets (Fig. 4.1(b)). The assembly is constructed by taking two membrane sheets and sealing them together at three edges to yield a membrane leaf, that looks like an open envelop (Fig. 4.2(b)). The open side of the leaf is connected to a perforated collector tube for the permeate gas and the leaf is rolled around the collector tube together with the feed and the permeate spacers. The membrane modules described here are assembled in stages where they are arranged in parallel to provide as much mem-
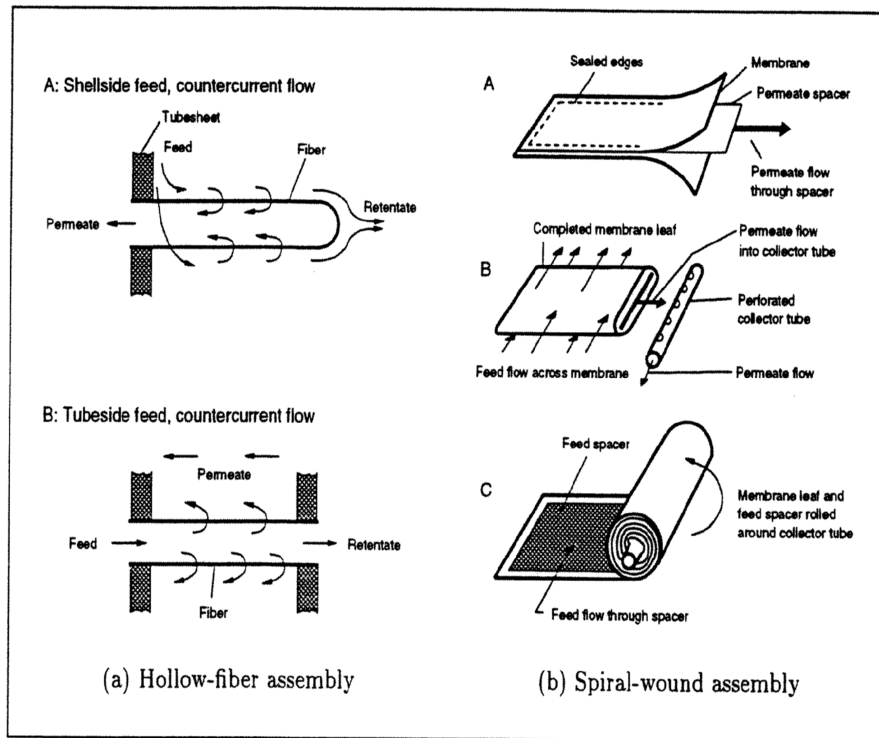
Figure 4.2: Schematic diagram of different commercial assemblies of membrane-based separation modules [48]

brane area as needed for the specific separation task.

The usage of tubular membranes in liquid and gas separations is not very popular owing to their low area/volume utilization. Table 4.1 compares the area to volume ratio of hollow fiber and film membranes [61].

Table 4.1: Area/Volume utilization for hollow-fiber and film membranes

Membrane configuration	A/V (ft^{-1})
Hollow-fiber	
OD 50 μ m	12,000
OD 100 μ m	6,000
OD 200 μ m	3,000
OD 300 μ m	2,000
Flat membrane, spiral wound	150-200
Tubular membrane, 0.5 in OD	50

In this chapter, the models are developed for the most common configurations of membrane modules: the hollow-fiber and flat sheet membrane configurations. In the following sections, development of the models for the membrane-based separation processes are shown for these two configurations. For case studies involving liquid separation with phase change mostly flat membranes are used while for gas separation hollow-fiber membranes are used.

67

The process models developed in this thesis contain balance equations that are derived from laws of conservation of mass, energy and momentum. Balances are first made for a small volume element and then integrated to cover the entire membrane volume. The structure of the whole model is shown in Fig. 4.3. The outer most later of the model describes the overall mass, energy and momentum balances. The balance equations are usually a function of mass and energy flux. The constitutive equations giving mass and energy flux are required to evaluate the balance equations at each discrete point. The mass and heat flux through the membrane depends on the physical phenomena that in turn depends mainly on the structure of the membrane. In order to evaluate the flux, there is a need of constitutive equations that mathematically represent the physical phenomena governing the flux in the membrane. Various phenomena that affect the flux could be heat and mass transfer through the boundary layers around the membrane, flow through membranes and vapor liquid equilibrium at the membrane wall in case of phase change. The mathematical equations representing them mainly depend on the physical/chemical properties of the pure components and the mixtures in the process, properties of the polymers like pore size, porosity and tortousity properties of polymer-penetrant molecule properties like solubility and diffusivity. So, for the evaluation of the constitutive equations representing the physical phenomena governing flux, there is a need of another set of constitutive equations for these properties.
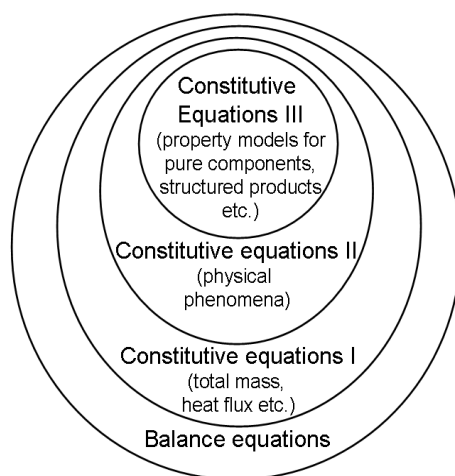
Figure 4.3: The model structure for membrane-based separation processes

For the reverse algorithm, the model for the process is solved independently of the property model for the structured materials. This is schematically represented in Fig. 4.4.

Both the process models, a general model for the liquid separation with phase change using flat sheet membrane module and membrane-based gas separation using hollow-fiber membrane module follow the same model structure. For the liquid separation with phase change using membranes the different processes for the which the model is developed are membrane distillation and pervaporation. The modeling objective is to be able to do the simultaneous design of the membrane based separation processes and the design of the structured product (polymer), model analysis
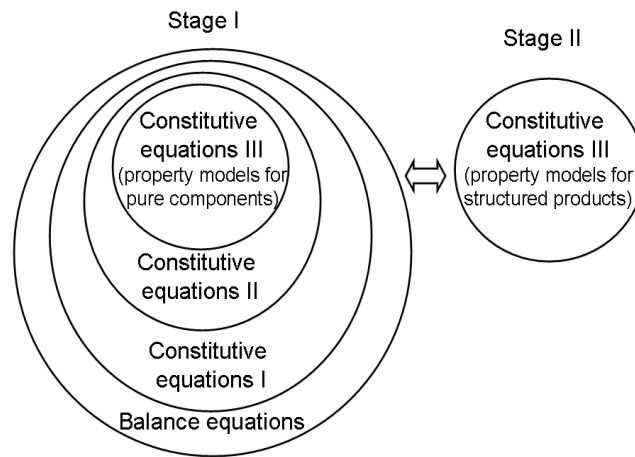
Figure 4.4: The model structure for membrane-based separation processes for the reverse design algorithm

and validation of the design.

4.2 Model derivation: Membrane based liquid separation

In this section, a general model giving the balance equations and constitutive equations for liquid separations with phase change using membrane using flat-sheet membrane module is presented. Then based on different conditions and assumptions, equations for individual processes (VMD, DCMD, SGMD, OMD, PV) can be derived from this general model. The model structure is given below:

- I. Balance equations: A mass and energy balance is made over the membrane module. This gives the mass and temperature profiles on each side of the membrane (i.e. feed and the permeate side) along the length of the module.

- II. Constitutive equations I: These equations are the mass and energy flux equations, derived for the mathematical representation of the transport through the membrane.

- III. Constitutive equations II: In order to describe the underlying physical phenomena in the membrane based separation processes for liquid separations with phase change, and to predict the effects of concentration and temperature polarization on the overall process performance the membrane module is divided in different sections: bulk feed and permeate side, liquid film on the feed side of the membrane wall, vapor film on the permeate side of the membrane wall and the membrane itself. The constitutive equations must address the following effects:

    - Mass and heat transfer resistances over the membrane module.

69

  – Transfer in films at the wall of the membrane by polarization model.

  – Liquid/vapor equilibrium at the feed/membrane interface.

  – Enthalpy balance at interface.

  – Effect of membrane characteristics on the performance.

- Constitutive equations IV: These equations represent property models for predicting pure component properties and properties for the polymers.

For a flat-sheet membrane module, a parallel flow of feed and permeate streams are shown in Fig. 4.5, where the boundaries of the system are defined.
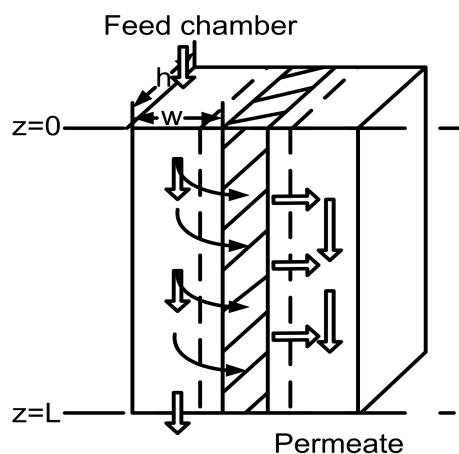
Figure 4.5: Flat-sheet membrane module

4.2.1 Model assumptions

- An average value of pore size and porosity of the membrane is assumed.

- A constant thickness of the membrane along the length is assumed.

- Pressure is assumed to be constant along the length of the membrane and so the momentum balance is not considered in this case.

- There is no consumption or production of mass during the separation process.

- In the case of VMD, there are no temperature gradients in the membrane, due to the presence of the vacuum on the permeate side.

- In the case of pervaporation, diffusion coefficients can be assumed to be constant under conditions where concentration of the penetrant gases in the membrane is assumed to be low.

- The heat of absorption of the components on the feed side of the membrane in pervaporation is assumed to be equal to the heat of desorption on the permeate side, hence making the heat of vaporization the only heat required during the transport of the components through the membrane.

- When the molar volumes in the membrane phase and liquid phase are assumed different, the difference can be modeled by a term called the molar volume correction factor. The molar volume correction factor is however assumed insignificant for pervaporation applications [119].

4.2.2 Balance equations

4.2.2.1 Mass balance

The membrane channel has a height h, a width w and a length L. A mass balance is made for a control volume of height h, width w and length Δz in the flow direction. The derivation of balance equations are shown for only feed side as the equations for the permeate side are analogous but with a different sign. Fig. 4.6 shows the cross section of the feed side of the membrane module and the mass balance over length Δz is:
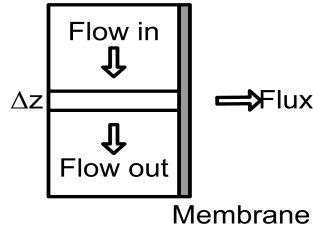
Figure 4.6: Cross section of the feed side of the membrane module

Feed side: Mass flow in = Mass flow out + Mass flux through membrane.

$$m_f|_z = m_f|_{z+\Delta z} + N_{total} \cdot \Delta A \tag{4.1}$$

$$\frac{m_f|_{z+\Delta z} - m_f|_z}{\Delta z} = -N_{total} \cdot w \tag{4.2}$$

where, m_f is the molar flow rate on the feed side and N_{total} is the total flux through the membrane. For $\Delta z \to 0$:

$$\frac{dm_f}{dz} = -N_{total} \cdot w \tag{4.3}$$

with, initial conditions defined at the inlet of the membrane module on the feed side as:

$$m_f (z = z_0) = m_{f,0} \tag{4.4}$$

71

The mass flow m_f can be converted to volumetric flow V_f, by dividing it by density:

$$V_f = \frac{m_f}{\rho_f} \tag{4.5}$$

and

$$V_p = \frac{m_p}{\rho_p} \tag{4.6}$$

For a constant density system, the balance for the volumetric flow can be written as:

$$\frac{dV_f}{dz} = \frac{-N_{total} \cdot w}{\rho_f} \tag{4.7}$$

Linear mass velocity is given as:

$$u_f = V_f * Am \tag{4.8}$$

and

$$u_p = V_p * Am \tag{4.9}$$

The mass balance equation at the permeate side is written as:

$$\frac{dm_p}{dz} = N_{total} \cdot w \tag{4.10}$$

with, initial conditions defined at the inlet of the membrane module on the permeate side as:

$$m_p \left(z = z_0 \right) = m_{p,0} \tag{4.11}$$

For each component i in the system, the component mass balance for the feed and permeate side is given:

$$\frac{dm_{f,i}}{dz} = -N_i \cdot w \ for \ i = 1, N \tag{4.12}$$

$$\frac{dm_{p,i}}{dz} = N_i \cdot w \ for \ i = 1, N \tag{4.13}$$

where, N_i is the mass flux. Flux equation of the following form is required for calculating the mass balance equations (Eq. 4.12, 4.13):

$$N_i = N_i(T, \Delta p_i, M_i, D_{i,j}, ...)$$ (4.14)

With the assumption of no production or consumption, the sum of flux of all component is the total flux:

$$N_{total} = \sum_i^N N_i$$ (4.15)

4.2.2.2 Energy balance

The energy balance will be first established for a control volume of height h, width w and length Δz (see Fig. 4.6). The heat balance for the feed side of the membrane is shown. For the small length Δz:

$$E_f|_z = E_f|_{z+\Delta z} + Q_{process} \cdot \Delta A$$ (4.16)

On the feed side, the energy E_f can be written as:

$$E_f|_z = m_f \cdot Cp_f \cdot T_f|_z$$ (4.17)

$$E_f|_{z+\Delta z} = m_f \cdot Cp_f \cdot T_f|_{z+\Delta z}$$ (4.18)

Inserting Eq. 4.5, 4.17 and 4.18 into Eq. 4.16 and taking the limit $\Delta z \to 0$, we get:

$$\frac{d\left(V_f \rho_f Cp_f T_f\right)}{dz} = -Q_{process} \cdot w$$ (4.19)

Rearranging the above equation for a constant density system and substituting $\frac{dV_f}{dz}$ with Eq. 4.7:

$$\frac{dT_f}{dz} = -\frac{1}{V_f} \left[\frac{Q_{process} \cdot w}{Cp_f \cdot \rho_f} + \frac{R_{total} \cdot T_f \cdot w}{\rho_f} \right]$$ (4.20)

Similarly the rate of change of temperature on the permeate side, T_P is derived to be:

$$\frac{dT_p}{dz} = \frac{1}{V_p} \left[\frac{Q_{process} \cdot w}{Cp_p \cdot \rho_p} - \frac{R_{total} \cdot T_p \cdot w}{\rho_p} \right]$$ (4.21)

where, the following initial conditions apply:

$$T_f\left(z = z_0\right) = T_{f,0} \tag{4.22}$$
$$T_p\left(z = z_0\right) = T_{p,0} \tag{4.23}$$

4.2.2.3 Analysis of balance equations

In this section, all the balance equations are analyzed to identify the variables that are needed to evaluate the balance equations. Table 4.2 shows different variables that are required to evaluate the balance equations. It can be seen from the table that apart from the physical properties of the streams on feed and permeate side (constitutive equations III), total and individual mass flux and heat flux (constitutive equations I) are required for the evaluation of the balance equations.

Table 4.2: Variables needed to evaluate the balance equations

Equation for	Equation number	Variables needed
Total mass balance (feed side)	Eq. 4.3	R_{total}, w
Total mass balance (permeate side)	Eq. 4.10	R_{total}, w
Component mass balance (feed side)	Eq. 4.12	R_i, w
Component mass balance (permeate side)	Eq. 4.13	R_i, w
Energy balance (feed side)	Eq. 4.20	$Q_{process}$, V_f, w, Cp_f, ρ_f, R_{total}
Energy balance (permeate side)	Eq. 4.21	$Q_{process}$, V_p, w, Cp_p, ρ_p, R_{total}

4.2.3 Constitutive equations I

The evaluation of the mass and energy balance equations (Eq. 4.3, 4.10, 4.12, 4.13, 4.20 and 4.21) requires the evaluation of component flux R_i and heat flux $Q_{process}$ respectively at each discrete point. In an MD process, the fluxes are assumed to be proportional to the partial pressure difference of the components across the membrane [63]. According to Darcy's law:

$$N_i = B\Delta P_i \tag{4.24}$$

Where, B is the overall coefficient, which depends on temperature, pressure and composition within the membrane as well as membrane characteristics like porosity,

tortousity etc. The coefficient B, can be evaluated in different ways for different resistances, because the resistances arise from collisions between diffusing molecules and either other molecules or the pore walls of the membrane. Dusty gas model (DGM) is the most commonly used model for flux through porous media. According to this model the flux is composed of diffusive and viscous components [27]:

$$N_i^G = N_i^D + N_i^V \tag{4.25}$$

The diffusive component N_i^D is given by Stefan-Maxwell equations [84]:

$$\frac{N_i^D}{D_{kie}} + \sum_{\substack{j=1 \\ j \neq i}}^{n} \frac{p_j N_i^D - p_i N_j^D}{D_{ije}^0} = -\frac{1}{RT}\nabla p_i, \ for \ i = 1, N \tag{4.26}$$

where D_{kie} is the effective Knudsen diffusivity for species i for molecular mass M_i and D_{ije}^0 is the pressure independent diffusivity

The viscous flux contribution is given by the d'Arcy equation with a constant mixture velocity. Thus:

$$N_i^V = -x_i \frac{p}{RT}\left(\frac{B_0}{\mu}\right)\nabla p \tag{4.27}$$

$$= -\frac{p_i}{RT}\left(\frac{B_0}{\mu}\right)\sum_{j=1}^{n}\nabla p_j \tag{4.28}$$

Eq. 4.26 and 4.27 comprise the dusty gas model. Different kind of membrane distillation processes differ from each other depending on the prevailing mechanism. Applying the assumptions of each mechanism to DGM, various flux models can be derived. Different flux equations used in literature are discussed below.

4.2.3.1 Knudsen-limited diffusion

When the mean free path of the diffusing molecules is larger than the pore size of the membrane, then molecule-pore wall collisions are dominant in membranes with small pores ($\langle r \rangle << \lambda$). The flux across the membrane can be effectively modeled by [9, 11]:

$$N_i = \frac{K_0}{RT}\left(\frac{8RT}{\pi M_i}^{0.5}\frac{\Delta p_i}{\delta}\right) \tag{4.29}$$

The flux of permeating species is directly proportional to the difference of partial pressures. In general, in MD process the separation is mainly due to the vapor-liquid equilibrium but some selectivity is imparted due to the presence of the $1/M_i^{0.5}$ term in the flux equation. So, in Knudsen-limited case the membrane imparts some favor (on molar basis) toward lighter molecules [73].

4.2.3.2 Knudsen-viscous transition diffusion

In the case where mean free path of diffusing species, λ is similar to the membrane pore diameter, the governing phenomena is Knudsen-viscous diffusion [71]. The complete Knudsen-viscous transition equation is given as:

$$N_i = \frac{1}{RT_{avg}\delta}\left[K_0 \frac{8RT}{\pi M_i}^{0.5}\Delta p_i + B_0 \frac{p_{i,avg}}{\mu}\Delta P\right] \tag{4.30}$$

The values of K_0 and B_0 can also be measured from gas permeation experiments of a pure gas. These parameters does not depend on the gas but only on the basic polymer structural parameters.

4.2.3.3 Knudsen-molecular diffusion

For membranes with smaller air filled pores (approximately less than 0.5 μm) molecular-pore collisions begin to occur as frequently as molecule-molecule collisions, and the Knudsen resistance must be taken into account. From DGM:

$$N_i = \frac{-1}{RT}\left[\frac{1}{D_{1e}^k} + \frac{P_p}{D_{12e}^0}\right]^{-1}\nabla P_f \tag{4.31}$$

For Knudsen-molecular diffusion the above equation should be used.

4.2.3.4 Solution-diffusion mechanism

For pervaporation and membrane-based gas separation usually non-porous membranes are considered which are also more attractive for commercial purposes. The mass transfer mechanism is very different as compared to the porous membranes. In this case the transport of the vapor is by three steps. The vapor first get dissolved at the feed side of the membrane then diffuse through the membrane and finally dissolves in the permeate flow. The mechanism is hence called *solution-diffusion mechanism*. Hence this mechanism is both thermodynamically (solution) and kinetically (diffusion) driven.

The solution-diffusion model is the most widely used transport model for permeation in non-porous polymer membranes. The model allows the membrane separation processes of dialysis, reverse osmosis, gas separation and pervaporation to be described by a series of interrelated equations. So, here the derivation of flux equations for membrane-based gas separation and pervaporation will be shown. For convenience, the equations for gas separation are also derived simultaneously with pervaporation as the transport mechanism is very similar. In the next section, where the model of gas separation is developed flux equation will be referred from this section. Solution-diffusion equations generally found in literature contain a simplifying assumption that the molar volume of each permeant in the membrane phase is equal to the permeant molar volume in the liquid phases in contact with the membrane [119]. But the equations for molar volume correction will be shown for pervaporation, which is usually insignificant and can be neglected in those cases.

Since diffusion is a kinetic process, classical thermodynamics does not explain the rate at which the diffusion process occurs. The movement of the gas molecules in a non-porous polymeric membrane can well be described by Fick's first law of diffusion. The unidimensional flux N_{Mi} of component i through a flat membrane is given by [26]

$$N_{Mi} = -D_i(c)\frac{dc_i}{dl} \tag{4.32}$$

where, $D_i(c)$ is the concentration dependent diffusion coefficient of component i in the membrane. dc_i/dl is the concentration gradient in the permeate direction inside the membrane. For constant diffusion coefficient, the integration of the equation above gives

$$N_{Mi} = \frac{D_i}{\delta}(c_{Ri} - c_{Pi}) \tag{4.33}$$

where, δ is the thickness of the membrane's active layer and c_{Ri} and c_{Pi} are concentration of component i at the retentate and the permeate face of the membrane, respectively. At the interface of the membrane there is an existence of phase equilibrium. This equilibrium relation can be used to connect the concentration of the components in the bulk feed solution and the concentration of the gas at the face of the membrane.

Since the interfaces are in equilibrium states, the concentrations in the membrane at the feed/membrane and membrane/permeate interfaces can be expressed in terms of the concentrations outside the membrane. This implies

$$\mu_{i,f} = \mu_{i,wf} \tag{4.34}$$

and

$$\mu_{i,p} = \mu_{i,wp} \tag{4.35}$$

where μ ($atmcm^3/mol$) is the chemical potential. The subscripts f and p represent the feed and the permeate side. And subscript w represent the membrane surface (wall of the membrane).

According to solution-diffusion mechanism the gas separation via membranes occur via pressure driven diffusion. Diffusion can only take place if there is a negative gradient of chemical potential. From thermodynamics, the chemical potential of a component i in a gas mixture μ_i is given by

$$d\mu_i = R_g T d\left(ln\left(f_i\right)\right) \tag{4.36}$$

where R is the gas constant, T the temperature (K), f_i is the fugacity of the component i.

The change in the chemical potential from feed to the permeate side is then given by

$$\mu_{Pi} - \mu_{Ri} = R_g T ln\left(\frac{f_{Pi}}{f_{Ri}}\right) \tag{4.37}$$

subscripts P and R represent the permeate and the retentate side of the membrane respectively. In order to have a negative chemical potential gradient, the value of $ln\left(f_{Pi}/f_{Ri}\right)$ should be negative. To achieve this condition it is required that $f_{Pi} < fRi$. Therefore the difference in fugacities (in case of ideal gas, partial pressures) provide the driving force for the transport of gas molecules across the membrane.

In incompressible phases, such as a liquid phase or a solid membrane phase, the molar volume is essentially independent of pressure. Integration of Eq. 4.37 with respect to concentration and pressure then gives

$$\mu_i = \mu_i^0 + RTln\left(\gamma_i^L x_i\right) + v_i^L\left(p - p_i^{sat}\right) \tag{4.38}$$

where μ_i^0 is the reference chemical potential of pure i at the saturation vapor pressure of i, p_i^{sat} (atm).

For compressible gases, the molar volume changes pressure and using the ideal gas law to integrate Eq. 4.37 gives

$$\mu_i = \mu_i^0 + RTln\left(\gamma_i^G y_i\right) + RTln\left(\frac{p}{p_i^{sat}}\right) \tag{4.39}$$

The equilibrium equation (Eq. 4.34 and 4.35) then take the following form for a liquid phase in contact with the membrane

$$\mu_i^0 + RTln\left(\gamma_i^L x_i\right) + v_i^L\left(p - p_i^{sat}\right) = \mu_i^0 + RTln\left(\gamma_{i,w} x_{i,w}\right) + v_{i,w}\left(p - p_i^{sat}\right) \tag{4.40}$$

and for a gas phase in contact with the membrane

$$\mu_i^0 + RTln\left(\gamma_i^G y_i\right) + RTln\left(\frac{p}{p_i^{sat}}\right) = \mu_i^0 + RTln\left(\gamma_{i,w} x_{i,w}\right) + v_{i,w}\left(p - p_i^{sat}\right) \tag{4.41}$$

The equilibrium equations (Eq. 4.40 and 4.41) can be combined with the diffusion equation (Eq. 4.33) to yield the solution-diffusion transport equations for gas separation and pervaporation.

Membrane-based gas separation: In gas separation, the membrane is in contact with two gas phases, and the equilibrium equations for the two membrane interfaces yield the following equations for the concentrations in the membrane at the feed and permeate interfaces

$$x_{i,wf} = \frac{\gamma_i^G}{\gamma_{i,w}}\frac{p_f}{p_i^{sat}}y_{i,f}exp\left(\frac{-v_{i(m)}\left(p_f - p_i^{sat}\right)}{RT}\right) \tag{4.42}$$

and

$$x_{i,wp} = \frac{\gamma_i^G}{\gamma_{i,w}}\frac{p_p}{p_i^{sat}}y_{i,p}exp\left(\frac{-v_{i(m)}\left(p_f - p_i^{sat}\right)}{RT}\right) \tag{4.43}$$

The gas phase sorption coefficient can be defined as:

$$K_i^G = \frac{\gamma_i^G}{\gamma_{i,w} p_i^{sat}} \tag{4.44}$$

Substituting Eq. 4.44 in Eq. 4.42 and 4.43 gives

$$x_{i,wf} = K_i^G y_{i,f} p_f exp\left(\frac{-v_{i(m)}\left(p_f - p_i^{sat}\right)}{RT}\right) \tag{4.45}$$

and

$$x_{i,wp} = K_i^G y_{i,p} p_p \left(\frac{-v_{i(m)}\left(p_f - p_i^{sat}\right)}{RT}\right) \tag{4.46}$$

which combined with diffusion equation Eq. 4.33, yields gas transportation equation

$$N_{M,i} = \rho_w \frac{D_i K_i^G}{l} exp\left(\frac{-v_{i(m)}\left(p_f - p_i^{sat}\right)}{RT}\right)\left(y_{i,f} p_f - y_{i,p} p_p\right) \tag{4.47}$$

or

$$N_{M,i} = \frac{P_i}{l} exp\left(\frac{-v_{i(m)}\left(p_f - p_i^{sat}\right)}{RT}\right)\left(y_{i,f} p_f - y_{i,p} p_p\right) \tag{4.48}$$

where the permeability coefficient, P_i $(molcm/(cm^2 satm))$, is defined by

$$P_i = \rho_w D_i K_i = \frac{\rho_w \gamma_i^G D_i}{\gamma_{i,w} p_i^{sat}} \tag{4.49}$$

The Poynting correction factor present in Eq. 4.48 is close to unity in most gas separation applications because the molar volume of the permeants involved are relatively small (vapor separation being a potential exception). Eq. 4.48 is then approximated very well by the expression

$$N_{Mi} = \frac{P_i}{l}\left(p_{i,f} - p_{i,p}\right) \tag{4.50}$$

which is the gas separation transport (flux) equation most commonly used.

Pervaporation: In the case of pervaporation, the membrane is in contact with a liquid phase on the feed side and with a vapor phase on the permeate side. So the equilibrium equations derived in the same way as for the gas separation case are:

$$x_{i,wf} = K_i^L x_{i,f} exp \left(\frac{\left(v_i^L - v_{i,w} \right) \left(p_f - p_i^{sat} \right)}{RT} \right) \tag{4.51}$$

on the feed side, and for the permate side its same as in the case of gas separation membrane (Eq. 4.46). The following relationship between the gas phase and liquid phase sorption coefficients is then applicable

$$K_i^G = \frac{\gamma_i^G}{\gamma_i^L p_i^{sat}} K_i^L \tag{4.52}$$

The transport equation for pervaporation can then be written as:

$$N_{Mi} = \frac{P_i^G}{l} \left[x_{i,f} \frac{\gamma_i^L}{\gamma_i^G} p_i^{sat} exp \left(\frac{\left(v_i^L - v_{i,w} \right) \left(p_f - p_i^{sat} \right)}{RT} \right) - y_{i,p} p_f exp \left(\frac{\left(-v_{i,w} \right) \left(p_f - p_i^{sat} \right)}{RT} \right) \right] \tag{4.53}$$

Using the following expression for the partial vapor pressure of i in the feed liquid, $p_{i,f}^{vapor}$

$$p_{i,f}^{vapor} = x_{i,f} \frac{\gamma_i^L}{\gamma_i^G} p_i^{sat} exp \left(\frac{-v_i^L \left(p_f - p_i^{sat} \right)}{RT} \right) \tag{4.54}$$

The pervaporation transport equation can be written in terms of a partial vapor pressure driving force as

$$N_{Mi} = \frac{P_i}{l} exp \left(\frac{-v_{i,w} \left(p_f - p_i^{sat} \right)}{RT} \right) \tag{4.55}$$

In actual practice, the feed pressures in pervaporation applications are normally low, so the Poynting and molar volume corrections are close to unity, which leads to

$$p_{i,f}^{vapor} = \frac{\gamma_i^L}{\gamma_i^G} p_i^{sat} \tag{4.56}$$

and

$$N_{Mi} = \frac{P_i}{l} \left(p_{i,f}^{vapor} - x_{i,p} p_p \right) = \frac{P_i}{l} \left(x_{i,f} \frac{\gamma_i^L}{\gamma_i^G} p_i^{sat} - x_{i,p} p_p \right) \tag{4.57}$$

4.2.3.5 Heat flux

The heat flux $[J/m^2 s]$ through the membrane can be calculated by considering the heat transfer through the film on the feed side of the membrane. Assuming no loss of heat during the transfer this is the total heat flux through the membrane. The heat transfer from bulk of the feed to the permeate side of the membrane can be described by simple heat transfer equations [51, 105]:

$$Q_{process} = h_f \left(T_f - T_{wf} \right) \tag{4.58}$$

where h_f is the heat transfer coefficient of the film on the feed side of the membrane. T_f and T_{wf} represent the temperature of bulk feed and at the surface of the membrane on the feed side respectively.

4.2.3.6 Analysis of flux equations

In this section, the flux equations for mass and heat flow are analyzed to identify the set of variables for which constitutive equations are required. The analysis is given in Table 4.3.

Table 4.3: Equation analysis - flux equations

Equation for	Equation number	Variables needed
Knudsen diffusion	Eq. 4.29	K_0, R,T,M_i,p_i,δ
Knudsen-Viscous diffusion	Eq. 4.30	K_0, R,T,M_i,p_i,δ, B_0, μ
Knudsen-Molecular diffusion	Eq. 4.31	D_{ie}^k,D_{12e}^0, R,T
Solution-diffusion mechanism	Eq. 4.57	P_i, δ, P_i^{sat}, $x_{i,p}$
Heat Flux	Eq. 4.58	h_{film}, T_{wf}

In these equations, K_0 and B_0 are parameters related to the membrane that are a function of the its structure (constitutive equations III). D_{ie}^k and D_{12e}^0 are Knudsen and molecular diffusivities, which are also a function of membrane structure and parameters like K_0 and B_0 (constitutive equations III). Component properties like viscosity (μ) and saturation pressure (P^{sat}) are also given by constitutive equations III. While, intermediate molar fractions and temperatures, x_p and T_{wf} respectively, can be evaluated by transport equations derived from the governing physical phenomena (constitutive equations II). Heat transfer coefficient for the film (h_{film}) is evaluated using film theory (constitutive equations II).

4.2.4 Constitutive equations II

4.2.4.1 Transfer resistances

The dusty gas model (DGM) is a comprehensive transport model that accounts for different mechanisms for mass transfer in porous media [27, 84]. Fig. 4.7 illustrates different mass transfer resistances in MD as described by DGM. As can be seen from the figure, the resistances correspond to the boundary layers next to the membrane and resistance within membrane. Molecular diffusion across the boundary layer

contributes substantially and is usually the rate limiting step in MD [73]. Within the membrane, the resistances are a consequence of transfer of momentum to the supported membrane (viscous or momentum transfer resistance), or of collisions of a diffusing molecule with other molecules (molecular resistance) or with membrane itself (Knudsen resistance).
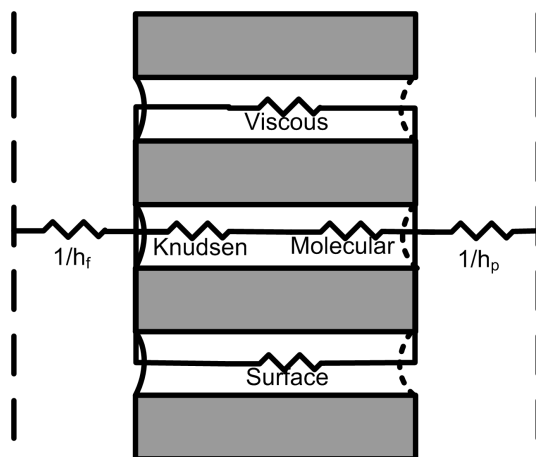
Figure 4.7: Mass transfer resistances in MD

Fig. 4.8 illustrates different kinds of heat transfer resistances in MD. Similar to mass transfer, the thermal boundary layer imparts resistance to the heat transfer. The liquid vaporizes at the surface of the membrane and the vapors are transported to the permeate side. The heat is transferred across the membrane at a rate corresponding to the heat of vaporization. And in addition to that, heat is transferred through the membrane material and the vapors that fill the membrane. On the cold side, the vapor condenses and the heat is transferred through the thermal boundary layer on the permeate side.
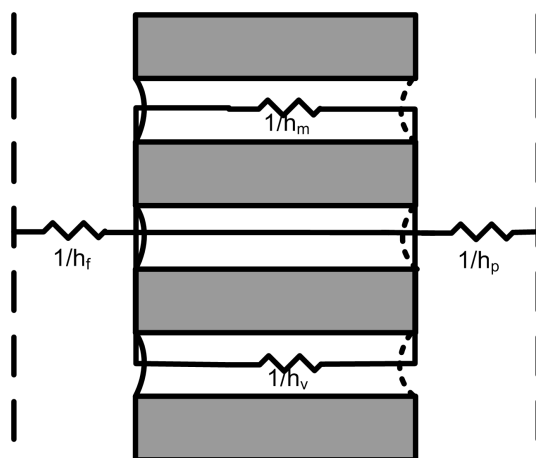
Figure 4.8: Heat transfer resistances in MD

4.2.4.2 Heat transfer resistances

Fig. 4.8 shows the heat transfer mechanism in liquid separation. Different heat transfer resistances are shown in the schematic diagram. The energy balance is made as a series parallel resistance model. At steady state the amount of heat transported through each medium Q must be the same to avoid accumulation of heat [73]. First the heat is transferred across the thermal boundary layer to the membrane surface (see Eq. 4.58) h_f in this equation can be calculated by Nusslet's correlation 4.80. Heat transfer through the membrane takes place via two mechanisms. It is a summation of the heat of vaporization Q_v and the heat conducted through the membrane and the vapor that fills the pores Q_m. So, the heat transfer through the membrane is given as:

$$Q = Q_v + Q_m = N_{total} \cdot \Delta H_v + h_m \cdot (T_w f - T_{wp}) \tag{4.59}$$

h_m is the heat transfer coefficient through the membrane and it depends on the porosity (ϵ) of the membrane:

$$h_m = \epsilon h_{mg} + (1 - \epsilon) h_{ms} \tag{4.60}$$

Since, the heat transfer coefficient of the gas in the membrane h_{mg} is usually much smaller than the coefficient of the solid membrane material h_{ms}. So, the heat losses by conduction can be minimized by increasing the membrane porosity.

For the thermal boundary layer on the permeate side, a similar expression can be formulated as on the feed side boundary layer:

$$Q = h_p \cdot (T_w p - T_p) \tag{4.61}$$

and h_p can be calculated similarly by Nusselt's equations.

Equating the three heat transfer terms Q the intermediate temperatures at the membrane surfaces (T_{wf}, T_{wp}) can be calculated implicitly.

4.2.4.3 Vapor liquid equilibrium

As mentioned above, the driving force in a MD process is the difference in the vapor pressures of component vapors across microporous hydrophobic membranes, which is imposed by a temperature difference (DCMD) or by vacuum, sweep gas or electrolyte solution on the permeate side. At the pores of the feed side of the membrane surface, liquid feed vaporizes and the vapors and liquid are assumed to be in equilibrium state corresponding to the temperature at the membrane surface and the pressure within the membrane pores. This assumption of vapor liquid equilibrium (VLE) can then be used to determine the partial pressures of components on the feed side. The partial pressure of the non ideal mixtures can then be given as [105]:

$$p_{i,wf} = P_i^{sat}(T_{wf}) \cdot \gamma_i(T_{wf}, x_{i,wf}) \cdot x_{i,wf} \ for \ i = 1, N \tag{4.62}$$

Where, P_i^{sat} is the saturation pressure at temperature T_{wf}. The subscript w corresponds to the conditions at the wall of the membrane. the pure component saturation pressure P_i^{sat} can then be calculated by Antoine equation [105]:

$$P_i^{sat} = exp\left[A - \frac{B}{C+T}\right] \tag{4.63}$$

In most of the cases in this work it has been calculated with the following correlation:

$$P_i^{sat} = \exp\left(A + B/T_{wf} + C.\ln(T_{wf}) + D.T_{wf}^E\right) \tag{4.64}$$

γ_i is the activity coefficient which is a function of temperature and composition and can be calculated by a number of different available models like UNIFAC, NRTL, UNIQUAC etc. or the experimental values can be obtained from literature.

For the permeate side, the partial pressures can be calculated as a function of the total pressure and the molar fractions in the vapor phase, in the cases where there is vapor phase on the permeate side, i.e. VMD and SGMD:

$$p_{i,wp} = P_p \cdot y_{i,wp} \tag{4.65}$$

For DCMD, there is a liquid phase on the permeate side, so the partial pressure on the permeate side can be calculated similarly as for the feed side:

$$p_{i,wp} = P_i^{sat}(T_{wp}) \cdot \gamma_i(T_{wp}, x_{i,wp}) \cdot x_{i,wp} \; for \; i = 1, N \tag{4.66}$$

For OMD, the liquid phase on the permeate side is the salt solution, hence the activity coefficients (γ_i^e) would be calculated from a model that incorporates terms for the electrolyte solutions, such as, extended UNIQUAC which includes terms like Born's term for the salt effect. The partial pressures can then be calculated as:

$$p_{i,wp} = P_i^{sat}(T_{wp}) \cdot \gamma_i^e(T_{wp}, x_{i,wp}) \cdot x_{i,wp} \; for \; i = 1, N \tag{4.67}$$

This relationship between p_i, liquid temperature and composition requires the iterative solution of MD heat and mass transfer equations.

The driving force, for each component i, transporting through the membrane can then be calculated as [11]:

$$\Delta P_{i,w} = p_{i,wf} = P_i^{sat}(T_{wf}) \cdot \gamma_i(T_{wf}, x_{i,wf}) \cdot x_{i,wf} - P_p \cdot y_{i,wp} \tag{4.68}$$

The heat and mass transfer resistances in the boundary layers can be neglected if instead of using the surface values in Eq. 4.68 the bulk values are used to calculate the driving force and get approximately the same value for driving force [11]. Same flux can be obtained either considering or neglecting the liquid-phase resistances. To make sure if the boundary layers offer the resistance or not, the flux of each component R_i, can be plotted vs. the driving force calculated at bulk conditions $\Delta P_{i,b}$. If the slope of this plot is equal to $K_m/\sqrt{M_i}$, then it can be concluded that the liquid phase resistance can be neglected.

4.2.4.4   Mass and heat transfer through boundary layers

Concentration and temperature polarization in the boundary layers are the rate limiting steps in liquid separations using membranes for mass and heat transfer respectively. Since separation in MD depends on the differences in volatility and diffusion rates of the components, some components permeate faster than others. So, their concentration decreases on the feed side. This reduces the partial pressure of this component hence changing the driving force which affects the flux through the membrane. This concentration drop of faster permeating species in the thin film on the membrane surface is called concentration polarization. Mass transfer across the boundary layers or concentration polarization may play an important role in the performance of an MD system. The boundary layers can increase the overall resistance to mass transfer, and they can cause undesirable solute concentrations at the membrane surface, which can lead to spontaneous wetting of the membrane. Such mass transfer through the liquid phase can be adequately described by the film theory model [51]:

$$N_{total} = k_m \times C_t \times \ln\left(\frac{x_{i,wf} - x_{i,p}}{x_{i,f} - x_{i,p}}\right) \tag{4.69}$$

where N_{total} is the total flux through the membrane, which is the sum of individual fluxes of all components in the system, k_m is the mass transfer coefficient, which can be calculated from Sherwood number as:

$$k_m = \frac{D_{AB}.\text{Sh}}{dh} \tag{4.70}$$

The Sherwoods correlations are then used to calculate the Sherwood number, and the correlation can take three different forms depending on whether the flow is laminar, transitional or turbulent [18, 87]:

$$\text{Sh} = f\left(\text{Re, Sc}, dh, L, \mu\right) \tag{4.71}$$

$Re < 2100$ Laminar regime

$$\text{Sh} = 1.86\left(\text{Re.Sc.}\frac{dh}{L}\right)^{0.33}\left(\frac{\mu_{bf}}{\mu_{wf}}\right)^{0.14} \tag{4.72}$$

$2100 < Re < 10000$ Transition regime

$$\text{Sh} = 0.116\left(\text{Re}^{2/3} - 125\right).\text{Sc}^{0.33}.\left(1 + \left(\frac{dh}{L}\right)^{2/3}\right)\left(\frac{\mu_{bf}}{\mu_{wf}}\right)^{0.14} \tag{4.73}$$

$Re > 10000$

$$\text{Sh} = -0.023.\text{Re}^{0.8}.\text{Sc}^{0.33}\left(\frac{\mu_{bf}}{\mu_{wf}}\right)^{0.14} \tag{4.74}$$

where,

$$\text{Re} = \frac{u_f.\rho.dh}{\mu} \tag{4.75}$$

$$\text{Sc} = \frac{\nu}{D_{AB}} \tag{4.76}$$

dh is the hydraulic radius and can be defined as:

$$dh = \frac{2.w.h}{w + h} \tag{4.77}$$

Similarly, heat transfer resistance in the boundary layer can be explained by the temperature polarization phenomena. It is the rate limiting step for the mass transfer in liquid separation, as a large amount of heat must be supplied to the surface of the membrane to vaporize the liquid. This can be modeled analogously to mass transfer. The heat transfer from bulk of the feed to the permeate side of the membrane can be described by simple heat transfer equations [51, 105]. For the heat transfer coefficient h_f Nusselt's Equations can be used [105]:

$$h_f = \frac{k_h \cdot Nu}{dh} \tag{4.78}$$

This equation is used on each side of the membrane where there is a liquid film on each side like DCMD and OMD. For VMD this film does not exist and for SGMD there is a gas film. For air as the sweeping gas stream, heat transfer coefficient on the permeate side for SGMD process is given as [63]:

$$h_p = 0.209 \frac{k_h}{dh} Pr^{0.36} \tag{4.79}$$

Nusselt's number again depends on the flow regime (divided into three regions) [18, 87]:

$$\text{Nu} = f\left(\text{Re}, \text{Pr}, dh, L, \mu\right) \tag{4.80}$$

where,

$$Pr = \frac{\mu Cp}{\lambda} \tag{4.81}$$

$Re < 2100$ Laminar regime

$$\text{Nu} = -1.86 \left(\text{Re}. \text{Pr}. \frac{dh}{L}\right)^{0.33} \left(\frac{\mu_{bf}}{\mu_{wf}}\right)^{0.14} \tag{4.82}$$

$2100 < Re < 10000$ Transition regime

$$\text{Nu} = -0.116 \left(\text{Re}^{2/3} - 125\right). \text{Pr}^{0.33}. \left(1 + \left(\frac{dh}{L}\right)^{2/3}\right) \left(\frac{\mu_{bf}}{\mu_{wf}}\right)^{0.14} \tag{4.83}$$

$Re > 10000$

$$\text{Nu} = -0.023. \text{Re}^{0.8}. \text{Pr}^{0.33} \left(\frac{\mu_{bf}}{\mu_{wf}}\right)^{0.14} \tag{4.84}$$

The variables needed to evaluate these equations are: porosity ϵ (related to polymer structure), length (L), width (w) and height (h) of the channel (known parameters for a given membrane module), pure component physical properties like liquid density (ρ_i), liquid viscosity (μ_i), heat of vaporization (ΔH_v) and activity coefficient (γ_i) (constitutive equations III).

4.2.5 Constitutive equations III

The third level of constitutive equations contain models for pure component physical properties and polymer properties (porous and non-porous).

4.2.5.1 Pure component physical properties

As far as pure component properties of the components are concerned the end-use property models are given here while the theory and their development is shown in next Section 4.2.5.1 in details. These include pure component liquid density (ρ_i), liquid viscosity (μ_i), specific heat (Cp_i), thermal conductivity (km_i), infinite dilution diffusion coefficients (D_i), gas viscosity (μ_{gi}), heat of vaporization (δH_i), vapor pressure (P^{sat}), activity coefficients (γ_i) etc.. In this work, a tool for property prediction called Pro-Pred [78], which is based on group contribution principles has been used to obtain property values at different temperatures. The properties were then fitted to the following expressions:

$$\text{Density} \left[\frac{\text{kmol}}{\text{m}^3}\right] : \rho = \frac{A}{B^{\left(1+\left(1-\frac{T}{C}\right)^D\right)}} \tag{4.85}$$

$$\text{Viscosity} \left[\frac{\text{kg}}{\text{m.s}}\right] : \mu = \exp\left(A + \frac{B}{T} + C.\ln(T) + D.T^E\right) \tag{4.86}$$

$$\text{Specific heat} \left[\frac{\text{J}}{\text{kmol.K}}\right] : Cp = A + B.T + C.T^2 + D.T^3 + E.T^4 \tag{4.87}$$

$$\text{Thermal conductivity} \left[\frac{\text{J}}{\text{m.s.K}}\right] : k_h = A + B.T + C.T^2 + D.T^3 + E.T^4 \tag{4.88}$$

$$\text{Diffusion coefficient} \left[\frac{\text{m}^2}{\text{s}}\right] : D^\infty = A + B.T + C.T^2 + D.T^3 + E.T^4 \tag{4.89}$$

$$\text{Gas Viscosity} \left[\frac{\text{kg}}{\text{m.s}}\right] : \mu_g = A.T^{\frac{B}{1+C/T+D/T^2}} \tag{4.90}$$

$$\text{Heat of Vaporization} \left[\frac{\text{J}}{\text{kmol}}\right] : H_{vap} = A.(1-Tr)^{B+C.Tr+D.Tr^2} \tag{4.91}$$

$$\text{Saturation pressure [Pa]} : P^{\text{sat}} = \exp\left(A + B/T_{\text{wf}} + C.\ln(T_{\text{wf}}) + D.T_{\text{wf}}^{\text{E}}\right) \tag{4.92}$$

After the calculation of pure component properties the mixture properties are then calculated using the following mixture rule:

$$Z_{mix} = \sum_{i=1}^{N} x_i Z_i \tag{4.93}$$

Where, Z represents a general property value.

For activity coefficients, wherever experimental values were not available, various models can be used depending on the system [105].

4.2.5.2 Polymer properties - porous membranes

This section contains equations for effective diffusivities of components through porous polymer and membrane parameters. The Knudsen diffusivity for species i is given as [73]:

$$D_{kie} = K_0 v_i = K_0 \left(\frac{8RT}{\pi M_i}^{0.5} \right) \tag{4.94}$$

where K_0 is the membrane parameter, M_i is the molecular weight of the component i passing through the membrane.

The pressure independent diffusivity is given as [73]:

$$D_{ije}^0 = p D_{ije} \tag{4.95}$$

The effective molecular diffusivity is given by [73]:

$$D_{ije} = K_1 D_{ij} \tag{4.96}$$

where K_1 is the membrane parameter. The constants K_0, K_1 and B_0 depend on membrane geometry and interaction of membrane and molecule. Due to complex geometries of most membranes, the direct calculations of these constant is difficult. So, it is better to use experimental values wherever possible. However, estimates of these constants can be obtained from membrane pore diameter r, porosity ϵ, tortousity factor τ (assuming membrane consists of uniform cylindrical pores):

$$K_0 = \frac{2r\epsilon}{3\tau} \tag{4.97}$$

$$K_1 = \frac{\epsilon}{\tau} \tag{4.98}$$

$$B_0 = \frac{r^2 \epsilon}{8\tau} \tag{4.99}$$

Tortousity factor is applied to correct for the fact that the actual distance traveled by a molecule through the membrane is larger than the membrane thickness. This is

due to variation in pore sectional area, pore tortousity and that some pores can be blind. Even though this factor has a physical meaning, it is generally used as a fitting parameter for correlating experimental data [50]. Some theoretical and empirical models are available for predicting this factor from porosity of the membrane. One of the most successfully applied empirical correlation is:

$$\tau = \frac{(2 - \epsilon)}{\epsilon} \tag{4.100}$$

This correlation has been successfully been applied for porous support layer of reverse osmosis membranes. For polymer structures of random clusters, fractal theories of random walks predicts a tortousity factor:

$$\tau = \frac{1}{\epsilon} \tag{4.101}$$

The difference between two groups of membranes is due to manufacturing methods and resulting pore morphologies.

4.2.5.3 Polymer properties: non-porous polymers

The properties of interest in this case are solubility and diffusivity and hence permeability of penetrants through the polymers. The models are given in Section 4.2.5.1 for the property models.

4.2.6 Definition equations

The definition of molar fractions of the components require that in all the cases it is necessary that the mole fractions on the permeate side and retentate side add to one. For example, the equation for the permeate side can be written as:

$$1 - \sum_{i=1}^{N_C} x_{i,P} = 0 \tag{4.102}$$

And molar fraction of the component i on the permeate side can be calculated by dividing the flux of that component by total flux on the permeate.

$$x_{i,p} = \frac{R_i}{\sum\limits_{i=1}^{N} R_i + R_{ex}} \tag{4.103}$$

where, subscript ex represents flux of any stream on the permeate side, for example, water flux in case of DCMD or gas stream in case of SGMD etc..

The performance of the processes is usually measured with recovery and concentration factor of the desired component. Recovery of a component i, is defined as the ratio of mass of component i in the permeate stream to that in the feed stream. Mathematically [89]:

$$\text{Recovery} = \frac{m_{i,p}}{m_{i,f}} \tag{4.104}$$

Concentration factor (CF) of component i is defined as the ratio of molar (or mass) fraction of component i in the permeate stream to that in the feed stream.

$$CF = \frac{x_{i,p}}{x_{i,f}} \tag{4.105}$$

4.2.7 Model analysis and solution

The model is implemented through a computer aided modeling toolbox, ICAS-MoT [40], which also provides options for simulation. The model is a Differential Algebraic Equation (DAE) system, containing 2N+4 ordinary differential equations (ODEs), where N is the number of components in the system. Since most of the case studies considered in the system are with binary mixtures, the model analysis is done for N=2. For a binary mixture, there are 8 differential variables (total and component mass on both feed and permeate side (m_f, m_p, $m_{f,i}$ and $m_{p,i}$), temperature of bulk feed, and permeate side (T_f, T_p)), 145 algebraic variables (explicit or implicit, calculated from 145 equations (see Table 4.4), and 56 known parameters.

Models for individual processes can be derived from this general model by applying simplifying assumptions. Individual model details and variable analysis for each model is presented in Appendix A.

4.3 Model derivation: Membrane-based gas separation

In this section, a model for hollow fiber membrane module for membrane-based gas separation is developed. This model includes the balance equations and constitutive equations for membrane based gas separation. The model structure is similar to the general model for liquid separations using membrane based separation processes.

4.3.1 Model assumptions

- This model is limited to non-porous membranes.

- A constant density system is assumed.

- The resistance to heat and mass transfer is assumed to be located only in the active membrane layer, that is, resistances due to boundary layers on the sides of the membrane layer can be neglected.

Table 4.4: Variables in general model for membrane-based liquid separation with phase change

Differential Variables (8)		Number
Mass flow	m_f, m_p, $m_{f,i}$, $m_{p,i}$	6
Temperature	T_f, T_p	2
Algebraic Variables (145)		**Number**
Process variables	V_f, V_p, R_i, R_{total}, Q_m, T_{wf}, T_{wp}, T_{avg}, $Q_{process}$, $p_{i,wf}$ $p_{i,wp}$, $x_{i,wf}$, $x_{i,wp}$, C_t, x_f u_f, u_p, Recovery, CF	24
Flow parameters	Sh, Re, Sc, Nu, Pr	10
Component /mixture properties	ρ, Cp, $\Delta H_{vap,i}$ P_i^{Sat}, D_{ij}, μ, $k_{h,i}$, $\mu_{gas,i}$	96
Polymer properties	K_0, K_1, B_0, D_{ie}^k, D_{ije}^0, τ, P_i	10
Module parameters	dh	1
Transfer coefficients	h_f, h_p, h_m, k_m	4
Known Variables (56)		**Number**
Process variables	P_f, P_p, $x_{i,f}$	3
Component properties	M_i, γ_i	4
Regressed variables	5 variables for each pure component property	40
Polymer properties	ϵ, r_p	2
Module parameters	w, δ_m, L, h, n_f	5
Constants	R_g, π	2
For a binary mixture the total number of variables:		**209**

Table 4.5: Equations to be solved for membrane-based liquid separation with phase change

Variables	Number	Equations
Differential variables	8	4.3, 4.10, 4.12, 4.13, 4.20 4.21
Process variables	24	4.5, 4.6, 4.8, 4.9, 4.31, 4.15, 4.58, 4.59, 4.61, 4.60, 4.62, 4.66, 4.69 4.102, 4.103, 4.104, 4.105
Flow parameters	10	4.71, 4.75, 4.81, 4.80, 4.76
Component properties	96	4.85, 4.86, 4.87, 4.88, 4.89, 4.90, 4.91, 4.92, 4.93
Polymer properties	10	4.94, 4.95, 4.96, 4.97, 4.98, 4.99, 4.101
Module parameters	1	4.77
Transfer coefficient	4	4.70, 4.78, 4.60, 4.79

- For transport of low molecular weight gases through the membrane it is reasonably assumed that the solubility and diffusivity of gases are constant and independent of compositions in cases where sorbed concentration are low.

- No production or consumption of the transported gases through the membrane is assumed.

- Due to large bulk flow in the axial direction and rather small fiber diameter to fiber length, axial backmixing can be neglected.

4.3.2   Balance equations

4.3.2.1   Material balance

The setup of material balance for the membrane gas separation device comes from the continuity equation for component i. Since the components are only being transported through the membrane and there is no production and consumption of the components, the equation can be written as [14]:

$$\frac{\partial c_i}{\partial t} + (\nabla \cdot N_i) = 0 \tag{4.106}$$

where, N_i is the vector of flux of all the components and c_i is the composition of component i. Due to the motion of component i, there is a change in the molar composition of component i and the above equation describes this change in a multicomponent mixture with respect to time in a differential volume element fixed in space. The flux is due to both convective and conductive transport through the membrane.

Fig. 4.9 shows a schematic diagram of co- and counter-current membrane module. A shell-side feed flow has been shown in this case, but even if it was a tube side feed flow arrangement the derivation would lead to the same model equations. The equations are developed by applying the continuity equation Eq. 4.106 to a differential volume of infinitely small length δz on the permeate side. Note that an equally legitimate possibility would be to derive the equations on the retentate side.

As shown in Fig. 4.2, the hollow-fiber co- and counter-current membrane modules the fibers are tubular in shape, so a cylindrical coordinate system is chosen with its z-axis being the fiber axis. The change of flux in the angular coordinates is assumed to be neglected, hence the flux has components in the radial direction r and axial direction z. With the assumption of no axial backmixing, the conductive part of flux is only present in the radial direction. Even if the flow through the membrane is small, the conductive part could be rather large due to a large diffusion coefficient. It is also important to consider this term as it will introduce the transmembrane flux in the equations. Further, it is also assumed that the convective transport is only in the axial direction.

Co-current flow: Applying these assumptions, the mass balance equation at steady-state can be written as:

$$\frac{\partial c_i v_z}{\partial z} - D_i \frac{1}{r} \frac{\partial}{\partial r} \left(r \frac{\partial c_i}{\partial r} \right) = 0 \tag{4.107}$$
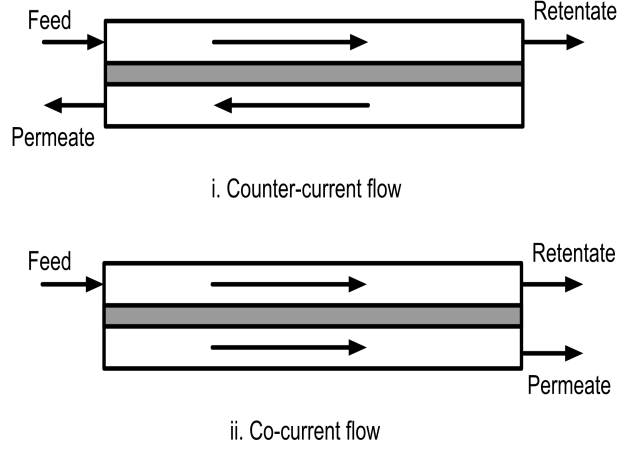
Figure 4.9: Flow patterns for gas separation membranes

where, v_z is the axial molar velocity coordinate resulting from axial pressure gradient. In the equation above D_i is the diffusion coefficient of component i in the gas mixture. Multiplying Eq. 4.107 with r and integrating between 0 and R, the inner radius of fiber bore, yields

$$\int_0^R r \left(\frac{\partial c_i}{\partial z} v_z + c_k \frac{\partial v_z}{\partial z} \right) dr - \int_0^R D_k \frac{\partial}{\partial r} \left(r \frac{\partial c_i}{\partial r} \right) dr = 0 \tag{4.108}$$

The axial velocity coordinate v_z can be written as

$$v_z = v_z(r, z) = v_{av}(z) F(r) \tag{4.109}$$

where, $v_{av}(z)$ is the axial average velocity (a function of z only), and $F(r)$ is a function of the radius covering the radial variation of v_z. In this way the axial velocity can be expressed in terms of an average velocity which does not depend on the radial coordinate can then can be taken out of the integral.

In case of parabolic velocity distribution the velocity profile in the radial direction is given by a function $F(r)$ as:

$$F(r) = 2 \left[1 - \left(\frac{\partial r}{\partial R}^2 \right) \right] \tag{4.110}$$

Substituting Eq. 4.109 and 4.110 into Eq. 4.108 and integrating, yields

$$\frac{\partial}{\partial z} \left(c_k v_{av} \right) \left(r^2 - \frac{1}{2R^2} r^4 \right) \Big|_0^R - D_k r \frac{\partial c_k}{\partial r} \Big|_0^R \tag{4.111}$$

subject to boundary condition at $r = 0$:

$$\frac{\partial c_k}{\partial r} \Big|_0 = 0 \tag{4.112}$$

and at $r = R$ as:

$$D_k \frac{\partial c_k}{\partial r}\bigg|_R = N_{Mi} \tag{4.113}$$

Substituting the boundary conditions into Eq. 4.111, we get

$$\frac{\partial}{\partial z}(c_k v_{av}) - \frac{2}{R} N_{Mi} \tag{4.114}$$

The factor 2/R in the above equation is related to the membrane A_M and the fiber bore volume V by equation:

$$a = \frac{A_M}{V} = \frac{2\pi RL}{\pi R^2 L} = \frac{2}{R} \tag{4.115}$$

where, L is the fiber length. Multiplying Eq. 4.114 by fiber bore volume we get:

$$L \frac{dn_{Pi}}{dz} - A_M N_{Mi} = 0 \tag{4.116}$$

where, n is the molar component flow rate of the streams on each side of membrane. The flux expression (Eq. 4.116) shows the mass flow for the permeate side. Variations are only considered in z-direction and no axial backmixing is assumed, so the only possibility for the permeate side of the membrane to change the component flow is through the membrane itself. In that case, a simple expression can be used to relate the retentate and the permeate side of the membrane. The change on the retentate component flow must be equal to the permeate component flow but in the opposite direction. So, the relation can be given as:

$$dn_{Pi} = -dn_{Ri} \tag{4.117}$$

where, n_{Pi} and n_{Ri} are the molar component flow rates on the permeate and the retentate respectively. The supplementary boundary condition is:

$$z = 0: \quad n_{Pi} = n_{Pi}^0 \tag{4.118}$$

Counter-current flow: In the counter-current case, since the directions of the flow of retentate and permeate are in the opposite directions, the corresponding relation is:

$$dn_{Pi} = dn_{Ri} \tag{4.119}$$

Integrating Eq. 4.117 and 4.119 from $z = 0$ to any arbitrary point z inside the module gives:

$$n_{Fi} + n_{Pi}^0 = n_{Pi}(z) + n_{Ri}(z) \tag{4.120}$$

where, subscript F represents the feed. For the counter-current case:

$$n_{Fi} = n_{Ri}(z) - n_{Pi}(z) + n_{Ri}^{ex} \tag{4.121}$$

where, subscript ex indicates flow rates at exit of the module. Similarly expressions to relate the total flow rates and permeate and retentate can be derived. Equations Eq. 4.120 and 4.121 express the retentate side component flow in terms of the permeate side component flow at each discrete point z of the membrane module.

as can be seen that the evaluation of the material balance equations, it is required to calculate the flux values on the retentate and the permeate side (constitutive equations I).

4.3.2.2 Momentum balance

In general, momentum balance describes the change of momentum with respect to time in a differential fluid volume element fixed in space, this change resulting from the net transport of the momentum into the volume element and the production or consumption of the momentum in the volume caused by the forces acting on the system. The momentum flux are expressed in terms of the velocity, hence the solution of the momentum balance yields the velocity profile in the volume element. Since velocity is represented by a value and a direction, the momentum balance is therefore a vector of differential equations which are in general coupled to the material balance over the velocity profile.

In order to simplify the solution, it is important to decouple the material balance from momentum balance. Since the formulation of the material balance requires molar flows using the average velocities, the velocities are not the dependent variables. Momentum balance can thus be reduced to obtain expressions to calculate pressure drop caused by the viscous flow of the gas in membrane module. Laminar flow is assumed in the module and the parameter of the resulting model can be described by *Hagen-Poiseuille equation.*

For a constant density, constant viscosity Newtonian fluid the velocity profile can be described by *Navier-Stokes equation*, given as:

$$\rho \left[\frac{\partial v}{\partial t} + (v \cdot \nabla v) \right] - \eta \nabla^2 v - \rho G + \nabla P = 0 \tag{4.122}$$

where, ρ and η are the density and viscosity of the mixture, respectively. ∇P is the pressure gradient representing the pressure drop. A pressure gradient is applied on the flow from an external source. Therefore the z-coordinate of the pressure gradient is non zero. A pressure gradient caused by volume forces (eg. gravity) are assumed to be negligible here. The axial pressure gradient must be independent from the radial coordinates, that is $\partial P / \partial r = 0$. Applying these assumptions Eq. 4.122 can be reduced to

$$\frac{dP}{dz} r = \eta \frac{d}{dr} \left(r \frac{dv_z}{dr} \right) = 0 \tag{4.123}$$

Integrating the above equations yields

$$\frac{dP}{dz} \frac{r}{2} = \eta \frac{v_z}{dr} \tag{4.124}$$

Applying the boundary condition $v_z(r = R) = 0$ due to adhesion, and integrating the above equation again:

$$v_z(r) = \frac{R^2}{4\eta} \left(-\frac{dP}{dz} \right) \left[1 - \left(\frac{r}{R^2} \right) \right] \tag{4.125}$$

The volumetric flow rate through the fiber bore $\dot{V}$ with $dA = 2\pi r dr$ is given as

$$\dot{V} = \int_0^R v_z(r) 2\pi r dr \tag{4.126}$$

where A is the cross sectional area of the fiber bore. Substituting velocity $v_z(r)$ in above equation with the parabolic velocity profile Eq. 4.125 in the equation above and integrating yields:

$$\dot{V} = \frac{\pi R^4}{8\eta} \left(-\frac{dP}{dz} \right) \tag{4.127}$$

Eq. 4.127 is called *Hagen-Poiseuille equation*. The average axial velocity is then given by:

$$v_{av} = \frac{\dot{V}}{A} = \frac{R^2}{8\eta} \left(-\frac{dP}{dz} \right) \tag{4.128}$$

which gives the velocity profile

$$v_z(r) = v_{av}2 \left(1 - \frac{r}{R}^2 \right) \tag{4.129}$$

This equation has been used to integrate the material balance in the previous section. The *Hagen-Poiseuille equation* (Eq. 4.127), expresses the pressure drop in terms of volumetric flow rate, the geometry of flow channel and the viscosity of the fluid. It is necessary to relate the pressure drop with the molar flow in order to be able to solve the material balance and momentum balance simultaneously with same reference frame. In general, the PVT-behaviour of the gas in the fiber bore can be written as

$$z = \frac{PV}{nR_gT} \tag{4.130}$$

where, n indicates the number of moles and z is the compressibility. For ideal case, $z = 1$, and then this equation can be used to substitute molar flow in Eq. 4.127 to give:

$$n = \frac{\pi R^4 P}{8\eta R_g T} \left(-\frac{dP}{dz} \right) \tag{4.131}$$

4.3.2.3   Energy balance

Membrane gas separation is in general a non isothermal process. This is due to *Joule-Thomson effect*, which comes into play when the gas is expanded across the membrane. In such a case of adiabatic expansion of real gas, the temperature may change to a large extent depending on the type of gas and applied pressure. In turn this temperature change can have an effect on the transport by effecting the permeabilities. The temperature dependency of the permeabilities can be can be introduced by an Arrhenius type expression. For the gas expanding from high pressure feed side to the low pressure permeate side, the internal energy change ΔU is given as:

$$\Delta U = U_P - U_F = -P_P V_P + P_F V_F \tag{4.132}$$
$$\Rightarrow U_F + P_F V_F = U_P + P_P V_P \tag{4.133}$$
$$\Rightarrow H_F = H_P \tag{4.134}$$

This implies that process is isenthalpic. The temperature change of this process is expressed by $(\partial T/\partial P)_H$, also known as **Joule-Thomson coefficient** μ_{JT}. For the enthalpy change of a reversible process can be written as

$$dH = VdP + TdS \tag{4.135}$$

Differentiating with respect to P at constant temperature gives

$$\left(\frac{\partial H}{\partial P}\right)_T = V + T\left(\frac{\partial S}{\partial P}\right)_T \tag{4.136}$$

From Maxwell's relations we have

$$-\left(\frac{\partial S}{\partial P}\right)_T = \left(\frac{\partial V}{\partial T}\right)_P \tag{4.137}$$

Substituting and rearranging

$$\left(\frac{\partial T}{\partial P}\right)_H = \mu_{JT} = -\frac{1}{C_p}\left[V - T\left(\frac{\partial V}{\partial T}\right)_P\right] \tag{4.138}$$

Depending on the relative magnitude of two terms between brackets the gas is either cooled or warmed upon pressurizing. For a real gas the isenthalps in a PT-plot have a bow shape so that any movement on the isenthalps due to a change in pressure results in a change in temperature. Estimation of temperature effects is of interest here, mainly because permeabilities of gases is a function of temperature and that can greatly change the transport of the gases. Also because a large temperature drop can lead to condensation of permeate gas. This can be avoided by preheating the feed gas. In general, application of such a model requires detailed knowledge of membrane, such as heat transfer coefficients and activation energies etc. A different approach is taken here, as these data are generally not available for commercial membranes.

A total energy balance around the entire membrane module assuming that no work is done on the system at steady-state yields

$$Q_{out} + H_F\left(T_F, P_F, n_{Fi}\right) - H_F\left(T_R, P_R, n_{Ri}\right) - H_F\left(T_P, P_P, n_{Pi}\right) = 0 \tag{4.139}$$

where H_F, H_R, and H_P are the enthalpies of the feed, retentate and permeate respectively, and Q_{out} denotes the heat release or uptake by module. If Joule-Thomson coefficient is very small then the process is isothermal and then $T_F = T_R = T_P$ and in that case the above equation can be used to calculate Q_{out}. In a second case, if adiabatic operation is assumed ($Q_{out} = 0$), then the outlet temperature $T_{out} = T_R = T_P \neq T_F$ can be calculated from the equation.

4.3.3 Constitutive equations I

This section evaluates the flux of different components through the membrane. Mass transfer in gas separation membranes is very similar to pervaporation process. In this work, non-porous membranes are considered which are also more attractive for

commercial purposes. The mass transfer mechanism is very different as compared to the porous membranes. In this case the transport of the gases is by three steps. The gas molecules first get dissolved at the feed side of the membrane then diffuse through the membrane and finally dissolves in the permeate flow. The mechanism is *solution-diffusion mechanism*, which is both thermodynamically (solution) and kinetically (diffusion) driven.

The derivation of the equations is given in Section 4.2.3.4. For any component i diffusing through the polymer it can be given as:

$$N_{Mi} = \frac{P_i}{\delta_m} (p_{i,f} - p_{i,p})$$ (4.140)

where P_i is the permeability of the gas i through the polymer, δ_m is the membrane thickness, $p_{i,f}$ and $p_{i,p}$ are partial pressure of component i on the feed and the permeate side of the membrane respectively.

For the evaluation of the partial pressure of the gases, constitutive equations II are given in next section.

4.3.4 Constitutive equation II

At the interface of the membrane there is an existence of phase equilibrium. This equilibrium relation can be used to connect the concentration of the components in the bulk feed solution and the concentration of the gas at the face of the membrane. Solution equilibrium for the permeate side gives

$$p_{Pi} = P_P y_i \phi_{Pi}$$ (4.141)

and for the retentate side it is given as

$$p_{Ri} = P_R x_i \phi_{Ri}$$ (4.142)

where, ϕ_{Ri} and ϕPi are the corresponding fugacities in the gas flow. x_i and y_i are the molar composition on the retentate and the permeate side, while, P_R and P_P are the pressures on each side of the membrane. Fugacities are in general a function of temperature, pressure and composition.

For low sorbate compositions of low molecular weight components in rubbery polymers it can be assumed that solubility is constant and is independent of composition [58]. For ideal gases, the above expressions reduce to

$$p_{Pi} = P_P y_i$$ (4.143)

and

$$p_{Ri} = P_R x_i$$ (4.144)

Substituting, Eq. 4.141 and 4.142 in flux equation (4.33) yields the transmembrane mass flux given as:

$$N_{Mi} = P_i \left(x_i \phi_{Ri} P_R - y_k \phi_{Pi} P_P \right)$$ (4.145)

Equation 4.145 gives a non linear driving force with respect to composition. The fugacity coefficients can be calculated using any suitable equation of state. However, in case where ideal gas mixture can be assumed, the fugacities are equal to one and the above flux equation gives a linear driving force with respect to composition. Substituting this flux equation in the material balance equation (4.116):

$$L\frac{dn_{Pi}}{dz} - P_i A_M \left(\frac{n_{Ri}}{n_{RT}}\phi_{Ri}P_R - \frac{n_{Pi}}{n_{PT}}\phi_{Pi}P_P\right) = 0 \tag{4.146}$$

Further simplification can be obtained by substituting the component molar flow on the retentate side (Eq. 4.120, 4.121) in the equation above. For the counter-current case:

$$L\frac{dn_{Pi}}{dz} - P_i A_M \left(\frac{n_{Fi} + n_{Pk}^0 - n_{Pi}}{n_{FT} + n_{PT}^0 - n_{PT}}\phi_{Ri}P_R - \frac{n_{Pi}}{n_{PT}}\phi_{Pi}P_P\right) = 0 \tag{4.147}$$

For the co-current case:

$$L\frac{dn_{Pi}}{dz} - P_i A_M \left(\frac{n_{Fi} + n_{Pi} - n_{Pi}^{ex}}{n_{FT} + n_{PT} - n_{PT}^{ex}}\phi_{Ri}P_R - \frac{n_{Pi}}{n_{PT}}\phi_{Pi}P_P\right) = 0 \tag{4.148}$$

In both cases it is necessary that the mole fractions on the permeate side and retentate side add to one. For example, the equation for the permeate side can be written as:

$$n_{PT} - \sum_{i=1}^{N_C} n_{Pi} = 0 \tag{4.149}$$

4.3.4.1 Dimensionless equations

For better scaling of the model, dimensionless variables have been introduced as:

$$X = \frac{z}{L} \quad u_i = \frac{n_{Pi}}{n_{FT}} \quad U = \frac{n_{PT}}{n_{FT}} \quad z_i = \frac{n_{Fi}}{n_{FT}} \quad p_P = \frac{P_P}{P_P^{ex}} \quad p_R = \frac{P_R}{P_F} \tag{4.150}$$

So, inserting dimensionless variables in the material balance equations 4.147 and 4.148, we get:

$$\frac{du_i}{dX} - Q_i \left(\frac{z_i + s_i - u_i}{1 + S - U}\phi_{Ri}p_R - \gamma\frac{u_i}{U}\phi_{Pi}p_P\right) = 0 \tag{4.151}$$

for the co-current case, and

$$\frac{du_i}{dX} - Q_i \left(\frac{z_i + s_i - u_i^{ex}}{1 + U - U^{ex}}\phi_{Ri}p_R - \gamma\frac{u_i}{U}\phi_{Pi}p_P\right) = 0 \tag{4.152}$$

for the counter-current case. The dimensionless sweep stream component and overall flow rates are denoted by s_i and S, respectively and are obtained by normalization on feed flow rate. the boundary condition becomes:

$$X = 0: \quad u_k = s_k \tag{4.153}$$

the dimensionless parameters Q_i and γ are defined as:

$$Q_i = \frac{q_i A_M P_F}{n_{FT}} \quad and \gamma = \frac{P_P^{ex}}{P_F} \tag{4.154}$$

where, Q_i can be interpreted as ratio of maximum possible flow of component i through the membrane to that of feed flow. Dimensionless form of Eq. 4.149 is given by

$$U - \sum_{i=1}^{N_C} = 0 \tag{4.155}$$

These equations simultaneously with retentate side equations are then solved to get profiles for u_k and U.

Dimensionless form of the momentum balance is given as:

$$p_P \frac{dp_P}{dX} + K_P U = 0 \tag{4.156}$$

where,

$$K_P = \frac{8\eta R_g T L n_{FT}}{\pi R^4 P_P^{ex2} n_f} \tag{4.157}$$

where n_f is the number of fibers. And this equation is supplemented by the dimensionless boundary condition

$$X = 1 : \quad p_P = 1 \tag{4.158}$$

The momentum balance states that the pressure drop is proportional to the molar flow rate of the respective flow.

4.3.5 Model analysis and solution

The model was implemented through a computer aided modeling toolbox, ICAS-MoT [102], and solved as in the case of membrane-based liquid separations. The model is a Differential Algebraic Equation (DAE) system, containing 2N+2 ordinary differential equations (ODEs), where N is the number of components in the system. In this case also binary mixtures are considered and the model analysis is illustrated for N=2. The model has 33 variables, out of which 6 are differential equations (mass flow on retentate and permeate side for each component ($n_{P,i}$ and $n_{R,i}$), pressure of bulk feed, and permeate side (P_F, P_P)), 16 algebraic variables (solved by 16 implicit or explicit equations) and 11 known variables. All these variables are shown in Table 4.6.

In order to simulation the model for membrane-based gas separation equations given in Table 4.7.

Table 4.6: Variables in membrane-based gas separation model

Differential Variables		Number
Mass flow rates	$n_{P,i}$ and $n_{R,i}$	4
Pressure	P_F, P_P	2
Algebraic Variables		**Number**
Process variables	$N_{m,i}, p_{i,F}, p_{i,P}, y_i, x_i$,	10
Component properties	$\phi_{P,i}$, $\phi_{R,i}$	4
Polymer properties	P_i	2
Known Variables		**Number**
Process variables	$n_{F,i}, T_F, T_P$	4
Module parameters	R, δ_m, L, A_M, n_f	5
Constants	R_g, π	2
For a binary mixture the total number of variables:		**33**

Table 4.7: Model equations to be solved to simulate the membrane-based gas separation model

	Equations	Number
Differential variables	4.116, 4.117, 4.119 and 4.156	6
Process variables	4.140, 4.120, 4.121, 4.139, 4.141, 4.142, 4.143, 4.144, 4.149	10
Component properties	ϕ_i: SRK model is used	4
Polymer properties	P_i : Closed-form model is used	2
Module parameters	A_M: 4.115	1

4.4 Property models

In this section, property models will be shown to relate the properties to not only process parameters like temperature but also to various functional groups in the component in case of component properties and product (polymer) parameters like monomer structure, chain length of the polymer, branch length etc. in case of polymer property models. Various property models shown in the subsequent sections are based on group contribution methods and atomistic simulations.

4.4.1 Group contribution models

The basic idea behind Group Contribution estimates is the addition of empirically-derived quantities, each characteristic of a chemical subunit of the compound in question. The derivation of parameters and the subsequent summation are performed to a prescribed formula in order to arrive at an estimate of the desired material property.

Group contribution methods, also known as Group Additivity relationships, are useful for correlating a material property with the chemical composition and state of matter of a substance. Useful methods have arisen for correlating properties of

small molecule gases and liquids, crystals, and polymeric materials.

The underlying idea of any Group Contribution method is as follows: whereas there are thousands of chemical compounds of interest to science and technology, the number of structural and functional groups which constitute all these compounds is very much smaller. The basic assumption is made that the physical property of a material (gas, liquid or solid) is a sum of contributions from each of the material's component parts. The fundamental assumption is additivity of these contributions.

The development and use of Group Contribution methods proceeds in two stages:

- The properties of known materials are correlated with their chemical structure, in order to identify the basic groups and their Additive Molar Quantities (AMQ's), in the nomenclature of van Krevelen.

- The properties of unknown materials are estimated through direct addition of AMQ's from constituent chemical groups, or through the use of additive quantities to estimate parameters in more accurate correlations.

These methods are largely empirical. In some cases, theoretical knowledge about the interdependence of material properties may be used as a guide in developing correlations.

Nevertheless, the definition of constituent "groups" is a very subjective matter. At one extreme, one may assume that only the basic atoms need be distinguished. However, we know that carbon in diamond exhibits very different properties from carbon in graphite. Even further, a carbonyl in a ketone is likely to exhibit different properties from the carbonyl in an organic acid. However, experience suggests that the carbonyl in most ketones, at least, are similar. Of course, the accuracy of any group contribution method increases as more and more distinctions are made between groups, until ultimately every compound comprises its own "group". The utility in the method comes from the wise selection of groups such that the number of groups remains small, but the accuracy of property estimation is still acceptable.

4.4.1.1 Pure component properties

A computer aided property predictive tool called "Pro-Pred" which is based on group contribution methods has been used in this work to predict pure component properties [78]. In computer aided process and product design, simple, efficient, and reliable methods for the estimation of properties of organic compounds from their molecular structure are essential for the analysis and design of products and processes. In particularly, for the cases where experimental physical property data is not readily available for various process conditions.

The basic group contribution (GC) method consists contributions for the first-order functional groups. These groups are used as building blocks to describe molecular structures. And the summation of the contributions times the number of occurance of the functional group in the molecule is the prediction for that property. For any

property GC model can be written as [114]:

$$f(Y) = \sum_i N_i C_i \qquad (4.159)$$

where $f(Y)$ is a property function for the property Y to be estimated, N_i is number of times the group G_i appears in the molecule, and C_i is the contribution of the group G_i to the property function $f(Y)$. The contribution of each functional group in the molecule is usually obtained through regression over a data set of chemical compounds and their corresponding experimentally measured values for property Y.

The estimation is done in this work using Marrero-Gani group contribution method [78, 79]. Brief introduction to the model are presented here to give the reader some idea of the prediction approach. Details can be read in the journal articles. In this approach, a new method has been developed where the molecular structure of a compound is considered to be a collection of three types of groups: first-order groups, second-order groups and third-order groups. The first-orders groups are intended to describe a wide variety of organic compounds, while the role of the second and third-order groups is to provide more structural information about molecular fragments of compounds whose description is insufficient through the first-order groups. Thus, the estimation is performed at three successive levels, where, the first level provides an initial approximation that is improved at the second level and further refined (if necessary) at the third level. The ultimate objective of this multilevel scheme of estimation is to enhance the accuracy, reliability and the range of application for a number of important pure component properties.

The first order groups contain a wide variety of chemical classes including both aromatic and aliphatic hydrocarbons. The idea is that each group should be as small as possible because very large groups are not desirable. The set of first-order groups also allows the distinction between groups occurring in cyclic and acyclic structures. In this model, first-order groups describe the entire molecule. In other words, there is no fragment of a given molecule that cannot be represented by first-order groups. It is be also required that no atom of the molecule can be included in more than one group, which implies that no group is allowed to overlap any other first-order group. And lastly, the contribution of any first-order group is independent of the molecule in which the group occurs, which satisfies one of the fundamental principles of the group-contribution approach.

The second level involves groups that permit a better description of polyfunctional compounds and differentiation among isomers. At the second level of approximation, there are some compounds that do not need any second-order group. The properties of these compounds (simple and monofunctional) are expected to be satisfactorily estimated after a first level of approximation. Contrary to the case of first-order groups, the entire molecule does not need to be described with second-order groups. Second-order groups are intended to describe only molecular fragments that could not be adequately described by first-order groups, and thereby yielded a poor estimation at the first level. The set of second-order groups should allow the differentiation among isomers. Accordingly, specific groups are provided with this

objective in mind. Second-order groups are allowed to overlap each other. That is, a specific atom of the molecule may be included in more than one group, contrary to the case of first-order groups. The contribution of any group should be equal in whichever molecule the group occurs, which makes it possible to satisfy one of the fundamental principles of the group-contribution approach in the case of second-order groups.

The criteria used for the identification of third-order groups are analogous to those used for second-order groups. These groups allow a quite detailed representation of systems of fused aromatic rings, systems of fused aromatic and non-aromatic rings, and systems of non-fused rings joined by chains in which can occur different functional groups.

The proposed property-estimation model in this case has the form of the following equation:

$$f\left(\underline{\xi}\right) = \sum_i N_i C_i + \omega \sum_j M_j D_j + z \sum_k O_k E_k \qquad (4.160)$$

where, C_i is the contribution of the first-order group of type i that occurs N_i times, D_j the contribution of the second-order group of type j that occurs M_j times and E_k the contribution of the third-order group of type k that has O_k occurrences in a compound. In the first level of estimation, the constants w and z are assigned zero values because only first-order groups are employed. In the second level, the constants w and z are assigned unity and zero values, respectively because only first- and second-order groups are involved while in the third level, both w and z are set to unity values. The left-hand side of Eq. 4.160 is a simple function $f(X)$ of the target property X. The determination of the adjustable parameters of the models, that is, the contributions C_i, D_j and E_k has been divided into a three-step regression procedure.

1. Regression is carried out to determine the contributions (C_i) of the first-order groups and the universal constants of the models while w and z are set to zero.

2. Then w is set to unity, z is set to zero and another regression is performed using the C_i and the universal constants calculated in the previous step to determine the contributions (D_j) of the second-order groups.

3. Finally, both w and z are assigned to unity and, using the universal constants of the models (C_i and D_j obtained as results of the previous steps), the contributions (E_k) of the third-order groups are determined.

This model is implemented in a property prediction tool Pro-Pred, which has been used in this work to predict liquid density (ρ_i), liquid viscosity (μ_i), specific heat (Cp_i), thermal conductivity (k_i), infinite dilution diffusion coefficients (D_i), gas viscosity (μ_{gi}), heat of vaporization (δH_i), vapor pressure (P^{sat}) and Critical temperature (T_C).

4.4.1.2 Permeability of gases in polymers

A lot of efforts have been put in order to obtain experimental data of gas permeability in various polymers. Such experimental data is available in literature and attempts have been made to learn the principals that govern the relationship between gas permeability and polymer repeat unit in order to be able to design better gas separation units. To be able to have a guideline for the development of new polymers there is a need to quantitatively correlate this information in literature. Several empirical/semi-empirical group contribution type models have been developed. For example, 'Permachor' approach where Permachor parameter has been calculated for each polymer calculated from empirically derived factors for each chemical group in polymer repeat unit [114]. Bicerano [12] has proposed model that considers cohesive energy, packing and rotational degrees of freedom of the polymers. The model predicts permeabilities for low permeability polymers. In this work, we have followed the group contribution model proposed by Paul et.al. [95] based on fractional free volume.

The diffusion coefficient of the gas through a polymer varies from polymer to polymer to a much larger extent as compared to the solubility coefficient. The most important factor on which the diffusion coefficient and solubility coefficient depends is the free volume of the polymer. And so it is reasonable to correlate the permeability coefficient to the free volume. Extensive work has been done to show the utility of the expression in the following form:

$$P_i = A_i exp \left[\frac{-B_i}{FFV_i} \right] \tag{4.161}$$

Where, A_i and B_i are constants for a particular gas i. The fractional free volume, FFV_i, has been defined as

$$FFV_i = \frac{[V - (V_0)_i]}{V} \tag{4.162}$$

Here, V is the volume of the polymer which is obtained from experimental measurement of the polymer density at the temperature of interest. The term V_0 is the volume occupied by polymer chains. Most commonly V_0 has been modeled by using Bondi's group contribution method where occupied volume is computed from van der Waals volume V_W of various groups in the polymer. For any gas i:

$$(V_0)_i = \sum_{n=1}^{N} \gamma_{in} (V_W)_n \tag{4.163}$$

and

$$V = \sum_{n=1}^{N} \beta_n (V_W)_n \tag{4.164}$$

Where, γ_{in} and β_n represents a set of empirical factors.

4.4.2 Molecular modeling

Molecular modeling has been mainly used in this work to generate pseudo-experimental data relating permeability to the structure of polymer. The next step is to use the generated data to develop higher order group contribution methods and/or closed form property models that take into account the parameters that define the branched architecture of polymers and relate them to the properties of interest.

In this work, the properties of interest here, namely, diffusion coefficient and solubility of small gases in polymer matrices are predicted using MD simulations. To do so, a hierarchical modeling approach (see Fig. 4.10) is proposed as follows.

Stage I: MD simulations to extract information about the density, radius of gyration and static structure factor (i.e. local packing of polymer atoms) and to obtain extensively equilibrated trajectories.

Step 1: Choose a monomer structure and temperature

In this step, the monomer structure of the polymer whose barrier properties are to be predicted is chosen. A simulation box (amorphous cell) is created with the polymer chains of a length at which we want to predict the permeability. While choosing the number of chains in the simulation box, care must be taken to have approximately 4000 "united atoms" or about 30 Åbox length to avoid system size effects [85]. For small systems, the number of molecules in the system might be too small to have good statistics.

Step 2: Obtain force field parameters of the groups in the polymer

It is crucial to have very good force fields to realistically and very closely reproduce all inter atomic interactions and very efficient methods to relax the systems within modest time. United-atom approach have been employed at this step, which means treating groups of atoms like -CH3, -CH2- as single sites. This greatly reduces the computational complexity and computation time. The algorithm require a reliable polymer force field that predicts the static properties of the polymer as closely as possible. Various parameters needed for the calculation of potential energy are listed in Table 4.8. This step might include tuning of force field parameters, which could involve some trial and error iterations (see Fig. 4.10). An extremely important static property in our case is the density since it dominates both the dynamics and the barrier properties of the studied polymer. Density, in turn is very sensitive to the non-bonded Lennard/Jones potential parameters ϵ/σ. For example, we can tune Lennard/Jones potential to match experimental density. Either by increasing ϵ or decreasing σ the density increases. It is critical that the calculated density value closely resembles the experimental. A difference exceeding 2-3 % of experimental data may distort calculated quantities from the simulations (like self-chain diffusivity or the barrier properties (S, D, P)).
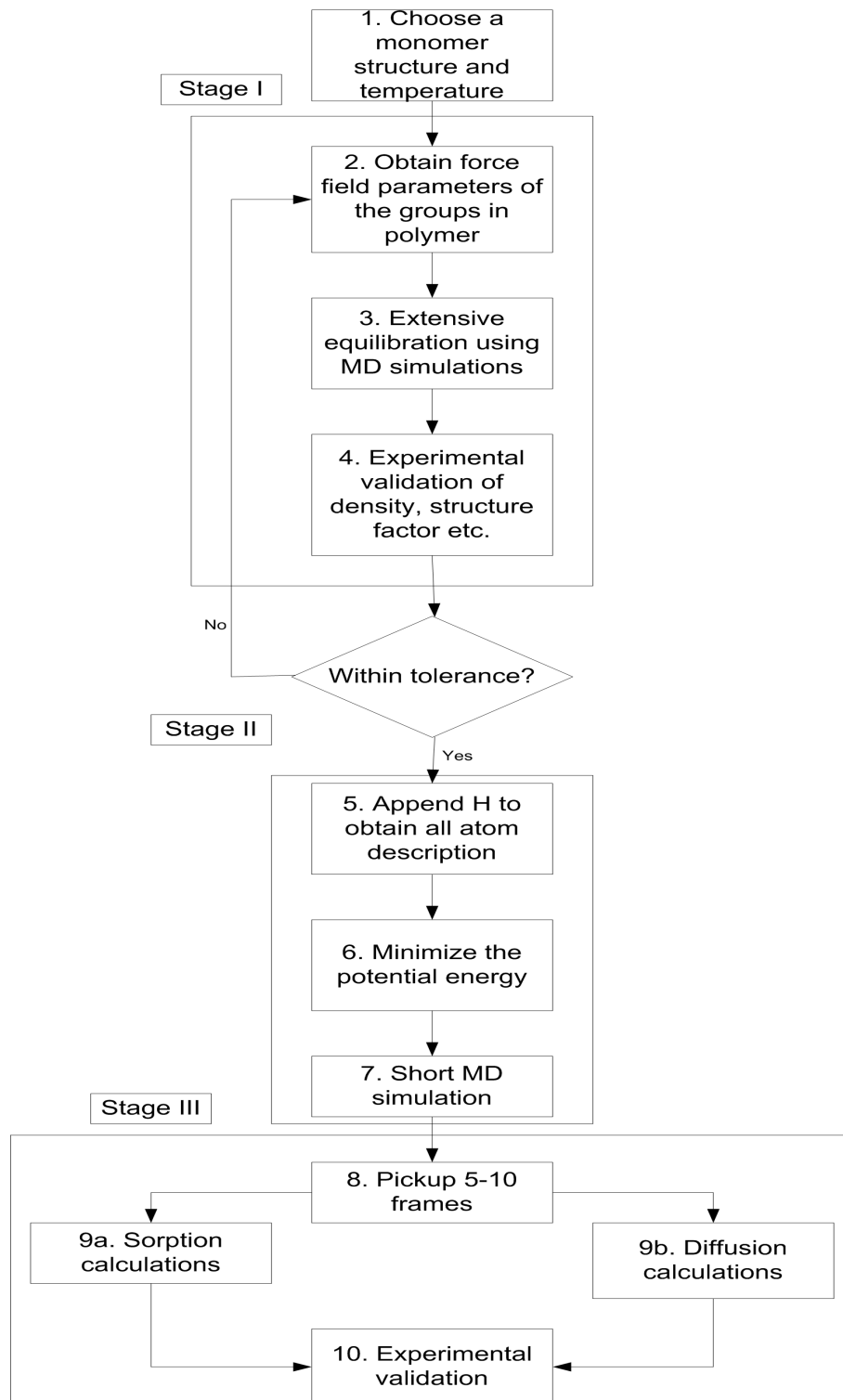
Figure 4.10: Hierarchal procedure to predict permeability properties of small penetrant gases in polymers

Potential terms	Parameters
i. Harmonic bond stretching	k_r, R_0
ii. Harmonic bond bending	k_θ, θ_0
iii.Torsional potential	k_ϕ
iv. Non bonded potential (Lennard/ Jones 6-12)	ε, σ

Table 4.8: Forcefield parameters

Step 3: Extensive equilibration using MD simulations

To ensure good initial structures (initial atomic positions and velocities) for MD simulations, the first step is to minimize the static energy of the amorphous cell with periodic boundaries. Then MD simulations are made to obtain equilibrated structures. Good results require realistic (in terms of system size) and fully equilibrated structures (atomic positions and velocities ensuring that the system has been relaxed meaning that the polymer chains have forgotten their initial configuration).

MD program LAMMPS has been used. The only input to this program is the initial minimized configuration (i.e. atomic positions and velocities). The generated three-dimensional structure undergoes extensive equilibration using NPT (ensemble) -simulation. Full-scale equilibration is obtained when:

- The system density (total mass of polymer atoms divided by the (fluctuating) simulation box volume) reaches a plateau value after a number of MD steps.

- The chain dimensions oscillate around a plateau value as quantified by the mean square end-to-end distance, $< R^2 >$ or the radius of gyration, $< Rg^2 >$ (for large molecular weights: $< Rg^2 >=< R^2 > /6$).

- The atomic packing is realistic. This is quantified mainly through the static structure factor, $S(k)$, which can be calculated experimentally.

All these properties normally oscillate around average values. Trajectories are picked to possess density and chain dimensions resembling averages obtained over all equilibrated frames of the MD trajectory.

Step 4: Experimental validation of physical, thermodynamical properties etc.

The results obtained up to this point allow to establish values of the properties like density, radial distribution function, distribution of bond lengths, bond angles, dihedral distributions etc. which are then compared against experimental data.

Stage II: Obtain all atom description.

Step 5: Obtain "all atoms" description by appending hydrogen atoms to the united atoms

A critical point for the barrier properties is that even the hydrogen atoms play a very important role in permeation. In the previous MD simulations (Step 3 of Stage I) we have used united atom descriptions (-CH2- and -CH3 are considered as (effective) single sites), so that no hydrogen atoms exist in the system. This is mainly done to save CPU time. For the properties calculated in Step 4, little difference is usually found. But for barrier properties, it is important to switch to an all-atom representation, which is done by appending hydrogen atoms to the center of mass of the "united atoms" to get an explicit atom representation.

Step 6: Minimize the potential energy

Upon addition of hydrogen to form new structures (bearing all atoms), overlaps between atoms may be created. This may lead to very high potential energies and unreliable property values later. So, it is crucial to minimize the static energy.

Step 7: Molecular dynamic simulation

A comparatively short canonical ensemble (NVT) MD simulation is done in order to equilibrate the newly added hydrogen atoms. This MD simulation is carried out for around 500 ps.

Stage III: Calculation of the end use properties.

This stage is the post processing stage where the barrier properties are calculated. It includes post-processing of the data (including both brute-force MD and Monte Carlo (MC) simulations) to extract information about the free volume, solubility, diffusivity and permeability of small gas molecules to a polymer matrix.

Step 8: Pick up frames

In this step, 5-10 repersenrative frames with density approximately equal to average density from the trajectory with appended hydrogen atoms obtained in the Step 7 are picked [77].

Step 9a: Prediction of solubility of penetrants in polymers

The built-in module for solubility calculations in Material studios [1] called Sorption is invoked in order to predict solubility (S) of small gas molecules in the polymer matrix. Average loading of small penetrants in a polymer for different fugacities can be calculated from Monte-Carlo simulations. Then a graphical method is employed to calculate solubility (or Henry's constant) of the penetrant. To do this, average loading of the gas molecules is plotted as a function of pressure and the slope gives Henry's constant (solubility).

Step 9b: Prediction of diffusivity of penetrants in polymers

109

A rather short MD (about 500 ps) is done after inserting the gas molecules in the already equilibrated polymer matrix. The mean squared displacement of the gas molecules is calculated and averaged over number of molecules. MSD versus time which is a straight line is plotted and the slope gives the diffusion coefficient. As mentioned in Chapter 3, diffusion of small molecules in polymer melts using MD simulation is most frequently calculated by means of the Einstein relationship given as:

$$D_\alpha = \frac{1}{6N_\alpha} \lim_{t \to \infty} \frac{d}{dt} \sum_{i=1}^{N_\alpha} \left\langle [r_i(t) - r_i(0)]^2 \right\rangle \tag{4.165}$$

where, r_i denotes the position vector of center of mass of species α, and angular brackets denote averaging over all choices of time origin within a dynamic trajectory. From an MD run, long enough to ensure that the system has reached the normal diffusive regime (when slope of the log of mean square displacement (MSD) as a function of log(t) is close to unity), a few well equilibrated and uncorrelated trajectories are extracted. The mean-square displacement (MSD) averaged over number of atoms (N) is plotted against time. The slope of this plot divided by 6 gives the diffusion coefficient of the penetrant molecule in the polymer matrix.

Once the solubility and diffusivity of small penetrants is calculated, the product of the two quantities gives the permeability of the penetrants.

4.5 Discussion/Conclusion

This chapter gives detailed models for liquid separation with phase change and for membrane-based gas separation. These models are very general and flexible that it is convinient to rearrange equations to be solved in either forward or reverse way. Various pure component property models needed by the process models as a function of temperature are presented. Property models for predicting barrier properties of the polymers used as membranes be using group contribution methods and molecular modeling are presented. A hierarchal approach for predicting permeability of small gases through polymers of different structures and at different conditions is presented in this chapter.

<div align="right">

5

</div>

<div align="right">

Case Studies

</div>

This chapter presents case studies from membrane-based separation processes to highlight different components of the model-based design framework and reverse design approach. This chapter is divided in two sections, the first section demonstrates the application/development of property models to predict pure component and polymer properties, and in the second section motivating examples illustrating the employment of the design framework developed in Chapter 2 for simultaneous process-product design.

Section 5.1 dealing with property prediction, describes in a step by step procedure to predict solubility and diffusivity of oxygen and nitrogen in polyisobutylene at various temperatures. This section also presents pure component property prediction of aroma compounds in black currant juice using group contribution models.

Section 5.2 demonstrates the process-product design for the case of enrichment of oxygen from air and of carbon dioxide from natural gas. A process-product design of recovery of aroma compounds from black currant juice is presented next in this section. A comparative case study to compare the process performance of various MD processes in terms of fluxes and end-use product purity is presented.

5.1   Property Prediction

5.1.1   Permeability calculations for Polyisobutylene using molecular modeling

The objective of this case study is to illustrate the application of a molecular modeling based hierarchal step-wise procedure for the prediction of diffusivites and solubilities of small gases through polymers at different temperatures. In particular the hierarchal procedure presented in Chapter 4 is applied here to predict the diffusivities and solubilities of oxygen and nitrogen at different temperatures in polymer polyisobutylene (PIB). Polyisobutylene is a synthetic rubber, or elastomer. Polyisobutylene, sometimes called butyl rubber, is a vinyl polymer. It is made from the monomer isobutylene, by cationic vinyl polymerization. The monomer structure is:

$$[-CH_2 - C\,(CH_3)_2 -]_n$$
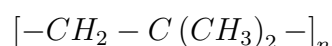
This polymer has been chosen because of the modeling challenge due to the presence of two methyl groups (CH_3) at every alternate carbon atom in the polymer chain and because we have permeability data for nitrogen and oxygen in polyethylene but none for higher olefins.

Permeability, which is a product of solubility and diffusivity, is obtained from the calculated solubilities and diffusivities of nitrogen and oxygen at temperatures ranging from 350-550 K for PIB of chain length of 48 carbon atoms. The application of the hierarchal procedure is highlighted for one value of diffusivity, solubility and permeability. all the calculated property values are presented in the form of tables at the end of the chapter together with a discussion on the computational time, accuracy and difficulties encountered during the calculation steps.

Stage I

The objective of Stage I is to run long MD simulations to extract information about the local packing of polymer atoms by calculating the density, radial distribution, etc. and to obtain extensively equilibrated trajectories. These simulations are very expensive and require a lot of CPU time. So, it is advantageous to run the simulations parallelly on a cluster of computers. LAMMPS is a molecular dynamic simulator that can run on single processor or parallel by using message-passing parallelism (MPI) technique. So, it was used for the stage I calculations. These calculations are performed in collaboration with ICE-FORTH, Patras, Greece, because of the availability of clusters of computers, source code for LAMMPS and a lot of experience in this field.

Step 1: Choose a monomer structure and temperature

PIB with 48 number of carbon atoms in each chain were chosen and 80 such chains were taken in the simulation box. To avoid system size effects the box length approximately above 30 Åand/or at least 4000 united atoms should be chosen. So, in this case the number of united atoms is 3840. This simulation was made at 500 K.

Step 2: Obtain force field parameters of the groups in the polymer

For Stage I calculations, "united atoms" were used to considerably save CPU time. In the PIB chain structure four group types are present, $> C <$, $-CH <$, $-CH_2-$, and $-CH_3$. A trial and error method was used to obtain the values of the force field parameters for a refined estimation of structural properties. The initial values taken from literature and are presented in Table 5.1 to 5.4 along with the new values from this work.

For bond stretching (two-body interaction), harmonic form of potential is used. It has the following form [16]:

$$E_{str} = \frac{1}{2} k_{str} \left(r - r_0 \right) \tag{5.1}$$

The parameters in the equation ($k_s tr$ and r_0) are given in Table 5.1. Details of these potential forms and the variables are presented in Chapter 3.

For bond bending (three-body interaction) also harmonic form of potential is used.

Table 5.1: Constants for potential function for bond stretching for the groups in PIB molecule

k_{str} (kcal/mol/Å²)	r_0 (Å)	Reference
633.35	1.54	[16]
1920.0	1.54	This work

It has the following form [93]:

$$E_\theta = \frac{1}{2} k_\theta \left(\theta - \theta_0\right) \tag{5.2}$$

The parameters in the equation (k_θ and θ_0) are given in Table 5.2

Table 5.2: Constants for potential function for bond angles for the groups in PIB molecule

Angle type	k_θ (kcal/mol/rad²)	θ_0 (rad)	Reference
CHx-C-CHx	124.2	109.47	[93]
	248.4	109.47	Current work
C-CHx-C	124.2	114.0	[93]
	248.4	116.0	Current work

For torsion potential (four-body interaction) following form of potential is used [16, 93]:

$$E_\phi = \frac{1}{2} V_3 \left(1 - cos3\phi\right) \tag{5.3}$$

The parameters in the equation are given in Table 5.3

Table 5.3: Constants for potential function for torsion angles for the groups in PIB molecule

Angle type	V_3 (kcal/mol)	Reference
CH$_2$-C-CH$_2$-C	3.25	[16]
(chain backbone)	3.25	Current work
CH$_3$-C-CH$_2$-C	3.25	[93]
	1.625	Current work

For non-bonded interaction Lennard-Jones (6-12) form of potential is used. It is given as [93]:

$$U_{LJ} = \epsilon \left[\left(\frac{\sigma}{r}\right)^{12} - \left(\frac{\sigma}{r}\right)^6 \right] \tag{5.4}$$

The parameters in the equation are given in Table 5.4

113

Table 5.4: Parameters for Lennard-Jones non-bonded potential for the groups in PIB molecule

Atom type	ϵ (kcal/mol)	σ (Å)	Reference
C	0.0338	3.91	
CH	0.0338	3.91	[93]
CH$_2$	0.091	3.93	
CH$_3$	0.148	3.91	

Step 3: Extensive equilibration using MD simulations

This step gives a simulation box with all the polymer chains which is at a relaxed state, i.e. the polymeric chains in the simulations box have moved to new positions and have no memory of the initial state. This can be obtained by extensively equilibrating the polymer chains through molecular dynamic (MD) simulation. This was done using a molecular dynamics simulator LAMMPS (details of this software are presented in Chapter 1). The simulations were made for an canonical ensemble (NVT) up to 100 ns real time which takes about 4-5 weeks on cluster of computers. During an MD simulation, various frames of the simulation box can be saved at various times. Frames are like pictures of the positions of the molecules in the system at different time points.

Step 4: Experimental validation of physical, thermodynamical properties etc.

In this step, various structural and static properties of the polymer can be compared to the available experimental values. Here, comparison is shown with density, radial distribution function, probability distribution of bond angles and torsional angles. Simulated vs experimental density is shown in Fig. 5.1.

The experimental densities of PIB at different temperatures is given by Boyd et.al.(1991) [16]. The simulated density of PIB with chain length of 48 carbon atoms is on an average 6-7% smaller than the experimental cases. This is due to the fact that the experimental values are measured at the polymeric regime with very high molecular weights. But for the simulated values, the chain length of the polymer is rather small (48 in number), and so has a low molecular weight. Due to the presence of more chain ends in a unit volume, due to smaller chains, the density of the polymer is smaller. Karayiannis et.al.(2002) has also reported a difference of about 6-8% between polymeric regime polyethylene and simulated polyethylene with 48 number of carbon atoms in the chain structure of polyethylene [58].

Fig. 5.2 shows the radial distribution function of PIB. A radial distribution function (RDF), describes how the density of surrounding matter varies as a function of the distance from a particular point. It gives some idea about the structure of the molecule. For example, the first peak in the figure is around 1.55 Å, which corresponds to the C-C bond (equilibrium value of C-C bond is 1.54 Å [93]).

Fig. 5.3 shows the bond angle distribution for PIB chains and a comparison is
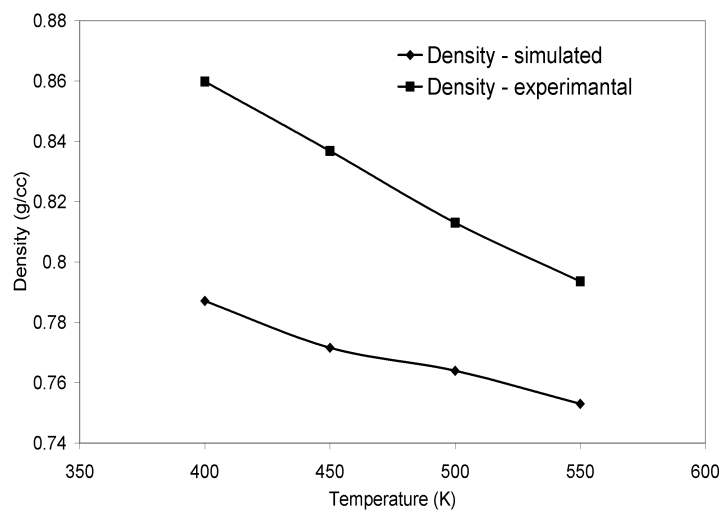
Figure 5.1: Density of PIB with chain length of 48 carbon atoms at different temperatures
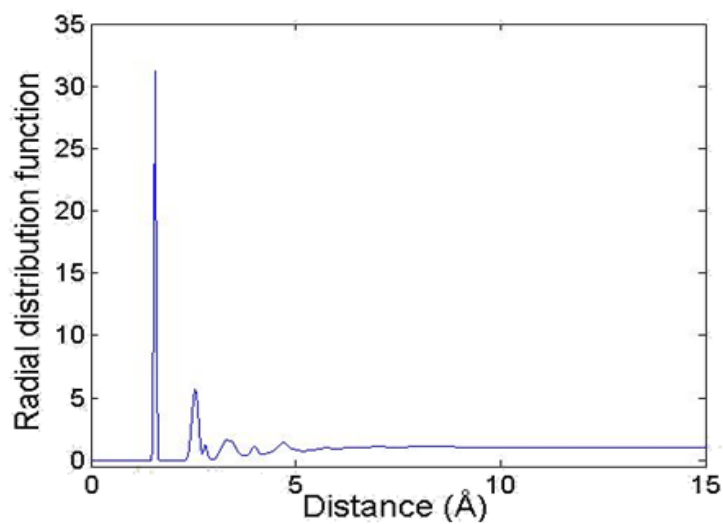
Figure 5.2: Radial distribution function of PIB: calculated by Georgia Tsolou at ICE-FORTH, Patras, Greece

given in Table 5.5.
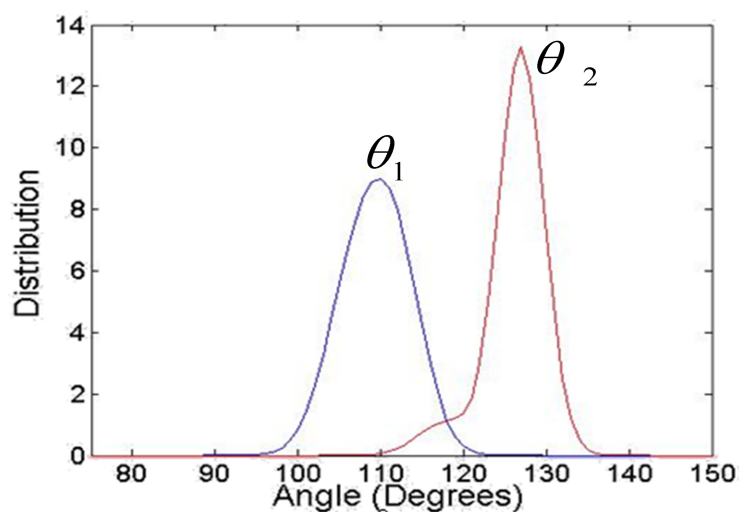
Figure 5.3: Bond angle distribution for PIB: calculated by Georgia Tsolou at ICE-FORTH, Patras, Greece

	Experimental [16]	Simulation
θ_1 : CH$_2$-C-CH$_2$	110°	109°
θ_2 : C-CH$_2$-C	128°	127°

Table 5.5: Comparison of bond angle of PIB chains: calculated by Georgia Tsolou at ICE-FORTH, Patras, Greece

Fig. 5.4 shows the torsion angle distribution for PIB chains and a comparison is given in Table 5.6.

	Experimental [93]	Simulation
T+	15°	13°
T-	-15°	-13°
G'+	127°	128°
G'-	106°	106°
G+	-106°	-106°
G-	-127°	128°

Table 5.6: Comparison of torsion angle for PIB chains

The equilibrated trajectories at different temperatures were provided by Georgia Tsolou. The structural properties shown above are comparable to the experimental values. After this confirmation that the trajectories resemble the real polymer in terms of the properties, few frames for the post processing to predict the diffusivity and the solubility are picked. The frames that have density values very close to the average density of the whole trajectory are chosen.
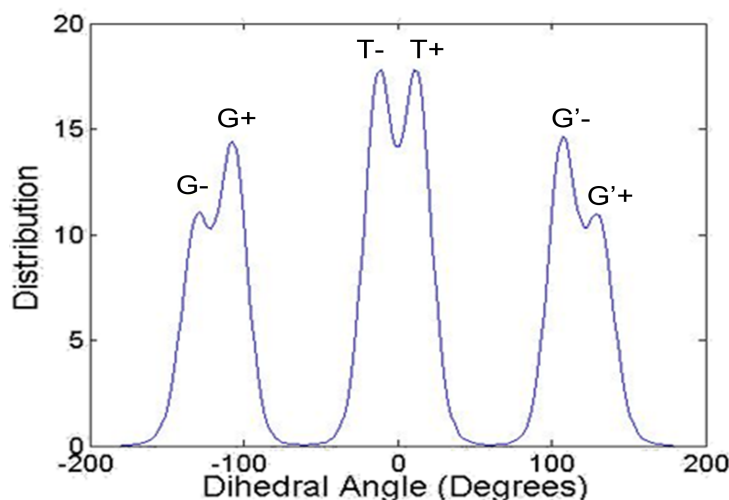
Figure 5.4: Torsion angle distribution for PIB

Stage II

In Stage I, for the extensive equilibration of the simulation box, "united-atoms" description was used. But for the prediction of the barrier properties, it is better to have an "all atoms" description because presence of the hydrogen atoms will have an effect on the free volume and hence the barrier properties of the polymer. So, the objective of this stage is to append hydrogens to the polymer chains and then equilibrate the simulation box again to relax the hydrogen atoms.

Step 5: Obtain "all atoms" description

Hydrogen atoms are appended to center of mass of the united atoms in the polymeric chains using Material Studio 4.0 (MS) from Accelrys.

Step 6: Minimize the potential energy

Potential energy of the simulation box might rise due to the addition of the hydrogen atoms, as some of them might overlap with each other during the addition. For this step also Material Studio was used. Genetic algorithms provided, as an option for the solution of the optimization problem, in the software has been used to obtain minimized energy. This calculation takes about 3-4 hours of CPU time.

Step 7: Molecular dynamic simulation

A comparatively short canonical ensemble (NVT) MD simulation is done in order to equilibrate the newly added hydrogen atoms. This MD simulation was done for about 500 ps which took approximately 4-5 weeks of CPU time for each simulation. In the end of this run hydrogen atoms are equilibrated.

Stage III

This stage is the post processing stage where the barrier properties are calculated.

Step 8: Pick up frames

In this step, 5 frames with density approximately equal to average density from the trajectory with appended hydrogen atoms obtained in the Step 7 were picked. These frames are then used to predict the solubility first and then the values are averaged for all the 5 frames.

Step 9a: Prediction of solubility of oxygen and nitrogen in PIB

In this step, the adsorption isotherm is obtained by plotting average loading of gas molecules at different pressures. The calculations are made in Material Studio's in-built tool to plot the adsorption isotherm. This tool used Metropolis Monte-Carlo method where trial configurations are generated without bias. The gas molecules are inserted into the polymer matrix and these insertions are accepted or rejected based on change of the total energy of the system (see Chapter 3). The adsorption isotherms for each of the 5 frames are plotted for both oxygen and nitrogen at 500K and are shown in Fig. 5.5 and Fig. 5.6 respectively. The average slope of this plot gives the Henry's constant and the inverse of slope is the solubility of the gas in the polymer [121]. The inverse of average slope for adsorption isotherm of oxygen at 500 K gives $S_{O_2} = (2.57\pm0.2)$e-5 mol/m^{3}Pa, and for Nitrogen gives $S_{N_2} = (2.33\pm0.4)$e-5 mol/m^{3}Pa. These calculations are reported for different temperatures and the results are shown at the end of this section.
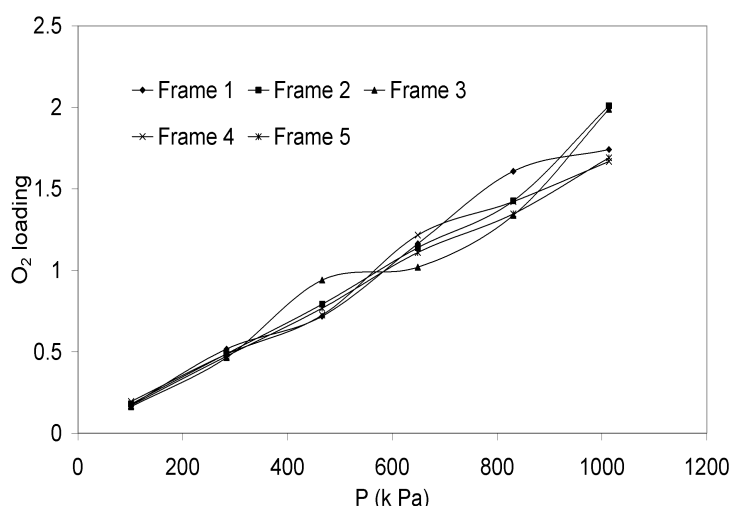
Figure 5.5: Adsorption isotherm for Oxygen in Polyisobutylene at 500 K

Step 9b: Prediction of diffusivity of oxygen and nitrogen in PIB
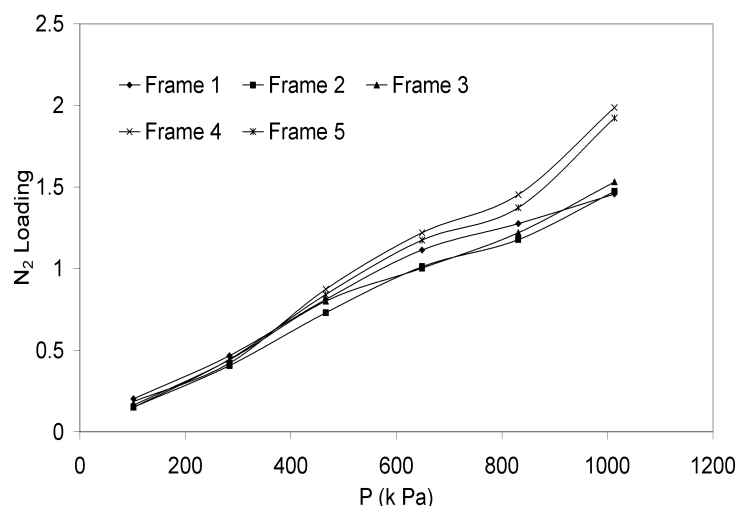
Figure 5.6: Adsorption isotherm for Nitrogen in Polyisobutylene at 500 K

For this step, 5-7 gas (oxygen or nitrogen in this case) molecules are inserted in the polymer matrix. The simulation box now containing the polymer chains and the gas molecules is then subjected to energy minimization to equilibrate the gas molecules in the simulation box. Then a simulation for about 150-200 ps is made using isobaric-isothermal (NPT) ensemble. To make sure that the system has reached the Fickian diffusion regime a plot of log of time vs. log of mean squared displacement (MSD) is evaluated. If the slope of this plot is close to 1 then the polymeric system is in the Fickian regime [58]. This plot for oxygen and nitrogen at 500K is shown in Fig. 5.7 and Fig. 5.8. In both these cases the slope of the graph is shown on the plot and is close to 1.
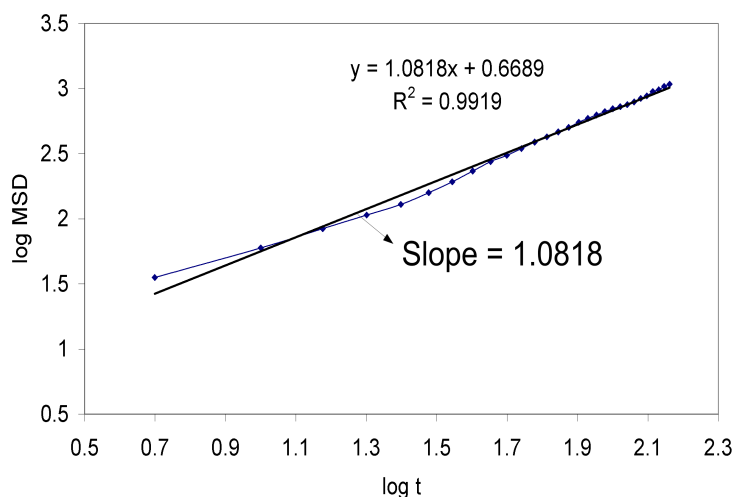
Figure 5.7: log(MSD) vs log(t) for Oxygen in Polyisobutylene at 500 K

The density plots Fig. 5.9 and Fig. 5.10 show the running average of density and the point density of the simulation box for oxygen and nitrogen respectively.

The Fig. 5.11 and Fig. 5.12 show the plots of time vs MSD. The slope of these
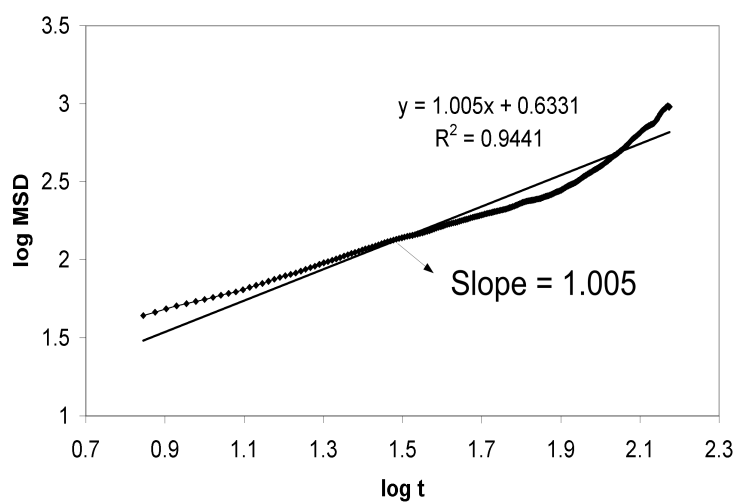
Figure 5.8: log(MSD) vs log(t) for Nitrogen in Polyisobutylene at 500 K
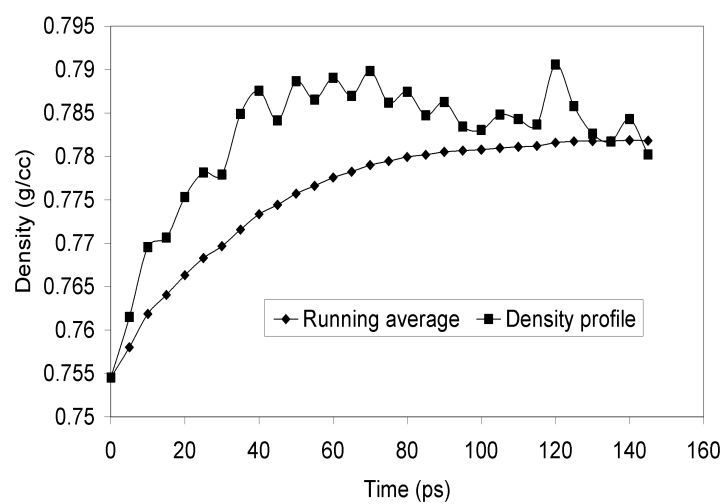
Figure 5.9: Density profile and running average of density for Oxygen in Polyisobutylene at 500 K
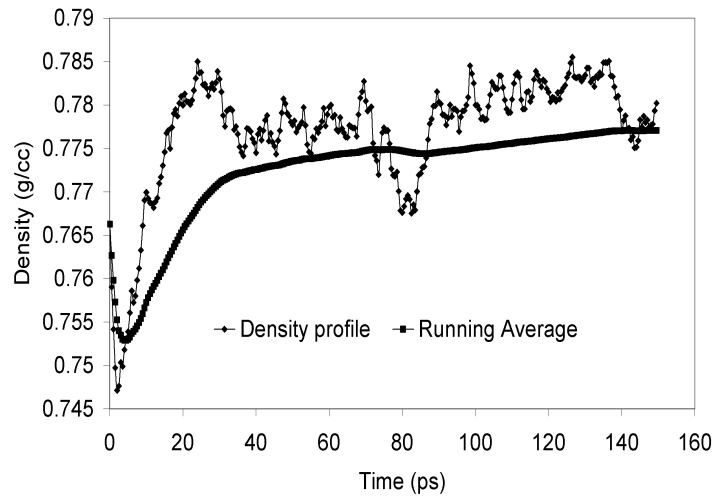
Figure 5.10: Density profile and running average of density for Nitrogen in Polyisobutylene at 500 K

plots divided by 6 gives the diffusivity of oxygen and nitrogen respectively in PIB at 500 K (see Chapter 3).
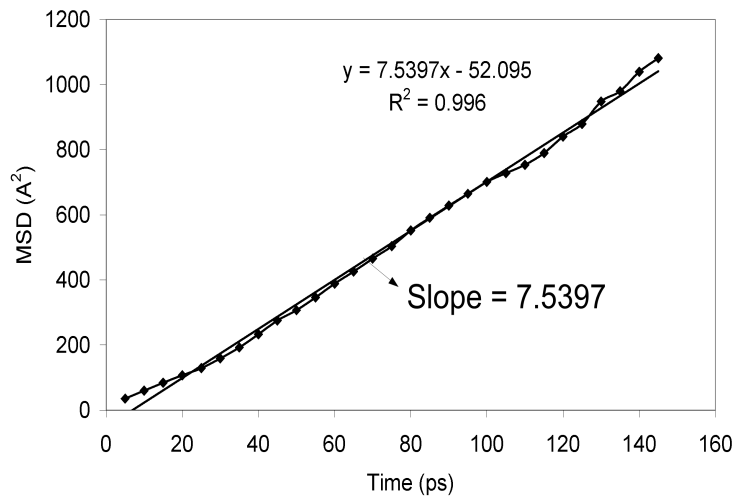
Figure 5.11: Mean squared displacement (MSD) vs time for Oxygen in Polyisobutylene at 500 K

Using Eq. 3.26 (from Chapter 3) and values of the slopes (see Fig. 5.11 and 5.11), the diffusivity of oxygen and nitrogen is calculated to be 1.26e-9 m^2/s and 0.949e-9 m^2/s respectively.

The simulation results for the temperatures ranging from 350K to 550K are given below. Adsorption isotherms for oxygen and nitrogen at 350 K are shown in Fig. 5.13 and 5.14

Adsorption isotherms for oxygen and nitrogen at 400 K are shown in Fig. 5.15 and 5.16

121
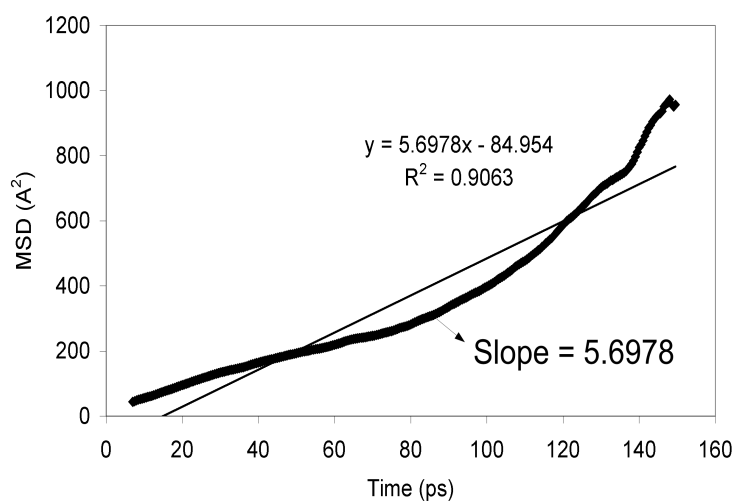
Figure 5.12: Mean squared displacement (MSD) vs time for Nitrogen in Polyisobutylene at 500 K
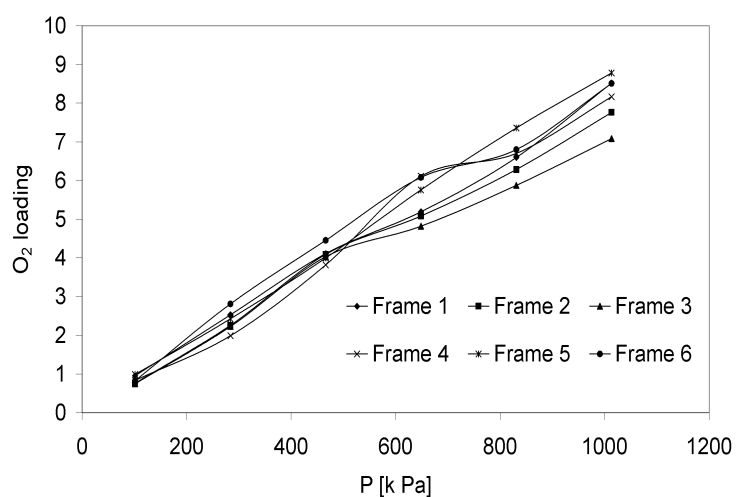
Figure 5.13: Adsorption isotherm for Oxygen in Polyisobutylene at 350 K
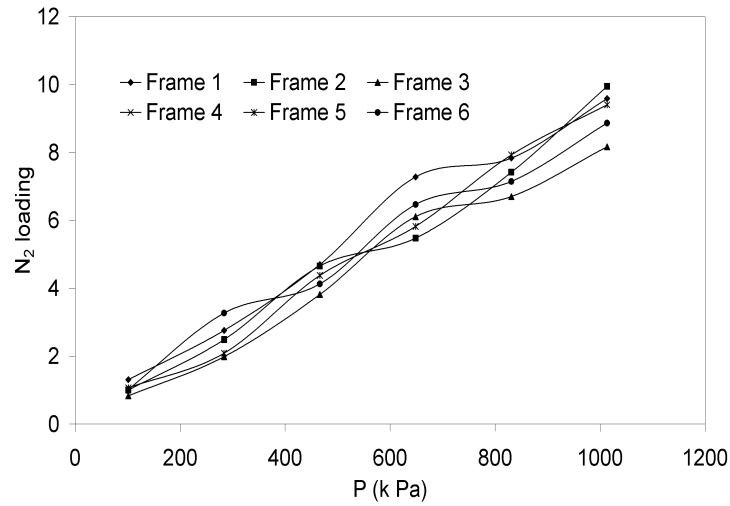
Figure 5.14: Adsorption isotherm for Nitrogen in Polyisobutylene at 350 K
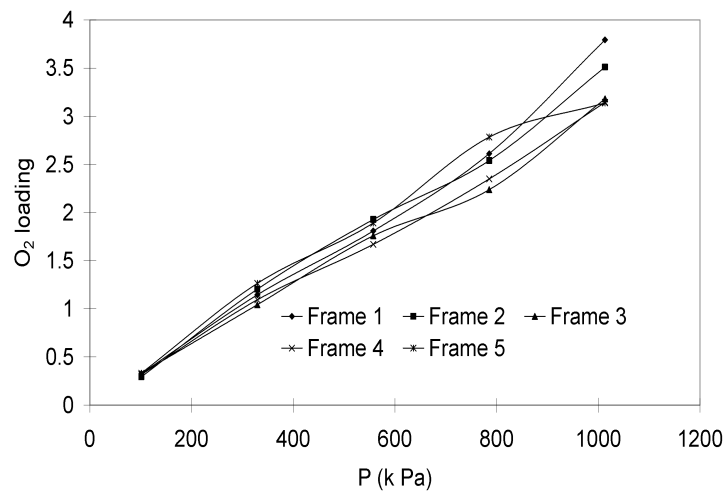
Figure 5.15: Adsorption isotherm for Oxygen in Polyisobutylene at 400 K
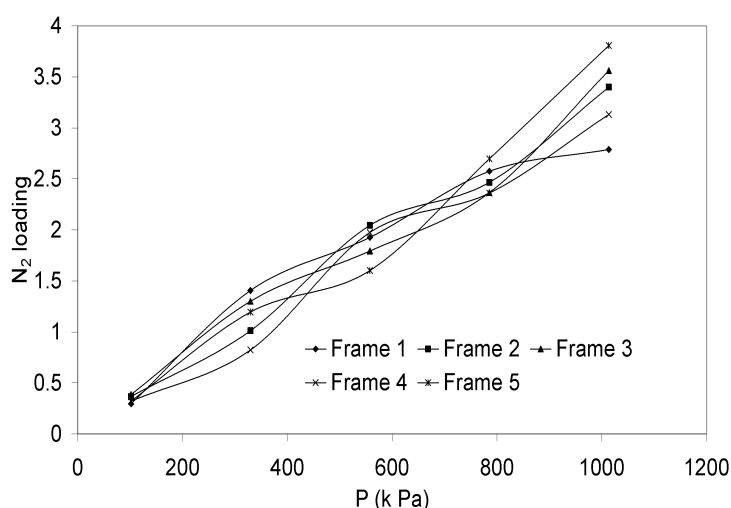
Figure 5.16: Adsorption isotherm for Nitrogen in Polyisobutylene at 400 K

Adsorption isotherms for oxygen and nitrogen at 450 K are shown in Fig. 5.17 and 5.18
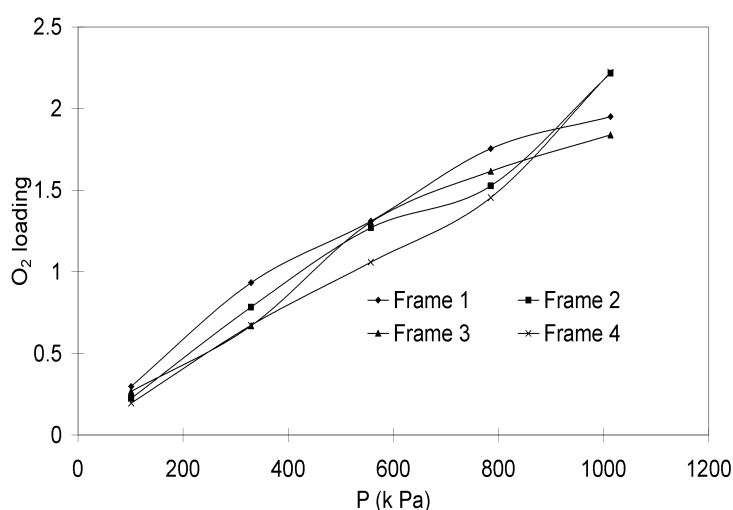
Figure 5.17: Adsorption isotherm for Oxygen in Polyisobutylene at 450 K

Adsorption isotherms for oxygen and nitrogen at 450 K are shown in Fig. 5.19 and 5.20

Based on the simulation results (Fig. 5.13- 5.20), the calculated values of solubility of oxygen and nitrogen at different temperature are listed in Table 5.7

Next the simulation results needed for the calculations for diffusivity calculation are shown. Fig. 5.21 gives log(t) vs log(MSD) and Fig. 5.22 gives time vs MSD for oxygen at 350 K in PIB.

Fig. 5.23 gives log(t) vs log(MSD) and Fig. 5.24 gives time vs MSD for oxygen at 400 K in PIB.

Fig. 5.25 gives log(t) vs log(MSD) and Fig. 5.26 gives time vs MSD for oxygen at 550 K in PIB.
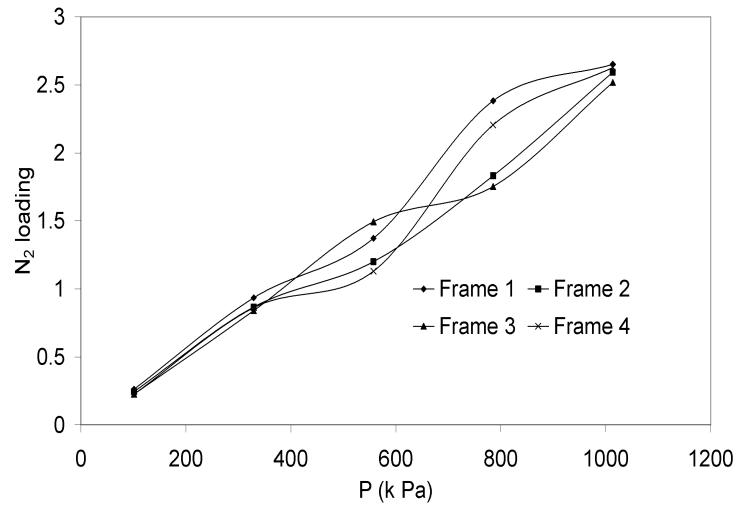
Figure 5.18: Adsorption isotherm for Nitrogen in Polyisobutylene at 450 K
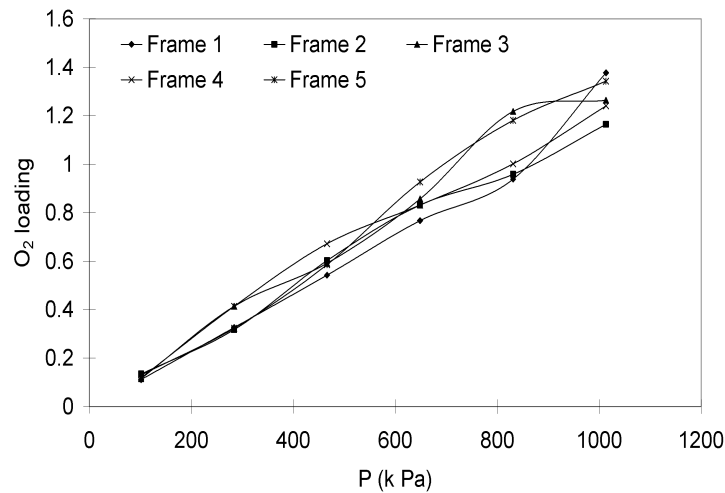
Figure 5.19: Adsorption isotherm for Oxygen in Polyisobutylene at 550 K

Temperature	S_{O_2}	S_{N_2}
(K)	$(\mathrm{mol/m^3/Pa}) \times 10^5$	$(\mathrm{mol/m^3/Pa}) \times 10^5$
350	11.5±0.4	12.9±0.7
400	4.76±0.6	4.80±0.7
450	2.93±0.3	2.87±0.2
500	2.57±0.2	2.33±0.4
550	1.95±0.1	1.79±0.04

Table 5.7: Calculated solubilities of oxygen and nitrogen in PIB at different temperatures

125
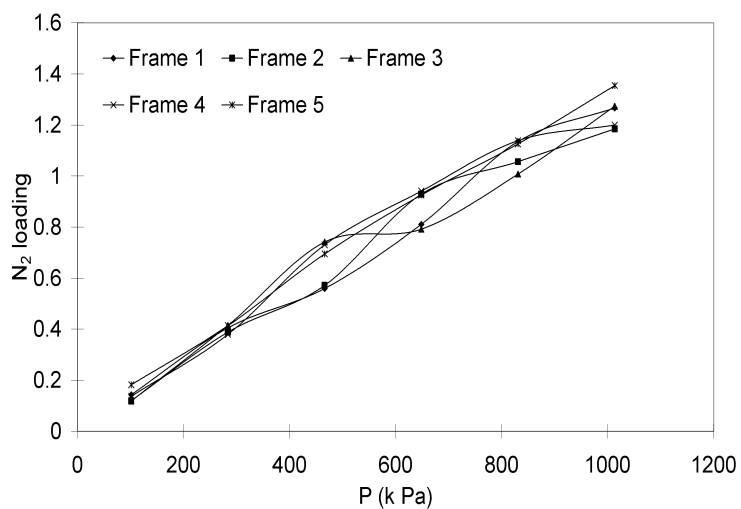
Figure 5.20: Adsorption isotherm for Nitrogen in Polyisobutylene at 550 K
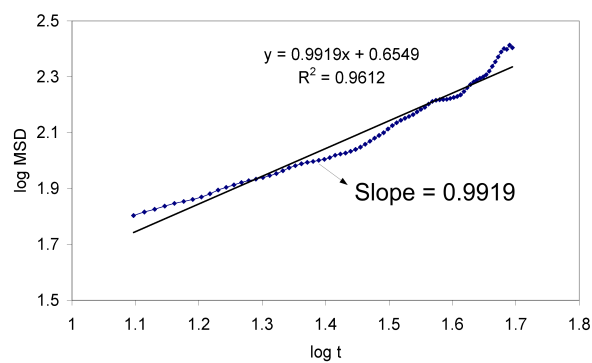
Figure 5.21: log(MSD) vs log(t) for Oxygen in Polyisobutylene at 350 K
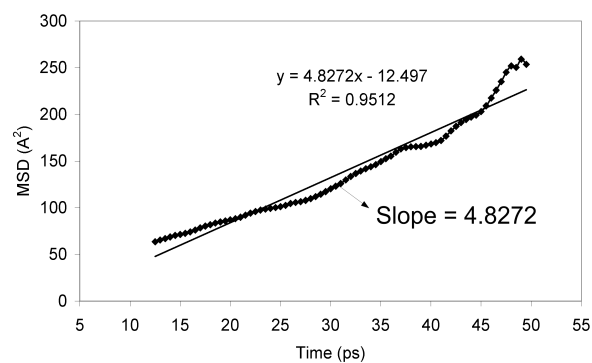
Figure 5.22: Mean squared displacement (MSD) vs time for Oxygen in Polyisobuty-
lene at 350 K
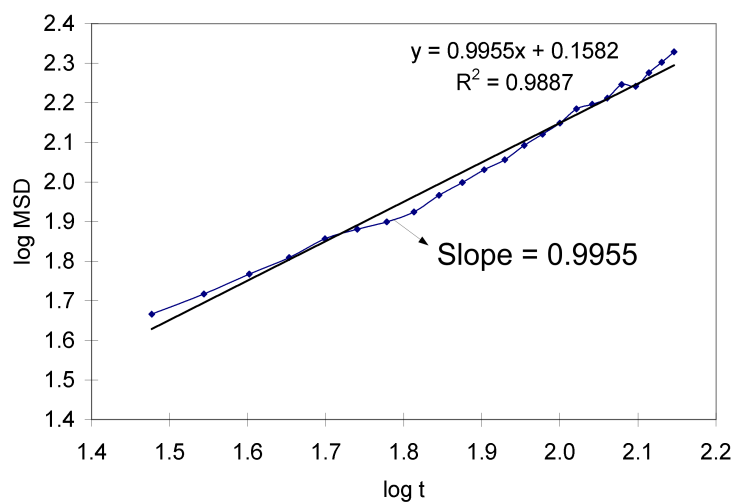
Figure 5.23: log(MSD) vs log(t) for Oxygen in Polyisobutylene at 400 K
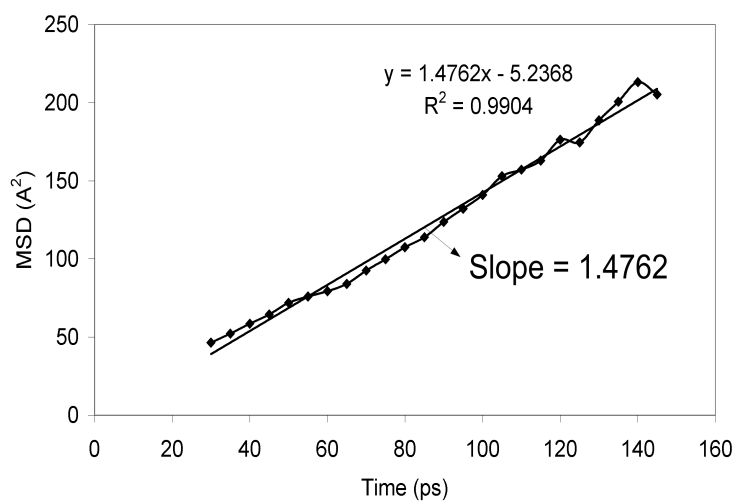
Figure 5.24: Mean squared displacement (MSD) vs time for Oxygen in Polyisobuty-lene at 400 K
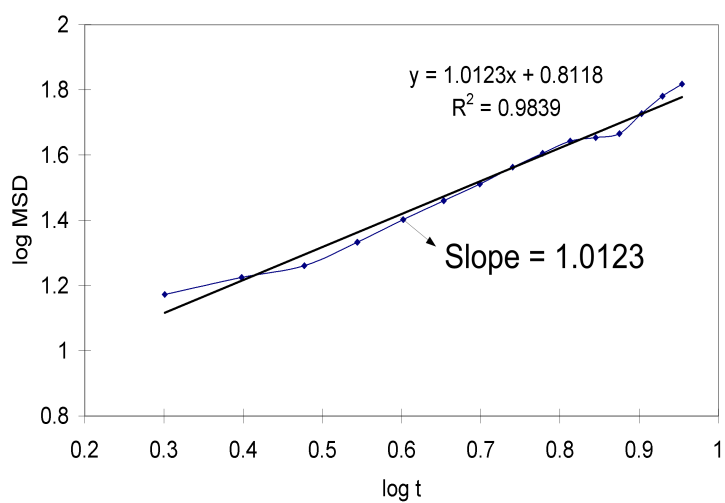
Figure 5.25: log(MSD) vs log(t) for Oxygen in Polyisobutylene at 550 K
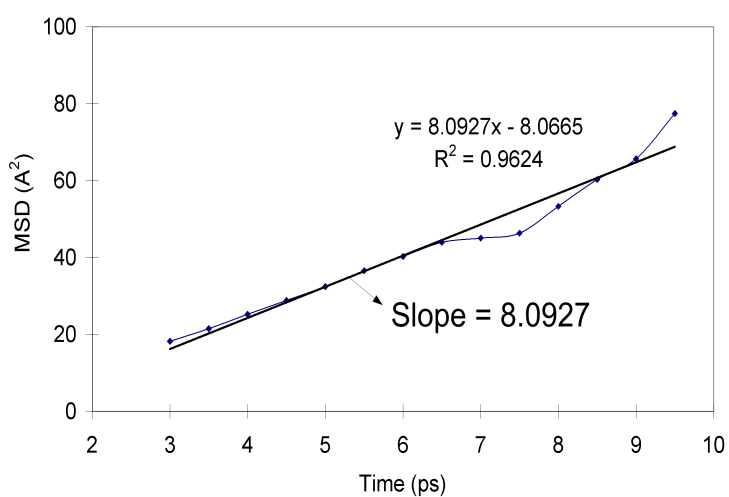
Figure 5.26: Mean squared displacement (MSD) vs time for Oxygen in Polyisobuty-
lene at 550 K

Fig. 5.27 gives log(t) vs log(MSD) and Fig. 5.28 gives time vs MSD for oxygen at 450 K in PIB.
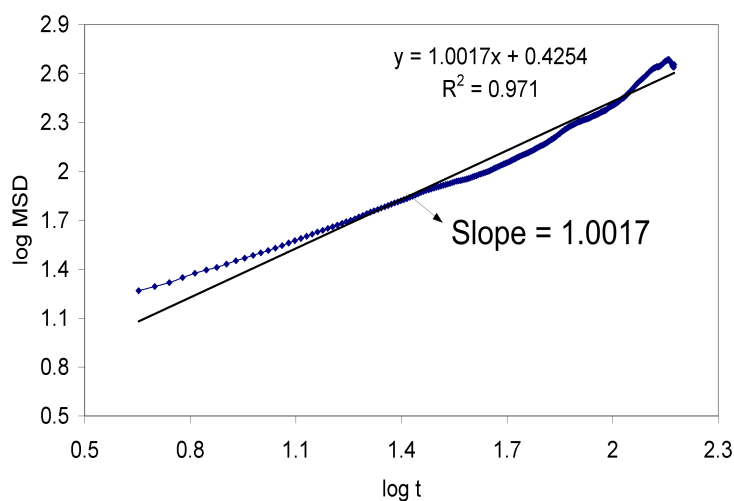
Figure 5.27: log(MSD) vs log(t) for Nitrogen in Polyisobutylene at 450 K
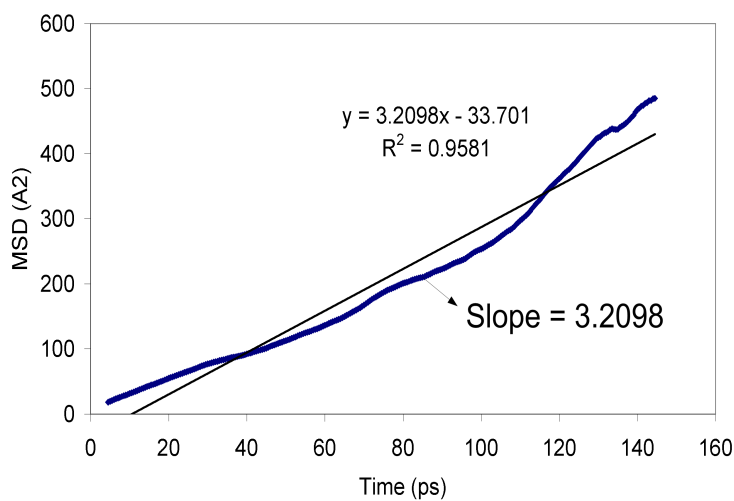
Figure 5.28: Mean squared displacement (MSD) vs time for Nitrogen in Polyisobutylene at 450 K

Fig. 5.25 gives log(t) vs log(MSD) and Fig. 5.26 gives time vs MSD for oxygen at 550 K in PIB.

Based on time vs MSD plots, the values of diffusivities are calculated for oxygen and nitrogen and are listed in Table 5.8

Some of the values of the diffusivities are not reported because the Fickian regime was not achieved as the slope of the log MSD vs log t was not close to 1. And since these simulations take about 4-5 weeks each for each temperature, due to time constraint, the results were not reproduced.
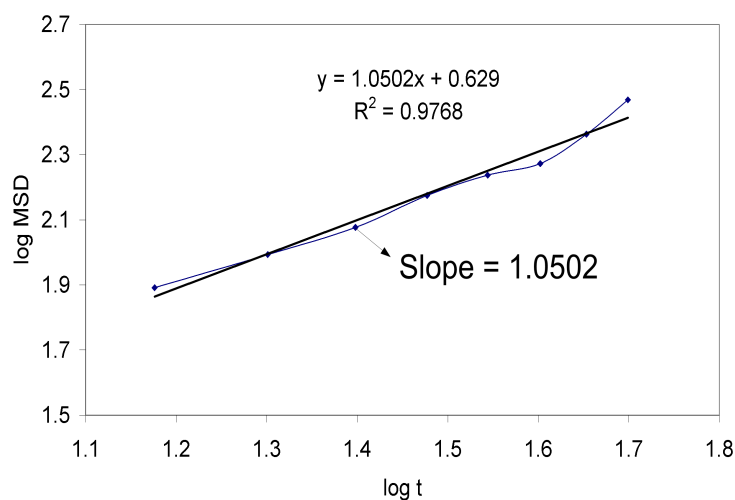
Figure 5.29: log(MSD) vs log(t) for Nitrogen in Polyisobutylene at 550 K
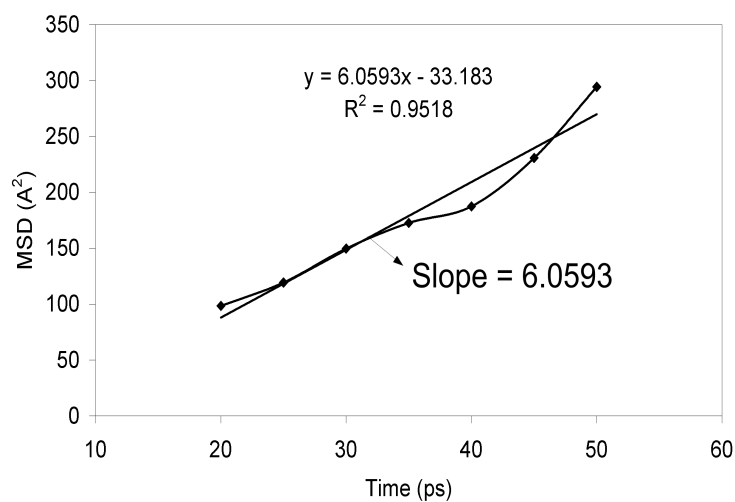
Figure 5.30: Mean squared displacement (MSD) vs time for Nitrogen in Polyisobutylene at 550 K

Temperature (K)	D_{O_2} $(\text{m}^2/\text{s}) \times 10^9$	D_{N_2} $(\text{m}^2/\text{s}) \times 10^9$
350	0.803	-
400	0.247	-
450	-	0.535
500	1.257	0.95
550	1.348	1.01

Table 5.8: Diffusivities of oxygen and nitrogen in PIB at different temperatures

The permeability values, which is the product of solubility and diffusivity, reported in Table 5.9.

Temperature (K)	P_{O_2} (mol/m/Pa/s)$\times10^{14}$	P_{N_2} (mol/m/Pa/s)$\times10^{14}$
350	9.24	-
400	1.18	-
450	-	1.54
500	3.23	2.23
550	2.63	1.81

Table 5.9: Permeabilities of oxygen and nitrogen in PIB at different temperatures

5.1.1.1 Discussion

In this case study the application of a hierarchal procedure developed in this work has been demonstrated to predict the solubilities and diffusivities of nitrogen and oxygen in PIB with 48 carbon atoms in each chain. The hierarchal procedure is quite general and can be used for most cases for polymers above glass transition temperature. For polymers around or below glass transition temperature, predicting diffusivities using brute force MD is difficult as it would take large CPU time to equilibrate the system (as the polymer is in glassy state). But for polymers well above glass transition temperature, based on the results for PIB and the previously reported values of PE [58], it is fairly reasonable to apply the given hierarchal procedure.

Taking into account all the steps in the hierarchal procedure, to predict permeability of one small gas molecule at one temperature in a polymer matrix took approximately around 12 weeks of CPU time. It gets economical when more than one prediction of diffusivity and solubility of different gases in the same polymer are made at one temperature, then long MD simulations in Stage I do not have to repeated for each gas molecule.

5.1.2 Property prediction of Aroma compounds

One of the case-studies in this work involves modeling, design and analysis of the recovery of aroma compounds from black currant juice using vacuum membrane distillation. The model equations require the evaluation of physical and chemical properties, such as density, viscosity, heat of vaporization, specific heat, vapor pressure etc., of aroma compounds as a function of temperature. Group contribution method given by Marrero and Gani (2001) (MG) [78], Constantinou and Gani (1994) (CG) [25] and Joback and Reid (1983) (JR) [53] have been used in this case study to predict the pure component properties of the aroma compounds from which the temperature dependant properties have been predicted.

Aroma compounds present in fruit juices usually comprise a mixture of a large number of volatile organic compounds. The individual aroma components present

in black currant juice differ according to their molecular structure, which in turn defines the solubility, the boiling point, and the volatility of each type of compound. In general, the aroma compounds are present in different concentrations and combinations, where the concentrations of individual aroma compounds in common fruit juices usually range from less than 1 to 20 ppm [55]. The aroma profile of black currant juice comprise of specific profiles of terpenoids, aliphatic esters, carbonyl compounds and alcohols that make up the characteristic black currant aroma of the juice. The twelve aroma compounds, representing various chemical groups, used in this study are shown in Fig. 5.31.
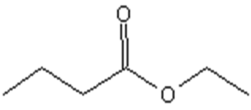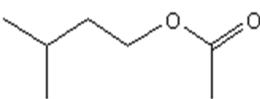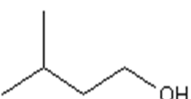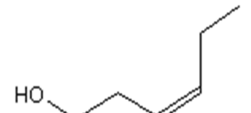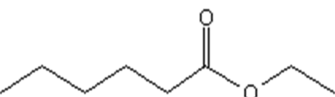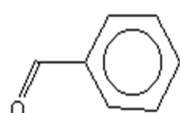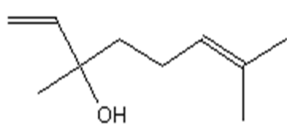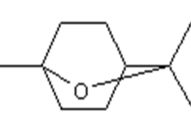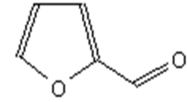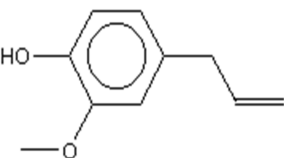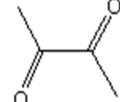
Figure 5.31: Characteristic aroma compounds for black currant juice

Various properties of the aroma compounds that are needed for the model are liquid density, liquid viscosity, liquid and ideal gas heat capacity, heap of vaporization, vapor pressure, infinite dilution diffusion coefficient in water and thermal conductivity. Group contribution method is used to predict these properties at different temperatures. A tool called Pro-Pred is used where the group contribution models have been implemented [78]. The properties are then plotted as a function of temperature and then regressed to obtain parameters to fit the end-use property model. OriginPro 7.5 is used in this work for regression. The parameters of the end-use property models with the regressed parameter values for the twelve aroma compounds are given in tables 5.10 to 5.12.

$$* \rho = A + B.T + C.T^2 + D.T^3 \tag{5.5}$$

Table 5.10: Coefficients for liquid density (kmol/m^3)

Aroma	Coefficients					Method
	A	B	C	D	E	
Ethyl Butanoate	0.63566	0.25613	571	0.27829	-	ICAS-DB
Iso amyl acetate	0.59955	0.26505	599	0.3009	-	ICAS-DB
3-methyl-1-butanol	0.837	0.27375	577.2	0.22951	-	ICAS-DB
Cis-3-hexene-1-ol*	6.63167	0.72023	308	0.99257	-	Pro-pred
Ethyl Hexanoate	4.76398	0.72941	308	0.99277	-	Pro-pred
Benzaldehyde	0.79368	0.25711	695	0.28673	-	ICAS-DB
Linalool	4.65927	0.74459	308	0.99363	-	Pro-pred
Octanal	0.56833	0.26939	638.1	0.26975	-	ICAS-DB
1,8 Cineole	4.56069	0.74736	308	0.99271	-	Pro-pred
Furfural	1.0586	0.26674	670.15	0.29968	-	ICAS-DB
Diacetyl	5.4391	0.6781	371.15	0.981	-	Pro-pred
Eugenol	4.737	0.7755	308	0.992	-	Pro-pred

Table 5.11: Coefficients for liquid viscosity (kg/m/s)

Aroma				Coefficients		Method
	A	B	C	D	E	
Ethyl Butanoate	-15.485	1325.6	0.6432	-	-	ICAS-DB
Iso amyl acetate	-12.128	1332.8	0.10018	-	-	ICAS-DB
3-methyl-1-butanol	-37.409	3747.7	3.3772	-	-	ICAS-DB
Cis-3-hexene-1-ol	95.331	-997.2	-17.668	3.21E-05	2	Pro-pred
Ethyl Hexanoate	63.793	-998.25	-12.138	2.20E-05	2	Pro-pred
Benzaldehyde	-17.062	1609.3	0.89088	-	-	ICAS-DB
Linalool*	-17.592	0.01844	856046	2.8891	-	Pro pred
Octanal	-10.191	1072.4	-0.0306	-	-	ICAS-DB
1,8 Cineole	-94.554	0.00455	215840	24.8908	-	Pro-pred
Furfural	-77.247	4384.4	9.8452	-	-	ICAS-DB
Diacetyl	46.9138	-997.74	-9.0466	1.16E-05	2	Pro-pred
Eugenol	60.467	-998.36	-11.548	2.10E-05	2	Pro-pred

133

Table 5.12: Coefficients for liquid specific heat (J/mol/K)

Aroma	Coefficients					Method
	A	B	C	D	E	
Ethyl Butanoate	82434	422.45	0.20992	-	-	ICAS-DB
Iso amyl acetate	120000	431.15	-	-	-	ICAS-DB
3-methyl-1-butanol	-53777	883.42	-	-	-	ICAS-DB
Cis-3-hexene-1-ol	20884.1	3120.28	-16.848	0.04079	-3.60E-05	Pro-pred
Ethyl Hexanoate	20532.9	3008.61	-14.844	0.03548	-3.10E-05	Pro-pred
Benzaldehyde	122530	98.307	0.22846	-	-	ICAS-DB
Linalool	-479.97	1497.85	-0.7081	-0.0033	4.58E-06	Pro-pred
Octanal	130650	463.61	-	-	-	ICAS-DB
1,8 Cineole	24625.7	675.731	1.41217	-0.004	2.76E-06	Pro-pred
Furfural	93551	215.94	-	-	-	ICAS-DB
Diacetyl	857.419	1567.13	-5.7379	0.00955	-5.10E-06	Pro-pred
Eugenol	56021.1	2522.55	-12.422	0.03038	-2.70E-05	Pro-pred

Table 5.13: Coefficients for thermal conductivity (J/m/s/K)

Aroma	Coefficients					Method
	A	B	C	D	E	
Ethyl Butanoate	0.21043	-2.49E-04				ICAS-DB
Iso amyl acetate	0.2024	-2.44E-04				ICAS-DB
3-methyl-1-butanol	0.22247	-2.74E-04				ICAS-DB
Cis-3-hexene-1-ol	65404.8	-1.08E+03	7.1723	-0.0238	3.94E-05	Pro-pred
Ethyl Hexanoate	-	-	-	-	-	-
Benzaldehyde	0.20655	-1.81E-04	-	-	-	ICAS-DB
Linalool	-	-	-	-	-	
Octanal	0.20143	-2.11E-04	-	-	-	ICAS-DB
1,8 Cineole	-	-	-	-	-	
Furfural	0.2295	-1.94E-04	-	-	-	ICAS-DB
Diacetyl	-	-	-	-	-	
Eugenol	-	-	-	-	-	

Table 5.14: Coefficients for infinite dilution diffusion coefficients (1e9*m^2/s)

Aroma	Coefficients					Method
	A	B	C	D	E	
Ethyl Butanoate	9.30272	-0.08075	0.00019	5.00E-08	0	Pro-pred
Iso amyl acetate	8.82157	-0.07665	0.00018	-4.92E-08	0	Pro-pred
3-methyl-1-butanol	-5.7409	0.02193	0	0.00E+00	0	Pro-pred
Cis-3-hexene-1-ol	9.45728	-0.08206	0.00019	-5.02E-08	0	Pro-pred
Ethyl Hexanoate	8.4059	-0.073103	0.00017	-4.86E-08	-	Pro-pred
Benzaldehyde	1	-	-	-	-	Pro-pred
Linalool	7.94316	-0.069157	0.00016	-4.79E-08	-	Pro-pred
Octanal	8.5259	-0.074125	0.00018	-4.88E-08	-	Pro-pred
1,8 Cineole	8.2096	-0.071429	0.00017	-4.83E-08	-	Pro-pred
Furfural	11.1104	-0.09615	0.00022	-5.25E-08	-	Pro-pred
Diacetyl	19.2252	-0.17519	0.00048	-3.33E-07	-	Pro-pred
Eugenol	8.1419	-0.07085	0.00017	-4.82E-08	-	Pro-pred

Table 5.15: Coefficients for gas viscosity (kg/m/ s)

Aroma	Coefficients					Method
	A	B	C	D	E	
Ethyl Butanoate	1.62E-07	0.7163	142.27	3590	-	ICAS-DB
Iso amyl acetate	2.90E-07	0.64	250	-	-	ICAS-DB
3-methyl-1-butanol	8.83E-08	0.80433	75.255	-	-	ICAS-DB
Cis-3-hexene-1-ol	-	-	-	-	-	
Ethyl Hexanoate	-	-	-	-	-	
Benzaldehyde	1.03E-07	0.7873	122	-	-	ICAS-DB
Linalool	-	-	-	-	-	
Octanal	1.03E-07	0.7589	121.26	-	-	ICAS-DB
1,8 Cineole	-	-	-	-	-	
Furfural	5.02E-08	0.91577	45.096	-	-	ICAS-DB
Diacetyl	-	-	-	-	-	
Eugenol	-	-	-	-	-	

Table 5.16: Coefficients for heat of vaporization (J/kmol)

Aroma	Coefficients					Method
	A	B	C	D	E	
Ethyl Butanoate	5.64E+07	0.37985	0	0	0	ICAS-DB
Iso amyl acetate	5.95E+07	0.38877	0	0	0	ICAS-DB
3-methyl-1-butanol	8.08E+07	0.50185	0	0	0	ICAS-DB
Cis-3-hexene-1-ol	1.00E+11	40.472	-88.262	58.1373	-	Pro-pred
Ethyl Hexanoate	1.00E+11	41.3748	-91.806	61.6779	-	Pro-pred
Benzaldehyde	6.19E+07	0.38194	-	-	-	ICAS-DB
Linalool	1.00E+11	26.6014	-40.749	17.0979	-	Pro-pred
Octanal	6.83E+07	0.41039	-	-	-	ICAS-DB
1,8 Cineole	1.00E+11	43.2862	-98.043	67.339	-	Pro-pred
Furfural	6.00E+07	0.34837	-	-	-	ICAS-DB
Diacetyl	1.00E+11	36.459	-68.004	36.9368	-	Pro-pred
Eugenol	1.00E+11	46.856	-116.92	89.713	-	Pro-pred

Table 5.17: Coefficients for vapour pressure (Pa)

Aroma	Coefficients					Method
	A	B	C	D	E	
Ethyl Butanoate	57.661	-6346.5	-5.032	8.25E-18	6	ICAS-DB
Iso amyl acetate	67.918	-7376.6	-6.4182	6.45E-18	6	ICAS-DB
3-methyl-1-butanol	107.02	-10237	-11.695	6.80E-18	6	ICAS-DB
Cis-3-hexene-1-ol*	-171.338	-1006.3	32.7478	-7.66E-05	2	Pro-Pred
Ethyl Hexanoate*	-169.46	-1006.2	32.3164	-7.50E-05	2	Pro-Pred
Benzaldehyde	116.28	-9331.2	-14.639	1.19E-02	1	ICAS-DB
Linalool*	-211.873	-1007.3	38.3831	-8.84E-05	2	Pro-Pred
Octanal*	250.25	-16162	-33.927	2.24E-05	2	Pro-Pred
1,8 Cineole*	-136.617	-1005.1	26.5167	-6.02E-05	2	Pro-Pred
Furfural	94.57	-8372.1	-11.13	8.82E-03	1	ICAS-DB
Diacetyl*	-47.53	-1003.9	10.846	-1.58E-05	2	Pro-Pred
Eugenol*	-197.579	-1007.1	36.9203	-8.29E-05	2	Pro-Pred

Table 5.18: Critical temperature (K) and infinite dilution activity coefficients (-)

Aroma	Tc (K)	Method		γ^∞	Reference
Ethyl Butanoate	571	ICAS-DB	[40]	UNIFAC	-
Iso amyl acetate	599	ICAS-DB	[40]	2980	[54]
3-methyl-1-butanol	577.2	ICAS-DB	[40]	208	[54]
Cis-3-hexene-1-ol	611.8	Pro-Pred	[78]	320	[54]
Ethyl Hexanoate	623.01	Pro-Pred	[78]	14200	[54]
Benzaldehyde	695	ICAS-DB	[40]	UNIFAC	-
Linalool	658.9	Pro-Pred	[78]	14127	[54]
Octanal	638.1	Pro-Pred	[78]	6594.4	[54]
1,8 Cineole	635.1	Pro-Pred	[78]	56500	[54]
Furfural	670.15	ICAS-DB	[40]	80	[54]
Diacetyl	610.4	Pro-Pred		14	[54]
Eugenol	706.407	Pro-Pred	[78]	5236	[54]

5.2 Product-Process design

5.2.1 Design of Air purification

Oxygen and Nitrogen are the primary components of air. Oxygen is present at 21 vol% and nitrogen at 78%. Consequently these two gases are primary products of air separation. Since their source is both free and abundant, the recovery is not much of an issue as the purity. New membrane technology has reduced the cost of air separation to levels at which it can be competitive in many applications with on-site delivery of cryogenically produced gases. Therefore, it has become one of the fastest growing applications of gas separation membrane in recent years [61].

Oxygen enrichment has its application for medical and biotechnological purposes and for enhanced combustion. Commercial membranes have oxygen/nitrogen selectivities ranging from 3.5 to 5.5 which leads to low recovery and limits oxygen purities to be 30-45% range [61]. Oxygen with an enrichment of 25-40% is generally of interest for enhanced combustion [89].

5.2.1.1 Comparative case study

Mulder (1996) [89] has given an example for enrichment of oxygen using membranes. The available data for the case-study is given in the table below (Table 5.19).

The model for membrane based gas separation given in Chapter 4 has been used to study the enrichment of oxygen. The input data for the gas separation is given in Table 5.20).

A hollow fiber having area of 14 m^2 membrane module with a fiber diameter of 1 cm and 6 m length with 75 number of fibers was used. The simulated results from the membrane-based gas separation are shown in the flow diagram and compared to the data from Mulder (1996) (see Fig. 5.32). As can be seen from the flow sheets that

Table 5.19: Membrane based air separation - relevant data for calculation([89])

Variable	Value
Oxygen feed concentration	0.21
Oxygen permeate concentration	0.33
Polymer selectivity	2.2
Permeate flow rate	10 m^3/h
Oxygen permeability	600 Barrer
Membrane thickness	1 μm
Membrane area	14 m^2
Upstream pressure	1 bar
Downstream pressure	0.2 bar
Oxygen flux	2.92e-3 $mol/m^2\ s$

Table 5.20: Membrane based air separation - Input data for the model

Variable	Value
Oxygen feed concentration	0.21
Polymer selectivity	2.2
Oxygen permeability	600 Barrer
Membrane thickness	1 μm
Membrane area	14 m^2
Upstream pressure	1 bar
Downstream pressure	0.2 bar

the calculated values from the model are reasonably accurate for practical purposes. The calculated recovery of oxygen in the permeate stream as compared to the feed stream is 2.15e-3.

5.2.1.2 Design problem

Normally, oxygen of more than 30 vol% purity for combustion and more than 40 vol% purity for medical use is required. The modeling objective is to describe the behavior of systems under study. Membrane-based gas separation model is then applied to find design alternative for the polymer that can be used in this membrane based separation process, that would satisfy the performance criteria given as in Fig. 5.33. A higher purity and recovery as compared to the previous case is desired in this design problem.

The reverse design algorithm is used to design the polymer in this case. The step by step procedure presented in Chapter 2 has been applied.

Stage A: Setting the property targets

Step A-I: For a given feed $\underline{I}$ and performance criteria $\underline{P}$, the first step is to select/derive the rigorous process model and identify the design variables.

138

a. Data from Mulder (1996)

$X_{O2,f} = 0.21$

$X_{O2,p} = 0.33$
Flow rate = 0.124 mol/s
Flux O_2 = 2.92e-3 mol/m^2 s

$X_{O2,f} = 0.21$

$X_{O2,p} = 0.36$
Flow rate = 0.123 mol/s
Flux O_2 = 3.23e-3 mol/m^2 s

b. Simulated data
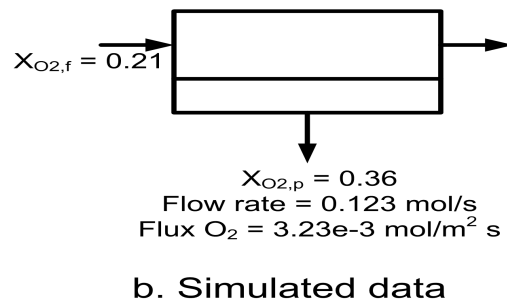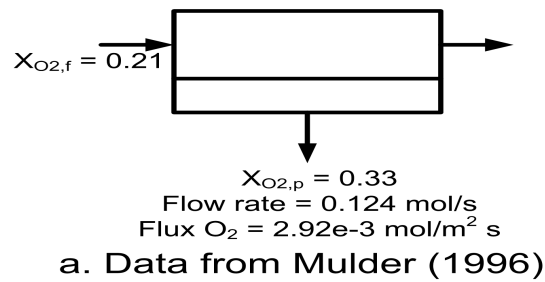
Figure 5.32: Single stage membrane based separation process for oxygen enrichment

$X_{O2,f} = 0.21$
Feed = 200 mol/s
T = 298 K
P = 1 bar

$X_{O2,p} = 0.50$
Oxygen recovery = 3.8e-3
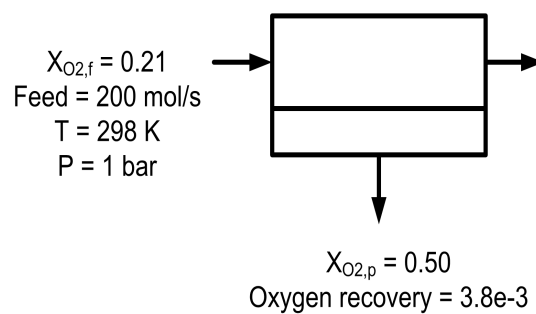
Figure 5.33: Design problem for oxygen enrichment using membrane based gas separation process

The process model for membrane-based separation process presented in Chapter 4 has been used. Different types of variables are listed in Tables 5.21 and 5.22.

Table 5.21: Types of variables in the membrane-based separation process model

State	Property	Constitutive	Module parameter
2 - Total mass flows	2 - P_{O_2} and P_{N_2}	2 - $x_{N_2,P}$, $x_{N_2,F}$	4 - L,R, δ_m, N_f
4 - Comp. mass flows			
2 - Pressures on	4 - $\mu_{i,P}$, $\mu_{i,F}$	2 - N_{O_2}, N_{N_2}	
each side of membrane	4 - $\phi_{i,P}$, $\phi_{i,F}$		

Table 5.22: Known and unknown variables in the membrane-based separation process model

Known ($\underline{I}$)	Unknown ($\underline{P}$)
1 - Feed flow rate	1 - Molar fraction
1 - Comp. flow rate	of O_2 in permeate
1 - Feed temperature	1 - CF of O_2
1 - Feed pressure	

In this case, vector $\underline{I}$ and vector $\underline{P}$ are known. In the Table 5.22, variables $\underline{P}$ then move to the column of known variables. So, now there are two more variables as compared to the number of variables. So, two variables, (P_{O_2} and P_{N_2} in this case) can be calculated from the model. The vector $\underline{I}$ and vector $\underline{P}$ are given as:

$$\underline{I}:$$
$$n_{Ft} = 200\text{mol/s}$$
$$x_{f,O_2} = 0.21$$
$$T_f = 298.15K$$
$$P_f = 1\text{bar}$$

and

$$\underline{P}:$$
$$\text{CF of Oxygen} = 2.38$$
$$\text{Oxygen recovery} = 3.8e-3$$

The design variables are identified as the structural parameters of the polymers (repeat unit or the microscopic structure of the polymer).

Step A-II: Using the values of the performance criteria ($\underline{P}$), the outlet variables ($\underline{X}$) are calculated.

Using the purity and recovery of oxygen the outlet variables (Eq. 4.104 and 4.105) of the membrane module are calculated as:

$$\underline{X}:$$
$$x_{O_2,P} = 0.5$$
$$N_{O_2} = 6.5e-4 \text{ mol/m}^2\text{s}$$

When molar fraction of oxygen in the permeate and transmembrane flux of oxygen are known and substituted in the process model, two variables that were originally known/specified can be calculated from the model. In this case, the two permeabilities ((P_{O_2} and P_{N_2})) are calculated from the model.

Step A-III: With specified inlet and outlet variables, the target property values, defined by $\underline{\theta}_{target}$ are calculated.

The model can be solved to obtain the target values of the permeabilities of oxygen and nitrogen that would give the desired performance criteria. Model equations were solved with known values of $x_{O_2,P}$ and N_{O_2} to give the following values of the target properties:

$$\underline{\theta}_{target}$$
$$P_{O_2} \geq 4.0 \text{ Barrer}$$
$$P_{N_2} \geq 0.889 \text{ Barrer}$$

Once θ_{target} has been calculated, the next step is to find the candidate polymer, either from the literature or by identifying the repeat unit of the polymer from group contribution methods or through the microscopic structure of the polymer from molecular simulations, with properties matching θ_{target}.

<u>Stage B</u>: **Design/Select polymers matching property targets**

Step B-IV: Once the targets for the properties are set ($\underline{\theta}_{target}$), in the second stage, different property models are solved in order to get the structured products. In this stage, an extensive database search could also be made to identify the product with ($\underline{\theta}_{target}$) property values.

Before, searching for polymers with different permeabilities for oxygen and nitrogen, it is important to establish conversion for different units of permeabilities. A number of units for can be found in the literature, and the most common of them is Barrer.

$$1 \text{ Barrer} = 10^{-10} \text{cm}^3(\text{STP})\text{cm cm}^{-1}\text{s}^{-1}\text{cm Hg}^{-1}$$
$$= 3.346\text{e} - 16 \text{ mol m m}^{-2} \text{ s}^{-1} \text{ Pa}$$

Another unit for permeability is

$$1 \text{ cm}^3(\text{STP})\text{cm cm}^{-2}\text{s}^{-1} \text{ Pa} = 4.462\text{e} - 3 \text{ mol m m}^{-2} \text{ s}^{-1} \text{ Pa}$$

(a) Literature search: Some polymers were selected from a polymer database [17]. They are listed in Table 5.23.

(b) Predictive model : Van Krevelan (1990) has given predictive group contribution based models to estimate solubility and diffusivity of oxygen and nitrogen in

Table 5.23: Permeability of polymers from literature [17]

Polymer	Permeability [Barrer]	
	Oxygen	Nitrogen
Poly(ethylene) LDPE	2.933	0.973
Poly(ethylene) HDPE	0.227	0.124
Poly(ethylene-hexene-1)	0.883	0.239
Poly(propylene)	2.240	0.565
Poly(styrene)	2.666	0.787
Poly(ethyl methyl acrylate)	1.185	0.227
Poly(tetrafluoroethylene)	4.266	1.333
Poly(butadiene)	19.065	6.453
Poly(oxydimethylsilylene)	489.292	226.647
Poly(dimethylsiloxane)	926.588	470.627
Poly(methyloctylsiloxane)	191.984	87.059
Ethyl cellulose	14.665	4.426
Silicone rubber	600.000	280.000
Poly(1-trimethylsilyl-1-propyne)	7600	5400
Poly(4-methy-1-pentene)	30.0	7.1
Polyimide	7.900	1.300
Polysulphone	1.100	0.180
Polyaramide	3.100	0.460
Tetrabromo bis polycarbonate	1.4	0.180
6FDA-6FpDA*	16.000	3.400
6FBPA/TERE**	12.000	2.950

* 6FDA-6FpDA: polyimide of 2,2-bis(3,4-dicarboxyphenyl) hexafluoropropane dianhydride and 4,4-(hexafluoro isopropylidene)-dianiline

** 6FBPA/TERE: polyester of hexafluoro bisphenol-A and terephthalic diacid chloride

some common polymers [114]. Table 5.24 lists the ones with high permeabilities or selectivities at 298 K. The predictive equations by van Krevelan provided values of solubility and diffusivity up to ±2% accurate estimates.

Table 5.24: Solubility and diffusivity of polymers at 298 K [114]

Polymer	Solubility [mol/m³Pa]		Diffusivity [m²/s]	
	Oxygen	Nitrogen	Oxygen	Nitrogen
Silicon rubber	5.62E-05	3.61E-05	2.5E-09	1.5E-09
Cis-1,4-polyisiprene	5.0E-05	2.45E-05	1.6E-10	1.1E-10
Polybutadiene	4.33E-05	2.01E-05	1.5E-10	1.1E-10
Styrene-butadiene rubber	4.19E-05	2.14E-05	4.3E-11	2.9E-11

The model parameters given by Krevelan have values that are specific to polymer-penetrant pair, so this method can not be used to generate new polymers.

(c) Group contribution model: As mentioned in Chapter 4, Park et.al. (1997) [95] have proposed a group contribution model based on free volume to predict permeabilities of gases through polymers. The polymers whose properties were generated using the group contribution method of Park et.al. are presented in Table 5.25. The predicted values are compared with experimental values (see Fig. 5.34).

Table 5.25: Predicted permeability of polymers from group contribution model [95]

Polymer	Permeability [Barrer]	
	Oxygen	Nitrogen
BPA-PC	0.405	1.757
BPA-PS	0.185	1.096
TMPC	2.822	12.509
TMPS	1.275	6.4899
HFPC	2.601	10.963
TM-HFPC	4.625	19.702
HFPS	1.297	6.193
TM-HFPS	2.618	12.120
PDMPO	1.255	5.935
PDPPO	1.515	7.505

Full names of the polymers are given in Appendix A

(d) Molecular modeling: Lastly, structurally different polymers obtained from molecular modeling were used in this case study. Barrier properties, such as diffusivity, solubility and permeability coefficients, are calculated for polyethylene (PE) melts using well-equilibrated, computer-generated linear polyethylene samples as input. PE at lower molecular weights have very high permeabilities for oxygen and nitrogen, so higher fluxes can be achieved. Two different molecular architectures of
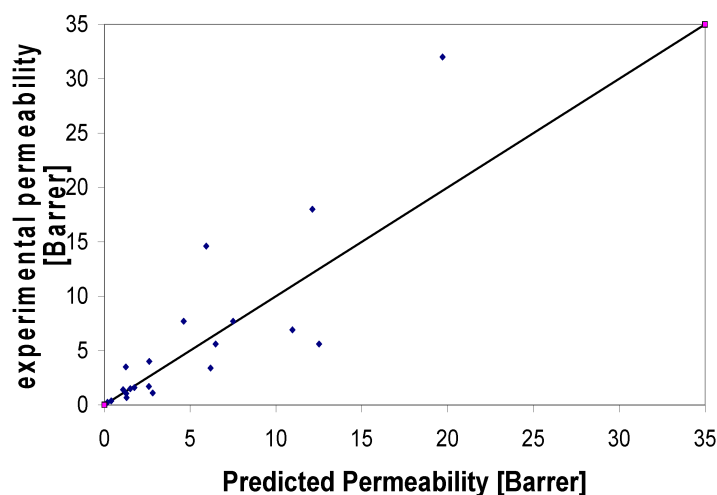
Figure 5.34: Comparison of permeabilities of oxygen and nitrogen from group contribution method [95]

PE were studied: purely linear systems denoted as "C_N" where N is the total number of carbon atoms per chain and short-chain branched (SCB) analogs referred to as "SCB_(Nbr + 1)Nfreq_NbrCb" where Nbr is the number of branches distributed regularly along the main (linear) backbone, Cb is the (constant) branch length (i.e. the number of carbon atoms of each branch) and Nfreq is the branching frequency (i.e. the number of carbon atoms along the main backbone between two successive branch points). In all cases studied, the SCB and linear systems are selected so as to correspond to the same (total) molecular weight (developed in collaboration with ICE/FORTH Patras, Greece). The adopted hierarchical simulation methodology consists of three main calculation phases:

- Application of chain-connectivity altering Monte Carlo (MC) moves [57, 59] for the rapid and robust equilibration of purely amorphous PE samples in the atomistic level of description (in a united-atom representation where carbons and bonded hydrogens are lumped into single, spherical interacting sites).

- Conversion of selected representative and uncorrelated configurations of the simulated systems to an explicit (all-atom) representation by appropriately adding the corresponding hydrogens. Application of short NVT (fixed number of molecules, volume and temperature) Molecular Dynamics (MD) simulations accompanied by static energy minimizations to afford additional local (segmental) relaxation because of the addition of hydrogen atoms.

- Application of the Gusev-Suter Transition State Theory (TST) [46] as implemented in InsightII commercial software by Accelrys Inc. to calculate the barrier properties of the computer-generated PE samples to O2 and N2 at conditions of infinite dilution (low concentration).

The simulated results are for linear polyethylene are shown in Table 5.26 and for the branched polyethylene (SCB) in Table 5.27.

Table 5.26: Permeabilities of oxygen and nitrogen in linear chain polyethylene at 300 and 450 K

PE System	P [10^{-12}cm^3(STP)cm/cm^{2}Pas]			
	Oxygen (T = 300K)	Nitrogen (T = 300K)	Oxygen (T = 450K)	Nitrogen (T = 450K)
C_{78}	3.85 ± 0.12	0.657 ± 0.20	25.0 ± 2.0	9.70 ± 1.0
C_{142}	3.05 ± 0.10	0.457 ± 0.15	19.7 ± 2.0	7.69 ± 0.8
C_{500}	1.82 ± 0.08	0.259 ± 0.10	17.1 ± 1.6	6.42 ± 0.7
C_{1000}	1.50 ± 0.06	0.202 ± 0.09	15.8 ± 1.8	5.83 ± 0.7

Table 5.27: Permeabilities of oxygen and nitrogen in branched structures of polyethylene at 300 and 450 K

PE System	P[10^{-12}cm^3(STP)cm/cm^{2}Pas]			
	Oxygen (T = 300K)	Nitrogen (T = 300K)	Oxygen (T = 450K)	Nitrogen (T = 450K)
SCB_11 × 12_10 × 1	1.59 ± 0.15	0.232 ± 0.08	19.4 ± 2.5	7.64 ± 0.9
SCB_9 × 14_8 × 2	2.17 ± 0.12	0.315 ± 0.02	21.6 ± 1.6	8.39 ± 0.7
SCB_7 × 16_6 × 5	2.80 ± 0.15	0.359 ± 0.06	20.9 ± 1.8	8.13 ± 0.7
SCB_5 × 22_4 × 8	2.39 ± 0.10	0.381 ± 0.05	21.7 ± 3.0	8.66 ± 0.6

To obtain end-use property models, the data generated through molecular modeling were fitted to closed-form equations. Fig. 5.35 and 5.36 shows the linear polyethylene permeabilities for oxygen and nitrogen respectively.
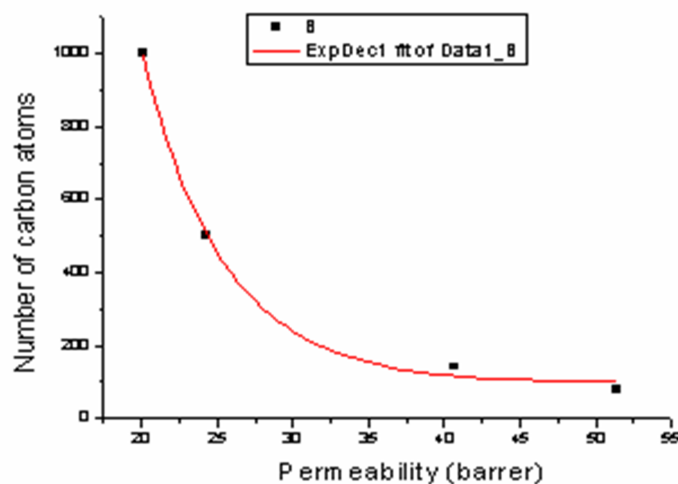
Figure 5.35: Permeability of oxygen as a function of number of carbon atoms in the linear chains of polyethylene

By analyzing these data, closed-form analytical expressions have been developed capable of relating these properties to features of molecular structure and conformation of the polymer. For the case of PE considered here, the permeability of oxygen

145
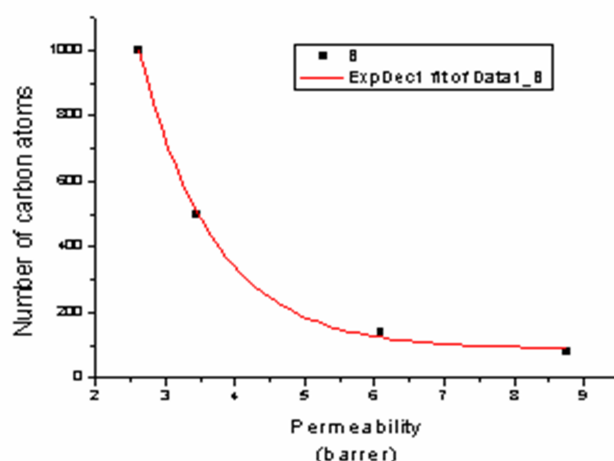
Figure 5.36: Permeability of nitrogen as a function of number of carbon atoms in the linear chains of polyethylene

and nitrogen has been related to the molecular length (number of carbon atoms) of the main chain backbone. Enough data is available to generate property models for PE giving permeabilities as a function of N_{Carbon} in the straight chain:

$$P_{O_2} = -\ln\left(\frac{N_{Carbon} - 67.42}{1.867e6}\right) 7.66e - 13 \text{ with } R^2 = 0.9989 \tag{5.6}$$

$$P_{N_2} = -\ln\left(\frac{N_{Carbon} - 65.96}{1.212e7}\right) 1.67e - 12 \text{ with } R^2 = 0.9984 \tag{5.7}$$

Stage C: Rigorous simulation to validate the polymer

Step C-V: Once the feasible set of products is proposed, then an analysis is made to validate the choices. This is done by doing the rigorous simulations using forward design algorithm for the products found in Stage II of the reverse design algorithm.

Polymers from literature, from group contribution methods and computer-generated ones (at T=300 K) were selected and plotted as shown in Fig. 5.37. Selectivity vs. permeability of oxygen is plotted. Selectivity gives an idea of the purity of oxygen, so it is chosen to be plotted instead of permeability of nitrogen. The horizontal and the vertical line on the plot represents the target values of the properties and the polymers that lie in the shaded region satisfy the property criteria.

The validation step was performed only for the candidate polymers lying in the shaded region. As can be seen from Table 5.28, that the desired performance criterion has been achieved for all the polymers possessing θ_{target} property values.

146
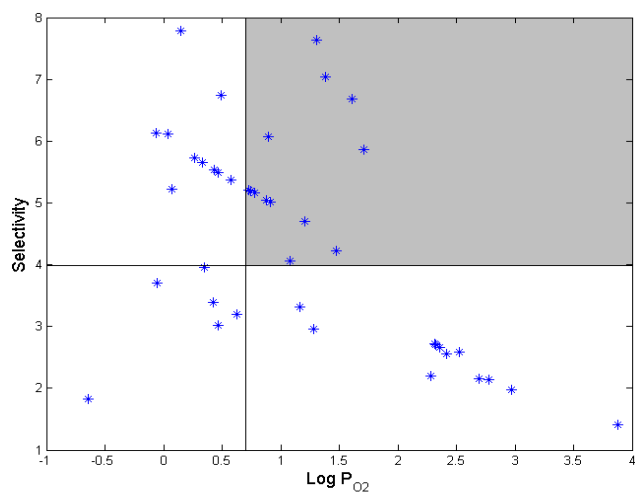
Figure 5.37: Polymers on property target plots

Table 5.28: Validation of the design obtained by reverse design algorithm

Polymer	Permeability		Selectivity	log P_{O2}	% Purity	Recovery
6FDA-6FpDA	16	3.4	4.705882	1.20412	54.24	2.90E-03
6FBPA/TERE	12	2.95	4.067797	1.079181	50.68	2.18E-03
HFPC	5.372923	1.031815	5.207254	0.730211	56.91	9.79E-04
TM-HFPC	8.163534	1.627455	5.016135	0.911878	55.95	1.49E-03
TM-HFPS	5.492173	1.056787	5.197048	0.739744	56.86	1.01E-03
TBr-HFPC	5.983086	1.160092	5.157424	0.776925	56.67	1.09E-03
PE-78	51.3549	8.7538	5.866585	1.710582	59.02	9.12E-03
PE-142	40.6626	6.0887	6.678345	1.609195	62.27	7.26E-03
PE-500	24.3176	3.4549	7.038666	1.38592	63.77	4.38E-03
PE-1000	20.0740	2.6296	7.633847	1.302634	65.69	3.63E-03

5.2.1.3 Discussion

This case study has highlighted the general work/data flow of the design framework for the simultaneous process and product design. Reverse design algorithm has been successfully applied to the oxygen enrichment design problem. It can be seen that using this design algorithm, it is very convenient to employ many different property models for the structured product to obtain polymers that would match the desired performance criteria.

The use of molecular modeling has been demonstrated to obtain properties of structurally different polymers at different temperatures for separation of oxygen from nitrogen. The polymers obtained from molecular modeling gave a very good performance (see Table 5.28). It can be seen that as the chain length of the polymer is decreased, the permeability increases. This could be attributed to the fact that with smaller chain lengths, there are more chain ending giving more free volume for the gases to diffuse faster.

5.2.2 Recovery of carbon dioxide from natural gas

Often natural gas contains carbon dioxide which must be removed prior to delivery to a pipeline as carbon dioxide is corrosive to the pipeline. The carbon dioxide rich stream has an application in the treatment of a gas containing carbon dioxide produced from a fractured well. High pressure carbon dioxide and water are injected into the well to fracture the tight formation trapping the natural gas. from 500 to 1200 tons of carbon dioxide are used in a typical well fracture, which can increase natural gas production 10-20 times [61].

Another application is carbon dioxide enhanced oil recovery [89]. Carbon dioxide flooding is often used to effectively enhance oil production from depleted oil fields and to extend the life of these oil fields. High pressure carbon dioxide is pumped in the ground on the periphery of the field. Carbon dioxide then diffuses through the formation and drives the residual oil to the already existing oil wells. In this recovery method, large quantities of carbon dioxide are required in the initial stages of injection program [61].

The objective of the gas separation is to claim both the natural gas and the carbon dioxide. The natural gas can be sold, and the recovered carbon dioxide can be re-compressed for re-injection into the field.

5.2.2.1 Design problem

Kesting et.al. have presented a case to concentrate carbon dioxide from 7% to 36.6% in a 300 mol/s at 850 psig using a polysulphone membrane. The design problem solved in this case study uses the same feed stream but with a higher purity of carbon dioxide in the permeate stream. The design problem is schematically shown in Fig. 5.38.
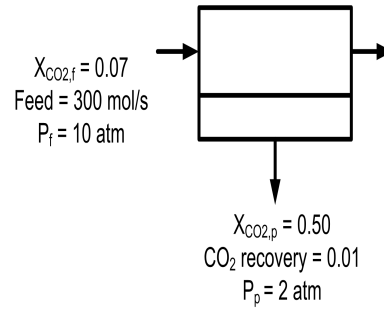
Figure 5.38: Design problem for carbon dioxide enrichment using membrane based gas separation process

In this case also the reverse design algorithm is used to find/design the polymer for recovery of carbon dioxide from natural gas. The step by step procedure presented in Chapter 2 has been applied.

Stage A: Setting the property targets

Step A-I: For a given feed $\underline{I}$ and performance criteria $\underline{P}$, the first step is to select/derive the rigorous process model and identify the design variables.

The process model for membrane-based separation process presented in Chapter 4 has been used. Different types of variables are listed in Tables 5.29 and 5.30.

Table 5.29: Types of variables in the membrane-based separation process model for recovery of carbon dioxide from natural gas

State	Property	Constitutive	Module parameter
2 - Total mass flows	2 - P_{CO_2} and P_{CH_4}	2 - $x_{CH_4,P}$, $x_{CH_4,F}$	4 - L,R, δ_m, N_f
4 - Comp. mass flows			
2 - Pressures on	4 - $\mu_{i,P}$, $\mu_{i,F}$	2 - N_{CO_2}, N_{CH_4}	
each side of membrane	4 - $\phi_{i,P}$, $\phi_{i,F}$		

Table 5.30: Known and unknown variables in the membrane-based separation process model

Known	Unknown
1 - Feed flow rate	1 - Molar fraction
1 - Comp. flow rate	of CO_2 in permeate
1 - Feed temperature	1 - Recovery of CO_2
1 - Feed pressure	

149

In this case, vector $\underline{I}$ and vector $\underline{P}$ is given as:

$$\underline{I}:$$
$$
\begin{aligned}
n_{Ft} &= 300\text{mol/s} \\
x_{f,CO_2} &= 0.07 \\
T_f &= 308.15K \\
P_f &= 10\text{atm}
\end{aligned}
$$

and

$$\underline{P}:$$
$$
\begin{aligned}
\text{Purity of } CO_2 &= 50\% \\
CO_2 \text{ recovery} &= 0.01
\end{aligned}
$$

The design variables are identified as the structural parameters of the polymers (repeat unit or the microscopic structure of the polymer).

Step A-II: Using the values of the performance criteria ($\underline{P}$), the outlet variables ($\underline{X}$) are calculated.

Using the purity and recovery of oxygen the outlet variables of the membrane module are calculated as:

$$\underline{X}:$$
$$
\begin{aligned}
x_{CO_2,P} &= 0.5 \\
N_{CO_2} &= 5.57e-3 \text{ mol/m}^2\text{s}
\end{aligned}
$$

For known values of $x_{CO_2,P}$ and N_{CO_2} in the process model, two variables that were originally known/specified can be calculated from the model. In this case also, the two permeabilities ((P_{CO_2} and P_{CH_4})) are calculated from the model.

Step A-III: With specified inlet and outlet variables, the target property values, defined by $\underline{\theta}_{target}$ are calculated.

The model can be solved to obtain the target values of the permeabilities of carbon dioxide and methane that would give the desired performance criteria. Model equations were solved with known values of $x_{CO_2,P}$ and N_{CO_2} to give the following values of the target properties:

$$
\begin{aligned}
\underline{\theta}_{target} \\
P_{O_2} &\geq 47.46 \text{ Barrer} \\
P_{N_2} &\geq 3.08 \text{ Barrer}
\end{aligned}
$$

Once θ_{target} has been calculated, the next step is to find the candidate polymer, either from the literature or by identifying the repeat unit of the polymer from group

contribution methods with properties matching θ_{target}. In this case, data from molecular modeling is not available.

Stage B: Design/Select polymers matching property targets

Step B-IV: Once the targets for the properties are set $(\underline{\theta}_{target})$, in the second stage, different property models are solved in order to get the structured products. In this stage, an extensive database search could also be made to identify the product with $(\underline{\theta}_{target})$ property values.

(a) Literature search: Some polymers with high permeabilities of carbon dioxide and methane were selected from a polymer database [95]. They are listed in Table 5.31. The full forms of the polymers is given in Appendix B.

(b) Group contribution model: Group contribution method proposed by Park et.al. (1997) [95] to predict permeabilities of gases through polymers is employed. The polymers whose properties were generated using the group contribution method of Park et.al. are presented in Table 5.32. The predicted values are compared with experimental values (see Fig. 5.39).
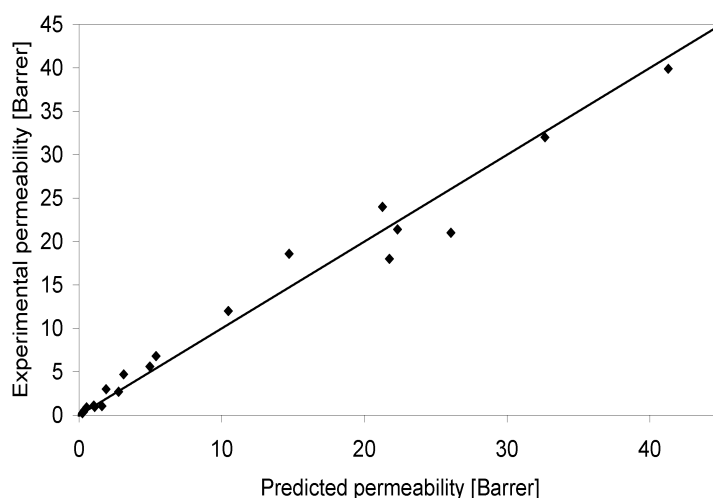
Figure 5.39: Comparison of permeabilities of carbon dioxide and methane from group contribution method [95]

Stage C: Rigorous simulation to validate the polymers

Step C-V: Once the feasible set of products is proposed, then an analysis is made to validate the choices. This is done by doing the rigorous simulations using forward algorithm for the products found in Stage II of the reverse algorithm.

Table 5.31: Permeability of carbon dioxide and methane in polymers from literature
[95]

Polymer	P_{CO2} (Barrer)	P_{CH_4} (Barrer)
TMPC	18.6	0.89
HFPC	24	1.05
TMHFPC	111	4.7
TMHFPSF	72	3
TBHFPC	32	0.89
TMBIPSF	31.8	1.27
PDMA-IPDA	27	0.9
6FDA-ODA	23	0.38
HMBIPSF	25.5	0.94
6FDA-6FpDA	64	1.6
6FBPA/TERE	47.1	2.74
SBI/TERE	55.7	4.2
6FBPA/BB	31.4	1.53
6FBPA/FO	29.9	0.981
PDMPO	65.5	4.1
PDPPO	39.9	2.7
BPA/Tbia	24.2	1.43
PhTh/Tbia	23.8	1.16
HPF/Tbia	36.8	2.38
TBBPA/TBIA	21.5	0.853
TBPHTH/TBIA	30.6	1.09
TBHPF/IA	20.4	0.567
TBHPF/TBIA	69.5	2.77
HFBPA/TBIA	56.9	3.47
6FDA-2,4-DATR	28.63	0.71
6FDA-3,5-DBTF	21.64	0.45
BPDA-6FPDA	27.4	0.761
PMDA-BATPHF	24.6	0.937
6FDA-BATPHF	22.8	0.703
6FDA-DAF	32.2	0.63
6FDA-TADPO PYRR	27.6	0.54

Table 5.32: Predicted permeability of polymers from group contribution model [95]

Polymer	Permeability [Barrer]	
	Carbon dioxide	Methane
BPA-PC	5.402	0.316
BPA-PS	4.955	0.232
TMPC	14.726	0.529
TMPS	26.06	1.094
HFPC	21.27	1.607
HFPS	10.46	0.368
PDPPO	41.30	2.772

Full names and the structures with the contributions of the groups in the polymers are given in Appendix A

Polymers from database and from group contribution methods were selected and plotted as shown in Fig. 5.40. Selectivity vs. permeability of carbon dioxide is plotted. The horizontal and the vertical line on the plot represents the target values of the properties and the polymers above these lines satisfy the property criteria.
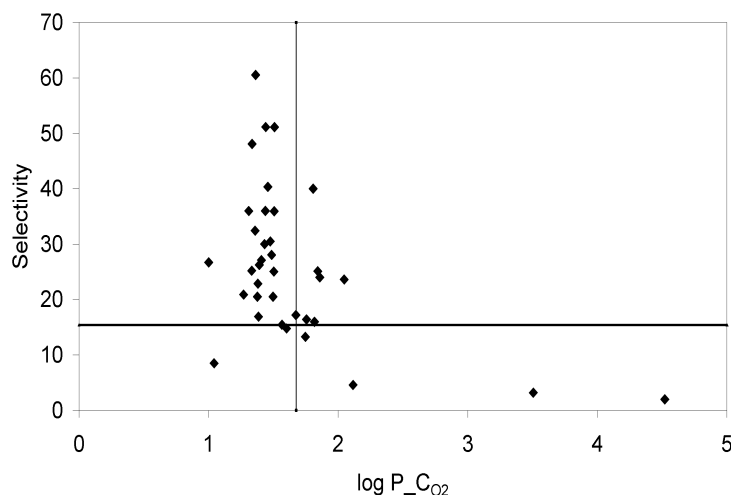
Figure 5.40: Polymers on property target plots

The validation step was performed only for the candidate polymers having the target properties. Table 5.33 shows that the desired performance criterion has been achieved for all the polymers possessing θ_{target} property values.

5.2.2.2 Discussion

This case study of enrichment of carbon dioxide from natural gas finds polymers at a repeat unit level. For obtaining methane rich stream with carbon dioxide content less than 2% as the retentate, polymers with very high carbon dioxide permeability (up to an order of 10^4 Barrer) should be chosen. And usually for such an operation multistage membrane-based separation unit is employed.

153

Table 5.33: Validation of the design obtained by reverse design algorithm

Polymer	Permeability		Selectivity	log P_{CO2}	% Purity	Recovery
TMHFPC	111	4.7	2.045323	23.61702	0.5912	0.0220
TMHFPSF	72	3	1.857332	24	0.596672	0.014366886
6FDA-6FpDA	64	1.6	1.80618	40	0.7032	0.0123
PDMPO	65.5	4.1	1.816241	15.97561	0.5052	0.0135
TBHPF/TBIA	69.5	2.77	1.841985	25.09025	0.6065	0.0138
HFBPA/TBIA	56.9	3.47	1.755112	16.39769	0.5116	0.0117

5.2.3 Recovery of aroma compounds from Black currant juice using vacuum membrane distillation

Fruit juice technology involves a purification operation where the juice is concentrated from 10-12% up to 65-75% by weight in order to reduce liquid volume, which not only lowers the costs in terms of storage, packaging and transportation, but also assists in preventing microbial spoilage of the juice concentrate. In industrial juice processing plants, juice concentration step is usually accomplished by aroma-stripping and the stripped aroma concentrate is later added back to the concentrated juice [55].

The more conventionally used method for fruit juice concentration comprises one or several multistage falling film vacuum evaporators connected to a separate aroma recovery plant. In the recovery units, aroma compounds are subject to high temperature rectification (counter-current distillation), condensation and washing. During high temperature distillation, the aroma profile of juices undergoes irreversible changes including heat induced transformations of sensory attributes (color, taste and aroma) and loss of nutrients (vitamin C).

Lately, membrane distillation, reverse osmosis and pervaporation have been considered as alternatives to the conventional techniques for the purification step in fruit juice industries. Lower operating temperatures and reduced vapor spaces (as compared to conventional distillation), lower operating pressures (as compared to other pressure driven membrane separations), reduced chemical interactions between membrane and process solutions and less demanding membrane mechanical property requirements are some of the benefits of membrane distillation over other more popular separation processes.

In this work, the use of the vacuum membrane distillation model described in Chapter 4 has been investigated for concentration of juice. The model was first validated with experimental data from literature for separation of ethanol, acetone and chloroform from water, respectively. Temperature, composition, flow rate of the liquid feed, and downstream pressure of the membrane are the main operational variables, and the effects of these variables are presented below.

5.2.3.1 Water ethanol separation

The accuracy of the VMD model has been evaluated by predicting the performance of VMD module for carrying out separation of ethanol from water. The experimental data reported by Lawson et.al.(1996) [71] has been used for validation of the developed model.

Module specifications: A square channel (flat-sheet membrane) of size 0.63×0.63 cm was used with a porous sintered metal support on the permeate side of the membrane. The total membrane area of 9.7 cm^2 has been used.

Membrane: Membranes provided by 3M Corporation were used. Results with 3MC membrane were used in this work for validation. The characteristics of this membrane are given in Table 5.34. In this case, as the experimental values of the constants K0 and B0 were given in the paper, so the corresponding model equations (Eq. 4.97, 4.99) were not used for validation.

Table 5.34: Membrane specifications for MC3 used for separation of water ethanol system using VMD

Maximum pore size (μm)	Free volume	Thickness (μm)	K_0 (10^{-7}m)	B_0 (10^{-14} m)
0.51	0.79	76	5.93	2.83

Experimental conditions: The feed solution contains 2 mol% ethanol in water. Unline other ethanol-water membrane-based separation studies, the data reported by Lawson et.al. [73] is appealing as the measurements were made at higher temperatures resulting in higher flux. The permeate pressure (P_{vacuum}) was kept constant at 3 kPa while the temperature was varied from 30 to 80°C. The feed flow rate of 63 cm^3/s was used.

The simulated results obtained with the developed VMD model are compared with experimental measurements in Fig. 5.41 and Fig. 5.42. A comparison of water and ethanol flux is made in Fig. 5.41 while a comparison of molar fraction of ethanol in the permeate side is made in Fig. 5.42. It can be noted that the simulations overpredict the values of the molar fraction of ethanol in permeate stream. As explained in the paper [71], that there could have been some experimental errors, as the tank containing water-ethanol solution used was open and there are chances that some of the ethanol might have evaporated.

5.2.3.2 Acetone water separation

The second comparison is done with experimental data from Sarti et. al. [9]. Acetone is recovered from a dilute binary solution of water and acetone. This case study shows the effect of varying the pressure on the permeate side of the membrane module. The vacuum side pressure is the major design factor since it greatly affects the separation efficiency.
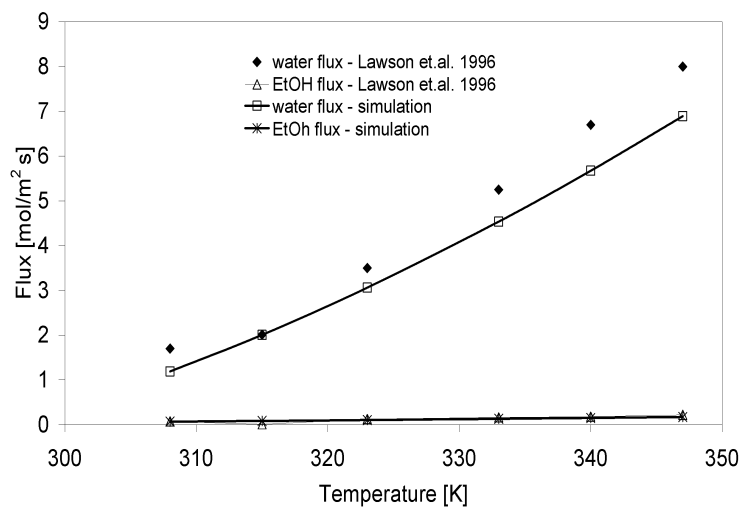
Figure 5.41: Water and ethanol flux - validation with experiments for water and ethanol separation
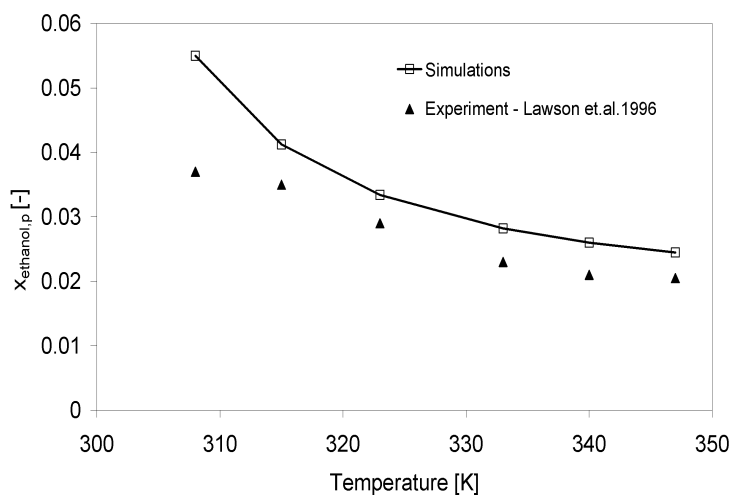
Figure 5.42: Molar fraction of ethanol in permeate - validation with experiments for water ethanol system

Module specifications: The membrane is located in the middle of a circular cell of 74 mm diameter and divides into two chambers of 2 mm depth. The useful membrane area for the process is 43 cm^2.

Membrane: Experiments were made by Sarti et.al. with flat PTFE membrane from Gelman Instruments Co. as TF200. The membrane has an average pore size of 0.2 m, a porosity of 60%, and a thickness of 60 μm.

Experimental conditions: The simulations were made at different conditions by varying the feed flow rate and the vacuum pressure on the permeate side. The simulated results were compared with 9 experimental data points for 3 different down stream pressures (20, 25 and 30 mbar) and 3 different flow rates (0.9, 1.75 and 2.6 L/min).

The comparison of the simulated results with reported experimental data are shown in Figs. 5.43- 5.45. Fig. 5.43 shows the comparison for water flux, while Fig. 5.44 shows the comparison for acetone flux. From a qualitative point of view the model has predicted the performance of the VMD process quite well at higher downstream pressures. It can be noted that as the downstream pressure increases, the trans-membrane flux decreases, which is due to the decrease in the driving force. Fig. 5.45 shows the comparison molar fraction of acetone in the permeate side which is very promising.
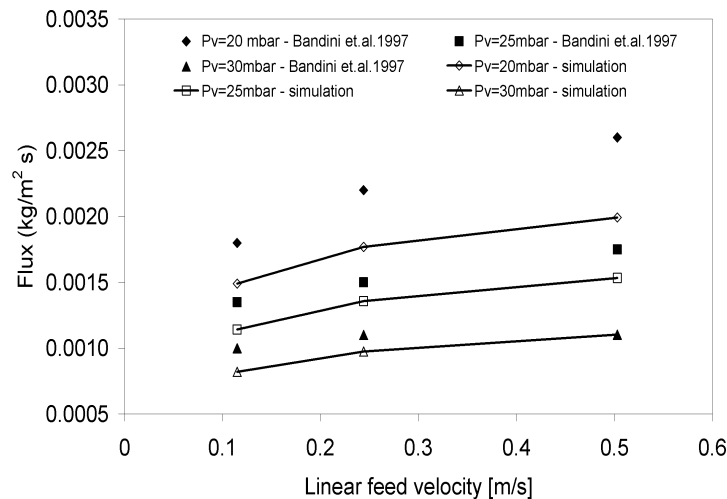
Figure 5.43: Water flux - validation with experiments for water acetone system

5.2.3.3 Water chloroform separation

Experimental data for a VMD module used to separate chloroform from water chloroform mixture has been reported by Urtiaga et.al.(2000) [113] in their experiments. The effect of varying the feed flow rate at low flow rates was studied here.

Module specifications: The aqueous feed was circulated through the lumen of
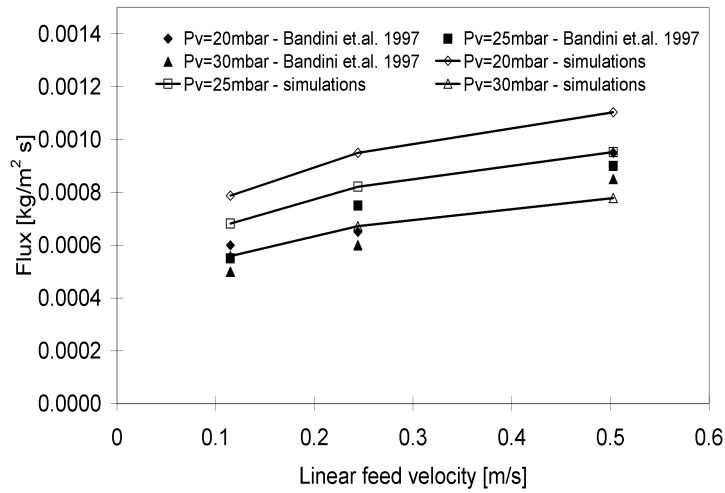
Figure 5.44: Acetone flux - validation with experiments for water acetone system
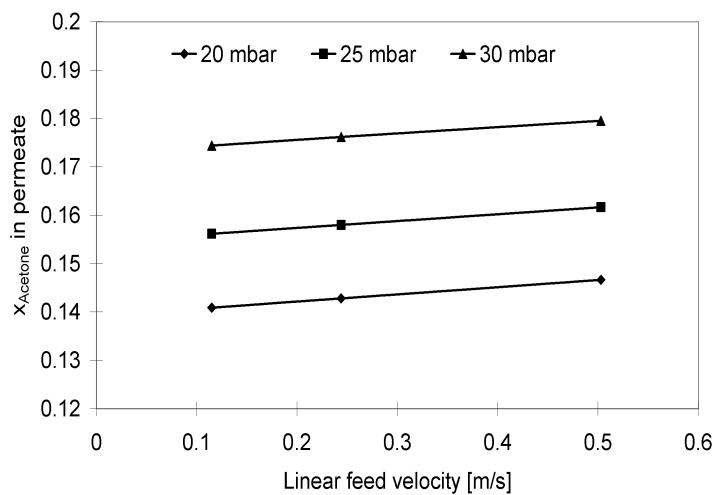
Figure 5.45: Acetone flux - validation with experiments for water acetone system

the hollow fibers and was introduced in a glass vessel with a capacity of 2 l. The module specifications are given in Table 5.35.

Table 5.35: Characteristics of membrane module for water-chloroform system using VMD

Inside diameter of the shell (m)	0.02
Inside diameter of hollow fiber (m)	5.5×10^{-3}
Thickness of membrane wall (m)	1.55×10^{-3}
Number of hollow fibers	3
Length of the module (m)	0.75
Total membrane area (m^2)	0.0389

Membrane: A hollow fiber membrane module with three porous polypropylene membranes was used. This membrane was obtained from Enka-Microdyne. The membrane has a pore size of 0.2 m and a porosity of 75%

Experimental conditions: The measurements were made bu Urtiaga et.al.(2000) at 25°C and with a downstream pressure of 9 mm Hg. The feed flow rate was varied from 0.23-1.43 l/min. The steady state water flux values were reported in the article which was used to validate the model.

The simulated results with the VMD model have been compared with experimentally measured data [113] of water flux values and are plotted in Fig. 5.46. The comparison seems reasonably precise. As can be seen from the results, the flux value does not change significantly with the change in flow rate of the feed at lower feed flow rates. These flow rates lead to a laminar flow regime with a calculated Reynolds number of 348 as compared to 333 from the experiments. The molar fraction of chloroform in the permeate stream is plotted in Fig. 5.47.
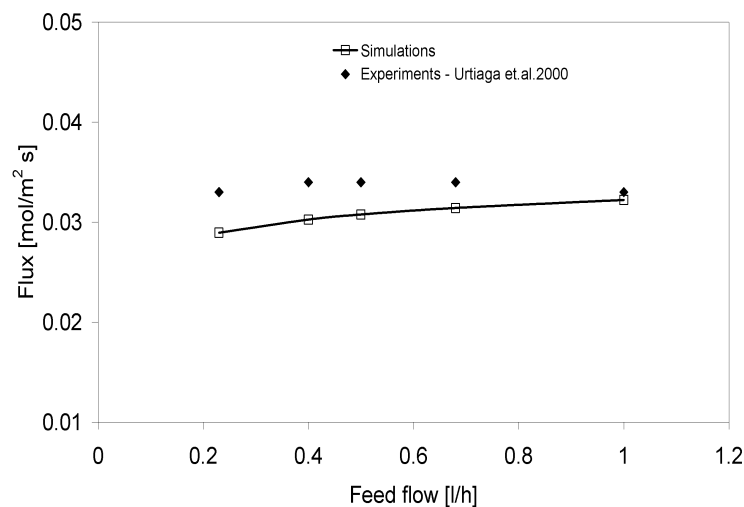
Figure 5.46: Total flux - comparison with experiments for water chloroform system
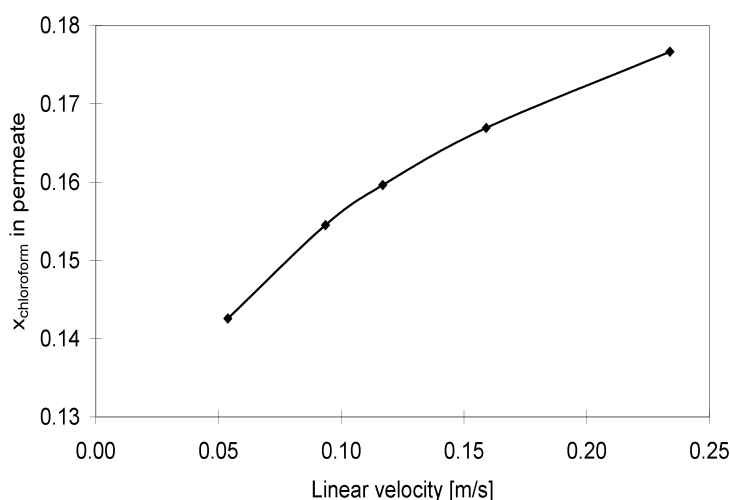
Figure 5.47: Molar fraction of chloroform in permeate

5.2.3.4 Recovery of aroma compounds from black currant juice

Simulations for the recovery of aroma compounds from Black currant juice using the VMD model was made under different conditions of operation. The unique aroma profile of black currant juice comprises more than 60 constituents but in this work, the twelve most characteristic aroma compounds have been used to validate the VMD model. The model requires calculation of pure component properties of all components of the system. The property models and the parameters needed to predict the properties of aroma compounds and water are given in Case study in Section 5.1.2. Since the properties are predicted and not all could be verified experimentally, it is important to check the effect of these properties on the concentration factors. In order to do so, a sensitivity analysis was made, where the property values were perturbed by ±5-20% and a change of concentration factor (CF) from the nominal value was plotted. If y is the output quantity on which the effect of the property ξ or the perturbed variable is to be seen, the the sensitivity is calculated as:

$$S_y = \frac{y(\xi) - y(\xi^*)}{y} \times 100 \tag{5.8}$$

where ξ is the reference value of the property and ξ^* is the value of the property after perturbation.

It was seen that molar fraction of aroma compounds in the permeate stream is not very sensitive to properties except activity coefficient and saturation pressure of the aroma compounds. The plots are shown in Fig. 5.48 and Fig. 5.49. This can be explained from the fact that the aroma compounds in the mixture are present in such small quantities that after applying the ideal mixing rule and calculating the mixture properties, the contribution of aroma part of the property is very small. However, activity coefficients and vapor pressures are used directly to calculate the partial pressures on each side of the membrane, which is the driving force to the process and have a large impact on the separation. So, care has to be taken while choosing the property models for these properties.

160
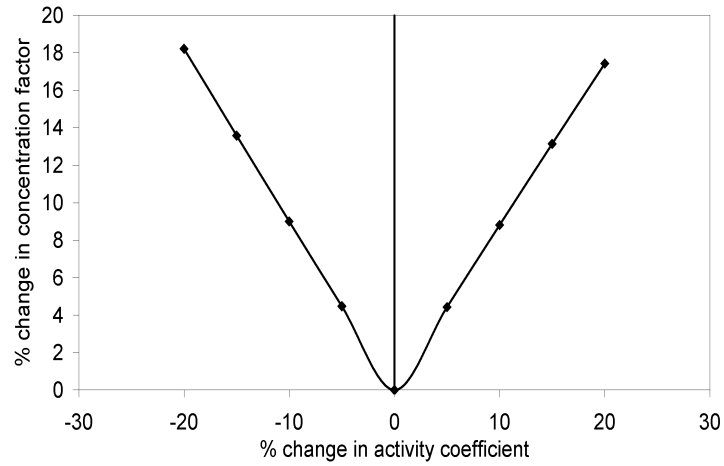
Figure 5.48: Sensitivity analysis for activity coefficients on the molar fraction of aroma compound in permeate
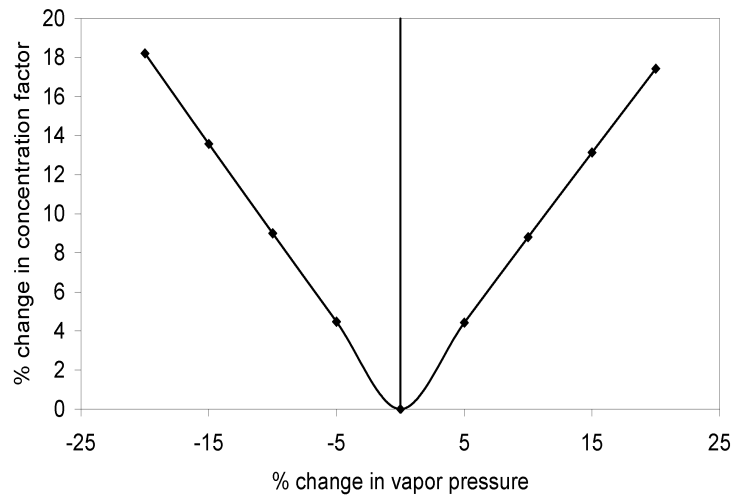
Figure 5.49: Sensitivity analysis for vapor pressure on the molar fraction of aroma compound in permeate

The membrane used in the experiments by Jorgensen et.al(2004) [55] was Polyte-
traflouroethane (PTFE). The properties of the membrane and specifications of the
membrane module are given in Table 5.36.

Table 5.36: Membrane specifications for polymer used for recovery of aroma com-
pounds from black currant juice

Membrane Specification	Value
Pore size, r_p [μm]	0.2
Porosity, ϵ [-]	0.75
Width, w, [cm]	3.8
Height, h, [cm]	0.1
Length, L, [cm]	9.75
Number of channels, n_c	1

For these membrane specifications, the prevailing mechanism for transport through
the membrane is Knudsen-viscous diffusion. The flux equation is then given by
Eq. 4.30 in Chapter 4. A term by term evaluation of the flux equation was also
performed in order to evaluate the effect of membrane parameters on the flux values.
The flux equation (Eq. 4.30) has two terms, as shown below:

$$\text{Flux} = \text{Term 1} + \text{Term 2} \tag{5.9}$$

$$\text{Term 1} = \frac{\left(D_{a,e}^i . \Delta p_i\right)}{R.T_{avg}.\delta_m} \tag{5.10}$$

$$\text{Term 2} = \frac{1}{R.T_{avg}.\delta_m}\left(B_0.\frac{p_{i,wf} + p_{i,wp}}{2.\mu_{gas}}.\Delta P\right) \tag{5.11}$$

The water flux at 303 K and 400 l/h is calculated to be 0.3391 mol/m²s and the
corresponding contribution of two the terms are: Term 1 = 0.3239, and, Term 2
= 0.0151 mol/m²s. This shows that in this case diffusive transport is much more
important than the convective transport. If the pore size is increased, the convective
term will become prominent because of the dependency on B_0 to a squared power
of the pore size (Eq. 4.99). The two terms are very sensitive to the values of the
membrane parameters K_0 and B_0 as a small change in these values creates a big
change in the value of the flux. These terms in turn depend on the value of the pore
size (r_p) and porosity (ϵ) of the membrane. So, a sensitivity analysis was performed
for both these variables (pore size and porosity) and their effect was seen on the flux
values (see Fig. 5.50 and Fig. 5.51). It can be seen that the flux is very sensitive to
the values of both these parameters and for a change of 15% there is approximately
a 13% change in flux value. So, in order to have accurate flux values from the
model, it is very important to have precise measurements of this variable. It was
seen that to have accuracy in the predicted flux value up to second decimal, it is
required to have accuracy of up to 8 decimal places for K_0. The partial pressure
and temperature were found to have a very small effect on the predicted values of
the flux.

Using the developed VMD model, the permeate concentration of the aroma com-
pounds and the flux were predicted, given the feed composition, operating temper-
ature and vacuum pressure. The feed concentration of the aroma compounds were
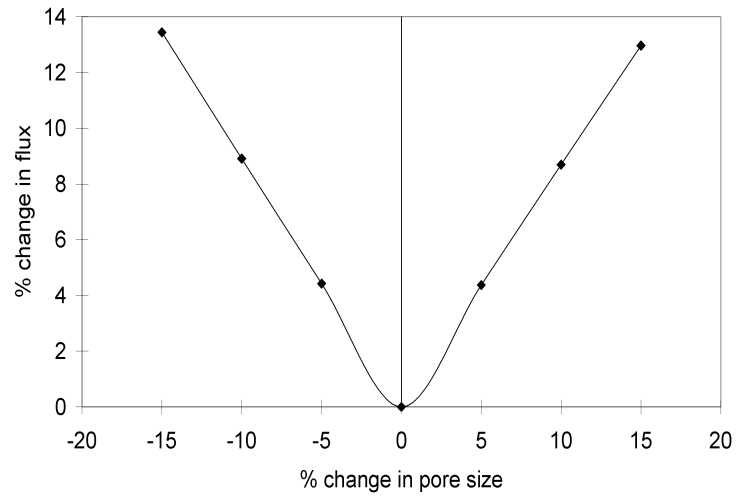
Figure 5.50: Sensitivity analysis of pore-size on total flux through membrane
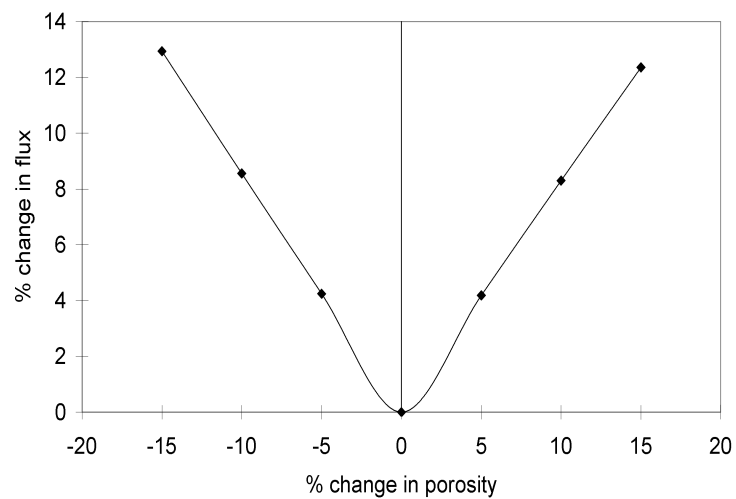
Figure 5.51: Sensitivity analysis of porosity on total flux through membrane

fixed at 1 ppm for the simulations (which is in accordance with the available experimental data). The concentration of aroma compounds in feed is so low that it was assumed that the presence of one aroma compound did not affect the transport of another. This assumption ultimately leads to the simplification of the system under study resulting in considering the total system as composed of twelve binary systems of each aroma compound with water rather than a single multicomponent system. The simulated results are shown in Fig. 5.52, where the concentration factors of aroma compounds in permeate from the model is compared versus those obtained from experiments [55] at three different feed flow rates (300, 400 and 500 l/h). The simulated values show a maximum deviation of 15% which is considered good in this case as the molar fractions are of the order of 1ppm. Total flux through the membrane is calculated at different flow rates (100, 300, 400 and 500 l/h) and was plotted in Fig. 5.53.
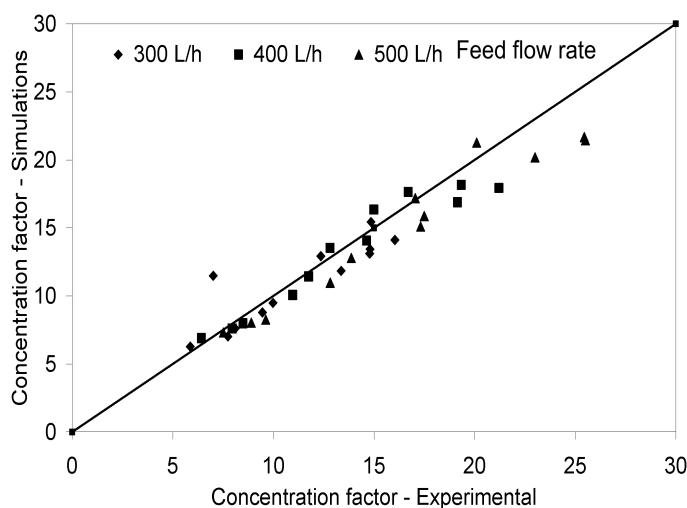
Figure 5.52: Comparison of concentration factors of aroma compounds from model and experiments at 30^oC and 300, 400 and 500 l/h

5.2.3.5 Post analysis

After the validation of the model, three aroma compounds, for which the infinite dilution activity coefficients were known as a function of temperature, were selected and simulations were made at different process conditions to study the behavior of the process variables on the separation factors. Calculations were made for ethyl butanoate, benzaldehyde and eugenol for temperatures ranging from 30^oC to 50^oC and flow rates from 300 l/h to 500 l/h. The plots comparing concentration factor of aroma for different temperatures and flow rates are shown in Fig. 5.54 to Fig. 5.56.

It can be seen from the plots that with the increase in temperature of the feed from 30^oC to 50^oC, the concentration factors (CF) of aroma compounds decrease. Increasing the flow rate, the concentration factors showed some increase but the change was not significant. The change in CF is much more when the temperature

164
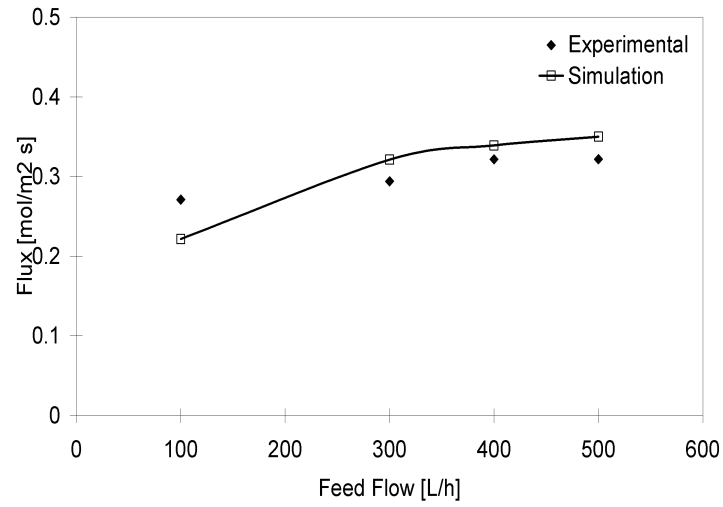
Figure 5.53: Comparison of flux through membrane from model and experiments at 30^oC and 100, 300, 400 and 500 l/h
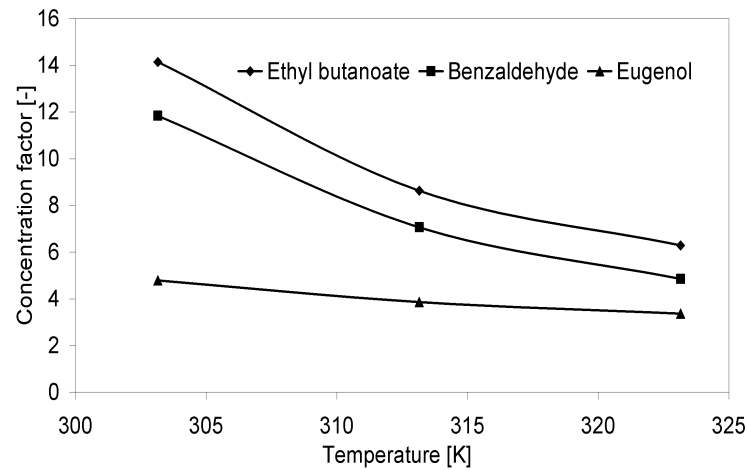
Figure 5.54: Comparison of concentration factor of aroma compounds at 300 l/h and T=30, 40, 50^oC

165
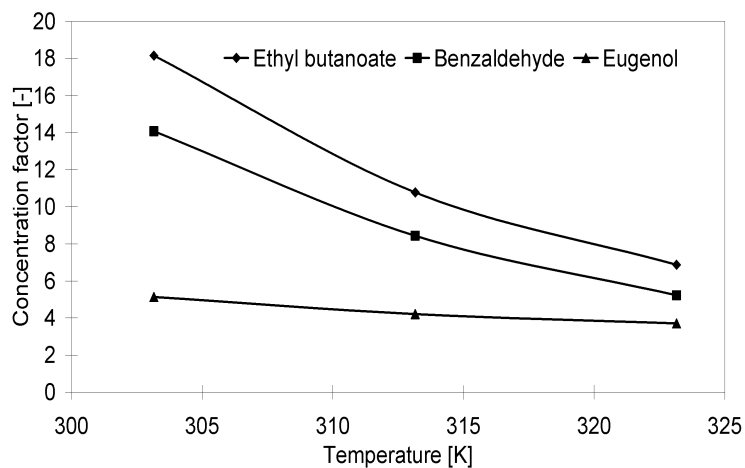
Figure 5.55: Comparison of concentration factor of aroma compounds at 400 l/h and T=30, 40, 50°C
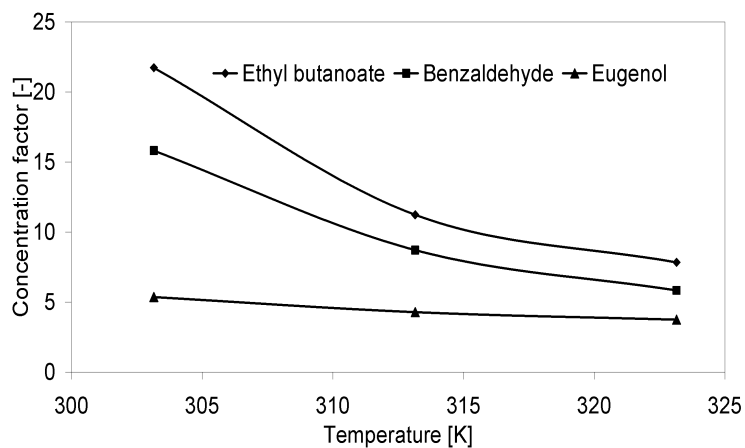
Figure 5.56: Comparison of concentration factor of aroma compounds at 500 l/h and T=30, 40, 50°C

is changed and the reason for this is that the infinite dilution activity coefficients and vapor pressures of the aroma compounds are sensitive to changes in temperature but not with the feed flow rate. The sensitivity analysis made on all properties also showed that the concentration factors of aroma compounds is very sensitive to activity coefficient and vapor pressures as compared to any other property. With a change of 20^oC in temperature the percentage change in the activity coefficients for ethyl butanoate, benzaldehyde and eugenol is 13.5%, 11.86% and 23.86%, respectively. While changes in flow rate from 300-500 l/h produced changes of CF of only around 0.01% for each compound. It was observed that even though all aroma compounds show a common trend, they change with a different degree with change in the process variables (see Fig. 5.54 to Fig. 5.56). This mainly depends on the different selectivities imparted by membrane to different compounds.

With the increase in temperature the permeate flux increases thereby the concentration of the individual aroma compounds at the membrane surface due to concentration polarization, which ultimately leads to the drop in CF. The effect of concentration polarization by varying the temperature was investigated by checking the concentration polarization in each case and the corresponding CF. Fig. 5.57 illustrates this effect on the concentrations of aroma compounds at the membrane surface as a function of temperature. The concentration factor drop is approximately 59%, 55% and 30% for benzaldehyde, ethyl butanoate and eugenol, respectively. This can be explained by noting the concentration polarization effect of these compounds at the membrane surface of the feed side of the membrane. The percentage concentration drop of the aroma compounds (x_{bf}/x_{wf}) is approximately 51%, 33% and 25% for benzaldehyde, ethyl butanoate and eugenol, respectively. This demonstrates the concentration polarization effect.
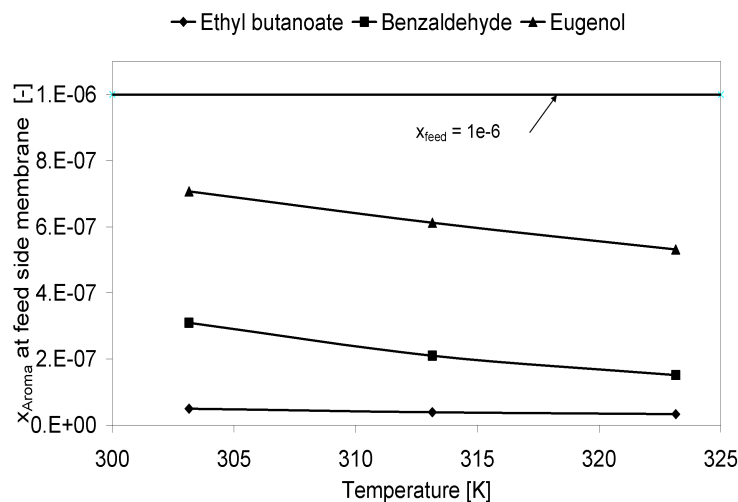
Figure 5.57: Comparison of molar fraction of aroma compounds at the membrane surface of the feed side of the membrane at 300l/h and T=30, 40, 50^oC

167

5.2.3.6 Simultaneous process-product design

To demonstrate simultaneous process-product design through the design framework, the case of benzaldehyde-water system is chosen. For a feed with 1 ppm concentration of benzaldehyde at 323.15 K and 300 l/h with PTFE membrane, the concentration factor (CF) of benzaldehyde is 4.85. To design a process for a much higher CF = 8.5 and a recovery of 5e-7, reverse design algorithm is used.

Stage A: Setting the property targets

Step A-I: For a given feed $\underline{I}$ and performance criteria $\underline{P}$, the first step is to select/derive the rigorous process model and identify the design variables.

The process model for VMD process presented in Chapter 4 has been used. The details of the model equations and variables are given in Appendix A.

The vector $\underline{I}$ and vector $\underline{P}$ are given as:

$$\underline{I}:$$
$$
\begin{aligned}
n_{Ft} &= 300 l/h \\
x_{f,O_2} &= 1 ppm \\
T_f &= 323.15 K \\
P_f &= 1 \text{bar}
\end{aligned}
$$

and

$$\underline{P}:$$
$$
\begin{aligned}
\text{CF of Oxygen} &= 8.5 \\
\text{Oxygen recovery} &= 5e-7
\end{aligned}
$$

The design variables could either be related to the process (d_1) or to the structured material (d_2). Two cases are considered here. Case A demonstrates the product design calculations where the design variables are identified as the structural parameters of the polymers (pore size and porosity of the polymer).

Case A: Product design If two variables CF and recovery are given in the model, two additional variables can be calculated from the model. If product design is intended, then the two design variables could be the pore size r_p and porosity ϵ of the polymer. So, in the first stage of the algorithm the values of the key properties (Knudsen diffusivities in this case) are calculated.

With the given feed conditions and the performance criteria in terms of CF and recovery, the model was solved for the Knudsen diffusivities. The values are:

$$
\begin{aligned}
D_{k,water} &= 5.4e-5 \\
D_{k,benzaldehyde} &= 2.26e-5
\end{aligned}
$$

Once θ_{target} has been calculated, the next step is to find the candidate polymer. In this case, the property models presented in Section 4.2 of Chapter 4 are used to find structure of the polymer, with properties matching θ_{target}.

Stage B: Find structure of polymers matching property targets

The pore size and the porosity are calculated as:

$$
\begin{aligned}
r_p &= 8.227e - 7m \\
\epsilon &= 0.57
\end{aligned}
$$

Case B: Process design: In this case the polymer was chosen to be PTFE, so the structural parameters of the polymer are already fixed (ϵ =0.75 and $r_p = 1\mu$m). In this case, the variables to be predicted from the model are, the feed temperature and the flow rate. The values calculated are:

$$
\begin{aligned}
T_f &= 312K & (5.12) \\
m_f &= 402l/h & (5.13)
\end{aligned}
$$

Similarly, if the membrane module is to be designed, the design variables could be the parameters related to the geometry of the membrane module like, the length or height of the channel.

5.2.3.7 Discussion/Conclusions

The VMD model was tested for the separation of volatile organic compounds from an aqueous solution. For the separation of Ethanol, Acetone and Chloroform from water the VMD model predicted the fluxes quite reasonably for different temperatures, feed flow rates, vacuum pressures, different polymers and module geometries. Experimental results for recovery of aroma compounds from black currant juice were used to validate the model. A sensitivity analysis was made to see the effect of physical properties of the components and of the membrane parameters on the concentration factors and fluxes. A comparison of the experimental and simulated values for the molar fractions of aroma compounds in the permeate stream exhibited a maximum of 15% relative error. So, it can be concluded that the model represents reasonably well, the physical behavior of the process.

A model-based analysis of the process made for three selected aroma compounds explained the experimentally observed trends with respect to the change in temperature and flow rate of the feed mixture. With the increase in temperature of the feed from 30ºC to 50ºC the concentration factors of aroma compounds decreased, while not much effect with respect to the change of the flow rate could be observed. The VMD model was able to predict the effects of concentration and temperature polarization well.

A simultaneous process product design example has been demonstrated to find the

structure of the polymer or the process conditions for a given performance criteria of the process.

5.2.4 Comparative study of various membrane distillation processes

The objective of this case study is to present a comparative study between the process performance of different kinds of membrane distillation processes (vacuum membrane distillation (VMD), sweeping gas membrane distillation (SGMD) and direct contact membrane distillation (DCMD)). A water-ethanol separation (during fermentation of biomass) using membrane distillation modules is used as the example mixture to highlight the differences between the different MD processes. The primary step in the production of various beverages and alcohol fuels is the fermentation of biomass (e.g. grains, starches, sugars, cellulose) to alcohols [63]. As fermentation proceeds, the increase in product concentration hampers the microbial activity by product inhibition. This is incentive to continually remove products of reaction. To do so, membrane distillation could be used.

But before the comparison is done, the process models for SGMD and DCMD are compared and validated with the experimental data (validation for VMD process model is presented in Section 5.2.3 of this chapter).

5.2.4.1 Sweep gas membrane distillation

The process performance of SGMD process depends on variables such as: feed flow, sweeping gas flow, feed temperatures and gas temperature. The experimental data reported by Khayet et.al.(2000) [63] demonstrates the effect of all these variables on the SGMD flux. In this case study, however, SGMD flux as a function of the sweeping gas velocity has been used for validation of the process model.

Module specifications: A flat-sheet membrane having an effective area of about 5.6e-3 m^2 is used.

Membrane: A hydrophobic membrane made of polytetraflouroethylene (PTFE) is used. the main characteristics of this membrane are: pore diameter 0.2 μm; thickness 178 μm and porosity 0.8.

Experimental conditions: The feed solution contains pure water. The sweeping air circulation velocity is varied between 0.5 and 2 m/s. Water circulation velocity is 0.15 m/s, water inlet temperature 65°C and air inlet temperature 20°C.

The simulated results obtained with the SGMD model are compared with experimental measurements in Fig. 5.58. A comparison of water flux is made and it can be noted that the simulations predict the flux values quite well.
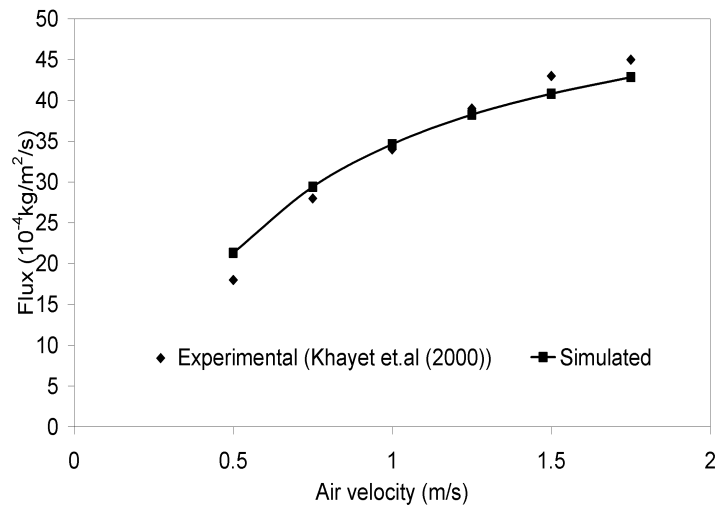
Figure 5.58: Total flux - comparison with experiments for sweep gas membrane distillation

5.2.4.2 Direct contact membrane distillation

The experimental data reported by Lawson et.al.(1996) [72] has been used for validation of the developed model.

Module specifications: A square channel (flat-sheet membrane) of size 0.63×0.63 cm was used with a porous sintered metal support on the permeate side of the membrane. The total membrane area of 9.7 cm^2 has been used.

Membrane: Membranes provided by 3M Corporation were used. Results with 3MA membrane were compared with the simulated results. The characteristics of this membrane are given in Table 5.37.

Table 5.37: Membrane specifications for 3MA used for DCMD process

Maximum pore size (μm)	Porosity	Thickness (μm)	K_0 (10^{-7}m)	B_0 (10^{-14} m)
0.29	0.66	91	2.61	0.934

Experimental conditions: The feed solution contains pure water. The temperature of the feed was varied from 30 to 80°C. The feed flow rate of 63 cm^3/s was used.

The simulated results obtained with the DCMD model are compared with experimental measurements in Fig. 5.59. As can be seen from the figure that the predicted fluxes with the model are quite precise.

5.2.4.3 Comparative study

The performance criteria in membrane-based separation processes is measured by the transmembrane flux and the product purity. In this case study, the effect of
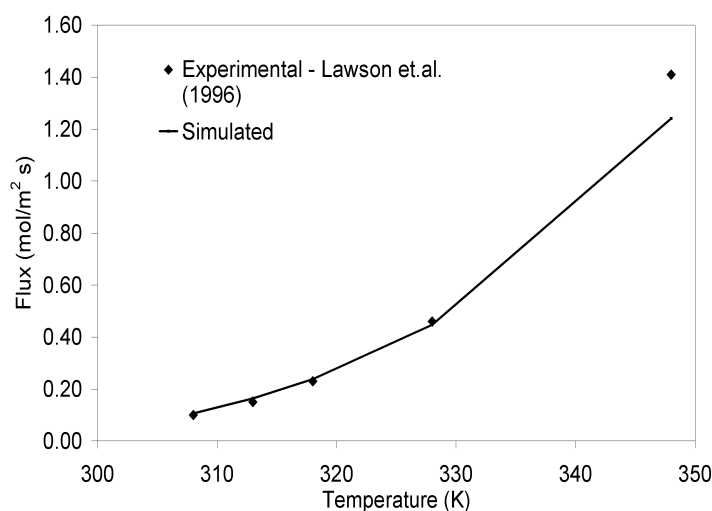
Figure 5.59: Total flux - comparison with experiments for direct contact membrane distillation

change of feed temperature is studied on the flux and the product purity for different MD processes. Water-ethanol separation using VMD process has already been presented in Section 5.2.3. The same configuration of the membrane module and the membrane is used in this case study as well. The process conditions are given below for VMD, SGMD and DCMD process.

VMD: Linear feed velocity of 1.56 m/s (corresponding to 63 cm^3/s feed flow rate from water-ethanol case study in Section 5.2.3) is chosen. A vacuum pressure of 3000 Pa is applied.

SGMD: Linear feed velocity of 1.56 m/s and a linear permeate velocity of 10 m/s is chosen. As the velocity of gas on the permeate side is low, the residence time is longer, and hence the gas is very saturated in the solute when it leaves the module. This increases the partial pressure of solute, thereby reducing the flux values. Therefore a higher linear permeate velocity is chosen. An inlet temperature of gas is chosen as 20°C.

DCMD: Linear feed and permeate velocity of 1.56 m/s is used with an inlet temperature of 20°C on the permeate side.

The feed temperature in each case is varied from 30°C to 45°C. With these conditions the simulations are made for all the three processes. Fig. 5.60 shows the effect of change in the feed temperature on the total flux through the membrane.

As can be seen from the figure, for all the cases the flux increases monotonically with the increase in the feed temperature. This is due to increase in partial pressure on the feed side of the membrane. It can be seen from the Fig. 5.60 that for VMD process the increase in flux is much more than the others. The main reason for
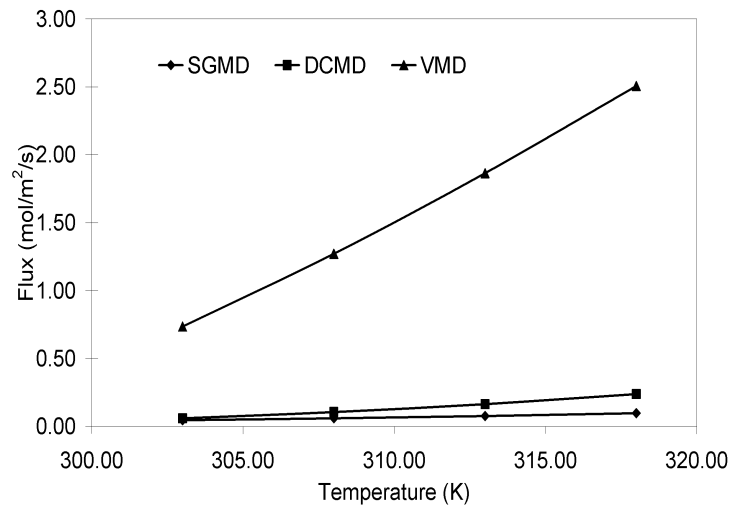
Figure 5.60: Total flux - comparison with experiments for sweep gas membrane distillation

that is the fact that the partial pressure on the feed side increases with increase in temperature but the partial pressure on the permeate side remains constant as it is only influenced by the vacuum pressure on the permeate side. While for DCMD process, partial pressure increases on the feed side, but simultaneously the partial pressure on the permeate side also increases due to large heat transfer through the membrane thereby increasing the permeate temperature. For SGMD process, the flux increases a bit in the beginning, but soon the gas starts to be concentrated on the permeate side hence increasing the partial pressure and reducing the driving force.

Fig. 5.61 presents molar fraction of ethanol on the permeate side as a function of temperature. It can be noted that even though the fluxes generated by VMD were the highest, the CF of the product is very low as compared to SGMD and it also decreases with increase in temperature. This can be explained by temperature and concentration polarization phenomena in these processes. These phenomena are much more prevalent in VMD and SGMD due to very fast evaporation of ethanol. The concentration and temperature polarization effects are shown Fig. 5.62 and 5.63 respectively.

Fig. 5.62 shows the molar fraction of ethanol at the wall of the feed side of the membrane. The bulk feed molar fraction of ethanol is 2%. It can be noted that for DCMD it remains almost the same, while for VMD there is a huge drop. This is due to very high fluxes in VMD, that leads to low concentration of ethanol at the feed side of the membrane. This explains the reduced purities at higher temperatures for VMD process. Its the same phenomena for SGMD For DCMD, the increase in feed temperature increases the partial pressure on the feed and also the temperature and partial pressure on the permeate side is increased. For lower feed temperatures, the flux is not that high, so polarization effect can not be seen very prominently. But with the increase in temperature and hence the flux, some polarization effect can be seen for higher temperatures. Fig. 5.63 shows the temperature polarization effect.

173
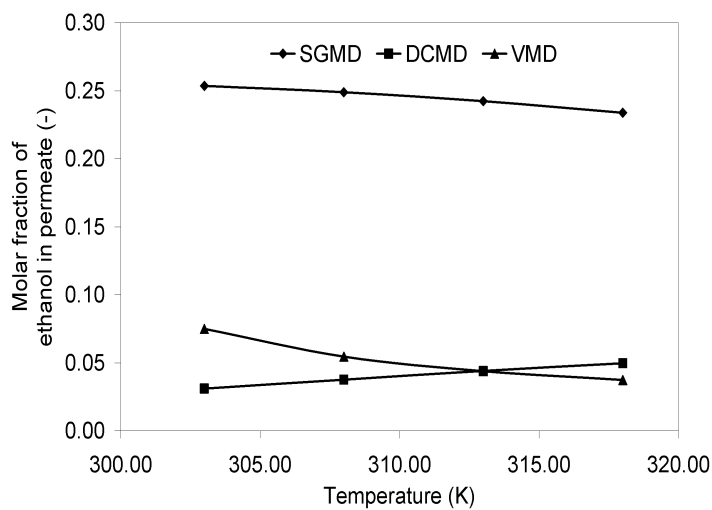
Figure 5.61: Molar fraction of ethanol in permeate - A comparison of VMD, SGMD and DCMD
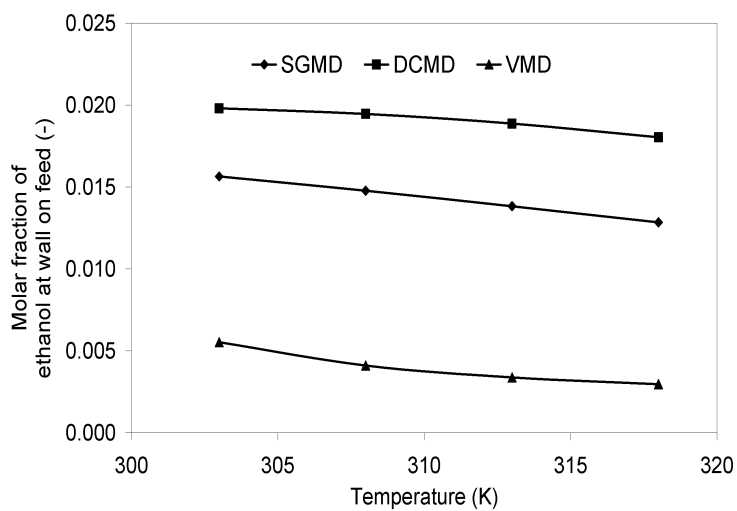
Figure 5.62: Molar fraction of ethanol on wall of the feed side of membrane - Concentration polarization effect
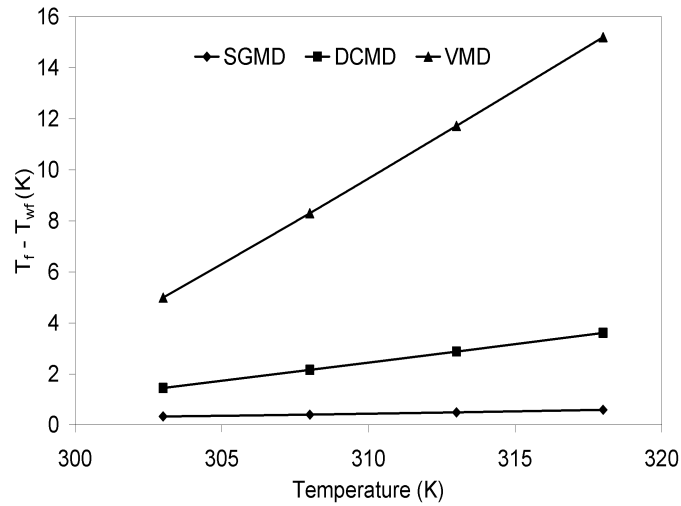
Figure 5.63: Temperature polarization effect for VMD, SGMD and DCMD

5.2.4.4 Discussion/Conclusions

The comparative study made in this case study highlights the polarization effect in membrane distillation processes and its effect on the product CF. It was seen from the results that with an increase in feed temperature, polarization effects are very high due to high fluxes in VMD and hence the product CF is very low as compared to SGMD and DCMD processes.

<div align="right">

6

</div>

Conclusions and future recommendations

6.1   Achievements

A computer-aided model-based design framework for the simultaneous design of processes and the assisting structured materials has been developed and its application illustrated with detailed examples. The major achievements of this PhD project are summarized below.

6.1.1   Design framework

The proposed design framework is a general framework for the simultaneous process-product design that contains model libraries for process models and property models for assisting structured materials and chemicals present in the process streams. The design framework is able to handle various multilevel models integrated together. The developed framework differs from other conventional design methods as it tracks the properties of the assisting structured materials rather than the composition and recovery of the end-use products of the process to match the desired process performance. This essentially gives a whole new dimension to the design problem as the properties of the structured material not only depends on the process conditions such as composition, temperature and pressure but also on their structure. The design framework establishes and illustrates through case studies the vital connections between process performance - properties of structured materials - microscopic structure of structured materials.

The design framework includes a robust design algorithm that solve the multilevel model equations with computational ease by decomposing the problem into two stages (sub-problems). The iterative nature of the conventional design algorithms is avoided by the reverse design algorithm for the application of the developed multilevel models for the simultaneous process-product design.

The applicability of the design framework has been illustrated through case studies demonstrating the simultaneous design of membrane-based separation process and the polymers that can be used as a membrane, that is, as a separation medium. It should be noted, however, the design framework is very general in nature and can be applied to many processes and products.

6.1.2 Process models

Generic process models for membrane-based liquid separation with phase change and membrane-based gas separations have been developed. The representation of the process with the model equations allows their easy rearrangement depending on the simulation method (forward or reverse) to be used. A model analysis in terms of number of variables (known, unknown, explicit and implicit), number of equations and degrees of freedom has been performed. That made the application and solution of the model equations through a computer-aided system quite simple and straight-forward.

The process model developed for membrane-based liquid separation with phase change is generic in nature and by introducing assumptions for individual processes it is possible to generate models for vacuum membrane distillation, sweep gas membrane distillation, direct contact membrane distillation, osmotic membrane distillation and pervaporation. The model is able to predict the effects of concentration and temperature polarization and calculates transmembrane fluxes based on Knudsen, viscous and/or molecular diffusion mechanisms. Knudsen, viscous and molecular diffusivities, that enhances or retards the process performance by affecting the flux of individual permeants, depend on the pore size and the porosity of the membrane material. Sensitivity analysis for these two structural properties to study their effects on the flux have been performed. The analysis showed that for a change of 15% in these properties the change in flux is about 12-13%. This reinforces the hypothesis that the process performance is dependent on the structure of the assisting structural material.

The process model for membrane-based gas separation based on solution-diffusion mechanism has been developed for counter-current and co-current operations. Permeability is shown to be the key property that affects the separation process. Case studies involving membrane-based gas separation, employing the developed process model, highlights the role of permeability in the design process. The uses of process model, in the reverse design algorithm, have been presented for simultaneous design of membrane-based gas separation process and polymers used as membrane.

6.1.3 Property models

Property models for prediction of properties of the assisting structured materials (in this case polymers) and the property models for chemicals present in the process streams have been compiled for use by the design framework. For properties of both polymer and chemicals in process streams, group contribution methods have been successfully applied.

The use of group contribution methods based on higher level of functional groups have been illustrated. Their application is demonstrated through the prediction of the properties of aroma compounds in black currant juice whose experimental values for properties like density, viscosity, vapor pressure etc., were not available as a function of temperature. The effect of these properties on the process performance

was also estimated through a sensitivity analysis. It was found that some properties such as activity coefficients and vapor pressures play a very important role for membrane-based liquid separations with phase change. So, their precise measurement/estimation is very important. For the case of recovery of aroma compounds from black currant juice, it was demonstrated that group contribution can predict the properties quite well to match the experimental results.

For the prediction of permeability of small gases in polymers, the uses of group contribution model based on fractional free volume of the polymer matrices have been presented. Design of polymers for required target properties, obtained from solving process models with given performance criteria, group contribution models have been used to design polymers at repeat unit level. Predictive models of Van Krevelan were also employed to design polymers at a repeat unit level.

Apart from group contribution methods, application of molecular modeling has been demonstrated by generating pseudo-experimental data for the diffusivities and solubilities of small gas molecules through the polymer. As experiments are sometimes time consuming, expensive and possible, molecular modeling has proved to be very useful, specially in the case where the properties have been predicted for polymers with structures that are not reported before. A hierarchal procedure for a step by step prediction of solubility and diffusivity of gases in polymers through molecular modeling have been presented. In most of the cases reported in the literature, the united atoms approach has been used to predict permeability of gases in polymers. In this work, the all atom approach has been employed to avoid the loss of precision resulting from the approximations made by the united atoms approach.

6.1.4   Reverse design algorithm

A design algorithm for the simultaneous process and product design has been proposed. This algorithm, called the reverse design algorithm, divides the solution steps in two stages. This is achieved by first defining the design targets in terms of the properties of the structured material assisting the process for the specified process performance (stage 1), and then finding (designing) structured materials that match the property targets (stage 2). In this way, the process model does not need a structured material property model, since the properties are the unknown variables. Once the property targets are obtained from the first stage, structured materials corresponding to these properties can be found using property models that relate the properties to the microscopic structure of the materials.

Application of this design algorithm avoids the iterative procedure in the forward design algorithm, where for each proposed design in terms of process or product variables the full set of process model equations need to be solved for every iteration. It has also been demonstrated, that splitting the solution steps in two stages makes the solution of the model computationally inexpensive as the property models need not be solved as an integrated part of the process model. Through case studies of the design of membrane-based separation processes, the uses of different kinds and different levels of property models were highlighted.

6.1.5 Case studies

Various case studies involving membrane-based separation processes have been developed to demonstrate the applications of the model-based design framework and the reverse design algorithm. The hierarchal procedure to predict the barrier properties of polymers using molecular modeling has been applied to predict solubility and diffusivity of oxygen and nitrogen in polyisobutylene with 48 carbon atoms and at different temperatures using the all atoms approach.

The simultaneous design of membrane-based gas separation and the polymer used as a membrane has been presented with case studies involving the enrichments of oxygen from air and carbon dioxide from natural gas. A process-product design case study involving the recovery of aroma compounds from black currant juice has also been developed along with the prediction of properties of aroma compounds using group contribution methods. A comparative study is made to highlight the polarization effects in membrane distillation processes and its effect on the product concentration factor.

6.2 Challenges and future directions

The development and application of the model-based design framework has progressed quite well. However, there is still a lot of scope for improvement and further developments. Some suggestions are given below.

- The application of the design framework has been demonstrated for membrane-based separation processes, so the models for both the processes and for the structured material properties are very specific. There is a need for development of models from different areas of application to widen the scope of application of the design framework and make it more generally applicable.

- To obtain closed form property models for permeability of gases through polymers a lot more data needs to be generated using molecular modeling at different structures of polymers at different process conditions. Having the appropriate closed-form models increase the application range while making the integration of the property model with the process model more simple and easy.

- The main difficulty with the application of molecular modeling is the enormous amount of real and CPU time required. To save some real time for these simulations, the simulation programs should be run on cluster of computers rather than single computers. For lesser CPU time for the same calculations, faster methods such as transition state theory could be applied to predict the diffusivities of gases in polymers instead of brute-force molecular dynamic simulations used in this work.

- Experimental validation and manufacturing of the polymers found in case studies is needed to validate the design framework and models experimentally.

- For the application of group contribution methods to generate new structures, rules for structure generation for polymers should be introduced.

A

Model details for MD and PV processes

This appendix gives the model generation and analysis of individual models for membrane-based liquid separation with phase change. For each process, different variables (differential, algebraic and known) are presented, along with the equations to be solved. Some of the variables are vectors, the number in parenthesis along with the variable represents the size of the vector. After the variables and the equations, the code that was implemented in ICAS-MoT is presented along with the variable analysis screen shot from the model test bed (ICAS-MoT). The right hand corner of screen shot shows the number of equations, degrees of freedom and number of differential variables of the model solved.

A.1   Direct contact membrane distillation

The model analysis for direct contact membrane distillation is given below. The model analysis is illustrated for a binary mixture (N=2). The model analysis is shown for Knudsen-molecular diffusion mechanism. The model for DCMD has 144 variables out of which 8 are differential variables; 80 algebraic variables (explicit or implicit, calculated from 80 equations) and 56 known variables. Table A.1 lists different variables in the DCMD. Table A.2 lists different equations that need to be solved for DCMD.

A.2   Osmotic membrane distillation

The model analysis for osmotic membrane distillation is given below. The model analysis is illustrated for a binary mixture (N=2). The model for OMD is very similar to DCMD, the only difference being the calculation of the activity coefficients of the mixture on the permeate side due to the presence of salt in the solution. The model for OMD has 144 variables out of which 8 are differential variables; 80 algebraic variables (explicit or implicit, calculated from 80 equations) and 56 known variables. Table A.3 lists different variables in the OMD. Table A.4 lists different equations that need to be solved for OMD.

Table A.1: Variables in DCMD model

Differential Variables (8)		Number
Mass flow	m_f, m_p, $\underline{m_{f,i}}(2)$, $\underline{m_{p,i}}(2)$	6
Temperature	$\overline{T_f}$, T_p	2
Algebraic Variables (80)		**Number**
Process variables	V_f, V_p, $\underline{R_i}(2)$, R_{total}, Q_m, T_{wf}, T_{wp}, $\overline{T}_{avg}$, $Q_{process}$, $\underline{p_{i,wf}}(2)$ $\underline{p_{i,wp}}(2)$, $x_{i,wf}(2)$, $\underline{x_{i,wp}}(2)$, $\overline{C_t}$, $\underline{x_f}$ (1) u_f, u_p, Recovery, CF	24
Flow parameters	Sh, $\underline{Re}$ (2), Sc, $\underline{Nu}$ (2), $\underline{Pr}$ (2)	8
Component /mixture properties	$\underline{\rho}(9)$, $\underline{Cp}(6)$, $\underline{\Delta H_{vap,i}}(2)$ $\underline{P_i^{Sat}}(2)$, D_{ij}, $\underline{\mu}(12)$, $\overline{k_{h,i}}(2)$, $\mu_{gas,i}(3)$	37
Polymer properties	K_0, K_1, $\underline{D_{ie}^k}(2)$, D_{ije}^0, τ	6
Module parameters	dh	1
Transfer coefficients	h_f, h_p, h_m, k_m	4
Known Variables (56)		**Number**
Process variables	P_f, P_p, $\underline{x_{i,f}}(1)$	3
Component properties	$\underline{M_i}(2)$ $\underline{\gamma_i}(2)$	4
Regressed variables	5 variables for each pure component property	40
Polymer properties	ϵ, r_p	2
Module parameters	w, δ_m, L, h, n_f	5
Constants	R_g, π	2
For a binary mixture the total number of variables:		**144**

Table A.2: Equations to be solved for DCMD process

Variables	Number	Equations
Differential variables	8	4.3, 4.10, 4.12, 4.13, 4.20 4.21
Process variables	24	4.5, 4.6, 4.8, 4.9, 4.31, 4.15, 4.58, 4.59, 4.61, 4.60, 4.62, 4.66, 4.69 4.102, 4.103, 4.104, 4.105
Flow parameters	8	4.71, 4.75, 4.81, 4.80, 4.76
Component properties	37	4.85, 4.86, 4.87, 4.88, 4.89, 4.90, 4.91, 4.92, 4.93
Polymer properties	6	4.94, 4.95, 4.96, 4.97, 4.98
Module parameters	1	4.77
Transfer coefficient	4	4.70, 4.78, 4.60

```
#------------------------------------------------------------------------------------
#Direct contact membrane distillation
#------------------------------------------------------------------------------------
-

xb_f = 1 - xa_f

#Density of water in the feed side
roa_f = 1000*Ma*ADippr101_0/(BDippr101_0^(1+(1-T_bf/CDippr101_0)^DDippr101_0))
rob_f = 1000*Mb*ADippr101_1/(BDippr101_1^(1+(1-T_bf/CDippr101_1)^DDippr101_1))

#Density of water in the permeate side
roa_p = 1000*Ma*dcoefA_a/(dcoefB_a^(1+(1-T_bp/dcoefC_a)^dcoefD_a))
rob_p = 1000*Mb*dcoefA_b/(dcoefB_b^(1+(1-T_bp/dcoefC_b)^dcoefD_b))

#Density of mix
ro_f = roa_f*xa_f+rob_f*xb_f

Tavg = (T_wf+T_wp)/2

# Linear velocity
uf = mf/(ro_f*Am)
up = mp/(ro_f*Am)

# Volumetric flows
Vf = uf*w*h*nc
Vp = up*w*h*nc

#Viscosity of water, ethanol and mix
visca_bf =
exp(ADippr108_0+BDippr108_0/T_bf+CDippr108_0*ln(T_bf)+DDippr108_0*T_bf^EDippr108_0)
viscb_bf =
exp(ADippr108_1+BDippr108_1/T_bf+CDippr108_1*ln(T_bf)+DDippr108_1*T_bf^EDippr108_1)
visc_bf =visca_bf*xa_f  + xb_f*viscb_bf

visca_bp = exp(vcoefA_a+vcoefB_a/T_bp+vcoefC_a*ln(T_bp)+vcoefD_a*T_bp^vcoefE_a)
viscb_bp = exp(vcoefA_b+vcoefB_b/T_bp+vcoefC_b*ln(T_bp))
visc_bp = visca_bp*xa_bp  + xb_bp*viscb_bp

visca_wp = exp(vcoefA_a+vcoefB_a/T_wp+vcoefC_a*ln(T_wp)+vcoefD_a*T_wp^vcoefE_a)
viscb_wp = exp(vcoefA_b+vcoefB_b/T_wp+vcoefC_b*ln(T_wp))
visc_wp = visca_wp*xa_bp  + xb_bp*viscb_wp

#Density of ethanol
rob_wf = 1000*Mb*ADippr101_1/(BDippr101_1^(1+(1-T_wf/CDippr101_1)^DDippr101_1))

#hidraulic diameter
dh = 2*w*h/(w+h)

#Heat capacity of ethanol
Cpa_f =
1/(Ma*1000)*(ADippr105_0+BDippr105_0*T_bf+CDippr105_0*T_bf^2+DDippr105_0*T_bf^3+EDippr105
_0*T_bf^4)
Cpb_f =
1/(Mb*1000)*(ADippr105_1+BDippr105_1*T_bf+CDippr105_1*T_bf^2+DDippr105_1*T_bf^3+EDippr105
_1*T_bf^4)
Cp_f = Cpa_f*xa_f + xb_f*Cpb_f

Cpa_p =
1/(Ma*1000)*(cpcoefA_a+cpcoefB_a*T_bp+cpcoefC_a*T_bp^2+cpcoefD_a*T_bp^3+cpcoefE_a*T_bp^4)
Cpb_p =
1/(Mb*1000)*(cpcoefA_b+cpcoefB_b*T_bp+cpcoefC_b*T_bp^2+cpcoefD_b*T_bp^3+cpcoefE_b*T_bp^4)
Cp_p = Cpa_p*xa_bp + xb_bp*Cpb_p

#Conductivity of water(=mix)
kh_f =
ADippr110_0+BDippr110_0*T_bf+CDippr110_0*T_bf^2+DDippr110_0*T_bf^3+EDippr110_0*T_bf^4
kh_p =
ADippr110_0+BDippr110_0*T_bp+CDippr110_0*T_bp^2+DDippr110_0*T_bp^3+EDippr110_0*T_bp^4

#VARIABLES IN THE FEED SIDE
```

```
#Reynolds
Re_f = dh*uf*ro_f/visc_bf
Re_p = dh*up*ro_p/visc_bp

#Schmidt
Sc_f = visc_bf/(ro_f*Dab)

#Prandtl
Pr_f =  (Cp_f*visc_bf)/kh_f
Pr_p =  (Cp_p*visc_bp)/kh_p

#Viscosities of mixture in the feed and permeate side
visca_wf =
exp(ADippr108_0+BDippr108_0/T_wf+CDippr108_0*ln(T_wf)+DDippr108_0*T_wf^EDippr108_0)
viscb_wf =
exp(ADippr108_1+BDippr108_1/T_wf+CDippr108_1*ln(T_wf)+DDippr108_1*T_wf^EDippr108_1)
visc_wf  = visca_wf*(1-xb_wf) + xb_wf*viscb_wf

#Density of water in the wall of feed side
roa_wf = 1000*Ma*ADippr101_0/(BDippr101_0^(1+(1-T_wf/CDippr101_0)^DDippr101_0))

#Thermal conductivity of vapour water
kv = ADippr111_0*Tavg^BDippr111_0/(1+CDippr111_0/Tavg+DDippr111_0/Tavg^2)

#Schmidt
Sh_f =
aux11*((1.86*(Re_f*Sc_f*dh/L)^0.33)*(visc_bf/visc_wf)^0.14)+aux12*(0.116*(Re_f^(2/3)-
125)*Sc_f^0.33*(1+(dh/L)^(2/3))*(visc_bf/visc_wf)^0.14)+aux13*(0.023*(Re_f^0.8)*(Sc_f^0.3
3)*(visc_bf/visc_wf)^0.14)

# Diffusivity
Dab = 1e-9

#transfer mass coefficient
Km_f = ((Sh_f*Dab)/dh)*(1+delkm)

#Nusselt
Nu_f =
aux11*((1.86*(Re_f*Pr_f*dh/L)^0.33)*(visc_bf/visc_wf)^0.14)+aux12*(0.116*(Re_f^(2/3)-
125)*Pr_f^0.33*(1+(dh/L)^(2/3))*(visc_bf/visc_wf)^0.14)+aux13*(0.023*(Re_f^0.8)*(Pr_f^0.3
3)*(visc_bf/visc_wf)^0.14)
Nu_p =
aux11*((1.86*(Re_p*Pr_p*dh/L)^0.33)*(visc_bp/visc_wp)^0.14)+aux12*(0.116*(Re_p^(2/3)-
125)*Pr_p^0.33*(1+(dh/L)^(2/3))*(visc_bp/visc_wp)^0.14)+aux13*(0.023*(Re_p^0.8)*(Pr_p^0.3
3)*(visc_bp/visc_wp)^0.14)

#Resistence to heat transfer
hh_f = (Nu_f*kh_f)/dh
hh_p = (Nu_p*kh_p)/dh

#viscosity of the gas inside the membrane
viscg_a=ADippr109_0*T_wf^(BDippr109_0)/(1+CDippr109_0/Tavg+DDippr109_0/T_wf^2)
viscg_b=ADippr109_1*T_wf^(BDippr109_1)/(1+CDippr109_1/Tavg+DDippr109_1/T_wf^2)
viscgas=xa_wp*viscg_a+(1-xa_wp)*viscg_b


#-----------------------------------------------------------------------
#MEMBRANE
tortuosity= 1/(epsilon)
K0 = (2*epsilon*Prad/(3*tortuosity))
K1 = epsilon/tortuosity

#Knudsen coefficients
Daeka = K0*sqrt(8*R*Tavg/(pi*Ma))
Daekb = K0*sqrt(8*R*Tavg/(pi*Mb))
Dabe0 = K1*4.46*10^(-6)*Tavg^2.334

#Vapour pressure in the feed side of the membrane
pvapa_wf = exp(pcoefA_a+pcoefB_a/T_wf+pcoefC_a*ln(T_wf)+pcoefD_a*T_wf^pcoefE_a)
pvapb_wf = exp(pcoefA_b+pcoefB_b/T_wf+pcoefC_b*ln(T_wf)+pcoefD_b*T_wf^pcoefE_b)
```

```
#Partial pressures at the permeate side of the membrane
pa_wp = xa_wp*Pvacuum
pb_wp = (1-xa_wp)*Pvacuum

#Partial pressures at feed side of the membrane
pa_wf = pvapa_wf*coefactab*(1-xb_wf)
pb_wf = pvapb_wf*coefactba*xb_wf

#Molar flux
Ra = Dabe0/(deltam*R*Tavg)*ln(((Ptotal-pa_wp)*Daeka+Dabe0)/((Ptotal-pa_wf)*Daeka+Dabe0))
Rb = Dabe0/(deltam*R*Tavg)*ln(((Ptotal-pb_wp)*Daekb+Dabe0)/((Ptotal-pb_wf)*Daekb+Dabe0))

#molar fraction in the wall of permeate side
0 = -xa_wp + (Ra/(Ra+Rb))
xb_wp = 1-xa_wp
xa_wf = 1 - xb_wf

#Density of mix
roab_wf = roa_wf*xmassa_wf+rob_wf*xmassb_wf
conc = roab_wf*(xmassa_wp/Ma + xmassb_wp/Mb)

#Enthalpy of evaporation
deltaHa = (1/Ma/1000)*ADippr103_0*(1-
T_wf/DB_Tc_0)^(BDippr103_0+CDippr103_0*(T_wf/DB_Tc_0)+DDippr103_0*(T_wf/DB_Tc_0)^2)
deltaHb = (1/Mb/1000)*ADippr103_1*(1-
T_wf/DB_Tc_1)^(BDippr103_1+CDippr103_1*(T_wf/DB_Tc_1)+DDippr103_1*(T_wf/DB_Tc_1)^2)

#Resistence to heat transfer of the membrane
h_m = (kv*epsilon + km*(1-epsilon))/deltam + energy/(T_wf - T_wp)


Qenergy=Na*deltaHa + Nb*deltaHb


0 = -xb_wf + (xb_f - xb_wp)*exp((Ra+Rb)/(conc*Km_f))+xb_wp
0 = -T_wf + T_bf-energy/hh_f
0 =  T_wp - (1/h_p*T_wf + 1/h_m*T_bp)/(1/h_p + 1/h_m)

# Heat flux throught the membrane
q = (T_wf - T_wp)/R_m

Rtotal = Ra+Rb

#Mass balance
dmf = -(Rtotal/conc)/(nc*h) + mf - mf
dmp = (Rtotal/conc)/(nc*h) + mp - mp

#Energy balance in feed side
dT_bf=1/Vf*(-Qenergy*w/(Cp_f*roa_f)+(liqflux)*w*T_bf)

#Energy balance in permeate side
dT_bp = 1/Vp*(q*w/(Cp_p*roa_p)-(liqflux)*w*T_bp)

# component permeate flows
dmasspA=Na*w + masspA - masspB
dmasspB=Nb*w + masspA - masspB

#component feed flows
dmassfA=-Na*w
dmassfB=-Nb*w + massfA - massfB

# Recovery and CF
Recovery = massfB/(uf*Am*ro_f*xb_f)
CF = xb_wp/xb_f
```

Figure A.1: MoT code for DCMD process
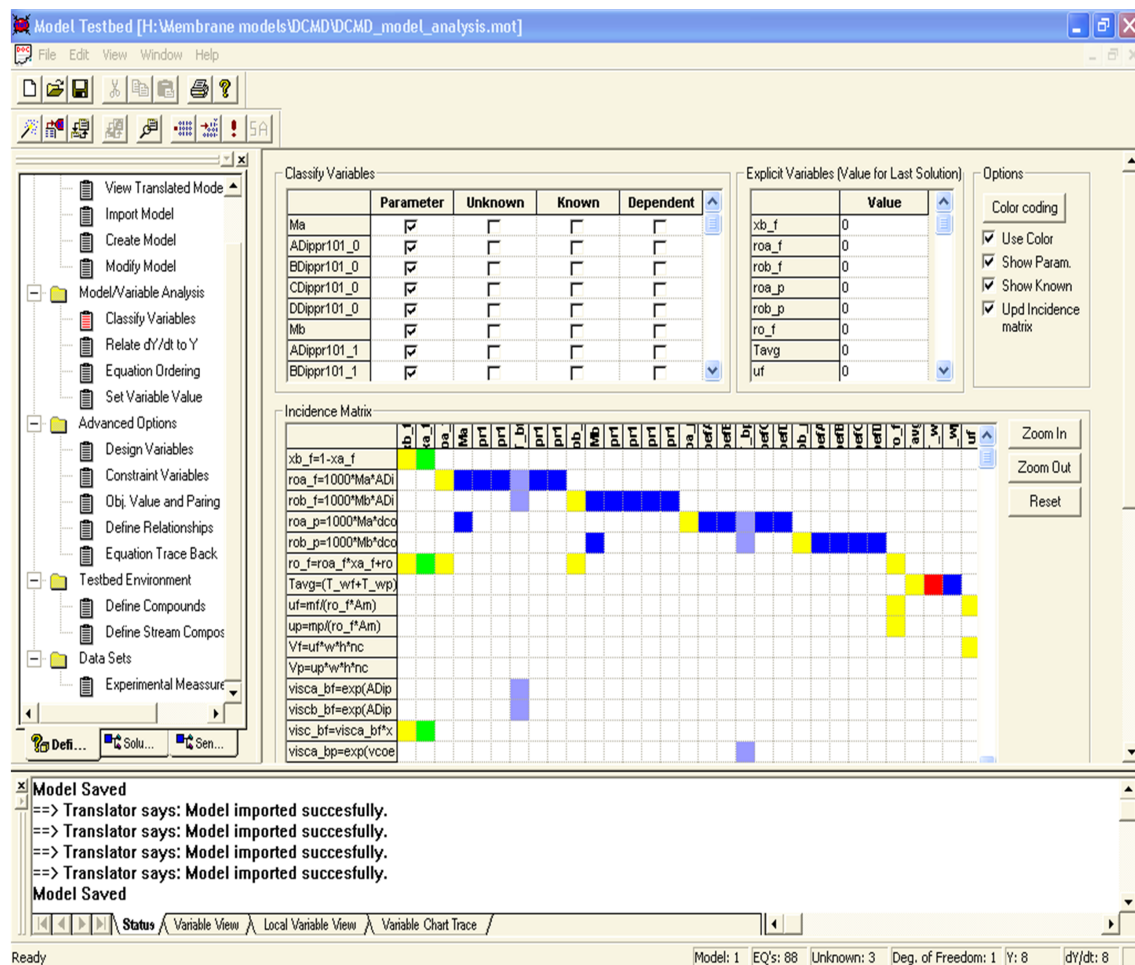
Figure A.2: Model analysis screen shot for DCMD process

Table A.3: Variables in OMD model

Differential Variables		Number
Mass flow	m_f, m_p, $\underline{m_{f,i}}(2)$, $\underline{m_{p,i}}(2)$	6
Temperature	T_f, T_p	2
Algebraic Variables		**Number**
Process variables	V_f, V_p, $\underline{R_i}(2)$, R_{total}, Q_m, T_{wf}, T_{wp}, T_{avg}, $Q_{process}$, $\underline{p_{i,wf}}(2)$ $\underline{p_{i,wp}}(2)$, $\underline{x_{i,wf}}(2)$, $\underline{x_{i,wp}}(2)$, $\overline{C_t}$, $\underline{x_f}$ (1) u_f, u_p, Recovery, CF	24
Flow parameters	Sh, $\underline{Re}$ (2), Sc, $\underline{Nu}$ (2), $\underline{Pr}$ (2)	8
Component /mixture properties	$\underline{\rho}(9)$, $\underline{Cp}(6)$, $\underline{\Delta H_{vap,i}}(2)$ $\underline{P_i^{Sat}}(2)$, D_{ij}, $\underline{\mu}(12)$, $\overline{k_{h,i}}(2)$, $\underline{\mu_{gas,i}}(3)$	37
Polymer properties	K_0, K_1, $\underline{D_{ie}^k}(2)$, $\overline{D_{ije}^0}$, τ	6
Module parameters	dh	1
Transfer coefficients	h_f, h_p, h_m, k_m	4
Known Variables		**Number**
Process variables	P_f, P_p, $\underline{x_{i,f}}(1)$	3
Component properties	$\underline{M_i}(2)$ $\overline{\gamma_i^e}(2)$	4
Regressed variables	5 variables for each pure component property	40
Polymer properties	ϵ, r_p	2
Module parameters	w, δ_m, L, h, n_f	5
Constants	R_g, π	2
For a binary mixture the total number of variables:		**144**

Table A.4: Equations to be solved for OMD process

Variables	Number	Equations
Differential variables	8	4.3, 4.10, 4.12, 4.13, 4.20 4.21
Process variables	24	4.5, 4.6, 4.8, 4.9, 4.31, 4.15, 4.58, 4.59, 4.61, 4.60, 4.62, 4.67, 4.69 4.102, 4.103, 4.104, 4.105
Flow parameters	8	4.71, 4.75, 4.81, 4.80, 4.76
Component properties	37	4.85, 4.86, 4.87, 4.88, 4.89, 4.90, 4.91, 4.92, 4.93
Polymer properties	6	4.94, 4.95, 4.96, 4.97, 4.98
Module parameters	1	4.77
Transfer coefficient	4	4.70, 4.78, 4.60

A.3 Sweeping gas membrane distillation

The model analysis for sweeping gas membrane distillation is given below. The model analysis is illustrated for a binary mixture (N=2). The model analysis is shown for Knudsen-molecular diffusion. The model differs from DCMD and OMD model due to the presence of gas film on the permeate side instead of the liquid film. The model for SGMD has 132 variables out of which 8 are differential variables; 67 algebraic variables (explicit or implicit, calculated from 67 equations) and 57 known variables. Table A.5 lists different variables in the SGMD. Table A.6 lists different equations that need to be solved for SGMD.

Table A.5: Variables in SGMD model

Differential Variables (8)		Number
Mass flow	m_f, m_p, $\underline{m_{f,i}}(2)$, $\underline{m_{p,i}}(2)$	6
Temperature	$\overline{T_f}$, T_p	2
Algebraic Variables (67)		**Number**
Process variables	V_f, V_p, $\underline{R_i}(2)$, R_{total}, Q_m,	
	T_{wf}, T_{wp}, $\overline{T_{avg}}$, $Q_{process}$, $\underline{p_{i,wf}}(2)$	24
	$\underline{p_{i,wp}}(2)$, $\underline{x_{i,wf}}(2)$, $\underline{x_{i,wp}}(2)$, $\overline{C_t}$, $\underline{x_f}$ (1)	
	u_f, u_p, Recovery, CF	
Flow parameters	Sh, $\underline{Re}$ (2), Sc, $\underline{Nu}$ (2), $\underline{Pr}$ (2)	8
Component	$\rho(6)$, $\overline{Cp}(3)$, $\underline{\Delta H_{vap,i}}(2)$	24
/mixture properties	$\underline{P_i^{Sat}}(2)$, $\overline{D_{ij}}$, $\underline{\mu}(6)$, k_h, $\underline{\mu_{gas,i}}(3)$	
Polymer properties	K_0, K_1, $\underline{D_{ie}^k}(2)$, D_{ije}^0, τ	6
Module parameters	dh	1
Transfer coefficients	h_f, h_p, h_m, k_m	4
Known Variables (57)		**Number**
Process variables	P_f, P_p, $\underline{x_{i,f}}(1)$	3
Component properties	$\underline{M_i}(2)$ $\underline{\gamma_i}(2)$, ρ_g	5
Regressed variables	5 variables for each pure component property	40
Polymer properties	ϵ, r_p	2
Module parameters	w, δ_m, L, h, n_f	5
Constants	R_g, π	2
For a binary mixture the total number of variables:		**132**

A.4 Vacuum membrane distillation

This model is different from other models due to the presence of vacuum on the permeate side. Due to which, the mean free path (λ) of the diffusing molecules is large (as λ is inversely proportional to pressure). Therefore the number of molecule-molecule collision is negligible compared to the number of molecule - pore wall collisions, and the molecular diffusion resistance can be omitted. So, the diffusion

```
#------------------------------------------------------------------------------------
#Sweeping gas membrane Distillation
#------------------------------------------------------------------------------------
-

xb_f = 1 - xa_f

#Density of water in the feed side
roa_f = 1000*Ma*ADippr101_0/(BDippr101_0^(1+(1-T_bf/CDippr101_0)^DDippr101_0))
rob_f = 1000*Mb*ADippr101_1/(BDippr101_1^(1+(1-T_bf/CDippr101_1)^DDippr101_1))

#Density of water in the permeate side
roa_p = 1000*Ma*dcoefA_a/(dcoefB_a^(1+(1-T_bp/dcoefC_a)^dcoefD_a))
rob_p = 1000*Mb*dcoefA_b/(dcoefB_b^(1+(1-T_bp/dcoefC_b)^dcoefD_b))

#Density of mix - feed
ro_f = roa_f*xa_f+rob_f*xb_f

#Density of mix - permeate
ro_p = roa_p*xa_wp+rob_p*xb_wp

Tavg = (T_wf+T_wp)/2

# Linear velocity
uf = mf/(ro_f*Am)
up = mp/(ro_f*Am)

# Volumetric flows
Vf = uf*w*h*nc
Vp = up*w*h*nc

#Viscosity of water, ethanol and mix
visca_bf =
exp(ADippr108_0+BDippr108_0/T_bf+CDippr108_0*ln(T_bf)+DDippr108_0*T_bf^EDippr108_0)
viscb_bf =
exp(ADippr108_1+BDippr108_1/T_bf+CDippr108_1*ln(T_bf)+DDippr108_1*T_bf^EDippr108_1)
visc_bf =visca_bf*xa_f  + xb_f*viscb_bf

#hidraulic diameter
dh = 2*w*h/(w+h)

#Heat capacity of ethanol
Cpa_f =
1/(Ma*1000)*(ADippr105_0+BDippr105_0*T_bf+CDippr105_0*T_bf^2+DDippr105_0*T_bf^3+EDippr105
_0*T_bf^4)
Cpb_f =
1/(Mb*1000)*(ADippr105_1+BDippr105_1*T_bf+CDippr105_1*T_bf^2+DDippr105_1*T_bf^3+EDippr105
_1*T_bf^4)
Cp_f = Cpa_f*xa_f + xb_f*Cpb_f

#Conductivity of water(=mix)
kh_f =
ADippr110_0+BDippr110_0*T_bf+CDippr110_0*T_bf^2+DDippr110_0*T_bf^3+EDippr110_0*T_bf^4

#viscosity of the gas inside the membrane
viscg_a=ADippr109_0*T_wf^(BDippr109_0)/(1+CDippr109_0/Tavg+DDippr109_0/T_wf^2)
viscg_b=ADippr109_1*T_wf^(BDippr109_1)/(1+CDippr109_1/Tavg+DDippr109_1/T_wf^2)
viscgas=xa_wp*viscg_a+(1-xa_wp)*viscg_b

# Flow parameters
#Reynolds
Re_f = dh*uf*ro_f/visc_bf
Re_p = dh*up*ro_sg/viscgas

#Schmidt
Sc_f = visc_bf/(ro_f*Dab)

#Prandtl
Pr_f =  (Cp_f*visc_bf)/kh_f
Pr_p = (1900*viscgas)/0.02
```

```
#Viscosities of mixture in the feed and permeate side
visca_wf =
exp(ADippr108_0+BDippr108_0/T_wf+CDippr108_0*ln(T_wf)+DDippr108_0*T_wf^EDippr108_0)
viscb_wf =
exp(ADippr108_1+BDippr108_1/T_wf+CDippr108_1*ln(T_wf)+DDippr108_1*T_wf^EDippr108_1)
visc_wf  = visca_wf*(1-xb_wf) + xb_wf*viscb_wf

#Schmidt
Sh_f =
aux11*((1.86*(Re_f*Sc_f*dh/L)^0.33)*(visc_bf/visc_wf)^0.14)+aux12*(0.116*(Re_f^(2/3)-
125)*Sc_f^0.33*(1+(dh/L)^(2/3))*(visc_bf/visc_wf)^0.14)+aux13*(0.023*(Re_f^0.8)*(Sc_f^0.3
3)*(visc_bf/visc_wf)^0.14)

# Diffusivity
Dab = 1e-9

#transfer mass coefficient
Km_f = ((Sh_f*Dab)/dh)*(1+delkm)

#Nusselt
Nu_f =
aux11*((1.86*(Re_f*Pr_f*dh/L)^0.33)*(visc_bf/visc_wf)^0.14)+aux12*(0.116*(Re_f^(2/3)-
125)*Pr_f^0.33*(1+(dh/L)^(2/3))*(visc_bf/visc_wf)^0.14)+aux13*(0.023*(Re_f^0.8)*(Pr_f^0.3
3)*(visc_bf/visc_wf)^0.14)
Nu_p =
aux11*((1.86*(Re_p*Pr_p*dh/L)^0.33)*(visc_bp/visc_wp)^0.14)+aux12*(0.116*(Re_p^(2/3)-
125)*Pr_p^0.33*(1+(dh/L)^(2/3))*(visc_bp/visc_wp)^0.14)+aux13*(0.023*(Re_p^0.8)*(Pr_p^0.3
3)*(visc_bp/visc_wp)^0.14)

#Resistence to heat transfer
hh_f = (Nu_f*kh_f)/dh
hh_p = 0.206*(0.02/dh)*Re_p^0.63*Pr_p^0.36

#-------------------------------------------------------------------------
#MEMBRANE
tortuosity= 1/(epsilon)
K0 = (2*epsilon*Prad/(3*tortuosity))
K1 = epsilon/tortuosity

#Knudsen coefficients
Daeka = K0*sqrt(8*R*Tavg/(pi*Ma))
Daekb = K0*sqrt(8*R*Tavg/(pi*Mb))
Dabe0 = K1*4.46*10^(-6)*Tavg^2.334

#Vapour pressure in the feed side of the membrane
pvapa_wf = exp(pcoefA_a+pcoefB_a/T_wf+pcoefC_a*ln(T_wf)+pcoefD_a*T_wf^pcoefE_a)
pvapb_wf = exp(pcoefA_b+pcoefB_b/T_wf+pcoefC_b*ln(T_wf)+pcoefD_b*T_wf^pcoefE_b)

#Partial pressures at the permeate side of the membrane
pa_wp = xa_wp*Pvacuum
pb_wp = (1-xa_wp)*Pvacuum

#Partial pressures at feed side of the membrane
pa_wf = pvapa_wf*coefactab*(1-xb_wf)
pb_wf = pvapb_wf*coefactba*xb_wf

#Molar flux
Ra = Dabe0/(deltam*R*Tavg)*ln(((Ptotal-pa_wp)*Daeka+Dabe0)/((Ptotal-pa_wf)*Daeka+Dabe0))
Rb = Dabe0/(deltam*R*Tavg)*ln(((Ptotal-pb_wp)*Daekb+Dabe0)/((Ptotal-pb_wf)*Daekb+Dabe0))

#molar fraction in the wall of permeate side
0 = -xa_wp + (Ra/(Ra+Rb))
xb_wp = 1-xa_wp
xa_wf = 1 - xb_wf

#Density of mix
conc = roab_wf*(xmassa_wp/Ma + xmassb_wp/Mb)

#Enthalpy of evaporation
deltaHa = (1/Ma/1000)*ADippr103_0*(1-
T_wf/DB_Tc_0)^(BDippr103_0+CDippr103_0*(T_wf/DB_Tc_0)+DDippr103_0*(T_wf/DB_Tc_0)^2)
```

Table A.6: Equations to be solved for SGMD process

Variables	Number	Equations
Differential variables	8	4.3, 4.10, 4.12, 4.13, 4.20 4.21
Process variables	24	4.5, 4.6, 4.8, 4.9, 4.31, 4.15, 4.58, 4.59, 4.61, 4.60, 4.62, 4.65, 4.69 4.102, 4.103, 4.104, 4.105
Flow parameters	8	4.71, 4.75, 4.81, 4.80, 4.76
Component properties	24	4.85, 4.86, 4.87, 4.88, 4.89, 4.90, 4.91, 4.92, 4.93
Polymer properties	6	4.94, 4.95, 4.96, 4.97, 4.98
Module parameters	1	4.77
Transfer coefficient	4	4.70, 4.78, 4.79, 4.60

```
deltaHb = (1/Mb/1000)*ADippr103_1*(1-
T_wf/DB_Tc_1)^(BDippr103_1+CDippr103_1*(T_wf/DB_Tc_1)+DDippr103_1*(T_wf/DB_Tc_1)^2)

#Resistence to heat transfer of the membrane
h_m = (kv*epsilon + km*(1-epsilon))/deltam + energy/(T_wf - T_wp)

Qenergy=Na*deltaHa + Nb*deltaHb

0 = -xb_wf + (xb_f - xb_wp)*exp((Ra+Rb)/(conc*Km_f))+xb_wp
0 = -T_wf + T_bf-energy/hh_f
0 =  T_wp - (1/h_p*T_wf + 1/h_m*T_bp)/(1/h_p + 1/h_m)

# Heat flux throught the membrane
q = (T_wf - T_wp)/R_m

Rtotal = Ra+Rb

#Mass balance
dmf = -(Rtotal/conc)/(nc*h) + mf - mf
dmp = (Rtotal/conc)/(nc*h) + mp - mp

#Energy balance in feed side
dT_bf=1/Vf*(-Qenergy*w/(Cp_f*ro_f)+(liqflux)*w*T_bf)

#Energy balance in permeate side
dT_bp = 1/Vp*(q*w/(Cp_p*ro_p)-(liqflux)*w*T_bp)

# component permeate flows
dmasspA=Na*w + masspA - masspB
dmasspB=Nb*w + masspA - masspB

#component feed flows
dmassfA=-Na*w
dmassfB=-Nb*w + massfA - massfB

# Recovery and CF
Recovery = massfB/(uf*Am*ro_f*xb_f)
CF = xb_wp/xb_f
```

Figure A.3: MoT code for SGMD process
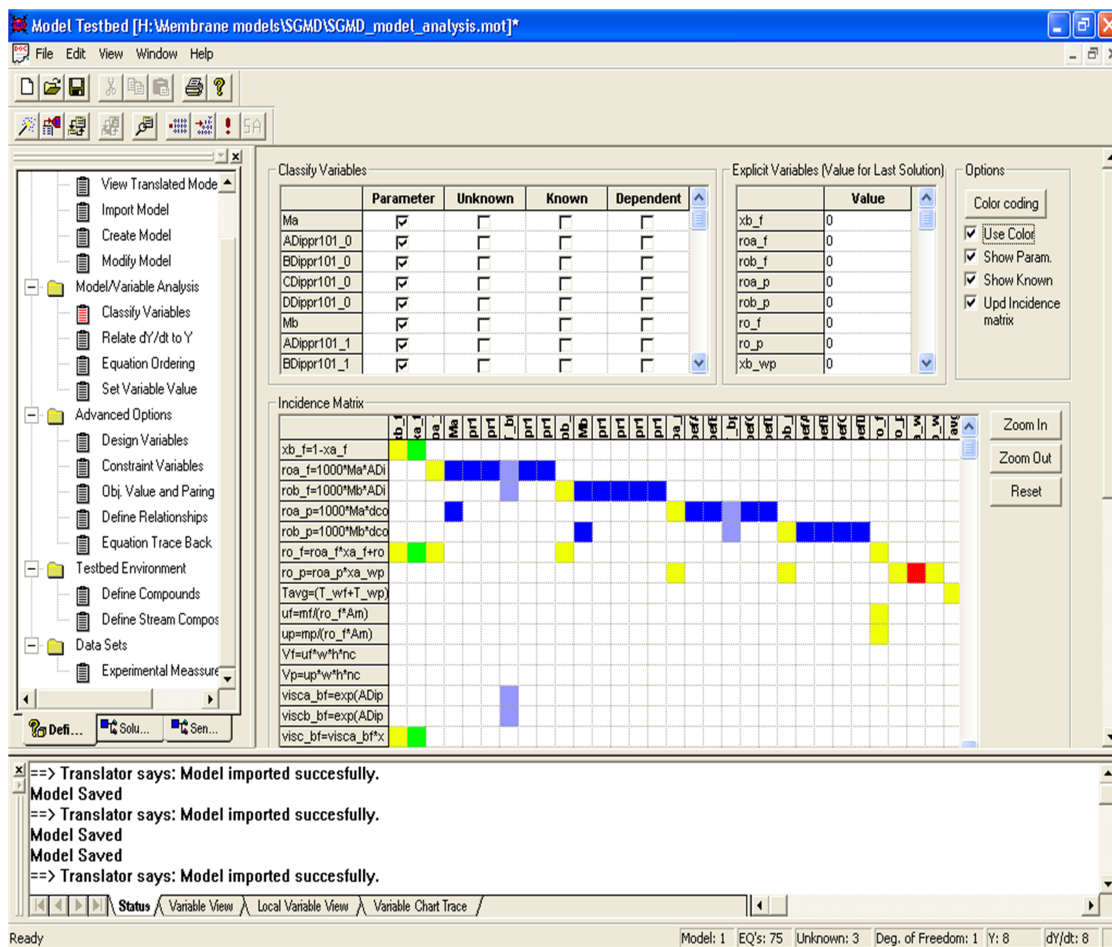
Figure A.4: Model analysis screen shot for SGMD process

through the membrane is according to Knudsen diffusion mechanism. But in a case of comparable size of the membrane pores to the mean free path, Knudsen-Viscous diffusion mechanism should be used.

The main resistance in VMD is considered to be located in the liquid phase. The vacuum on the permeate side of the membrane prevents the formation of a boundary layer, so the corresponding boundary layer resistance may be omitted.

There are no temperature gradients in the membrane. And this is also due to the presence of the vacuum on the permeate side.

The model analysis for vacuum membrane distillation is given below. The model analysis is illustrated for a binary mixture (N=2). The model analysis is shown for Knudsen diffusion. The model for VMD has 115 variables out of which 7 are differential variables; 52 algebraic variables (explicit or implicit, calculated from 52 equations) and 56 known variables. Table A.7 lists different variables in the VMD. Table A.8 lists different equations that need to be solved for VMD.

Table A.7: Variables in VMD model

Differential Variables (7)		Number
Mass flow	m_f, m_p, $\underline{m_{f,i}}(2)$, $\underline{m_{p,i}}(2)$	6
Temperature	T_f	1
Algebraic Variables (52)		**Number**
Process variables	V_f, V_p, $\underline{R_i}(2)$, R_{total} T_{wf}, $Q_{process}$, $\underline{p_{i,wf}}(2)$ $\underline{p_{i,wp}}(2)$, $\underline{x_{i,wf}}(2)$, $\underline{x_{i,wp}}(2)$, C_t, $\underline{x_f}$ (1) u_f, u_p, Recovery, CF	21
Flow parameters	Sh, Re, Sc, Nu, Pr	5
Component /mixture properties	$\underline{\rho}(3)$, $\underline{Cp}(3)$, $\underline{\Delta H_{vap,i}}(2)$ $\underline{P_i^{Sat}}(2)$, $\underline{D_{ij}}$, $\underline{\mu}(6)$, k_h, $\underline{\mu_{gas,i}}(3)$	21
Polymer properties	K_0, τ	2
Module parameters	dh	1
Transfer coefficients	h_f, k_m	2
Known Variables (56)		**Number**
Process variables	P_f, P_p, $\underline{x_{i,f}}(1)$	3
Component properties	$\underline{M_i}(2)$ $\underline{\gamma_i}(2)$	4
Regressed variables	5 variables for each pure component property	40
Polymer properties	ϵ, r_p	2
Module parameters	w, δ_m, L, h, n_f	5
Constants	R_g, π	2
For a binary mixture the total number of variables:		**115**

```
#-------------------------------------------------------------------------------------
#Vacuum membrane Distillation
#-------------------------------------------------------------------------------------
-

xb_f = 1 - xa_f

#Density of water in the feed side
roa_f = 1000*Ma*ADippr101_0/(BDippr101_0^(1+(1-T_bf/CDippr101_0)^DDippr101_0))
rob_f = 1000*Mb*ADippr101_1/(BDippr101_1^(1+(1-T_bf/CDippr101_1)^DDippr101_1))

#Density of mix
ro_f = roa_f*xa_f+rob_f*xb_f

# Linear velocity
uf = mf/(ro_f*Am)
up = mp/(ro_f*Am)

# Volumetric flows
Vf = uf*w*h*nc
Vp = up*w*h*nc


#Viscosity of water, ethanol and mix
visca_bf =
exp(ADippr108_0+BDippr108_0/T_bf+CDippr108_0*ln(T_bf)+DDippr108_0*T_bf^EDippr108_0)
viscb_bf =
exp(ADippr108_1+BDippr108_1/T_bf+CDippr108_1*ln(T_bf)+DDippr108_1*T_bf^EDippr108_1)
visc_bf =visca_bf*xa_f  + xb_f*viscb_bf

#hidraulic diameter
dh = 2*w*h/(w+h)

#Heat capacity of ethanol
Cpa_f =
1/(Ma*1000)*(ADippr105_0+BDippr105_0*T_bf+CDippr105_0*T_bf^2+DDippr105_0*T_bf^3+EDippr105
_0*T_bf^4)
Cpb_f =
1/(Mb*1000)*(ADippr105_1+BDippr105_1*T_bf+CDippr105_1*T_bf^2+DDippr105_1*T_bf^3+EDippr105
_1*T_bf^4)
Cp_f = Cpa_f*xa_f + xb_f*Cpb_f

#Conductivity of water(=mix)
kh_f =
ADippr110_0+BDippr110_0*T_bf+CDippr110_0*T_bf^2+DDippr110_0*T_bf^3+EDippr110_0*T_bf^4

#VARIABLES IN THE FEED SIDE
#Reynolds
Re_f = dh*uf*ro_f/visc_bf

#Schmidt
Sc_f = visc_bf/(ro_f*Dab)

#Prandtl
Pr_f =  (Cp_f*visc_bf)/kh_f

#Viscosities of mixture in the feed and permeate side
visca_wf =
exp(ADippr108_0+BDippr108_0/T_wf+CDippr108_0*ln(T_wf)+DDippr108_0*T_wf^EDippr108_0)
viscb_wf =
exp(ADippr108_1+BDippr108_1/T_wf+CDippr108_1*ln(T_wf)+DDippr108_1*T_wf^EDippr108_1)
visc_wf  = visca_wf*(1-xb_wf) + xb_wf*viscb_wf

# Diffusivity
Dab = 1e-9

#Schmidt
Sh_f =
aux11*((1.86*(Re_f*Sc_f*dh/L)^0.33)*(visc_bf/visc_wf)^0.14)+aux12*(0.116*(Re_f^(2/3)-
125)*Sc_f^0.33*(1+(dh/L)^(2/3))*(visc_bf/visc_wf)^0.14)+aux13*(0.023*(Re_f^0.8)*(Sc_f^0.3
3)*(visc_bf/visc_wf)^0.14)
```

```
#transfer mass coefficient
Km_f = ((Sh_f*Dab)/dh)*(1+delkm)

#Nusselt
Nu_f =
aux11*((1.86*(Re_f*Pr_f*dh/L)^0.33)*(visc_bf/visc_wf)^0.14)+aux12*(0.116*(Re_f^(2/3)-
125)*Pr_f^0.33*(1+(dh/L)^(2/3))*(visc_bf/visc_wf)^0.14)+aux13*(0.023*(Re_f^0.8)*(Pr_f^0.3
3)*(visc_bf/visc_wf)^0.14)

#Resistence to heat transfer
hh_f = (Nu_f*kh_f)/dh

#viscosity of the gas inside the membrane
viscg_a=ADippr109_0*T_wf^(BDippr109_0)/(1+CDippr109_0/Tavg+DDippr109_0/T_wf^2)
viscg_b=ADippr109_1*T_wf^(BDippr109_1)/(1+CDippr109_1/Tavg+DDippr109_1/T_wf^2)
viscgas=xa_wp*viscg_a+(1-xa_wp)*viscg_b


#-------------------------------------------------------------------------
#MEMBRANE
tortuosity = 1/(epsilon)
K0 = (2*epsilon*Prad/(3*tortuosity))

#Vapour pressure in the feed side of the membrane
pvapa_wf = exp(pcoefA_a+pcoefB_a/T_wf+pcoefC_a*ln(T_wf)+pcoefD_a*T_wf^pcoefE_a)
pvapb_wf = exp(pcoefA_b+pcoefB_b/T_wf+pcoefC_b*ln(T_wf)+pcoefD_b*T_wf^pcoefE_b)

#Partial pressures at the permeate side of the membrane
pa_wp = xa_wp*Pvacuum
pb_wp = (1-xa_wp)*Pvacuum

#Partial pressures at feed side of the membrane
pa_wf = pvapa_wf*coefactab*(1-xb_wf)
pb_wf = pvapb_wf*coefactba*xb_wf

#Molar flux
Ra = K0/(R*T_wf*deltam)*(8*R*T_wf/(pi*Ma))^0.5*(pa_wf-pa_wp)
Rb = K0/(R*T_wf*deltam)*(8*R*T_wf/(pi*Mb))^0.5*(pb_wf-pb_wp)

#molar fraction in the wall of permeate side
0 = -xa_wp + (Ra/(Ra+Rb))
xb_wp = 1-xa_wp
xa_wf = 1 - xb_wf

conc = roab_wf*(xmassa_wp/Ma + xmassb_wp/Mb)

#Enthalpy of evaporation
deltaHa = (1/Ma/1000)*ADippr103_0*(1-
T_wf/DB_Tc_0)^(BDippr103_0+CDippr103_0*(T_wf/DB_Tc_0)+DDippr103_0*(T_wf/DB_Tc_0)^2)
deltaHb = (1/Mb/1000)*ADippr103_1*(1-
T_wf/DB_Tc_1)^(BDippr103_1+CDippr103_1*(T_wf/DB_Tc_1)+DDippr103_1*(T_wf/DB_Tc_1)^2)

Qenergy=Na*deltaHa + Nb*deltaHb

0 = -xb_wf + (xb_f - xb_wp)*exp((Ra+Rb)/(conc*Km_f))+xb_wp
0 = -T_wf + T_bf-energy/hh_f

Rtotal = Ra+Rb

#Mass balance
dmf = -(Rtotal/conc)/(nc*h) + mf - mf
dmp = (Rtotal/conc)/(nc*h) + mp - mp

#Energy balance in feed side
dT_bf=1/Vf*(-Qenergy*w/(Cp_f*roa_f)+(liqflux)*w*T_bf)

# component permeate flows
dmasspA=Na*w + masspA - masspB
dmasspB=Nb*w + masspA - masspB
```

```
#component feed flows
dmassfA=-Na*w
dmassfB=-Nb*w + massfA - massfB

# Recovery and CF
Recovery = massfB/(uf*Am*ro_f*xb_f)
CF = xb_wp/xb_f
```

Figure A.5: MoT code for VMD process
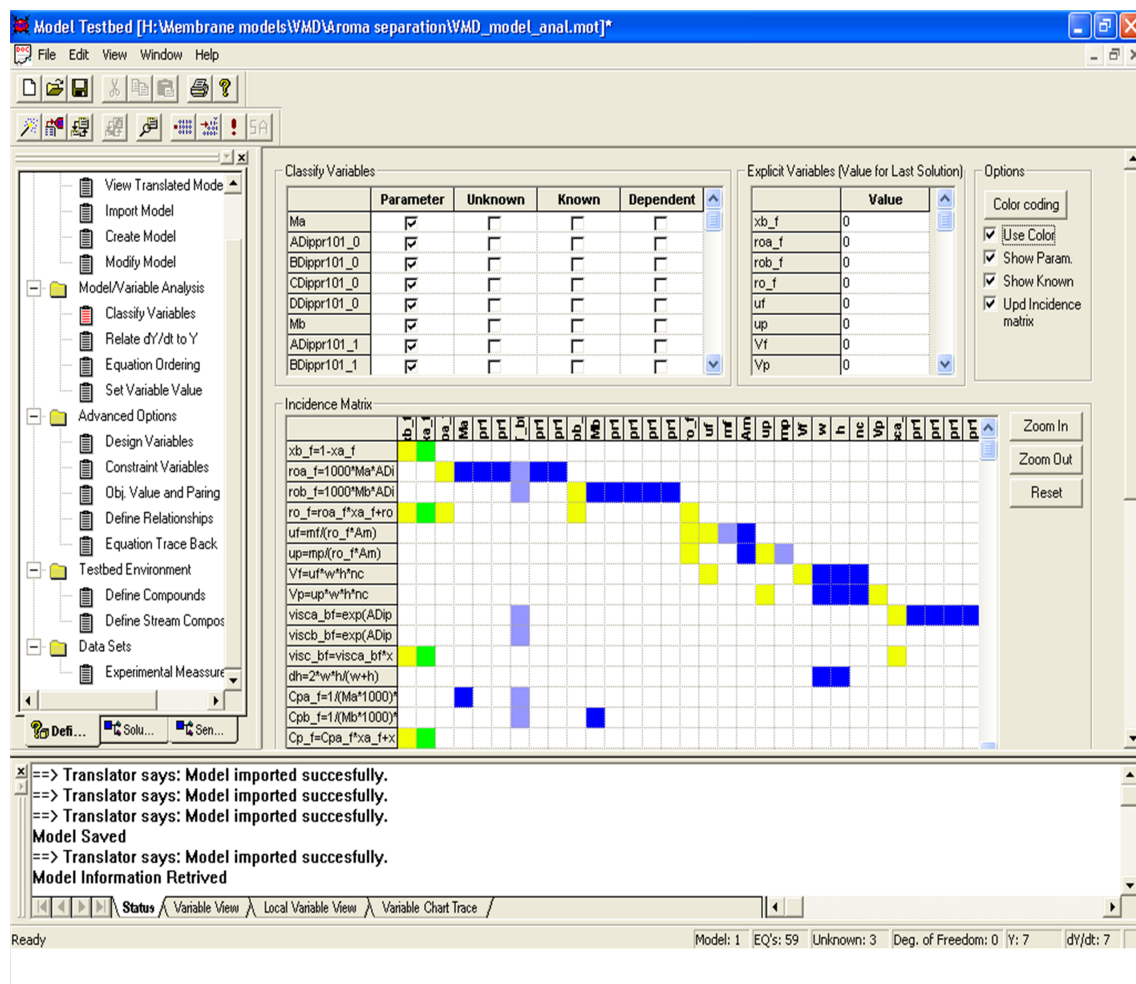
Figure A.6: Model analysis screen shot for VMD process

Table A.8: Equations to be solved for VMD process

Variables	Number	Equations
Differential variables	7	4.3, 4.10, 4.12, 4.13, 4.20
Process variables	21	4.5, 4.6, 4.8, 4.9, 4.29, 4.15, 4.58, 4.62, 4.65, 4.69 4.102, 4.103, 4.104, 4.105
Flow parameters	5	4.71, 4.75, 4.81, 4.80, 4.76
Component properties	21	4.85, 4.86, 4.87, 4.88, 4.89, 4.90, 4.91, 4.92, 4.93
Polymer properties	2	4.97, 4.101
Module parameters	1	4.77
Transfer coefficient	2	4.70, 4.78

A.5 Pervaporation

The model analysis for pervaporation is given below. The model analysis is illustrated for a binary mixture (N=2). This model is very similar to VMD model but differs due to the use of non-porous membrane instead of porous. So, the solution-diffusion mechanism prevails in this separation process. The model for PV has 115 variables out of which 7 are differential variables; 50 algebraic variables (explicit or implicit, calculated from 50 equations) and 58 known variables. Table A.9 lists different variables in the PV. Table A.10 lists different equations that need to be solved for PV.

Table A.9: Variables in PV model

Differential Variables (7)		Number
Mass flow	m_f, m_p, $\underline{m_{f,i}}(2)$, $\underline{m_{p,i}}(2)$	6
Temperature	$\underline{T_f}$	1
Algebraic Variables (50)		**Number**
Process variables	V_f, V_p, $\underline{R_i}(2)$, R_{total} T_{wf}, $Q_{process}$, $\underline{p_{i,wf}}(2)$ $\underline{p_{i,wp}}(2)$, $\underline{x_{i,wf}}(2)$, $\underline{x_{i,wp}}(2)$, C_t, $\underline{x_f}$ (1) u_f, u_p, Recovery, CF	21
Flow parameters	Sh, Re, Sc, Nu, Pr	5
Component /mixture properties	$\rho(3)$, $\underline{Cp}(3)$, $\underline{\Delta H_{vap,i}}(2)$ $\underline{P_i^{Sat}}(2)$, $\underline{D_{ij}}$, $\underline{\mu}(6)$, k_h, $\underline{\mu_{gas,i}}(3)$	21
Module parameters	dh	1
Transfer coefficients	h_f, k_m	2
Known Variables (58)		**Number**
Process variables	P_f, P_p, $\underline{x_{i,f}}(1)$	3
Component properties	$\underline{M_i}(2)$ $\underline{\gamma_i}(2)$	4
Regressed variables	5 variables for each pure component property	40
Polymer properties	$\underline{P_i}$ (2)	2
Module parameters	w, δ_m, L, h, n_f	5
Constants	R_g, π	2
For a binary mixture the total number of variables:		**115**

Table A.10: Equations to be solved for PV process

Variables	Number	Equations
Differential variables	7	4.3, 4.10, 4.12, 4.13, 4.20
Process variables	21	4.5, 4.6, 4.8, 4.9, 4.57, 4.15, 4.58, 4.62, 4.65, 4.69 4.102, 4.103, 4.104, 4.105
Flow parameters	5	4.71, 4.75, 4.81, 4.80, 4.76
Component properties	21	4.85, 4.86, 4.87, 4.88, 4.89, 4.90, 4.91, 4.92, 4.93
Module parameters	1	4.77
Transfer coefficient	2	4.70, 4.78

```
#------------------------------------------------------------------------------------
#Pervaporation
#------------------------------------------------------------------------------------
-

xb_f = 1 - xa_f

#Density of water in the feed side
roa_f = 1000*Ma*ADippr101_0/(BDippr101_0^(1+(1-T_bf/CDippr101_0)^DDippr101_0))
rob_f = 1000*Mb*ADippr101_1/(BDippr101_1^(1+(1-T_bf/CDippr101_1)^DDippr101_1))

#Density of mix
ro_f = roa_f*xa_f+rob_f*xb_f

# Linear velocity
uf = mf/(ro_f*Am)
up = mp/(ro_f*Am)

# Volumetric flows
Vf = uf*w*h*nc
Vp = up*w*h*nc


#Viscosity of water, ethanol and mix
visca_bf =
exp(ADippr108_0+BDippr108_0/T_bf+CDippr108_0*ln(T_bf)+DDippr108_0*T_bf^EDippr108_0)
viscb_bf =
exp(ADippr108_1+BDippr108_1/T_bf+CDippr108_1*ln(T_bf)+DDippr108_1*T_bf^EDippr108_1)
visc_bf =visca_bf*xa_f  + xb_f*viscb_bf

#hidraulic diameter
dh = 2*w*h/(w+h)

#Heat capacity of ethanol
Cpa_f =
1/(Ma*1000)*(ADippr105_0+BDippr105_0*T_bf+CDippr105_0*T_bf^2+DDippr105_0*T_bf^3+EDippr105
_0*T_bf^4)
Cpb_f =
1/(Mb*1000)*(ADippr105_1+BDippr105_1*T_bf+CDippr105_1*T_bf^2+DDippr105_1*T_bf^3+EDippr105
_1*T_bf^4)
Cp_f = Cpa_f*xa_f + xb_f*Cpb_f

#Conductivity of water(=mix)
kh_f =
ADippr110_0+BDippr110_0*T_bf+CDippr110_0*T_bf^2+DDippr110_0*T_bf^3+EDippr110_0*T_bf^4

#VARIABLES IN THE FEED SIDE
#Reynolds
Re_f = dh*uf*ro_f/visc_bf

#Schmidt
Sc_f = visc_bf/(ro_f*Dab)

#Prandtl
Pr_f =  (Cp_f*visc_bf)/kh_f

#Viscosities of mixture in the feed and permeate side
visca_wf =
exp(ADippr108_0+BDippr108_0/T_wf+CDippr108_0*ln(T_wf)+DDippr108_0*T_wf^EDippr108_0)
viscb_wf =
exp(ADippr108_1+BDippr108_1/T_wf+CDippr108_1*ln(T_wf)+DDippr108_1*T_wf^EDippr108_1)
visc_wf  = visca_wf*(1-xb_wf) + xb_wf*viscb_wf

# Diffusivity
Dab = 1e-9

#Schmidt
Sh_f =
aux11*((1.86*(Re_f*Sc_f*dh/L)^0.33)*(visc_bf/visc_wf)^0.14)+aux12*(0.116*(Re_f^(2/3)-
125)*Sc_f^0.33*(1+(dh/L)^(2/3))*(visc_bf/visc_wf)^0.14)+aux13*(0.023*(Re_f^0.8)*(Sc_f^0.3
3)*(visc_bf/visc_wf)^0.14)
```

```
#transfer mass coefficient
Km_f = ((Sh_f*Dab)/dh)*(1+delkm)

#Nusselt
Nu_f =
aux11*((1.86*(Re_f*Pr_f*dh/L)^0.33)*(visc_bf/visc_wf)^0.14)+aux12*(0.116*(Re_f^(2/3)-
125)*Pr_f^0.33*(1+(dh/L)^(2/3))*(visc_bf/visc_wf)^0.14)+aux13*(0.023*(Re_f^0.8)*(Pr_f^0.3
3)*(visc_bf/visc_wf)^0.14)

#Resistence to heat transfer
hh_f = (Nu_f*kh_f)/dh

#viscosity of the gas inside the membrane
viscg_a=ADippr109_0*T_wf^(BDippr109_0)/(1+CDippr109_0/Tavg+DDippr109_0/T_wf^2)
viscg_b=ADippr109_1*T_wf^(BDippr109_1)/(1+CDippr109_1/Tavg+DDippr109_1/T_wf^2)
viscgas=xa_wp*viscg_a+(1-xa_wp)*viscg_b


#-------------------------------------------------------------------------
#MEMBRANE
tortuosity = 1/(epsilon)
K0 = (2*epsilon*Prad/(3*tortuosity))

#Vapour pressure in the feed side of the membrane
pvapa_wf = exp(pcoefA_a+pcoefB_a/T_wf+pcoefC_a*ln(T_wf)+pcoefD_a*T_wf^pcoefE_a)
pvapb_wf = exp(pcoefA_b+pcoefB_b/T_wf+pcoefC_b*ln(T_wf)+pcoefD_b*T_wf^pcoefE_b)

#Partial pressures at the permeate side of the membrane
pa_wp = xa_wp*Pvacuum
pb_wp = (1-xa_wp)*Pvacuum

#Partial pressures at feed side of the membrane
pa_wf = pvapa_wf*coefactab*(1-xb_wf)
pb_wf = pvapb_wf*coefactba*xb_wf

#Molar flux
Ra = Pa/deltam*(pa_wp-pa_wf)
Rb = Pb/deltam*(pb_wp-pb_wf)

#molar fraction in the wall of permeate side
0 = -xa_wp + (Ra/(Ra+Rb))
xb_wp = 1-xa_wp
xa_wf = 1 - xb_wf

conc = roab_wf*(xmassa_wp/Ma + xmassb_wp/Mb)

#Enthalpy of evaporation
deltaHa = (1/Ma/1000)*ADippr103_0*(1-
T_wf/DB_Tc_0)^(BDippr103_0+CDippr103_0*(T_wf/DB_Tc_0)+DDippr103_0*(T_wf/DB_Tc_0)^2)
deltaHb = (1/Mb/1000)*ADippr103_1*(1-
T_wf/DB_Tc_1)^(BDippr103_1+CDippr103_1*(T_wf/DB_Tc_1)+DDippr103_1*(T_wf/DB_Tc_1)^2)

Qenergy=Na*deltaHa + Nb*deltaHb

0 = -xb_wf + (xb_f - xb_wp)*exp((Ra+Rb)/(conc*Km_f))+xb_wp
0 = -T_wf + T_bf-energy/hh_f

Rtotal = Ra+Rb

#Mass balance
dmf = -(Rtotal/conc)/(nc*h) + mf - mf
dmp = (Rtotal/conc)/(nc*h) + mp - mp

#Energy balance in feed side
dT_bf=1/Vf*(-Qenergy*w/(Cp_f*roa_f)+(liqflux)*w*T_bf)

# component permeate flows
dmasspA=Na*w + masspA - masspB
dmasspB=Nb*w + masspA - masspB
```

```
#component feed flows
dmassfA=-Na*w
dmassfB=-Nb*w + massfA - massfB

# Recovery and CF
Recovery = massfB/(uf*Am*ro_f*xb_f)
CF = xb_wp/xb_f
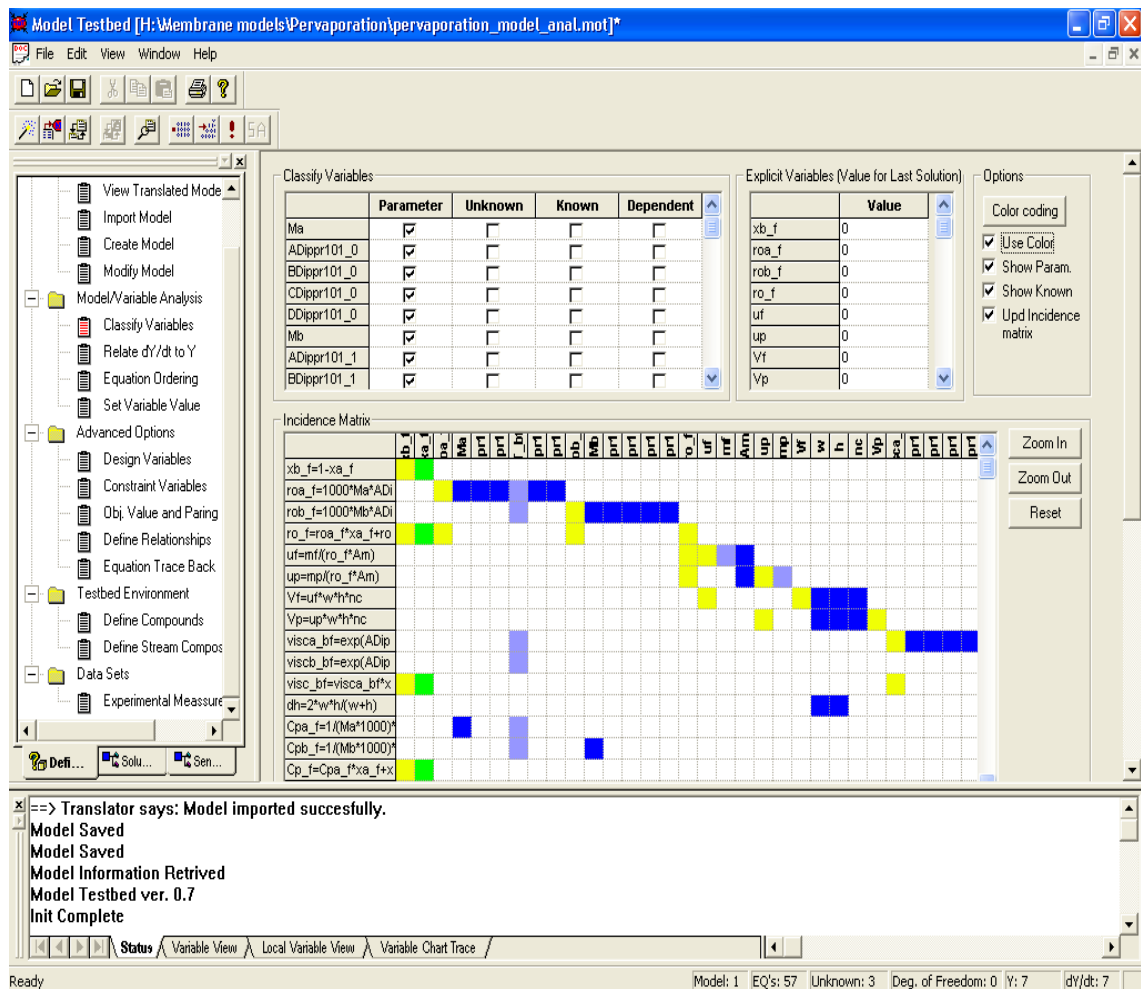```

Figure A.7: MoT code for VMD process



Figure A.8: Model analysis screen shot for PV process

# Polymer abbreviations

This appendix presents the full forms of the polymers whose abbreviations are used in Case studies presented in 5.2.1 and 5.2.2 in Chapter 5.

| Abbreviation | Full form |
| --- | --- |
| 6FDA-6FpDA | polyimide of 2,2-bis(3,4dicarboxyphenyl) hexafluoropropane dianhydride and 4,4'-(hexafluoro isopropylidene)-dianiline |
| 6FBPA/TERE | polyester of hexafluoro bisphenol-A and terephthalic diacid chloride |
| HFPC | hexafluoro bisphenol-A polycarbonate |
| TMHFPC | tetramethyl hexafluoro bisphenol-A polycarbonate |
| TMHFPSF | tetramethyl hexafluoro bisphenol-A polysulfone |
| TBrHFPC | tetrabromo hexafluoro bisphenol-A polycarbonate |
| TMPC | tetramethyl bisphenol-A polycarbonate |
| TMBIPSF | tetramethyl biphenol polysulfone |
| PMDA-IPDA | polypyromellitimide of isopropylidenedianiline |
| 6FDA-ODA | polyimide of 2,2-bis(3,4dicarboxyphenyl) hexafluoropropane dianhydride and oxydianiline |
| SBI/TERE | polyester of 6,6'-dihydroxy 3,3,3',3'-tetramethyl-1, 1'-spirobiindane and terephthalic diacid chloride |
| 6FBPA/BB | polyester of hexafluoro bisphenol-A and 4,4'-biphenol diacid chloride |
| PDMPO: | poly(2,6-dimethyl-1,4 phenylene oxide) |
| PDPPO: | poly(2,6-diphenyl-1,4 phenylene oxide) |
| BPA/tBIA: | poly(bisphenol-A tetrabutyl isophthalate) |
| PhTh/tBIA: | poly(phenolphthalein tetrabutyl isophthalate) |
| HPF/tBIA: | poly(fluorene bisphenol tetrabutyl isophthalate) |
| TBBPA/IA: | poly(tetrabromo bisphenol-A isophthalate) |
| TBPhTh/tBIA: | poly(tetrabromo bisphenol-A isophthalate) |
| TBPhTh/tBIA: | poly(tetrabromo phenolphthalein tetrabutyl isophthalate) |
| TBPAh/IA: | poly(tetrabromo phenolphthalein isophthalate) |
| 6FDA-2,4-DATr: | polyimide of 2,2-bis(3,4 dicarboxyphenyl) hexafluoropropane dianhydride and 2,4-diaminotoluene |
| 6FDA-3,5-DBTF: | polyimide of 2,2-bis(3,4) dicarboxyphenyl) hexafluoropropane dianhydride and 3,5-diaminobenzotrifluoride |

# Nomenclature

| | |
|---|---|
| $\alpha$ | Center of mass of species |
| $\epsilon$ | Porosity |
| $\delta_m$ | Thickness of membrane's active layer (m) |
| $\phi$ | Fugacity |
| $\Delta H$ | Heat of vaporization (J/mol) |
| $\gamma$ | Activity coefficient |
| $\lambda$ | Mean free path (m) |
| $\mu_g$ | Gas viscosity (kg/m/s) |
| $\mu_{JT}$ | Joule-Thompson coefficient |
| $\mu_L$ | Liquid viscosity (kg/m/s) |
| $\rho$ | Liquid density (kg/m$^3$) |
| $\underline{\theta}$ | Vector of properties assisting structured materials |
| $\tau$ | Tortousity |
| $\xi$ | vector of chemical and physical properties |
| $a$ | Acceleration (m/s$^2$) |
| $A_m$ | Area (m$^2$) |
| $\underline{A}$ | Vector of constitutive variables |
| $C_p$ | Specific heat (J/mol/K) |
| $C_T$ | Concentration (m$^3$/mol) |
| $D_F$ | Degrees of freedom |
| $D_{ij}$ | Diffusion coefficient (m$^2$/s) |
| $D_{ie}^k$ | Effective Knudsen diffusivity (m$^2$/s) |
| $D_{ie}^0$ | Pressure independent diffusivity (m$^2$/s) |
| E | Energy (J/mol) |
| $h$ | Heat transfer coefficient (J/s/m$^2$/K) |
| $H$ | Henry's constant (m$^3$ Pa/mol) |
| $\underline{I}$ | Vector of inlet variables |
| $K$ | Instantaneous kinetic energy (kg m$^2$/s$^2$) |
| $L$ | Length of membrane module (m) |
| $\underline{M}$ | Vector of parameters representing geometry of process module |
| $M_w$ | Molecular weight (g/mol) |
| $m$ | Molar flow (kg/s) |
| N | Number of moles (mol) |
| $N_{total}$ | Total flux through membranes (mol/m$^2$/s) |
| Nu | Nusselt's number |
| $k_v$ | Thermal conductivity (J/m/s/K) |
| $k_B$ | Boltzmann constant (J/s/m$^2$/K$^4$) |
| $p_i$ | Partial vapor pressure (Pa) |
| P | Pressure (Pa) |

| | |
|---|---|
| $P_i$ | Permeability coefficient (mol/m/s/Pa) |
| $\underline{P}$ | Vector of performance criteria |
| $P^{sat}$ | Vapor pressure (Pa) |
| Pr | Prandtl number |
| $Q$ | Partition function |
| Re | Reynold's number |
| $r_p$ | Pore radius [m] |
| R | Gas constant (Pa m$^3$/mol/K) |
| $R_g$ | Radius of gyration (m) |
| $S_i$ | Solubility (mol/m$^3$/Pa) |
| Sc | Schmidt's number |
| Sh | Sherwood number |
| $t$ | Time (s) |
| $T$ | Temperature (K) |
| $T_C$ | critical temperature (K) |
| $U$ | potential energy (kg m$^2$/s$^2$) |
| $U_r$ | Harmonic bond stretching potential (kg m$^2$/s$^2$) |
| $U_\theta$ | harmonic bend angle potential (kg m$^2$/s$^2$) |
| $v$ | linear mass velocity (m/s) |
| V | Volume (m$^3$) |
| $w$ | Width of the membrane module (m) |
| $x$ | Molar fraction in liquid phase |
| $\underline{X}$ | Vector of outlet variables |
| $y$ | Molar fraction in gas phase |
| $\underline{Y}$ | Vector of state variables |
| $z$ | Independent variable (space) |

**Subscripts**

| | |
|---|---|
| $\theta$ | property variables |
| $\xi$ | physical property variables |
| $av$ | average |
| $ex$ | flux of any stream entering the permeate side |
| $F$ | feed side of membrane module |
| $I$ | Input variables |
| $M$ | geometry variables |
| $N$ | process equations |
| $P$ | permeate side of membrane module |
| $R$ | retentate side of membrane module |
| $SM$ | structural material property equations |
| $SS$ | sorbet molecules |
| $w$ | wall of membrane module |
| $X$ | output variables |

**Superscripts**

| | |
|---|---|
| $G$ | gas phase |
| $L$ | liquid phase |
| $P$ | predicted |

# References

[1] Accelrys. *Material Studio manual*, version 4.0 edition.

[2] M.P. Allen. Introduction to molecular dynamics simulation. Technical report, John von Neumann Institute for Computing, Julich, 2004.

[3] M.P. Allen and D.J. Tildesley. *Computer simulation of liquids.* Clarendon Press: Oxford, U.K.,, 1987.

[4] C.R. Antonson, R.J. Gardner, C.F. King, and D.Y. Ko. Analysis of gas separation by permeation in hollow fibers. *Ind Eng Chem Process Des Dev*, 16 (4):463–469, 1977.

[5] R.B. Babu, N.K. Rastogi, and K.S.M.S. Raghavarao. Mass transfer in osmotic membrane distillation of phycocyanin colorant and sweet-lime juice. *Journal of Membrane Science*, 272:5869, 2006.

[6] R.W. Baker. *Membrane technology and applications.* Wiley and sons, 2004.

[7] F.A. Banat and J. Simandl. Removal of benzene traces from contaminated water by vacuum membrane distillation. *Chemical Engineering Science*, 51:1257–1265, 1996.

[8] S. Bandini, C. Gostoli, and G.C. Sarti. Role of heat and mass transfer in membrane distillation process. *Desubnatron*, 81:91–106, 1991.

[9] S. Bandini, A. Saavedra, and G.C. Sarti. Vacuum membrane distillation: Experiments and modeling. *AIChE Journal*, 43:398, 1997.

[10] S. Bandini and G.C. Sarti. Concentration of must through vacuum membrane distillation. *Desalination*, 149:253–259, 2002.

[11] S. Bandini and G.G. Sarti. Heat and mass transport resistances in vacuum membrane distillation per drop. *AIChE Journal*, 45 (7):1422–1433, 1999.

[12] J. Bicerano. *Prediction of polymer properties.* Marcel Dekker, Inc., New York, 1993.

[13] R.C. Binning, R.J. Lee, J.F. Jennings, and E.C. Martin. Separation of liquid mixtures by permeation. *Industrial and engineering chemistry*, 53 (1):45–50, 1961.

[14] R.B. Bird, W. Stewart, and E. Lightfoot. *Transport Phenomena.* John Wiley and sons, New York, 2000.

[15] G.C. Boulougouris, E.C. Voutsas, I.G. Economou, D.N. Theodorou, and D.P. Tassios. Henry's constant analysis for water and nonpolar solvents from experimental data, macroscopic models, and molecular simulation. *Journal of Physical Chemistry B*, 105 (32):7792–7798, 2001.

[16] R.H. Boyd and P.V. K. Pant. Molecular packing and diffusion in polyisobutylene. *Macromolecules ,,,* 24:6325–6331, 1991.

[17] J. Brandrup, E.H. Immergut, and E.A. Grulke. *Polymer handbook*. John Wiley and sons, 1999.

[18] V. Calabro, E. Drioli, and G. Jonsson. Mass transfer and thermodynamics in polarization phenomena in reverse osmosis and membrane distillation. Not published yet.

[19] V. Calabro, B.L. Jiao, and E. Drioli. Theoretical and experimental study on membrane distillation in the concentration of orange juice. *Industrial Engineering Chemist y Research*, 33:1803–1808, 1994.

[20] M. Celere and C. Gostoli. The heat and mass transfer phenomena in osmotic membrane distillation. *Desalination*, 147:133–138, 2002.

[21] S.G. Charati and S.A. Stern. Diffusion of gases in silicone polymers: Molecular dynamics simulations. *Macromolecules*, 31:5529–5535, 1998.

[22] R.T. Chern, W.J. Koros, and P.S. Fedkiw. Simulation of a hollow-fiber gas separator: The effects of process and design variables. *Industrial and Engineering Chemistry, Process Design and Development*, 24 (4):1015–1022, 1985.

[23] D.T. Coker, B.D. Freeman, and G.K. Fleming. Modeling multicomponent gas separation using hollow-fiber membrane contactors. *AIChE Journal*, 44 (6):1289–1302, 1998.

[24] L. Constantinou, K. Bagherpour, R. Gani, J.A. Klein, and D.T. Wu. Computer aided product design: problem formulations, methodology and applications. *Computers and Chemical Engineering*, 20 (6-7):685–702, 1996.

[25] L. Constantinou and R. Gani. New group contribution method for estimating properties of pure compounds. *AIChE Journal*, 40 (10):1697–1710, 1994.

[26] J. Crank. *The Mathematics of Diffusion*. Clarendon Press: Oxford, U.K.,, 1975.

[27] R. Datta, S. Dechapanichkul, J.S. Kim, and L.Y. Fang. A generalized model for the transport of gases in porous, non-porous, and leaky membranes. i. application to single gases. *Journal of Membrane Science*, 75 (3):245–263, 1992.

[28] G.C. Derringer and R.L. Markham. Computer based methodology for matching polymer structures with required properties. *Journal of Applied Polymer Science*, 30 (12):4609–4617, 1985.

[29] E. Drioli, Y. Wu, and V. Calabro. Membrane distillation in the treatment of aqueous solutions. *Journal of Membrane Science*, 33:277–284, 1987.

[30] I.G. Economou. Monte carlo simulation of phase equilibria of aqueous systems. *Fluid Phase Equilibria*, 183-184:259–269, 2001.

[31] K.A. Fattah, S.M. Hamam, G. Al-Enez, H.M. Ettoueny, and R. Hughes. A nonideal model for analysis of gas separation permeators. *Journal of Membrane Science*, 65 (3):247–257, 1992.

[32] X. Feng and R.Y.M. Huang. Concentration polarization in pervaporation separation processes. *Journal of Membrane Science*, 92:201–208, 1994.

[33] X. Feng and R.Y.M. Huang. Estimation of activation energy for permation in pervaporation process. *Journal of Membrane Science*, 118:127–131, 1996.

[34] X. Feng and R.Y.M. Huang. Liquid separation by membrane pervaporation: A review. *Ind. Eng. Chem. Res.*, 36:1048–1066, 1997.

[35] J.K. Franklin. Prediction of heat and free energies of organic compounds. *Industrial and Engineering Chemistry*, 41 (51):1070+, 1949.

[36] D. Frenkel and B. Smit. *Understanding molecular simulation.* Academic press, 2002.

[37] Frost and Sullivan. U.s. membrane separation systems market. Technical report, Frost & Sullivan, 2006.

[38] R. Gani and L. Constantinou. Molecular structure based estimation of properties for process design. *Fluid Phase Equilibria*, 116(1-2):75–86, 1996.

[39] R. Gani, P.M. Harper, and M. Hostrup. Automatic creation of missing groups through connectivity index for pure-component property prediction. *Ind. Eng. Chem. Res.*, 44:7262–7269, 2005.

[40] R. Gani, G. Hytoft, C. Jaksland, and A.K. Jensen. An integrated computer aided system for integrated design of chemical processes. *Computers and Chemical Engineering*, 21 (10):1135–1146, 1997.

[41] R. Gani and E.N. Pistikopoulos. Property modeling and simulation for product and process design. *Fluid Phase Equilibria*, 194197:4359, 2002.

[42] H. Gorissen. Temperature changes involved in membrane gas separations. *Chemical Engineering and Processing*, 22 (2):63–67, 1987.

[43] C. Gostoli. Thermal effects in osmotic distillation. *Journal of Membrane Science*, 163:7591, 1999.

[44] M. Gryta. Osmotic md and other membrane distillation variants. *Journal of Membrane Science*, 246:145156, 2005.

[45] M. Gryta and M. Tomaszewska. Heat transport in the membrane distillation process. *Journal of Membrane Science*, 144:211–222, 1998.

[46] A.A. Gusev, S. Arizzi, and U.W. Suter. Dynamics of light gases in rigid matrices of dense polymers. *Journal of Chemical Physics*, 99 (3):2221–2228, 1993.

[47] P.M. Harper, R. Gani, P. Kolar, and T. Ishikawa. Computer-aided molecular design with combined molecular modeling and group contribution. *Fluid Phase Equilibria*, 158160:337347, 1999.

[48] W.S.W. Ho and K.K. Sirkar. *Membrane handbook*, chapter 1, pages 3–15. Van Nostrand Reinhold, New York, 1992.

[49] S.T. Hwang and J.M. Thorman. Continous membrane contactors. *AIChE Journal*, 26 (4):558–566, 1980.

[50] S.B. Iversen, V.K. Bhatia, K. Dam-Johansen, and G. Jonsson. Characterization of microporous membranes for use in membrane contactors. *Journal of Membrane Science*, Vol.130 (1-2):205–217, 1997.

[51] M.A. Izquierdo-Gil and G. Jonsson. Factors affecting flux and ethanol separation performance in vacuum membrane distillation. *Journal of Membrane Science*, 214:113130, 2003.

[52] C. Jaksland. *Separation process design and synthesis based on thermodynamics insights*. PhD thesis, Department of chemical engineering, Technical university of Denmark, 1996.

[53] K.G. Joback and R. C. Reid. Estimation of pure-component properties from group contributions. *Chem. Eng. Commun.*, 57:233, 1983.

[54] R.B. Jorgensen. Personal correspondence.

[55] R.B. Jorgensen, A.S. Meyer, C. Varming, and G. Jonsson. Recovery of volatile aroma compounds from black currant juice by vacuum membrane distillation. *Journal of Food Engineering*, 64:23–31, 2004.

[56] Y.K. Kao, S. Chen, and S.T. Hwang. Effect of diffusion on the model of a capillary gas permeator. *Journal of Membrane Science*, 32:139–157, 1987.

[57] N.C. Karayiannis, A.E. Giannousaki, and V.G. Mavrantzas. An advanced monte carlo method for the equilibration of model long-chain branched polymers with a well-defined molecular architecture: Detailed atomistic simulation of an h-shaped polyethylene melt. *Journal of Chemical Physics*, 118 (6):2451–2454, 2003.

[58] N.C. Karayiannis, A.E. Giannousaki, V.G. Mavrantzas, and D.N. Theodorou. Atomistic monte carlo simulation of stictly monodisperse long polyethylene melts through a generalized chain bridging algorithm. *Journal of chemical physics*, 117 (11):5465–5479, 2002.

[59] N.C. Karayiannis, V.M. Mavrantzas, and D.N. Theodorou. A novel monte carlo scheme for the rapid equilibration of atomistic model polymer systems of precisely defined molecular architecture. *Physical Review Letters*, 88 (10):1055031–1055034, 2002.

[60] N.Ch. Karayiannis, V. G. Mavrantzas, and D. N. Theodorou. Detailed atomistic simulation of the segmental dynamics and barrier properties of amorphous poly(ethylene terephthalate) and poly(ethylene isophthalate). *Macromolecules*, 37:2978–2995, 2004.

[61] R.E. Kesting and A.K. Fritzsche. *Polymeric gas separation membranes*. John Wiley & Sons: New York, 1993.

[62] M. Khayet, M.P. Godino, and J.I. Mengual. Theoretical and experimental studies on desalination using the sweeping gas membrane distillation method. *Desalination*, 157:297–305, 2003.

[63] M. Khayet, P. Godino, and J. I. Mengual. Nature of flow on sweeping gas membrane distillation. *Journal of Membrane Science*, 170:243, 2000.

[64] M. Khayet, P. Godino, and J. I. Mengual. Theory and experiments on sweeping gas membrane distillation. *Journal of Membrane Science*, 165:261272, 2000.

[65] L. B. Kier and H. L. Hall. *Molecular Connectivity in Structure Activity Analysis*. John Wiley & Sons: New York, 1986.

[66] K. M. Klincewicz and R. C. Reid. Estimation of critical properties with group contribution methods. *AIChE Journal*, 30(1):137–142, 1984.

[67] P.A. Kober. Pervaporation, perstillation and percrystalization. *Journal of the Americal chemical society*, 39:944–948, 1917.

[68] W. Kunz, A. Benhabiles, and R. Ben-Aim. Osmotic evaporation through macroporous hydrophobic membranes: a survey of current research and applications. *Journal of Membrane Science*, 121 (1):25–36, 1996.

[69] H. Lababidi, G.A. Al-Enezi, and H.M. Ettouney. Optimization of module configuration in membrane gas separation. *Journal of Membrane Science*, 112 (2):185–197, 1996.

[70] LAMMPS. *Distributed by Sandia National Laboratories, a US Department of Energy (DOE) laboratory*. http://lammps.sandia.gov/.

[71] K.W. Lawson and D.R. Lloyd. Membrane distillation. i. module design and performance evaluation using vacuum membrane distillation. *Journal of Membrane Science*, 120:111–121, 1996.

[72] K.W. Lawson and D.R. Lloyd. Membrane distillation. ii. direct contact md. *Journal of Membrane Science*, 120:123–133, 1996.

[73] K.W. Lawson and D.R. Lloyd. Membrane distillation. *Journal of Membrane Science*, 124 (1):1–25, 1997.

[74] Y.M. Lee and E.M. Shin. Pervaporation separation of water-ethanol through modified chitosan membranes. 4. phosphorylated chitosan membranes. *Journal of Membrane Science*, 64:145, 1991.

[75] H.K. Lonsdale, U. Merten, and R.L. Riley. Transport properties of cellulose acetate osmotic membranes. *Journal of applied polymer science*, 9:1341–1362, 1965.

[76] S. Macchietto, O. Odele, and O. Omatsone. Design of optimal solvents for liquid-liquid extraction and gas absorption processes. *Chemical Engineering Research and Design*, 68 (5):429–433, 1990.

[77] Z. Makrodimitri, R. Dohrn, and I. Economou. Atomistic simulation of poly(dimethylsiloxane): Force field development, structure, and thermodynamic properties of polymer melt and solubility of n-alkanes, n-perfluoroalkanes, and noble and light gases. *Macromolecules*, 40 (5):1720–1729, 2007.

[78] J. Marrero and R. Gani. Group-contribution based estimation of pure component properties. *Fluid Phase Equilibria*, 183184:183208, 2001.

[79] J. Marrero and R. Gani. Group-contribution-based estimation of octanol/water partition coefficient and aqueous solubility. *Industrial and Engineering Chemistry Research*, Vol.41 (25):6623–6633, 2002.

[80] J.I. Marriot and E. Sorensen. A general approach to modelling membrane modules. *Chemical Engineering Science*, 58:4975–4990, 2003.

[81] J.I. Marriot, E. Sorensen, and I.D.L. Bogle. Detailed mathematical modeling of membane modules. *Computers and chemical engineers*, 25:693–700, 2001.

[82] L. Martinez and J.M. Rodriguez-Maroto. On transport resistances in direct contact membrane distillation. *Journal of Membrane Science*, 295:2839, 2007.

[83] L. Martinez-Diez and M.I. Vazquez-Gonzalez. A method to evaluate coefficients affecting flux in membrane distillation. *Journal of Membrane Science*, 173:225234, 2000.

[84] E.A. Mason and A.P. Malinauskas. *Gas transport in porous media: The dusty gas model.* Elsevier, New York, 1983.

[85] V. Mavrantzas. Personal correspondence , ice-forth, patras, greece.

[86] W.L. McCabe, J.C. Smith, and P. Harriot. *Unit operations of chemical engineering.* Mc Graw Hill Publications, 2005.

[87] J.I. Mengual, M. Khayet, and M.P. Godino. Heat and mass transfer in vacuum membrane distillation. *International Journal of Heat and Mass Transfer*, 47:865–875, 2004.

[88] A.-H. Meniai and D.M.T. Newsham. Selection of solvents for liquid-liquid extraction. *Chemical Engineering Research and Design*, 70 (1):78–87, 1992.

[89] M. Mulder. *Basic principles of membrane technology*. Kluwer academic publishers, 1996.

[90] S. Murad and S. Gupta. A simple molecular dynamics simulation for calculating henry's constant and solubility of gases in liquids. *Chemical Physics Letters*, 319 (1-2):60–64, 2000.

[91] S. Murad and S. Gupta. Molecular dynamics simulation for henry"s constant of oxygen in benzene. 187-188:29–37, 2001.

[92] N. Nagaraj, G. Patil, B.R. Babu, U.H. Hebbar, K.S.M.S. Raghavarao, and S. Neneb. Mass transfer in osmotic membrane distillation. *Journal of Membrane Science*, 268:4856, 2006.

[93] S.K. Nath and R. Khare. New forcefield parameters for branched hydrocarbons. *Journal of chemical physics*, 115(23):10837–10844, 2001.

[94] P.V.K. Pant and R.H. Boyd. Molecular dynamics simulation of diffusion of small penetrants in polymers. *Macromolecules*, 26:619–686, 1993.

[95] J.Y. Park and D.R. Paul. Correlation and prediction of gas permeability in glassy polymer membrane materials via a modified free volume based group contribution method. *Journal of Membrane Science*, 125 (1):23–39, 1997.

[96] G.B. Peters. *Enzyme Functionality*, chapter Computer simulations: A tool for investigating the function of complex biological macromolecules, pages 97–147. Marcel, Dekker Inc., New York, 2004.

[97] R. Rautenbach and W. Dahm. Simplified calculation of gas-permeation hollow-fiber modules for the separation of binary mixtures. *Journal of Membrane Science*, 28 (3):319–327, 1986.

[98] R. C. Reid, J. M. Prausnitz, and B. E. Poling. *The Properties of Gases and Liquids, 4th ed.* McGraw-Hill, New York, 1987.

[99] B.M. Russel, J.P. Henriksen, S.B. Jorgensen, and R. Gani. Integration of design and control through model analysis. *Computers and Chemical Engineering*, 24(2-7):967–973, 2000.

[100] D.M. Ruthven and S. Sirkar. Design of membrane and psa processes for bulk gas separation. *AIChE Symposium Series*, 91 (304):29–38, 1995.

[101] K. Sakai, T. Koyano, M. Tamura, and T. Muroi. Effects of temperature and concentration polarization on water vapour permeability for blood in membrane distillation. *The Chemical Engineering Journal*, 38:B33–B39, 1988.

[102] A.M. Sales-Cruz and R. Gani. *Development of a computer aided modeling system for bio and chemical process and product design*. PhD thesis, CAPEC, Technical University of Denmark, 2006.

[103] R.W. Schofield, A.G. Fane, and C.J.D. Fell. Heat and mass transfer in membrane distillation. *Journal of Membrane Science*, 33:299–313, 1987.

[104] J.D. Seader and E. Henley. *Separation process principles*. John Wiley & Sons: New York, 1998.

[105] J.M. Smith, H.C. Van Ness, and M.M. Abbott. *Introduction to chemical engineering thermodynamics*. McGraw-Hill International edition, 2005.

[106] K. Smolders and A.C.M. Franken. Terminology for membrane distillation. *Desalination*, 72 (3):249–262, 1989.

[107] S.A. Stern. Polymers for gas separations: the next decade. *Journal of Membrane Science*, 94:1–65, 1994.

[108] H. Takeuchi. A jump motion of small molecules in glassy polymers: A molecular dynamics simulation. *Journal of Chemical Physics*, 93 (3):2062 – 2067, 1990.

[109] H. Takeuchi and K. Okazaki. Molecular dynamics simulation of diffusion of simple gas molecules in a short chain polymer. *Journal of Chemical Physics*, 92 (9):5643–5652, 1990.

[110] R. Taylor and R. Krishna. *Multicomponent mass transfer*. Wiley and sons, 1993.

[111] S. Tessendorf. *Modeling, analysis, and design of membrane based gas separation systems*. PhD thesis, Technical University of Denmark, 1998.

[112] D.N. Theodorou. *Diffusion in Polymers*. Marcel Dekker: New York, 1996.

[113] A.M Urtiaga, G. Ruiz, and I. Ortiz. Kinetic analysis of the vacuum membrane distillation of chloroform from aqueous solutions. *Journal of membrane science*, 165:99–110, 2000.

[114] D.W. van Krevelan. *Properties of polymers*. Elsevier, Amsterdam, 1990.

[115] J. S. Vrentas and C. M. Vrentas. Evaluation of the free-volume theory of diffusion. *Journal of Polymer Science: Part B: Polymer Physics*, 41:501507, 2003.

[116] J.S. Vrentas, C.M. Vrentas, and N. Faridi. Effect of solvent size on solvent self-diffusion in polymer-solvent systems. *Macromolecules*, 29 (9):3272–3276, 1996.

[117] J. Weeks, D. Chandler, and H. C. Andersen. Role of repulsive forces in determining the equilibrium structure of simple liquids. *Journal of Chemial Physics*, 54:5237–5247, 1971.

[118] B. Widom. Some topics in the theory of fluids. *Journal of Chemical Physics*, 39 (11):2808–2812, 1963.

[119] J.G. Wijmans. The role of permeant molar volume in the solution-diffusion model transport equations. *Journal of Membrane Science*, 237:3950, 2004.

[120] J.G. Wijmans and R.W. Baker. The solution-diffusion model - a review. *Journal of Membrane Science*, 107:1–21, 1995.

[121] C. Wu, X. Li, J. Dia, and H. Sun. Prediction of henrys law constants of small gas molecules in liquid ethylene oxide and ethanol using force field methods. *Fluid Phase Equilibria*, 236:6677, 2005.

[122] J.M. Zielinski and J.L. Duda. Predicting polymer/solvent diffusion coefficients using free-volume theory. *AIChE Journal*, 38 (3):405–415, 1992.